Chapter 1 Introduction

1.1 The mitochondrion

Most eukaryotic cells contain mitochondria, organelles which are surrounded by a double membrane and are similar in cross-section to bacteria. The outer membrane is permeable to ions and small molecules less than 25 Å in diameter due to the presence of the voltage-dependent anion channel (VDAC) (Colombini, 2012), whilst the inner membrane is not. The 'tightness' of the inner membrane is the key feature that helps the mitochondrion accomplish its most well established function, the production of cellular energy in the form of adenosine 5'-triphosphate (ATP) by oxidative phosphorylation. The double membrane surrounds the mitochondrial matrix, a protein-dense interior containing, of note, multiple copies of self-replicating circular mitochondrial DNA (mtDNA) genomes. The mitochondrial organelles undergo fusion and fission depending on cell type and cues from the cellular environment. Mitochondria also play a role in the regulation of metabolism, the cell cycle and cell death (McBride *et al.*, 2006; Mitra *et al.*, 2009).

The primary function of mitochondria is the production of ATP by oxidative phosphorylation. Briefly, electrons derived from the oxidation of fatty acids, pyruvate and amino acids are transferred by nicotinamide adenine dinucleotide (NADH) to complex I, by flavoprotein dehydrogenases to electron-transferring flavoprotein:ubiquinone oxidoreductase (ETF-QO) or by succinate to complex II. The electrons which enter complex I, ETF-QO and complex II are carried by ubiquinol to complex III, and then by cytochrome *c* to complex IV. Concomitantly, protons are pumped by complexes I, III and IV from the mitochondrial matrix to the intermembrane region, generating a proton motive force which drives the synthesis of ATP from adenosine 5'-diphosphate (ADP) and phosphate (P_i) by ATP synthase. ADP is imported by the ADP/ATP carrier into the mitochondrial matrix for ATP synthesis and ATP is exported to replenish the cell with ATP needed to drive cellular reactions. In addition to energy conversion, the mitochondrion also plays a role in the oxidation of fatty acids, the synthesis and degradation of amino acids, iron-

sulphur cluster and haem assembly and the generation of heat by the dissipation of the proton gradient (Figure 1.1) (Kunji, 2004).

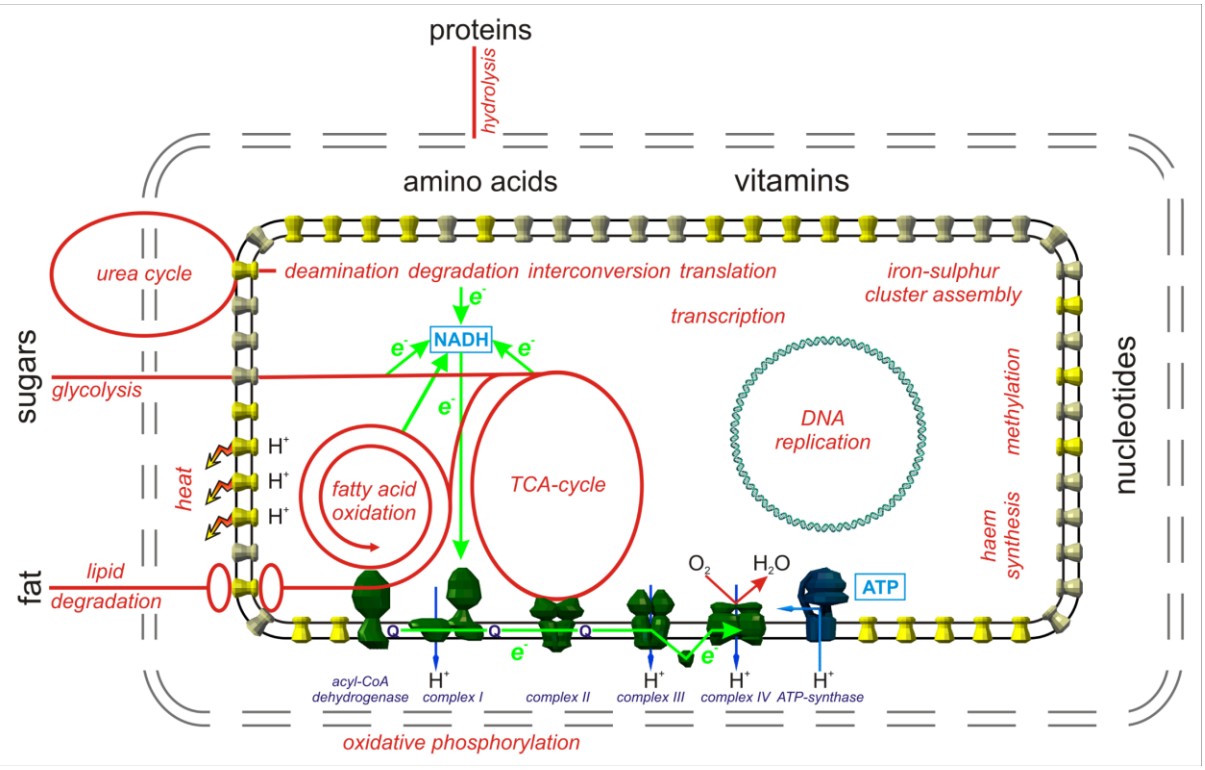

Figure 1.1 Metabolic pathways of the mitochondrion. Simplified diagram of the primary metabolic pathways involved in mammalian mitochondrial and cytosolic metabolism. Metabolic pathways (red), including fatty acid oxidation and the TCA cycle, generate NADH (light blue) and donate electrons (light green) to the respiratory chain (dark green). ATP synthase (dark blue) generates ATP (light blue). Mitochondrial carriers are depicted in yellow and metabolites in black. The permeable outer membrane (dotted double line) and the impermeable inner membrane (solid double line) are depicted. Figure courtesy of Dr Edmund R.S. Kunji.

1.1.1 Structural features

Fixed animal mitochondria were first imaged using two-dimensional transmission electron microscopy (Palade, 1952; Palade, 1953). The images showed individual mitochondria shaped as ellipses and confirmed the existence of a double, limiting membrane, a mitochondrial matrix and inner membrane ridges, which were named cristae (Figure 1.2 A). Electron microscope (EM) tomography, a modern imaging method, provided better insights into mitochondrial structure (Frey & Mannella, 2000). Three-dimensional EM tomography images of isolated mitochondria showed that the cristae are not highly invaginated, but are instead lamellar with narrow

tubular connections (Figure 1.2 B) (Perkins *et al.*, 1997; Frey & Mannella, 2000; Perkins & Frey, 2000). The narrow tubular connections have been termed cristae junctions. It is hypothesised that the cristae junctions may help maintain internal metabolite gradients, and thus help regulate the rate of ATP synthesis (Frey & Mannella, 2000).

Additionally, contact points between the inner and outer membranes have been identified (Hackenbrock, 1966; Perkins *et al.*, 1997). These punctate contact points are approximately 14 nm in length, and are randomly arranged with respect to cristae junctions. The translocase of the outer membrane (TOM) and translocase of the inner membrane (TIM) protein complexes, which translocate proteins into the membrane or inside the mitochondrion, are located at these junctions.

The general structure of mitochondria is as follows: the mitochondrial outer membrane contains the enzymes required for the β-oxidation of fatty acids, forming associations with the endoplasmic reticulum, which may help facilitate lipid transport from the endoplasmic reticulum to the mitochondrion (Perkins *et al.*, 1997; Okamoto & Shaw, 2005). The intermembrane region is between the outer and inner membranes. The mitochondrial inner membrane is the location of the electron transport chain enzyme complexes, the ATP synthase and the mitochondrial carrier family proteins, including the ADP/ATP carrier. In addition, the double membrane encapsulates the mitochondrial matrix, the site of metabolic processes such as iron-sulphur synthesis and the TCA cycle. Importantly, the circular mtDNA genome is found within the mitochondrial matrix, tethered to the inner membrane. The mtDNA encodes for 13 hydrophobic respiratory chain protein subunits and for ribosomal and messenger ribonucleic acid (RNA) (Kadenbach *et al.*, 1991; Sherratt, 1991). The post-transcriptional regulation of mitochondrial RNAs is a topic of active investigation (Rorbach & Minczuk, 2012).

Mitochondrial morphology is more complex than originally surmised. Mitochondria were thought to function independently, but it is now known that they are usually fused into a reticular network originating from near the cell's nucleus to facilitate the effective distribution of ATP and metabolites (Palmer *et al.*, 2011). However, mitochondria are dynamic, often undergoing fission and fusion, mediated by

conserved GTPases, to maintain or disrupt these networks (Okamoto & Shaw, 2005; Palmer *et al.*, 2011). Furthermore, mitochondria may undergo mitophagy to rid the cell of defective or unnecessary mitochondria. Mitophagy was identified and characterised in yeast, and it occurs in mammals during erythrocyte differentiation to rid the daughter cells of mitochondria (Youle & Narendra, 2011). Outer membrane associated proteins, parkin and PTEN-induced putative kinase protein 1 (PINK1) are major regulators of mitophagy, and they have been implicated in some forms of Parkinson's disease (Narendra *et al.*, 2010).

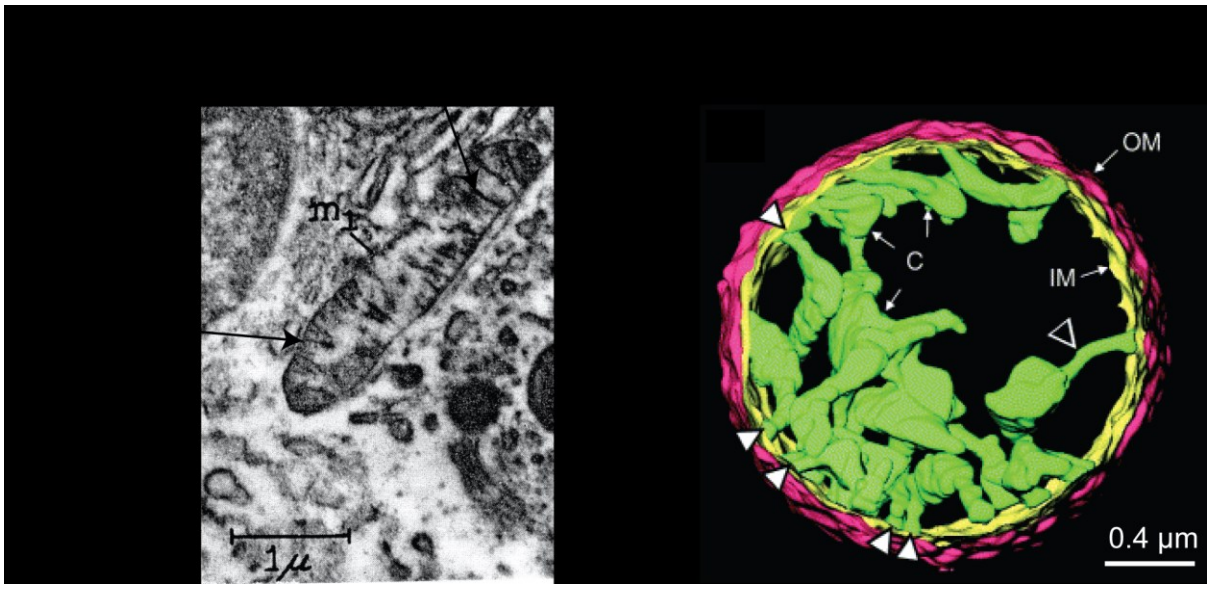

Figure 1.2 Mitochondrial structure. (**A**) Electron microscopy cross-sectional image of a rat pancreas mitochondrion. The mitochondrion is labelled m_1. The limiting membrane and the internal cristae are labelled. This image is from (Palade, 1952) (**B**) Three-dimensional electron tomography image of a rat liver mitochondrion. The outer membrane is labelled OM (red), the inner membrane is labelled IM (yellow), the crista are labelled C (green) and the crista junctions are indicated by white arrowheads. The tubular connection is indicated by a transparent arrowhead. This image is from (Mannella, 2000).

1.1.2 Oxidative phosphorylation

When the enzymatic reactions and chemical intermediates of glycolysis were discovered, it was believed that the synthesis of ATP was accomplished by a similar coupled reaction mechanism and that electron and proton transfer in oxidative systems worked in concert with substrate-level phosphorylation (Slater, 1953). However, the high-energy phosphate intermediate required to phosphorylate ADP to

ATP remained elusive. Peter Mitchell proposed an alternative mechanism, oxidative phosphorylation by chemiosmosis (Mitchell, 1961; Mitchell, 1979). Mitchell proposed four main postulates, which have been subsequently shown to be correct. Briefly, it was proposed that a chemiosmotic system should include a reversible ATP synthase with a defined proton to phosphorylation stoichiometry, membrane respiratory chains with a defined proton to electron stoichiometry across the membrane, proton-linked transporters for metabolite transport and osmotic maintenance and that all of these components be contained in an insulating membrane.

Knowledge about oxidative phosphorylation has expanded since Mitchell's revolutionary theory was published. Following glycolysis of glucose in the cytoplasm, pyruvate is transported across the mitochondrial inner membrane by the pyruvate transporter (Bricker *et al.*, 2012; Herzig *et al.*, 2012). Nicotinamide adenine dinucleotide (NAD^+) is reduced to NADH and flavin adenine dinucleotide (FAD) is reduced to $FADH_2$. Additionally, fatty acids cross the mitochondrial inner membrane and are oxidised by conversion to acetyl-CoA, which enters the tricarboxylic acid (TCA) cycle to form reducing equivalents. Electrons from NADH, flavoprotein dehydrogenases and succinate are transferred to protein complexes in the electron transport chain. The midpoint potential describes the affinity of a site for electrons; for example the midpoint potential $E_{m,7}$ of the NAD^+/NADH pair is -320 mV (Zu *et al.*, 2003) and $E_{m,7}$ for the fumarate/succinate pair is +30 mV (Pershad *et al.*, 1999). Electrons flow energetically 'downhill' to reduce O_2 to H_2O in the final step. The $O_2/2H_2O$ pair has an $E_{m,7}$ of +820 mV (Nicholls & Ferguson, 2002). It is at the end of the respiratory chain because is has the most positive midpoint potential. Concomitant with the flow of electrons energetically 'downhill', protons are pumped 'uphill' across the mitochondrial inner membrane from the mitochondrial matrix to the intermembrane region, generating a proton motive force.

The proton motive force, Δp, comprises the membrane potential, $\Delta\Psi$, and the pH difference, ΔpH, across the mitochondrial inner membrane. This relationship is defined as the following:

$$\Delta p\ (\mathrm{mV}) = \Delta\Psi\ (\mathrm{mV}) - \frac{\mathrm{RT}}{2\mathrm{F}}\ \Delta\mathrm{pH}$$

R is the gas constant, T is temperature (°C) and F is the Faraday constant. The ΔpH is quite small; approximately 0.5 in a respiring mitochondrion. The high buffering capacity of the mitochondrial matrix and the high capacitance of the inner membrane help keep ΔpH minimal. Therefore, $\Delta\Psi$ (~200 mV in a respiring mitochondrion) accounts for most of Δp (Nicholls & Ferguson, 2002).

Δp is generated with the aid of protein complexes in the electron transport chain, found in the mitochondrial inner membrane (Figure 1.3). The electron transport chain is primarily comprised of complex I, electron-transferring flavoprotein:ubiquinone oxidoreductase, complex II, complex III and complex IV. ATP synthase couples the proton motive force to the synthesis of ATP from ADP and P_i.

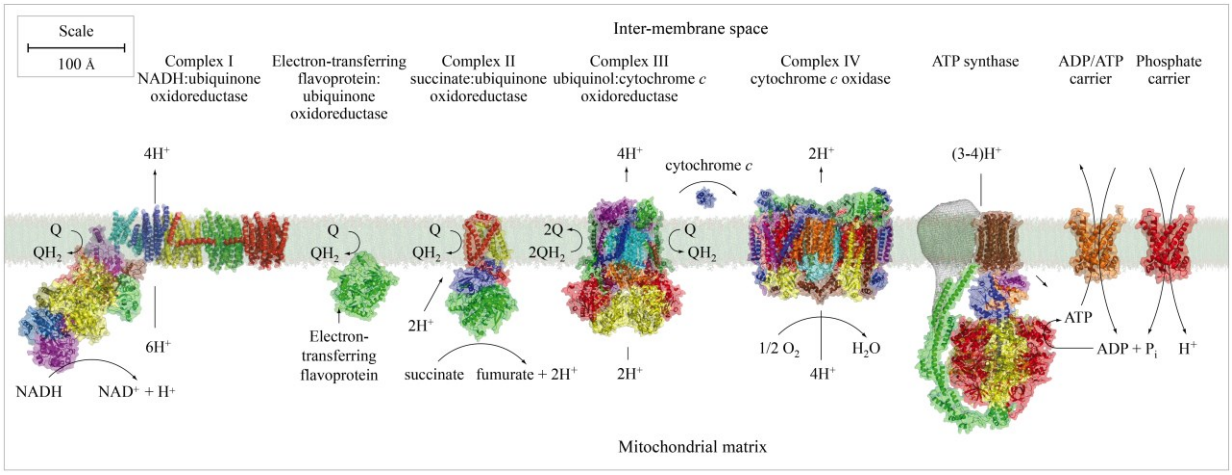

Figure 1.3 Primary protein complexes involved in mitochondrial energy transduction. For clarity, other proteins of the mitochondrial inner membrane are not shown. Images of three-dimensional structures and electron density maps were generated using PyMOL (DeLano scientific, 2002). The structure of the electron-transferring flavoprotein (PDB accession code: 2GMH) is from porcine mitochondria (Zhang *et al.*, 2006). Complex I is the low resolution structure of the enzyme from *T. thermophilus* (PDB: 3M9S) to 4.5 Å (Efremov *et al.*, 2010). Complexes III (PDB: 1BE3) and IV (PDB: 1OCC) are the high resolution structures of the bovine enzymes (Tsukihara *et al.*, 1996; Iwata *et al.*, 1998). Complex II (PDB: 1ZOY) is the porcine enzyme (Sun *et al.*, 2005). Cytochrome *c* (PDB: 1CXA) is from *Rhodobacter sphaeroides* (Axelrod *et al.*, 1994). ATP synthase (PDB: 2CLY) is a model from Professor John E. Walker's group (Dickson *et al.*, 2006). The mitochondrial ADP/ATP carrier (PDB: 1OKC) in complex with carboxy-atractyloside is also shown (Pebay-Peyroula *et al.*, 2003) as is the homologous phosphate carrier (no structure exists, although both are members of the mitochondrial carrier family). This figure was prepared by Dr Martin King.

Complex I (NADH:ubiquinone oxidoreductase) oxidises NADH, reduces ubiquinone and concomitantly translocates three to four protons across the mitochondrial inner membrane into the intermembrane region, contributing up to 40% of the Δ*p* (Wikström, 1984) (Figure 1.3). Complex I has two distinct domains; the hydrophilic domain contains a non-covalently bound flavin mononucleotide, the site of NADH oxidation, and eight or nine iron-sulphur clusters, seven of which form an electron-conducting wire linking the flavin to the site of ubiquinone reduction near the plane of the membrane (Sazanov & Hinchliffe, 2006). Electron leakage at the flavin site can lead to reactive oxygen species generation, and the initiation of redox cycling reactions that produce significant amounts of superoxide and hydrogen peroxide (Hirst *et al.*, 2008; Birrell *et al.*, 2011). The hydrophobic domain embedded in the mitochondrial inner membrane contains the subunits that are thought to be involved in proton pumping; three of the largest (NuoL, M and N in *Escherichia coli*) are homologous to Na^+/H^+ antiporters, and are each thought to pump one proton across the inner membrane (Efremov *et al.*, 2010; Efremov & Sazanov, 2011). The mechanism of by which NADH oxidation and ubiquinone reduction is coupled to proton translocation remains unclear. The recent success in the determination of the architectures of intact complex I from *Thermus thermophilus* (Efremov *et al.*, 2010) and *Yarrowia lipolytica* (Hunte *et al.*, 2010), and the atomic-resolution structure of the hydrophobic domain of *Escherichia coli* (*E. coli*) complex I (Efremov & Sazanov, 2011) will guide future research into the mechanism of complex I.

Electron-transferring flavoprotein:ubiquinone oxidoreductase (ETF-QO) transfers electrons from 11 types of flavoprotein dehyrogenase to ubiquinone to form ubiquinol (Figure 1.3). The electron-donating flavoprotein dehydrogenases catalyse β-oxidation of fatty acids, linking ETF-QO function to β-oxidation (Watmough & Frerman, 2010). ETF-QO loosely associates with the inner membrane from the matrix side and contains four iron-sulphur clusters and FAD, both of which accept electrons (Zhang *et al.*, 2006). After two electrons reduce ETF-QO, two electrons are transferred to ubiquinone. ETF-QO does not translocate protons.

Complex II (succinate:ubiquinone oxidoreductase) couples the two electron oxidation of succinate to fumarate to the two electron reduction of ubiquinone to ubiquinol (Figure 1.3). The structure of complex II has been determined for the bacterial and

mitochondrial forms, in inhibited and uninhibited states (Yankovskaya *et al.*, 2003; Sun *et al.*, 2005; Huang *et al.*, 2006). Complex II is comprised of a hydrophilic domain and a hydrophobic transmembrane domain. The hydrophilic domain contains a FAD binding protein, the site for succinate binding, and a three iron-sulphur cluster containing protein. The hydrophobic domain contains two subunits, with a haem situated between.

Complex I, ETF-QO and complex II all reduce membrane soluble ubiquinone to ubiquinol. Following reduction, ubiquinol diffuses to complex III (ubiquinol:cytochrome *c* oxidoreductase) (Figure 1.3). Complex III oxidises ubiquinol to ubiquinone, leading to the translocation of protons and the reduction of cytochrome *c* on the cytoplasmic side of the membrane. Bovine complex III is a functional dimer, with each monomer containing 11 subunits, including the Rieske protein, which contains an iron-sulphur cluster, two *b*-haems and a single cytochrome *c* haem (Iwata *et al.*, 1998). The proton motive ubiquinone cycle, or Q cycle, was formulated to describe the redox reactions of complex III (Mitchell, 1976).

Complex IV (cytochrome *c* oxidase) is the terminal enzyme of the respiratory chain (Figure 1.3), catalysing the reduction of molecular oxygen to water:

$O_2 + 4e^- + 4H^+ \rightarrow 2H_2O$

The oxygen diffuses into the mitochondrial inner membrane, the electrons are donated by cytochrome *c*, and the protons originate from the matrix side of the membrane. In addition to the four protons reacted to generate water, four protons are translocated across the membrane. The structure of the bovine complex IV is dimeric, with each monomer composed of 13 subunits (Tsukihara *et al.*, 1996; Yoshikawa *et al.*, 1998).

ATP synthase couples the proton motive force generated by the electron transport chain to the synthesis of ATP from ADP and P_i. F_1F_O ATP synthase is comprised of a soluble catalytic F_1 $\alpha_3\beta_3$ domain, a membrane motor F_O domain containing the c ring, the central stalk and the peripheral arm (Figure 1.3). During ATP synthesis, the translocation of a proton through each c subunit of the c ring drives rotation of the F_O

domain c ring. The rotation of the c ring is coupled to the rotation of the central stalk of F_1F_O ATP synthase. The asymmetric central stalk drives conformational changes in the F_1 $\alpha_3\beta_3$ domain (Abrahams *et al.*, 1994), resulting in the condensation of ADP and P_i to ATP in the β subunits (Stock *et al.*, 2000). The peripheral arm acts as a stator to stabilise the F_1 catalytic domain whilst the c ring and central stalk are rotating (Karrasch & Walker, 1999; Rubinstein *et al.*, 2003; Rees *et al.*, 2009).

Yeast have ten c subunits (Stock *et al.*, 1999; Dautant *et al.*, 2010; Symersky *et al.*, 2012) and metazoans have eight c subunits per c ring (Watt *et al.*, 2010). Interestingly, the number of c subunits in each c ring changes the catalytic efficiency of ATP synthase. Yeast require 3.3 protons, and metazoans 2.7 protons, respectively, to rotate 10 and eight membered c rings 120° to generate one ATP (Watt *et al.*, 2010). It is not understood fully how proton translocation occurs, but it is hypothesised to occur at the interface of the c subunits and the a subunit at a location equivalent to the middle of the membrane (Baker *et al.*, 2012).

Combined, the metazoan ATP synthase, the ADP/ATP carrier and the phosphate carrier catalyse the electroneutral transfer of 3.7 protons across the mitochondrial inner membrane (Figure 1.4). 2.7 protons are consumed when ATP synthase synthesises ATP, and one during the transport of P_i into mitochondria by the phosphate carrier. Consequently, 3.7 protons are required for every ATP synthesised.

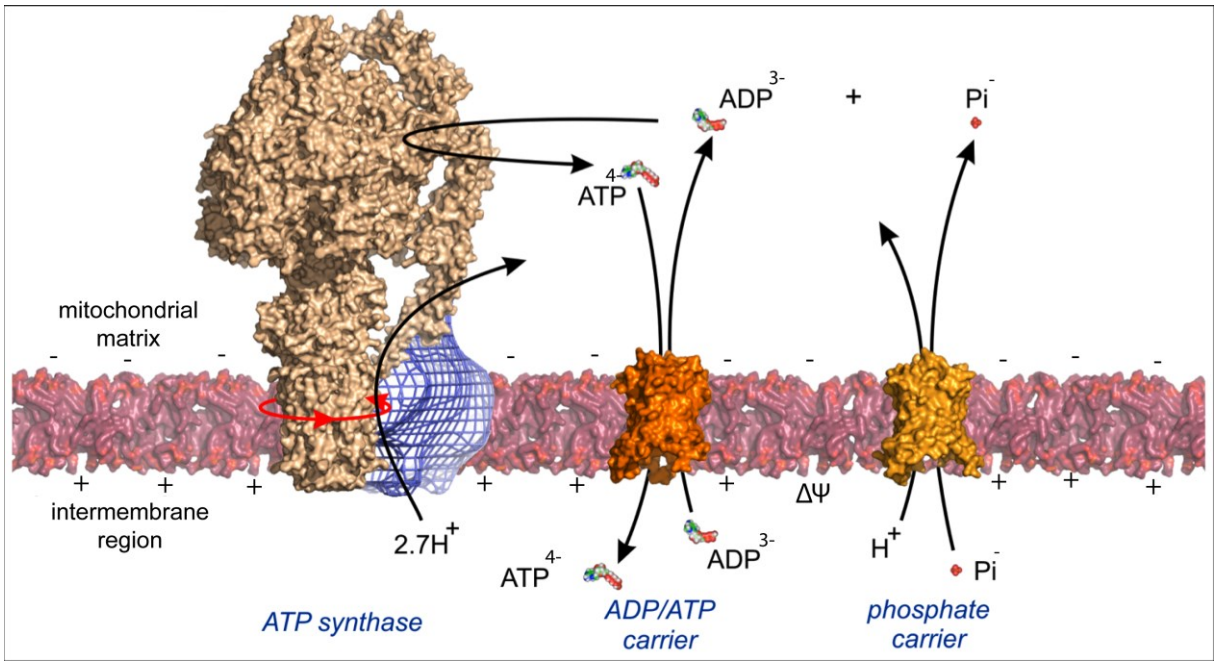

Figure 1.4 Stoichiometry of charge transfer across the mitochondrial inner membrane. Metazoan ATP synthase, the ADP/ATP carrier and the phosphate carrier synthesise ATP^{4-} in the mitochondrial matrix or transfer charged ATP^{4-}, ADP^{3-}, P_i^- and H^+ across the mitochondrial inner membrane. The mitochondrial inner membrane is coloured dark red. + and - denote the membrane potential across the membrane. This figure was generated by Dr Edmund R.S. Kunji and subsequently modified.

1.2 Mitochondrial carrier family

1.2.1 Initial discoveries and essential concepts

Swelling experiments of isolated mitochondria (Chappell & Greville, 1958; Chappell, 1968), and ADP and ATP, but not AMP uptake into isolated mitochondria (Pfaff *et al.*, 1965) provided some of the earliest evidence for protein-mediated transport of charged compounds across the mitochondrial inner membrane. These initial discoveries provided support for one of the four tenets of the chemiosmotic theory, that proton-linked transporters are required for metabolite transport across an insulating membrane (Mitchell, 1961; Mitchell, 1979).

Following initial discoveries in the 1960s, improvements in protein purification and sequencing were instrumental in the discovery of members of the mitochondrial carrier family. The first carrier to be identified was the bovine ADP/ATP carrier

(Riccio, Aquila & Klingenberg, 1975a; Riccio, Aquila & Klingenberg, 1975b; Aquila *et al.*, 1982). Not long after, the uncoupling protein (Aquila *et al.*, 1985), the phosphate carrier (Runswick *et al.*, 1987) and the 2-oxoglutarate/malate carrier (Runswick *et al.*, 1990) were identified. The role of mitochondrial carriers in providing connections between cytosolic and mitochondrial pathway is shown in Figure 1.1.

Despite the diversity of substrates transported, it was noted that a key feature of the mitochondrial carrier family of proteins is the presence of three homologous sequence repeats of ~100 amino acids (Saraste & Walker, 1982; Aquila *et al.*, 1987) (Figure 1.5), and is likely the by-product of gene triplication and divergent evolution from a single gene (Saraste & Walker, 1982). Mitochondrial carriers are about 300 amino acids in length, contain six transmembrane α-helices and a PX[DE]XX[KR] signature motif on the matrix side of each of the three odd-numbered α-helices. Yeast regain-of-function mutagenesis data and structural data have confirmed that the matrix signature motif is essential for the function of the ADP/ATP carrier (Nelson *et al.*, 1998; Pebay-Peyroula *et al.*, 2003). In addition, a second signature motif, [FY][DE]XX[RK], was identified on the cytoplasmic side of each of three even-numbered α-helices (Figure 1.15) (Robinson *et al.*, 2008).

Most eukaryotic mitochondria contain 35-55 types of mitochondrial carriers, which are encoded by the nuclear genome (Kunji, 2004). Alternatively, mitochondrial carrier family members may be expressed in mitosomes (Tsaousis *et al.*, 2008) and hyrogenosomes (van der Giezen *et al.*, 2002), which are mitochondrial remnants, but also in peroxisomes (L. Palmieri *et al.*, 2001), amyloplasts (Pozueta-Romero *et al.*, 1991) and chloroplasts (Neuhaus & Wagner, 2000).

Mitochondrial carriers can function as uniporters, proton couplers or strict exchangers by using substrate concentration gradients to drive transport. In addition to using substrate gradients, some mitochondrial carriers also utilise $\Delta\Psi$ or the proton electrochemical gradient.

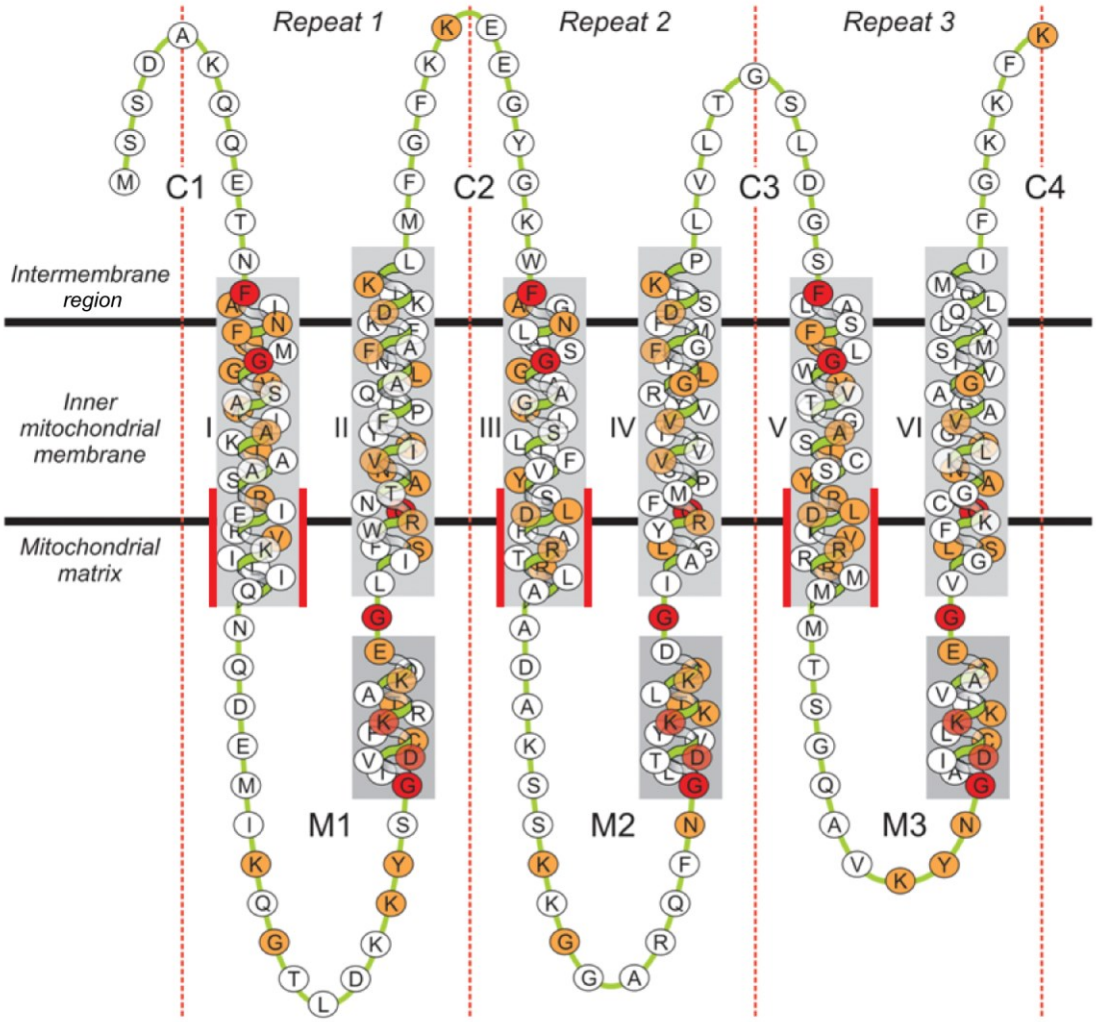

Figure 1.5 Three ~100 amino acid homologous sequence repeats of *S. cerevisiae* Aac3p. The secondary structure and amino acid sequence of yeast Aac3p are depicted. Individual amino acids are denoted by the one letter amino acid code, and the sequence of amino acids is connected by a single polypeptide chain, shown in green. The arrangement of the polypeptide chain is shown relative to the mitochondrial inner membrane, with grey shaded regions denoting sections of sequence embedded in the mitochondrial inner membrane. The six transmembrane α-helices are labelled I, II, III, IV, V and VI. The N- and C-termini and the cytoplasmic loops are labelled C1, C2, C3 and C4. The mitochondrial matrix loops are M1, M2 and M3, including partial matrix helices (grey). The red dashed line indicates the boundary for each of the three ~100 amino acid homologous sequences repeats. Residues conserved for 2 of the 3 repeats are coloured orange, and residues conserved in all 3 repeats are coloured red. The red bars indicate the regions containing the matrix signature motif. This figure was created by Dr Edmund R.S. Kunji.

1.2.2 Mitochondrial carriers as uniporters

Many mitochondrial carriers function as strict exchangers, but some have partial or significant uniport activity, defined as net importers into mitochondria. During uniport, substrate pools on either side of the membrane are equilibrated. Uniport activity can be predicted based on symmetry analysis (Robinson *et al.*, 2008) by comparing the cytoplasmic and matrix signature motifs, which are predicted or have been proven to form salt bridge networks, respectively. If the cytoplasmic salt bridge is incomplete and weak, and the matrix network is conserved and strong, then following substrate transfer from the cytoplasmic to the matrix side, the cytoplasmic network spontaneously breaks and the carrier converts from the matrix to the cytoplasmic state without a transport step.

An example of a uniporter is the ornithine carrier. The ornithine carrier is an amino acid transporter that electroneutrally exchanges citrulline and ornithine, products formed at the start and the end of the urea cycle (Indiveri *et al.*, 1997). The ornithine carrier has a weak cytoplasmic network, so some net import of ornithine is expected. In confirmation of ornithine carrier uniport, ornithine uptake has been observed in the absence of citrulline in rat liver mitochondria proteoliposomes (Indiveri *et al.*, 1999).

1.2.3 Mitochondrial carriers as proton couplers

Proton couplers or proton-substrate symporters, are defined as transporters that translocate a substrate and a proton concomitantly and transport substrates against the concentration gradient by coupling substrate transport to Δp. Proton couplers can be identified by the presence of acidic residues, such as aspartate or glutamate, located adjacent to basic residues in the central substrate binding site (Kunji & Robinson, 2010). The acidic residues form an ionic interaction with a proton and the alkaline residues interact with a substrate, which often contains a phosphate or carboxylate group.

The phosphate carrier is an inorganic ion transporter that transports P_i and H^+ into the mitochondrion thereby consuming Δp (Figure 1.4). At pH 7.0, the stoichiometry

of H^+ to P_i transported is 1.5, as predicted since an equimolar ratio of HPO_4^{2-} to $H_2PO_4^-$ exists (McGivan & Klingenberg, 1971). The phosphate carrier has a cluster of positively charged residues in the substrate binding site, with negatively charged residues located nearby to facilitate proton coupling (Kunji & Robinson, 2010).

1.2.4 Mitochondrial carriers as strict exchangers

Most mitochondrial carriers function as strict exchangers that exchange one substrate on one side of the mitochondrial membrane, for one different, but structurally related substrate on the opposite side of the membrane. It might be possible to predict strict exchange activity by estimating the interaction energy of the cytoplasmic and matrix salt bridge network (Robinson *et al.*, 2008). If the cytoplasmic and the matrix salt bridge networks have three ionic interactions, then this will form a high energy barrier that prevents the conversion to the other state in the absence of substrate. Only when a substrate binds will the conversion to the other state take place.

A good example of a strict exchanger is the carnitine/acylcarnitine carrier, which catalyses the exchange of cytosolic acylcarnitine for matrix carnitine. Once imported into the mitochondrial matrix, acylcarnitine is subsequently oxidised during β-oxidation of fatty acids. As expected, the carnitine/acylcarnitine carrier has strong cytoplasmic and matrix networks. Less than 0.5% of carnitine/acylcarnitine exchange is attributed to uniport as determined by kinetic assays, providing experimental confirmation that the carrier catalyses strict exchange (Indiveri *et al.*, 1994).

The quintessential strict exchanger, the ADP/ATP carrier, is discussed in detail in the next section.

1.3 The ADP/ATP carrier

1.3.1 Initial discoveries and essential concepts

In the late 1950s, it was proposed that nucleotides were exchanged between cytosolic and matrix compartments of isolated mitochondria, but the mechanism for this observation was unknown (Pressman, 1958). Further experiments on isolated mitochondria with an inhibitor of oxidative phosphorylation, atractyloside, provided evidence for a means of transport for adenine nucleotides across the mitochondrial inner membrane (Bruni & Luciani, 1962; Vignais *et al.*, 1962; Bruni *et al.*, 1964; Chappell & Crofts, 1965).

The ADP/ATP carrier protein catalyses equimolar exchange of cytosolic ADP for matrix ATP across the mitochondrial inner membrane. Substrate concentration gradients and the membrane potential, $\Delta\Psi$, drive exchange of ADP and ATP. In support of the strict equimolar exchange mechanism, the ADP/ATP carrier contains complete cytoplasmic and matrix salt bridge networks (Robinson *et al.*, 2008).

The ADP/ATP carrier (AAC) is one of most extensively studied mitochondrial carriers. The high abundance of AAC enables high protein yields to be isolated from native tissues such as bovine heart (Riccio, Aquila & Klingenberg, 1975a), and the existence of two strongly binding inhibitors makes it more amenable to structural and functional studies than other members of the mitochondrial carrier family which are present in lower abundance and lack specific, strongly binding inhibitors.

The human ADP/ATP carrier protein (hANT) is expressed as four isoforms encoded on separate genes. AAC1 is expressed in skeletal and heart muscle, AAC2 is found in proliferating cells, AAC3 is ubiquitous and AAC4 is expressed in testis, brain and liver (Fontanesi *et al.*, 2004; Dolce *et al.*, 2005). In *Saccharomyces cerevisiae*, isoforms Aac1p and Aac3p are not required for growth of yeast on non-fermentable carbon sources, but Aac2p is necessary for yeast survival on non-fermentable carbon sources (Drgon *et al.*, 1992). Yeast Aac2p is an orthologue of human and

bovine AAC1 because all are highly abundant and ubiquitously expressed. In the following chapters, results of studies of *S. cerevisiae* Aac2p will be presented.

1.3.2 Amino acid sequence

The ADP/ATP carrier was the first member of the mitochondrial carrier family to be sequenced (Aquila *et al.*, 1982). Following sequencing, it was noticed that the ADP/ATP carrier contained three ~100 amino acid sequence repeats (Figure 1.5) (Saraste & Walker, 1982). Like other members of the mitochondrial carrier family, the ADP/ATP carrier contains six transmembrane α-helices and its N- and C-termini face the intermembrane region (Pebay-Peyroula *et al.*, 2003). The ADP/ATP carrier contains an RRRMMM sequence motif. The first arginine of this motif on α-helix H5 corresponds to the arginine of the matrix signature motif, PX[DE]XX[KR]. The second arginine is part of the substrate binding site.

1.3.3 Substrates and inhibitors

The ADP/ATP carrier transports ADP and ATP, and is fully reversible. In the absence of a chemical substrate gradient, the ADP/ATP carrier will exchange ADP for ADP, or ATP for ATP. The ADP/ATP carrier only transports ADP and ATP. AMP (Brierley & O'Brien, 1965) ADP or ATP chelated to Mg^{2+}, Mn^{2+} or Ca^{2+} (Brandolin *et al.*, 1980), CDP, GDP and UDP (Pfaff *et al.*, 1965; Duee & Vignais, 1969) are not transported. There are various reports of the K_M of ADP or ATP, but it is approximately 10 μM (Brandolin *et al.*, 1980).

Two classes of specific transport inhibitors of the ADP/ATP carrier have been identified. The first class, the atractylosides, are isolated from the Mediterranean thistle *Atractylis gummifera* (Bruni & Luciani, 1962; Bruni *et al.*, 1964). Carboxy-atractyloside (CATR) contains two carboxylate groups on a diterpenoid ring, an isovaleric group, and a glucosidic group that contains two sulphates (Figure 1.6 A). Atractyloside (ATR) is similar in structure to CATR, but it lacks the second carboxylate group (Vignais *et al.*, 1971; Vignais *et al.*, 1973). The dissociation constant or K_I is in the low nanomolar range for both ATR and CATR. ATR and

CATR only inhibit the ADP/ATP carrier; they do not inhibit any other mitochondrial carrier proteins (Klingenberg, 2008).

The second class of inhibitor includes bongkrekic acid and isobongkrekic acid. Bongkrekic acid (BKA), produced by the bacterium *Pseudomonas cocovenanans*, was first shown to inhibit the ADP/ATP carrier by demonstration of its inhibition of adenine nucleotide uptake in rat liver mitochondria (Henderson & Lardy, 1970). Isobongkrekic acid was shown to inhibit the ADP/ATP carrier not long after (Lauquin & Vignais, 1976). BKA is a lipid mimic that contains three carboxylate groups (Figure 1.6 B), which, when protonated, allows it to cross membranes (Weidemann *et al.*, 1970). The deprotonated form binds to the ADP/ATP carrier with a K_I in the low nanomolar range (Klingenberg *et al.*, 1970). BKA might bind at or in the vicinity of the substrate binding site from the matrix side of the carrier, but this has not been confirmed structurally. BKA inhibition is affected by variables such as temperature, pH, timing of addition, amount of addition and presence or absence of adenine nucleotides (Henderson & Lardy, 1970; Henderson *et al.*, 1970; Kemp *et al.*, 1970; Klingenberg *et al.*, 1970; Erdelt *et al.*, 1972)

Antibody evidence has shown that CATR and BKA lock the ADP/ATP carrier in two distinct conformational states, termed the cytoplasmic-state (c-state), and the matrix-state (m-state), respectively (Buchanan *et al.*, 1976), and are considered to represent aborted conformational states of the transport cycle. CATR binds to the ADP/ATP carrier from the cytoplasmic side of the membrane and BKA binds from the matrix side. The cavity of the ADP/ATP carrier is open to the cytoplasmic side in the inhibited c-state (Pebay-Peyroula *et al.*, 2003), and the cavity is believed to be open to the matrix side in the m-state.

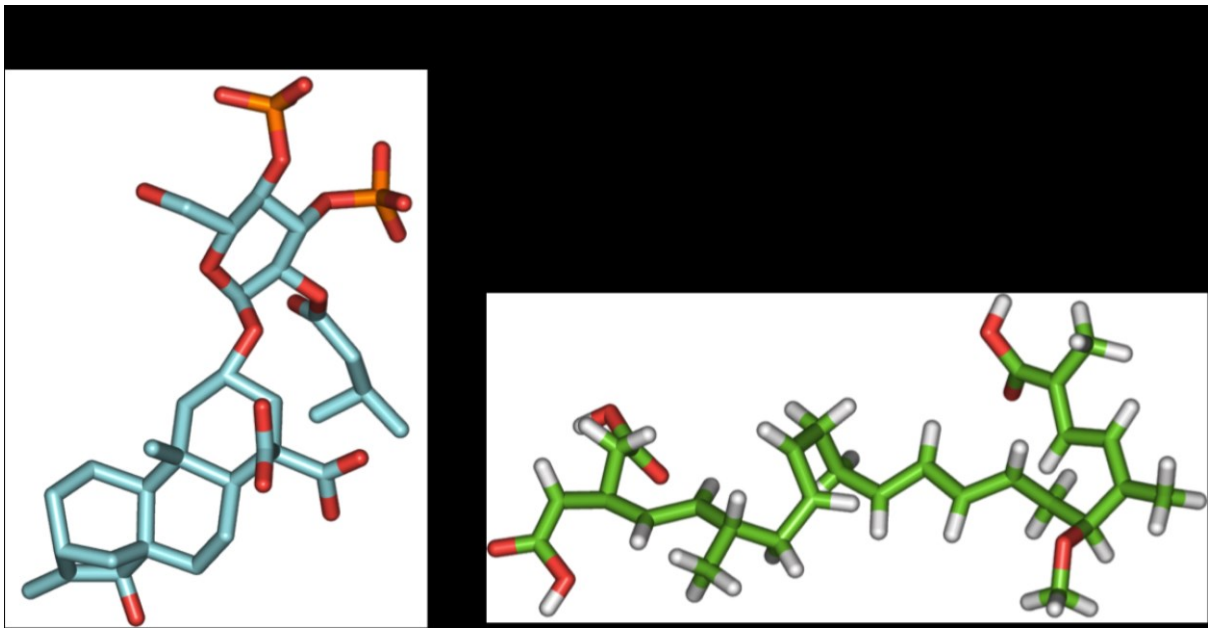

Figure 1.6 Three-dimensional structural representations of carboxy-atractyloside and bongkrekic acid. **(A)** CATR and **(B)** BKA are shown. Carbon is blue or green, respectively, for CATR and BKA. Oxygen is red and sulphur is orange. Hydrogens are not shown for CATR, but they are shown in white for BKA.

1.4 Structural features of the ADP/ATP carrier

1.4.1 Inhibited structures

Two inhibited structures of the ADP/ATP carrier are available; one projection structure with ATR bound and one three-dimensional structure with CATR bound. A two-dimensional electron microscopy projection structure of yeast Aac3p with ATR bound was solved to 5 Å resolution (Figure 1.7) (Kunji & Harding, 2003). The structure of Aac3p in the membrane confirmed that the ADP/ATP carrier is three-fold pseudo-symmetric, consisting of six transmembrane α-helices in agreement with the three homologous sequence repeats and topology model. The structure shows the protein is monomeric and has a central translocation pathway, suggesting that the carrier may function as a monomer, too (see below).

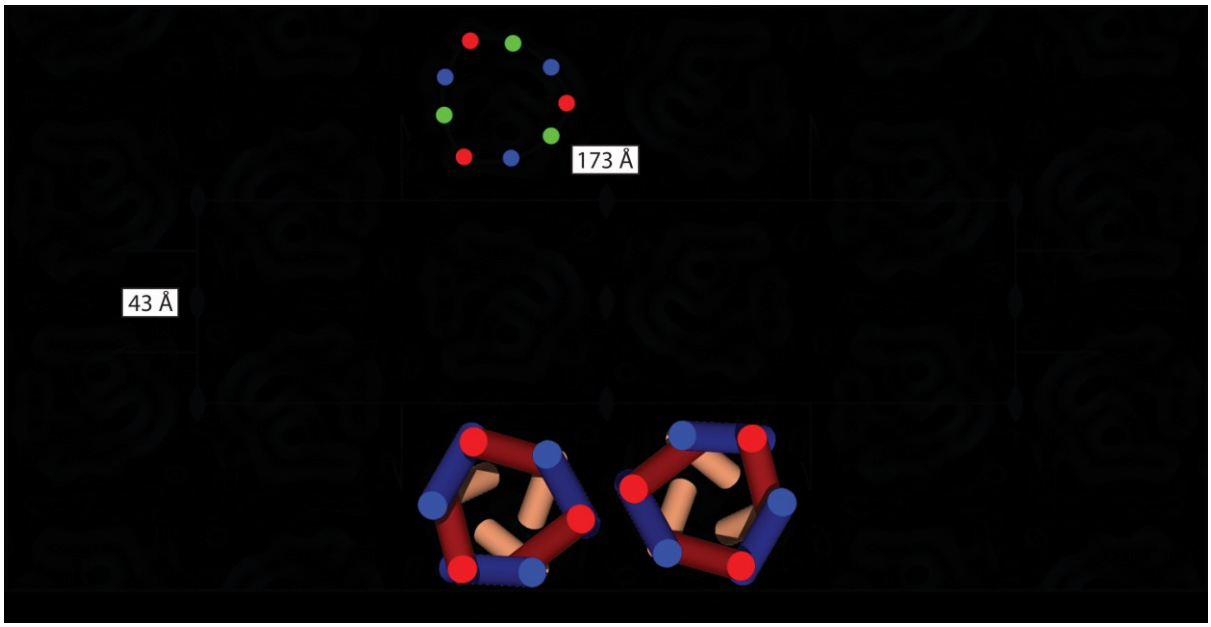

Figure 1.7 Projection electron density map of atractyloside inhibited yeast Aac3p. The two-dimensional electron microscopy density map of yeast Aac3p (Kunji & Harding, 2003). The resolution is 5 Å. The unit cell is 173 Å (horizontal) by 43 Å (vertical). Solid lines show density above the average and dotted lines show negative contours. Nine density peaks are indicated by red, blue and green dots. The transmembrane α-helices are coloured red and blue, and the C-terminal parts of the odd-numbered helices are tan. This image is from Dr Edmund R.S. Kunji.

The three-dimensional X-ray crystallography structure of the bovine ADP/ATP carrier inhibited by CATR has been solved to 2.2 Å (Figure 1.8) (Pebay-Peyroula *et al.*, 2003). The structure showed that the carrier is arranged as a bundle of six transmembrane α-helices, with three matrix α-helices lying parallel to the plane of the membrane. CATR binds in a central, water-filled cavity along α-helix H2 (Figure 1.8 A and B, Figure 1.9). The prolines of the PX[DE]XX[RK] motif are present at kinks in the odd-numbered α-helices and acidic and basic residues form a salt bridge network on the matrix side of the membrane in the CATR bound state (Figure 1.8 C and D). Structures of the BKA-inhibited or substrate bound ADP/ATP carrier have yet to be determined.

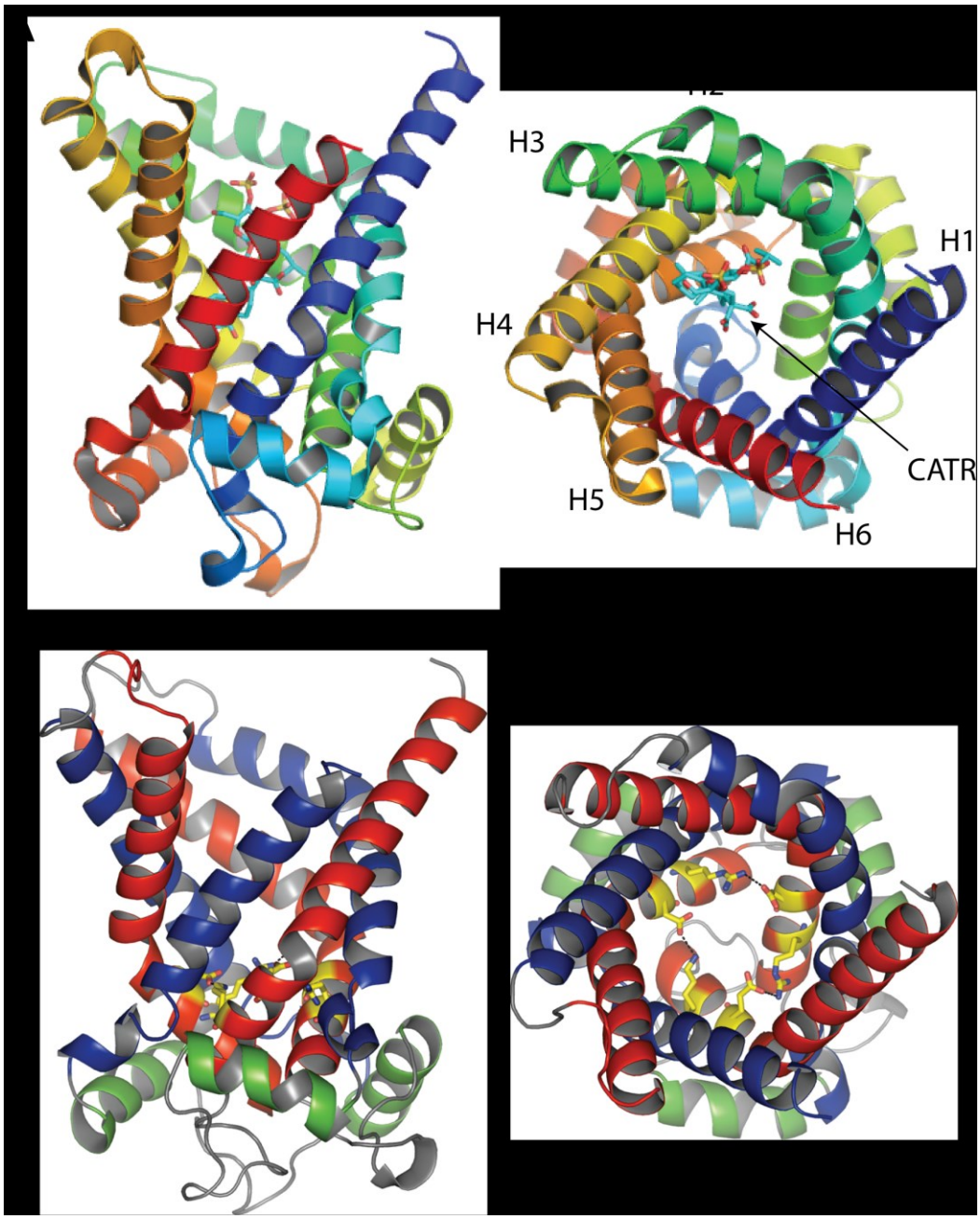

Figure 1.8 Carboxy-atractyloside inhibited structure of the bovine ADP/ATP carrier. The three-dimensional X-ray crystallography structure of bovine AAC1 (PDB code 1OKC) (Pebay-Peyroula *et al.*, 2003). **(A)** The lateral view and the **(B)** cytoplasmic view of the cavity showing the location of CATR binding are depicted. α-helix 1 (H1) is dark blue, α-helix (H2) is teal, α-helix (H3) is dark green, α-helix (H4) is yellow, α-helix (H5) is orange and α-helix (H6) is red. CATR is labelled. **(C)** The lateral view and the **(D)** cytoplasmic view of the cavity highlighting the matrix salt bridge network and the three-fold pseudo-symmetry of the CATR-inhibited bovine AAC1. The odd α-helices are red and the even α-helices are blue. The matrix α-helices are green. The matrix salt bridge network residues are coloured yellow. This figure was prepared by Dr Alex Hellawell.

1.4.2 Carboxy-atractyloside binding site

The structure shows clearly that CATR binds in the central, water-filled cavity along α-helix H2 (Figure 1.9) (Pebay-Peyroula *et al.*, 2003). Additionally, CATR associates with residues on all α-helices excluding α-helix H6 (Table 1.1). The CATR diterpenoid ring docks the inhibitor into the binding site. The glucosidic, sulphate and isovaleric groups of CATR prevent the ADP/ATP carrier from entering an alternate conformational state.

Table 1.1 Residues involved in CATR binding.

bovine residue	yeast residue	CATR binding location
R79	R96	α-helix H2, H-bonds to diterpenoid ring carboxyl
N87	N104	α-helix H2, H-bonds to sulphate
K91	K108	α-helix H2, H-bonds to sulphate
L127	L142	α-helix H3, hydrophobic contact
V130	V145	α-helix H3, hydrophobic contact
I183	I200	α-helix H4, hydrophobic contact
R187	R204	α-helix H4, H-bonds to sulphate
D231	D249	α-helix H5, H-bonds to diterpenoid ring hydroxyl
R234	R252	α-helix H5, H-bonds to diterpenoid ring hydroxyl
R279	R294	α-helix H6, H-bonds to diterpenoid ring carboxyl via a water

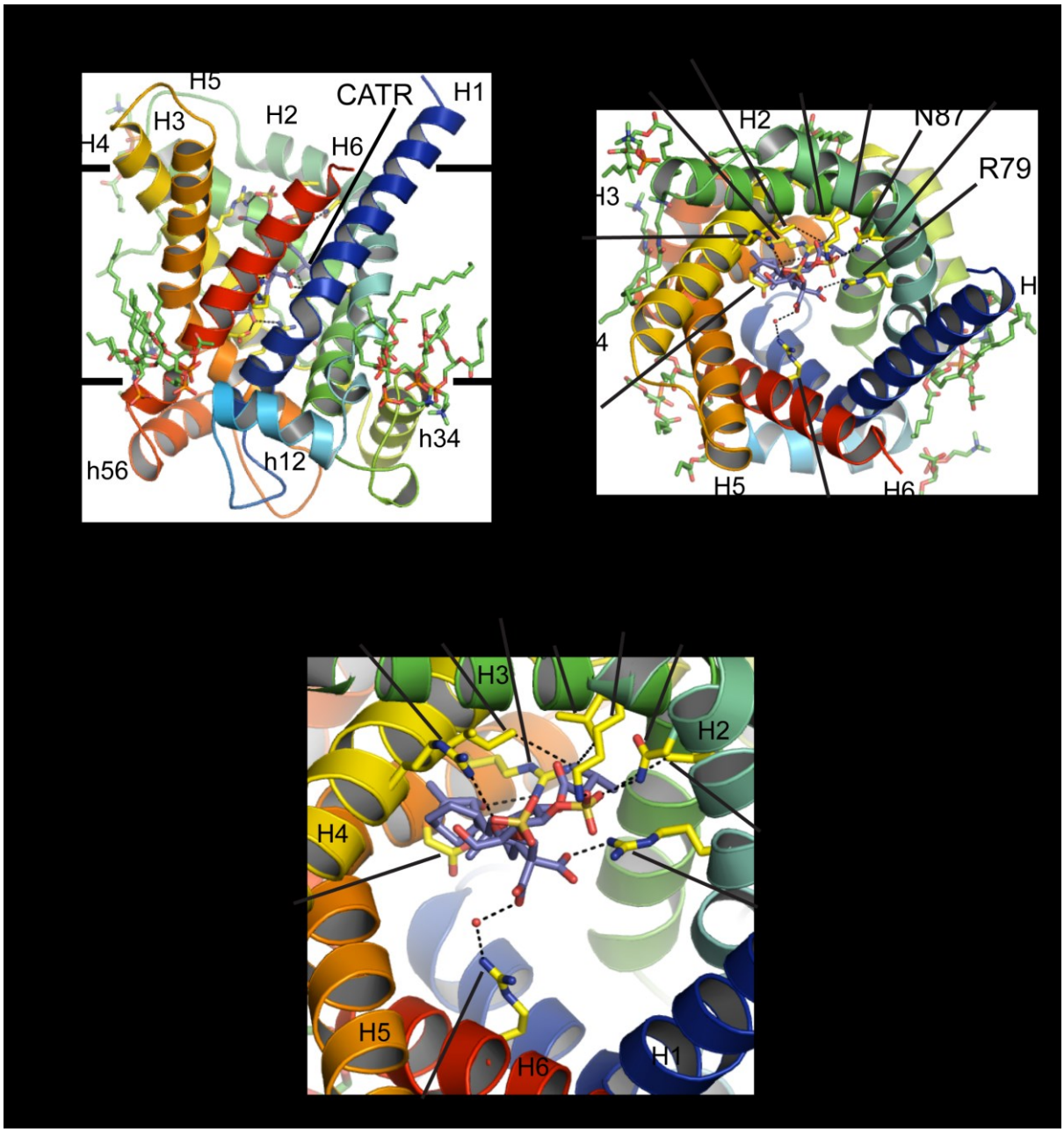

Figure 1.9 Carboxy-atractyloside binding site. The three-dimensional X-ray crystallography structure of bovine AAC1 (PDB code 1OKC) (Pebay-Peyroula *et al.*, 2003) with CATR bound. **(A)** The lateral view and the **(B)** cytoplasmic view of the cavity showing the location of CATR binding. **(C)** Close-up of the CATR binding site shown in (B). α-helix 1 (H1) is dark blue, α-helix (H2) is teal, α-helix (H3) is dark green, α-helix (H4) is yellow, α-helix (H5) is orange and α-helix (H6) is red. CATR is labelled in (A). The residues (yellow sticks) that interact with CATR (blue sticks) are labelled in (B) and (C).

1.5 The ADP/ATP carrier functions as a monomer

For the past 35 years, the ADP/ATP carrier was believed to function as a dimer in the mitochondrial inner membrane (reviewed in (Kunji & Crichton, 2010)). The ADP/ATP carrier was first suggested to function as a dimer when purified ADP/ATP carrier protein was identified as having a 1:2 stoichiometry of CATR to protein (Riccio, Aquila & Klingenberg, 1975a). However, the structure of the ADP/ATP carrier in a membrane environment (Kunji & Harding, 2003) (Figure 1.7) clearly demonstrated that the ADP/ATP carrier is monomeric. There is no interface for dimerization, and the central cavity is filled with basic residues for binding ADP indicating that the ADP/ATP carrier might function as a monomer. Subsequent studies showed that the ADP/ATP carrier is also monomeric in detergents (Bamber *et al.*, 2006; Bamber, Slotboom, *et al.*, 2007b; Kunji *et al.*, 2008) and functions as a monomer in mitochondrial membranes (Bamber, Harding, *et al.*, 2007a). Furthermore, all of the main structural and mechanistic features are three-fold symmetrical, indicating that the transport mechanism may also function in a symmetrical manner. No conserved asymmetric features are present on the surface that could plausibly constitute an interaction surface (Kunji & Crichton, 2010). It is likely that the previous claims of a dimeric structure were based on technical errors and misinterpretations.

1.6 Substrate binding site of the ADP/ATP carrier

1.6.1 Sequence analysis

Distance and chemical restraints were applied to comparative models of the ADP/ATP carrier to identify the location of the substrate binding site in all keto and amino acid carriers (Kunji & Robinson, 2006; Robinson & Kunji, 2006). Similarly, the identity of substrates and nucleotide co-factors for mitochondrial carrier family members of unknown substrate specificity could be predicted. The substrate binding site contains three major contact points located on the even α-helices in a location corresponding approximately to the middle of the membrane (Figure 1.10) (Robinson *et al.*, 2008). In yeast Aac2p, contact point I R96 and contact point III R294 interact with the phosphates of ADP, whereas contact point II, comprising G199, I200 and

Y203, forms a pocket for the adenine ring. The ADP binding site overlaps with the CATR binding site (Figure 1.11) (Section 1.4.2). The substrate binding site was also identified by analysing the sequences of three homologous repeats using symmetry analysis (Robinson *et al.*, 2008). It was proposed that substrates are asymmetrical in chemical and biophysical properties and thus the symmetry-related residues involved in substrate binding must also share this asymmetry. A cluster of asymmetrical residues was found in a similar position as the binding site identified by chemical and distance constraints in all carriers investigated.

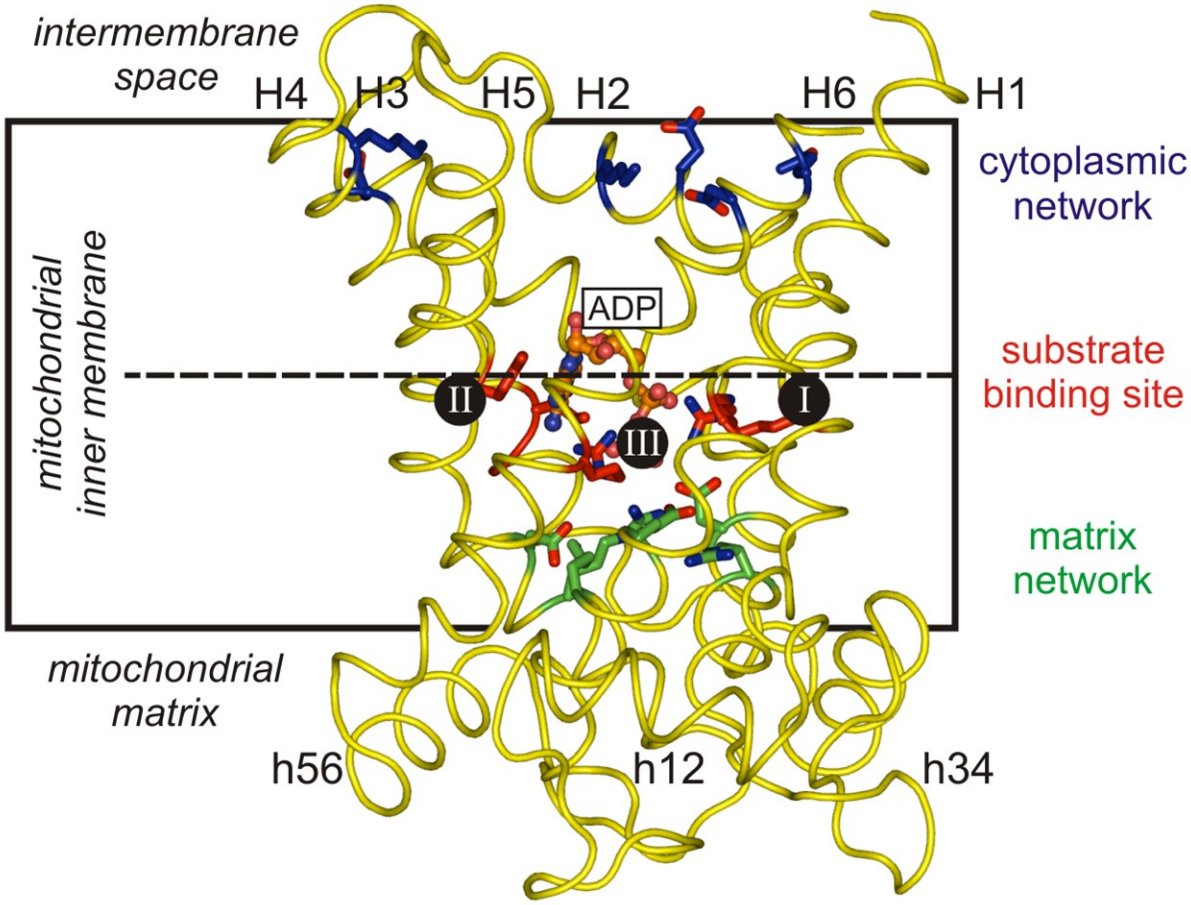

Figure 1.10 Substrate binding site and salt bridge networks of the ADP/ATP carrier. The yeast Aac2p model is based on the CATR-inhibited bovine AAC1 structure (PDB code 1OKC) (Pebay-Peyroula *et al.*, 2003). The ADP/ATP carrier is yellow. α-helices H1 to H6 and matrix α-helices h12, h34 and h56 are labelled. Residues of the cytoplasmic salt bridge network are blue. Residues of the matrix salt bridge network are green. The residues of central substrate binding site are red. ADP (orange), shown as a ball and stick model in the central binding site, is shown bound at contact points I, II and III. This image is from (Robinson *et al.*, 2008).

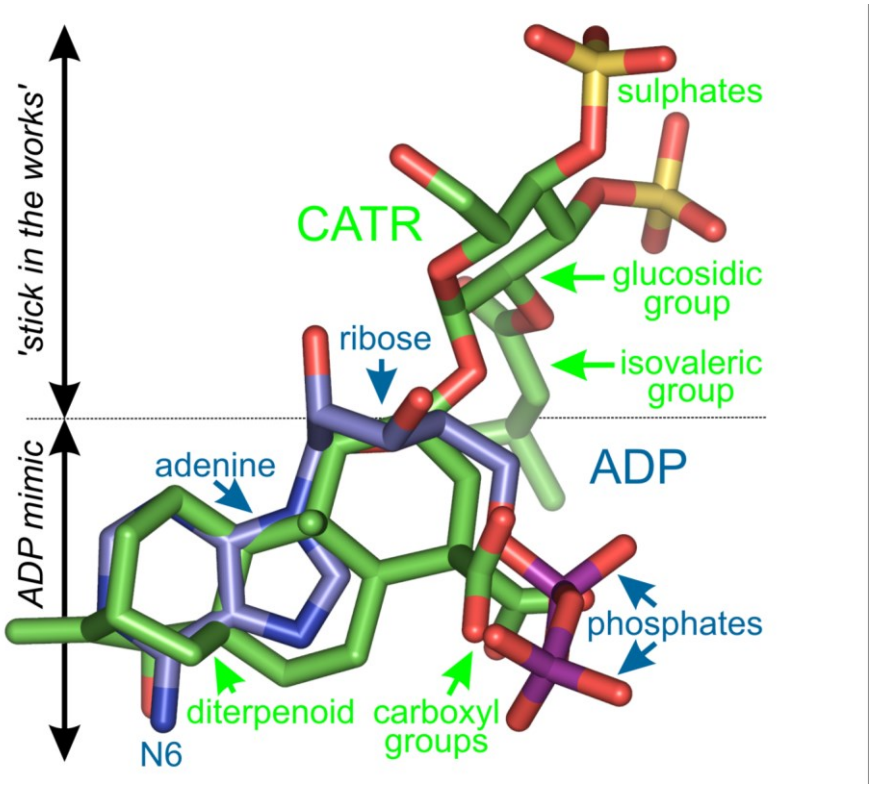

Figure 1.11 Superposition of ADP and CATR in the substrate binding site. Carbon is blue for ADP and green for CATR. Oxygen, phosphorous and sulphur are respectively red, purple and yellow. This figure is from (Kunji & Robinson, 2006).

1.6.2 Molecular dynamics simulations

In addition to sequence analysis, molecular dynamics of substrate binding to the bovine ADP/ATP carrier has also been investigated. Two studies of ADP binding from the cytoplasmic side of the membrane were carried out using the CATR-bound bovine ADP/ATP carrier model with CATR removed; in both cases, a monomeric ADP/ATP carrier was inserted into a membrane (Dehez *et al.*, 2008; Wang & Tajkhorshid, 2008). The water molecules from the crystal structure were either present (Wang & Tajkhorshid, 2008) or were removed and replaced with a dynamic water modelling system (Dehez *et al.*, 2008). The results suggest that ADP binds to the central binding site in both molecular dynamics situations, supporting the previously identified location (Kunji & Robinson, 2006; Robinson & Kunji, 2006), except that the β-phosphate of ADP binds to the second R (R253 in yeast) of the RRRMMM motif, which may help to break the matrix salt bridge network (Dehez *et al.*, 2008; Wang & Tajkhorshid, 2008). Both the binding site contact points and the

RRRMMM motif are highly conserved among ADP/ATP carriers (Robinson *et al.*, 2008).

1.7 Transport mechanism of mitochondrial carriers

1.7.1 Inhibitor studies

The transport mechanism of mitochondrial carriers was initially proposed by comparing the BKA- and CATR-inhibited states of the ADP/ATP carrier. Based on numerous inhibitor studies, a single-binding centre gate pore mechanism (Klingenberg, 1989; Klingenberg, 2005), which is essentially an alternating access mechanism (Jardetzky, 1966) was proposed. The sodium transporter, which pumps sodium ions against its chemical gradient, provides a good example of an alternating access mechanism (Figure 1.12). The cavity of the sodium pump is initially open to one side of the membrane; when sodium binds to the central binding site (Figure 1.12), the pump is phosphorylated, causing a conformational change allowing the transport of sodium to the opposite side of the membrane (Figure 1.12). The ADP/ATP carrier works similarly, except that it is the proton motive force and substrate gradients which drive transport, not phosphorylation. Additionally, cytoplasmic and matrix gates prevent uncontrolled leakage of ions across the tight mitochondrial inner membrane. This is the single-binding centre gated pore mechanism (Klingenberg, 1989; Klingenberg, 2005).

In support of the alternating access mechanism, it was shown that BKA and CATR binding are mutually exclusive, and that ADP or ATP is removed by inhibitor binding. In the first demonstration that BKA and CATR bind to distinct binding sites, the absorbance of mitochondria was found to increase upon BKA binding, indicating that conformational changes of the ADP/ATP carrier had occurred, but this absorbance increase was inhibited by ATR binding (Scherer & Klingenberg, 1974). In a separate study, [^{3}H]-BKA was found bound to rat liver mitochondria on the inside of the membrane (Lauquin & Vignais, 1976), demonstrating that BKA binds to the matrix side of the carrier. Additionally, [^{3}H]-BKA eqimolarly displaces [^{35}S]-ATR in mitochondria in an ADP concentration-dependent manner suggesting that the

ADP/ATP carrier undergoes an m- to c-state transition (Klingenberg *et al.*, 1983). Some of the strongest inhibitor evidence for the m-state and the c-state was that specific antibodies were produced against BKA- and CATR-inhibited bovine ADP/ATP carrier proteins (Buchanan *et al.*, 1976). Collectively, these inhibitor studies supported the alternating access mechanism.

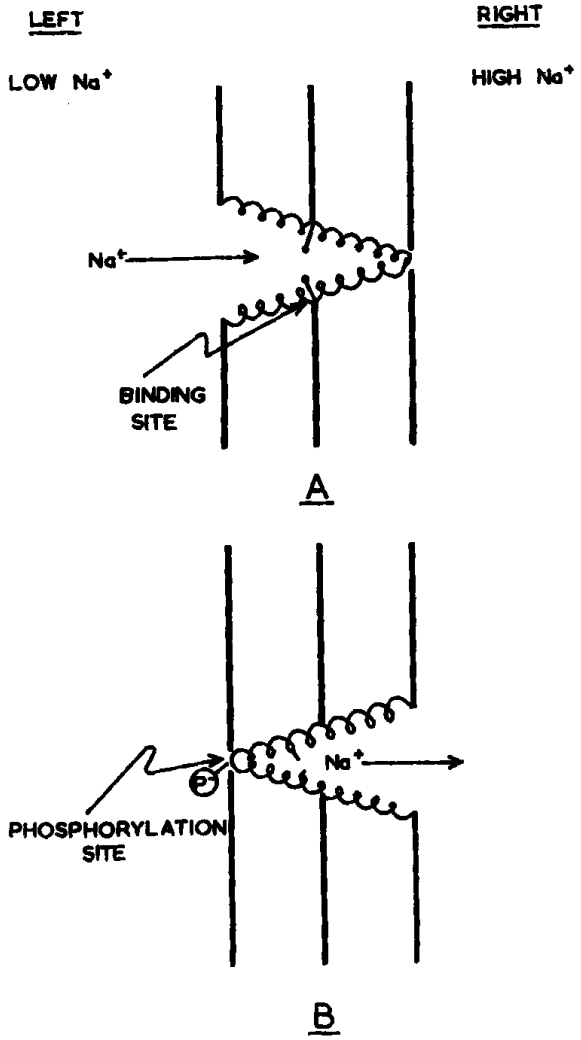

Figure 1.12 Alternating access transport mechanism of a sodium pump. **(A)** The unphosphorylated sodium pump changes conformation upon **(B)** phosphorylation of the pump. In the case of the sodium pump, phosphorylation changes the affinity of the pump for sodium. A sectional view of the pump (shown as helices) is depicted in the membrane (solid lines, middle line corresponds to middle of membrane). The labelled binding site corresponds to the middle of the membrane. The movement of sodium is shown by an arrow. The phosphorylation site is labelled. This figure is from (Jardetzky, 1966).

1.7.2 Kinetic studies

Whereas inhibitor studies provide strong support for the alternating access mechanism, kinetic studies provide more contentious evidence for the transport mechanism of mitochondrial carriers. The alternating access mechanism assumes that there is a single substrate binding site. In contrast, a sequential or simultaneous mechanism assumes dual substrate binding sites (Figure 1.13). The alternating access and sequential mechanisms were originally conceived with the assumption that mitochondrial carriers are dimers (Figure 1.13 B and D), but both mechanisms are fully compatible with mitochondrial carriers functioning as monomers (Figure 1.13 A and C). In the alternating access mechanism, one substrate binds and is transported at a time. In the sequential or simultaneous mechanism, two substrates bind to the carrier to form a ternary complex. The substrates bind one after or another (sequential), or at the same time (simultaneous), before transport occurs.

Kinetic studies of the ADP/ATP carrier (Duyckaerts *et al.*, 1980; Chan & Barbour, 1983) and the aspartate/glutamate carrier (Sluse *et al.*, 1991) in intact mitochondria provide support for the sequential or simultaneous mechanism. Kinetic studies of purified and reconstituted aspartate/glutamate carrier (Dierks *et al.*, 1988), oxoglutarate carrier (Indiveri *et al.*, 1991), dicarboxylate carrier (Indiveri *et al.*, 1993) and phosphate carrier (Stappen & Krämer, 1994) also support the sequential or simultaneous mechanism. In addition, of eight mitochondrial carriers, only one, the carnitine/acylcarnitine carrier, exhibits kinetic properties consistent with an alternating access mechanism when reconstituted in proteoliposomes (F. Palmieri, Indiveri, *et al.*, 1993b), whereas the other seven exhibit a sequential or simultaneous mechanism.

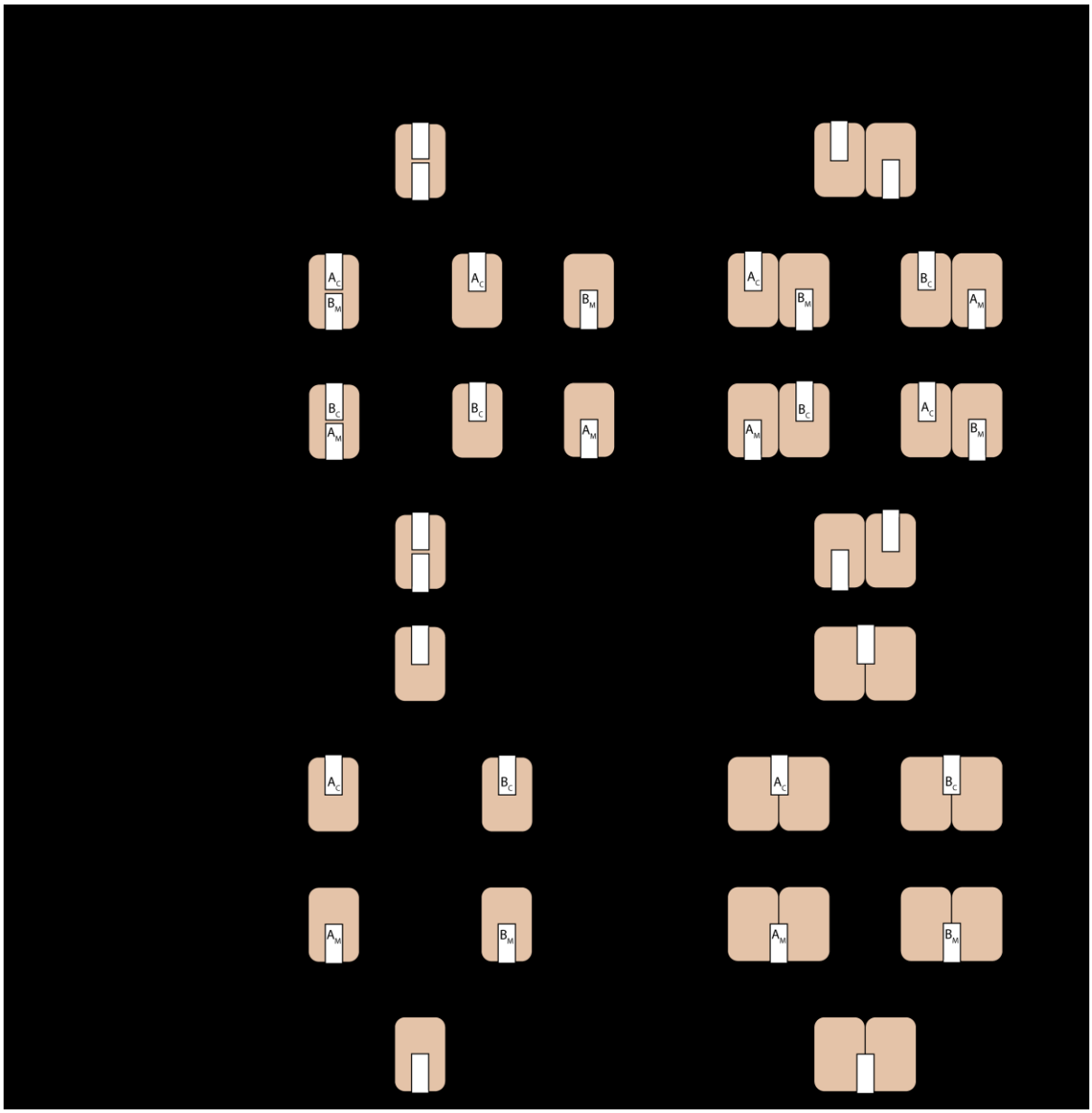

Figure 1.13 Kinetic mechanisms for mitochondrial carrier monomers and dimers. Possible kinetic mechanisms for the transport of substrate by mitochondrial carriers are shown. The carrier protein is coloured tan. A and B are potential substrates. A_C and B_C are substrates on the cytoplasmic side (above) of the protein. A_M and B_M are substrates on the matrix side (below) of the protein. **(A)** The sequential mechanism for a monomeric carrier. **(B)** The sequential mechanism for a dimerised carrier. **(C)** The alternating access mechanism for a monomeric carrier. **(D)** The alternating access mechanism for a dimerised carrier. (B) and (D) are based on (F. Palmieri, Indiveri, *et al.*, 1993b). This figure was prepared by Dr Alex Hellawell and subsequently modified.

In all of the kinetic studies supporting the sequential or simultaneous mechanism, the K_M/V_{max} ratio decreased with increasing internal substrate concentrations. In contrast, a constant K_M/V_{max} ratio would have been expected for a alternating access reaction mechanism. A caveat of these studies is that the K_M/V_{max} ratio is highly susceptible to being erroneously calculated, because small errors get amplified during the calculation of the ratio; consequently, any leakage of nucleotides across the membrane or issues with limiting substrate concentrations could affect K_M/V_{max}.

However, in addition to the finding that the K_M/V_{max} for the carnitine/acylcarnitine carrier is constant (F. Palmieri, Indiveri, *et al.*, 1993b) providing support for the alternating access mechanism, alternative kinetic studies also provided support for it. The capacitive currents generated by ADP/ATP carrier substrate transport were decreased when substrate was loaded on one side of the membrane only (Brustovetsky *et al.*, 1996), as expected for a carrier that has transported substrate, and must wait for a new substrate molecule. Further kinetic capacitive current studies suggested that the ADP/ATP carrier utilises an alternating access mechanism (Broustovetsky *et al.*, 1997; Gropp *et al.*, 1999). The mechanism of mitochondrial carriers as determined by kinetics is unresolved.

1.7.3 Mutagenesis studies supporting common substrate binding site

By the 1990s, advances in genetic engineering facilitated the feasibility of mutagenesis for studying protein function. The effect of mutagenesis on the transport activity of mitochondrial carriers was assessed, but the interpretation of why certain mutations were deleterious was limited in the absence of structural data. For instance, mutated charged cavity and matrix residues were found to have dramatic effects on the transport activity of yeast phosphate carrier reconstituted in proteoliposomes (Phelps *et al.*, 1996; Briggs *et al.*, 1999; Wohlrab *et al.*, 2002), but little could be interpreted about the transport mechanism. Now, based on symmetry analysis (Robinson *et al.*, 2008) it is thought that mutations R276A and K179A are likely to have abolished the activity of the phosphate carrier because the residues are part of the common substrate binding site (Wohlrab *et al.*, 2002).

A second highlight from the early literature was mutagenesis of acidic and basic yeast Aac2p residues that have since been implicated in substrate binding (K38, R96, R294) and substrate transport (R253) (Heidkämper *et al.*, 1996; V. Müller *et al.*, 1997). In all cases, mutagenesis of these residues that are critical for substrate binding resulted in reduced or ablated transport activity. The effect of mutagenesis on the transport activity of the citrate carrier (Kaplan *et al.*, 2000; Xu *et al.*, 2000), the oxoglutarate carrier (Stipani *et al.*, 2001) and yeast Aac2p residues in the α-helix 23 cytoplasmic loop (Kihira *et al.*, 2005) was determined before structural data became available.

The elucidation of the CATR-inhibited bovine ADP/ATP carrier structure (Pebay-Peyroula *et al.*, 2003) (Figure 1.8) was instrumental for mechanistically interpreting mutagenesis studies. For example, when prolines or equivalent residues at the ends of α-helix H1, H3 and H5 of yeast Aac2p were mutated to alanine or leucine (Babot *et al.*, 2012), it was shown that the alanine mutants did not affect Aac2p transport activity, whereas the leucine mutants led to abnormal yeast growth phenotypes. Remarkably, mild mutations to the Aac2p prolines were not detrimental to transport, suggesting that prolines may be functionally important, but not structurally important.

Carnitine/acylcarnitine carrier mutagenesis studies showed that transport was compromised for mutants of the proposed substrate binding site, providing evidence of a hydrophobic binding site ideally suited for hydrophobic carnitine and acylcarnitine binding (Tonazzi *et al.*, 2012).

The best evidence supporting the common substrate binding site was provided by a mutagenesis study in which two human mitochondrial ornithine carriers were used that differed in specificity and transport rate. The two isoforms differ in a single residue in contact point II of the substrate binding site, which is a glutamate or a glutamine. When the two residues are swapped by mutagenesis, substrate specificity and transport rate are also swapped (Monné *et al.*, 2012). The ornithine carrier mutagenesis study provided convincing evidence for the substrate specificity being determined at the proposed common substrate binding site of mitochondrial carriers.

1.7.4 Mutagenesis studies supporting mechanism

A pre-structural mutagenesis study of yeast Aac2p showed that replacement of acidic and basic residues resulted in reduced or ablated transport activity (Heidkämper *et al.*, 1996; V. Müller *et al.*, 1997). The affected residues included E45, K48, D149, R152, D249 and R252, which have since been implicated in the formation of the matrix salt bridge network.

Following the publication of the CATR-inhibited ADP/ATP carrier structure, a putative aromatic ladder was observed in the cavity of the bovine ADP/ATP carrier and implicated as having a role in facilitating the gliding of ADP toward the substrate binding site (David *et al.*, 2008). Equivalent residues in yeast Aac2p, Y203, Y207, F208 and Y211 were mutated to alanine. The transport activity for mutants Y203A and F208A was compromised, demonstrating that Y203 and F208 might be important for function. However, one of these belongs to the well-conserved [YF]XX[YF] motif, which is conserved symmetrically in all carriers, and the other is one of the residues that forms the adenine binding pocket, and thus there is no experimental evidence supporting the existence of the aromatic ladder in substrate gliding.

Carnitine/acylcarnitine carrier mutagenesis studies showed that transport is compromised for mutants of the matrix salt bridge network, providing evidence that the network is mechanistically important (Giangregorio *et al.*, 2010).

Of note, single cysteine mutants of the entire mitochondrial oxoglutarate carrier were assessed for transport activity (Cappello *et al.*, 2006; Cappello *et al.*, 2007; Miniero *et al.*, 2011). It was demonstrated that mutation of residues in the cavity, especially in the lower section, have a severe effect on transport activity, regardless of whether the residues are located on the even or odd-numbered α-helices. The residues in the lower cavity are believed to be crucial for substrate recognition, binding and ion coupling, so they are critical for the transport mechanism. In contrast, cytoplasmic loop, membrane-facing, inter-helical and less conserved matrix residues were not critical for transport, as expected for residues that do not play a key role in the transport mechanism. Overall, the data are consistent with the oxoglutarate carrier

functioning as a monomer, likely via an alternating access mechanism (Figure 1.10 C).

1.7.5 Genetic studies

The RRRMMM motif and the matrix salt bridge network were determined by genetic analysis to be important for the transport mechanism of the ADP/ATP carrier and the mitochondrial carrier family, respectively. Yeast Aac2p mutants were generated that did not allow growth of yeast on glycerol, which selects for respiration deficient yeast. Arginine to isoleucine mutations (R252I, R253I and R254I) were introduced into the RRRMMM motif, which causes reduced growth of yeast on glycerol (Nelson & Douglas, 1993; Nelson, 1996). Spontaneous mutations to residues on the cytoplasmic side of the carrier, near the membrane interface, were identified that allow robust growth on glycerol. These results show that the RRRMMM motif is important for the transport mechanism, and that second site revertants can compensate for its function.

Importantly, the first evidence for the formation of the matrix salt bridge network was generated by a similar genetic analysis approach to that described above. E45, K48, D149, R152, D249 and R252 of the PX[DE]XX[KR] motif, found on the odd numbered helices on the matrix side of the membrane, were neutralised by mutagenesis. All mutants except the E45 mutants abolished growth of yeast on glycerol. Interestingly, when one of the residues is neutralised, a second residue from the motif is also neutralised. This result led to the proposal that acidic-basic charge pairs are essential for the transport cycle of the ADP/ATP carrier. As the PX[DE]XX[KR] motif is conserved across the mitochondrial carrier family, it is proposed that charge pairs are also found in other carriers (Nelson *et al.*, 1998).

1.7.6 Structural analysis

The CATR-inhibited structure of the bovine ADP/ATP carrier (Figure 1.8) (Pebay-Peyroula *et al.*, 2003) provided some of the most convincing evidence for how the transport cycle functions. The structure shows that the CATR-inhibited c-state exists as originally postulated by inhibitor studies (Section 1.7.1). Additionally, the structure confirms that the ADP/ATP carrier is monomeric, after it had been shown to be monomeric in membranes (Kunji & Harding, 2003) (Figure 1.7), suggesting that it may function as a monomer, also. Furthermore, the structure shows that the matrix salt bridge network, originally postulated using genetic analysis of second site revertants (Section 1.7.5), is formed in the CATR-inhibited state (Figure 1.7 C and D).

Recently, a structure of uncoupling protein 2 was generated by nuclear magnetic resonance molecular fragment searching (Berardi *et al.*, 2011). The structure contains a bundle of six transmembrane α-helices, like the ADP/ATP carrier, but the α-helices are too far apart to form inter-helical interactions and the symmetry deviates significantly. The structure of uncoupling protein 2 is likely to be incorrect, possibly as a consequence of an insufficient number of reliable modelling restraints.

1.7.7 Sequence analysis

Recently, the three amino acid sequence repeats (Saraste & Walker, 1982) for all members of the mitochondrial carrier family were aligned (Figure 1.14 and 1.15), and their residues were classified as either asymmetric or symmetric (Robinson *et al.*, 2008) (Figure 1.16). The average symmetry and conservation scores for the yeast and human AAC are depicted on the carrier model (Figure 1.16 A-B, D-E). The symmetric residues (Figure 1.16 B, E) are postulated to be involved in the transport mechanism, whereas the asymmetric residues (Figure 1.16 A, D) are postulated to be important for substrate binding. Notably, most of the asymmetric residues are located in the centre of the cavity, indicating that there is only a single substrate binding site in the middle of the membrane (Figure 1.10).

A second feature that emerged from symmetry analysis was the presence of a conserved motif [YF][DE]XX[RK] found in the cavity on the cytoplasmic side of the membrane (Figure 1.15 and Figure 1.16 A-B, D-E). The motif is proposed to form a salt bridge on the cytoplasmic side of the membrane when the carrier is in the matrix-state as part of the gating mechanism in the transport cycle. Salt bridge networks have been identified on either side of the substrate binding site (Figure 1.16 C, F), consistent with the alternating access (Jardetzky, 1966) and the single-binding centre gated pore mechanisms (Section 1.7.1) (Klingenberg, 2005).

Mitochondrial carriers are predicted to operate primarily as strict equimolar exchangers (Figure 1.17 A) or as uniporters (Figure 1.17 B), based on the strength of their cytoplasmic salt bridge networks. Strong matrix networks are conserved across most of the mitochondrial carrier protein family. If the cytoplasmic network is also strong, strict equimolar exchange occurs (Figure 1.17 A), as conformational changes in the absence of substrate are prohibited by the energy barrier posed by the fully formed salt bridge network. Only when a substrate binds can the energy barrier be overcome, leading to conformational changes to the other state. If the cytoplasmic network is weak or incomplete, the energy barrier is low and the carrier converts to the c-state in the absence of substrate. Thus, net movement of substrate from the cytoplasmic side of the membrane to the matrix side occurs, leading to net import. Beside the salt bridge networks, conserved proline and glycine residues are postulated to be breaking points of the helices facilitating the opening and closure (F. Palmieri & Pierri, 2010), but this notion is likely to be incorrect as it would also require substantial hydrogen bond breaking. It is much more likely that the glycines and prolines are involved in maintaining the high curvature of the transmembrane helices, whereas GXXXG motifs facilitate inter-helical interactions during the transport cycle (Y. Liu *et al.*, 2002; Schneider & Engelman, 2004; Robinson *et al.*, 2008).

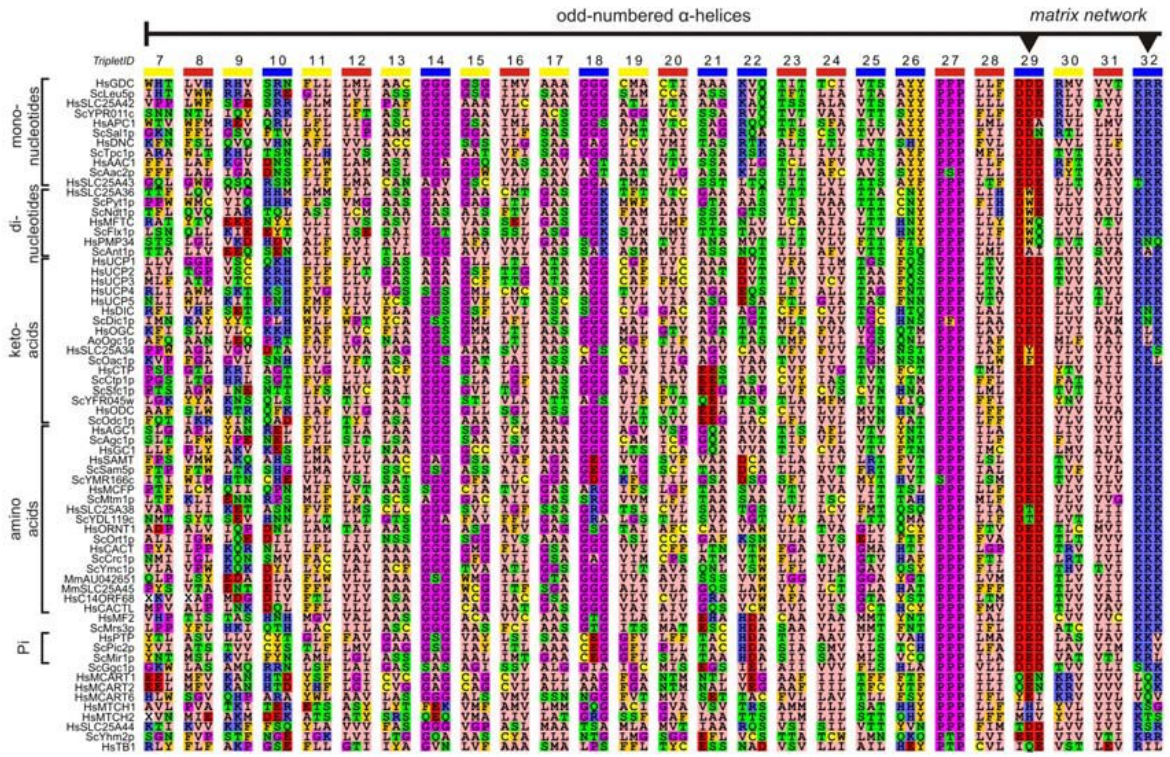

Figure 1.14 An alignment of the symmetry related triplets for α-helix H1, H3 and H5. CLUSTALW (Thompson *et al.*, 1994) was used to align mitochondrial carrier amino acid sequences from *Aspergillus oryzae* (Ao), *H. sapiens* (Hs), *M. musculus* (Mm) and *S. cerevisiae* (Sc) by sequence similarity. The triplet residues are arranged adjacent to show the symmetry of the three-fold repeat, and are numbered starting with the first repeat of the bovine AAC1. The bars beneath the TripletID show the topology of the residues, with dark blue for residues facing the cavity, red for residues facing the lipid bilayer and yellow for inter-helical facing residues. Amino acids are coloured based on their chemical properties. Acidic residues (D and E) are red, basic residues (H, K and R) are blue, polar (N, Q, S and T) are green, aliphatic (A, I, L, M and V) are pink, structural (G and P) are magenta and cysteine (C) is yellow. The residues comprising the matrix network are indicated by arrows. This figure is from Robinson *et al.* (2008).

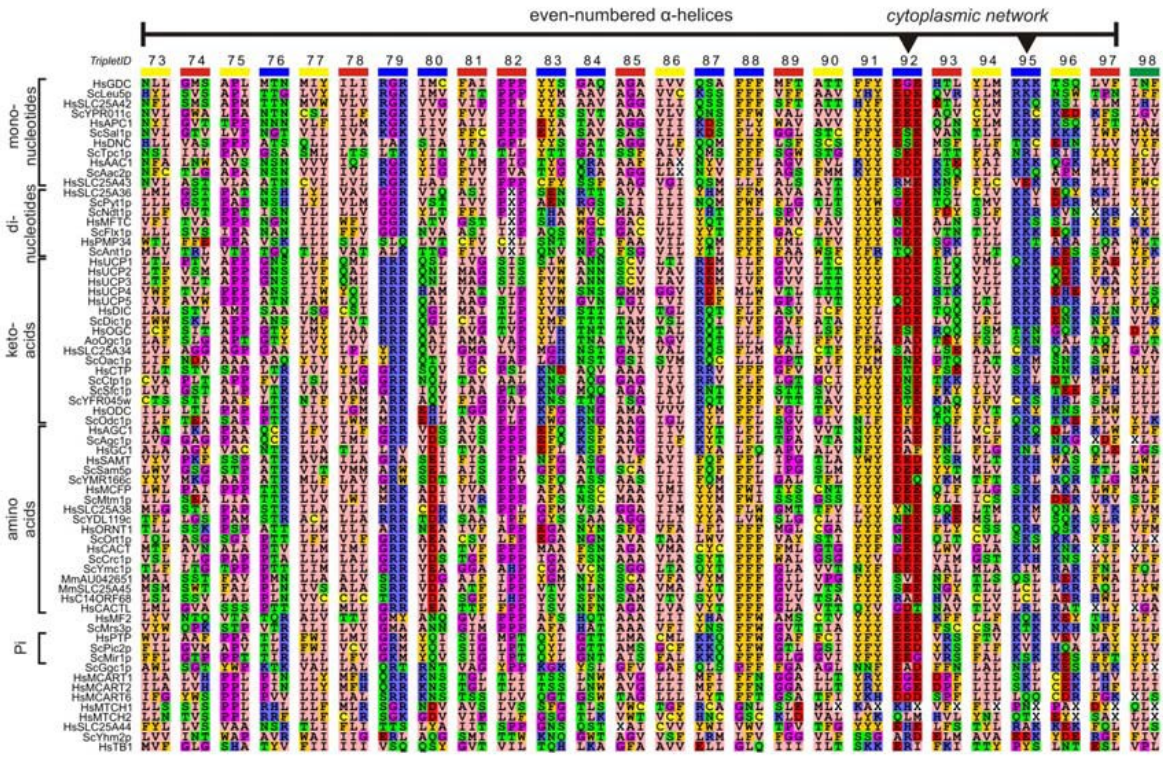

Figure 1.15 An alignment of the symmetry related triplets for α-helix H2, H4 and H6. For a description, please see the legend for Figure 1.14. The residues comprising the cytoplasmic network are indicated by arrows. The green bar underneath TripletID 98 indicates that the residues are in the cytoplasmic loop. This figure is from Robinson *et al.* (2008).

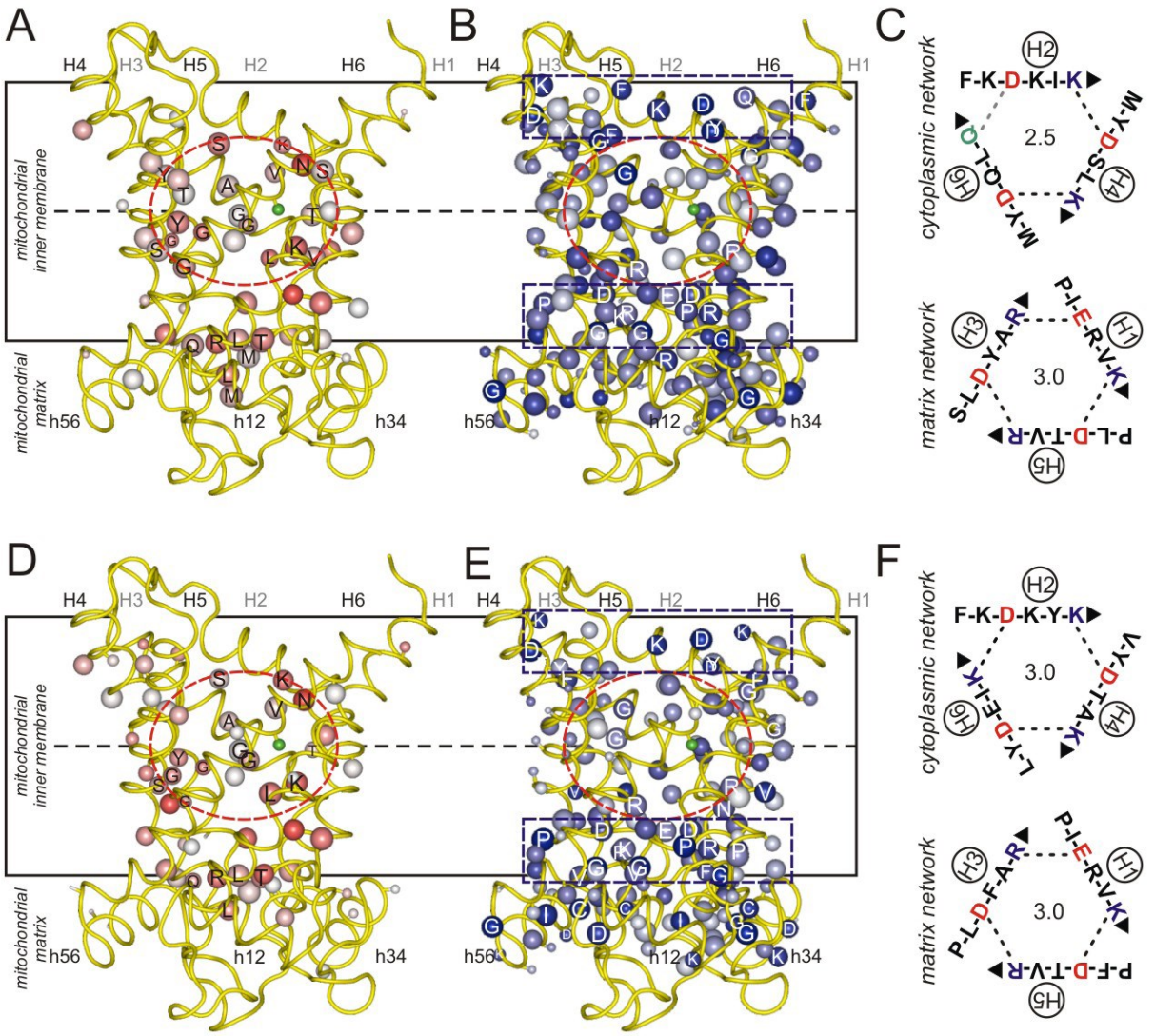

Figure 1.16 Asymmetry and symmetry of the yeast Aac2p and human AAC1. The bovine ADP/ATP carrier model (Pebay-Peyroula *et al.*, 2003) was used as a scaffold for **(A and B)** yeast Aac2p and **(D and E)** human AAC1, and the average symmetry and conservation scores are depicted as spheres. The size and colour of the C_β correlates to the score assigned. Negative scores, which correspond to asymmetric residues, are shown in red. Positive scores, which correspond to symmetric residues, are shown in blue. Labelled residues are highly symmetric. Residues absent from the repeat are coloured green. Dashed circles highlight the location of the substrate binding site. Dashed rectangles highlight the location of the salt bridge networks. **(C and F)** The cytoplasmic (upper) and matrix (lower) salt bridge networks for (C) yeast Aac2p and (F) human AAC1. Positive residues are blue, negative residues are red, and polar residues are green. The interaction energies (shown in the middle of each network diagram) were quantified by considering hydrogen bonds as half of the energy of an acidic or basic residue. Figure is from Robinson *et al.* (2008).

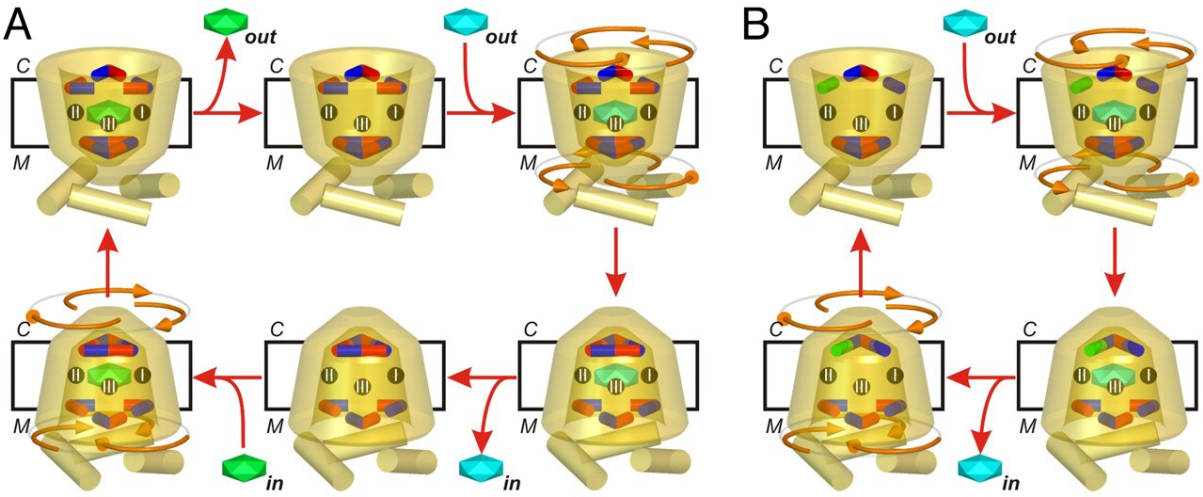

Figure 1.17 Strict equimolar exchange and uniport transport mechanisms. The mode of transport is dependent on the interaction energies of the salt bridge networks. **(A)** Strict exchange and **(B)** uniport mechanisms of transport. The carrier is coloured tan. The exported substrate is green and the imported substrate is cyan. The contact points I, II and III of the common substrate binding site are labelled. Basic, acidic and polar residues are shown as blue, red or green sticks, respectively. The red arrows show the direction of transport, as dictated usually by substrate gradients. During substrate transport, the salt bridge networks alternately open and close. The orange arrows indicate the proposed direction of the three-fold rotary twist of the α-helices. Figure is from Robinson *et al.* (2008).

1.7.8 Disease models

Many rare but severe mitochondrial diseases are associated with missense mutations of mitochondrial carrier family members (F. Palmieri, 2004; F. Palmieri, 2008). Two diseases, ADP/ATP carrier isoform 1 deficiency and autosomal dominant progressive external ophthalmoplegia (adPEO) are associated with missense mutations to human AAC1, an ortholog of yeast Aac2p. The A123D mutation, which is associated with ADP/ATP carrier isoform 1 deficiency, is found in the lower cytoplasmic cavity, close to the proposed common substrate binding site. In reconstituted liposomes, A123D completely abolishes substrate transport (L. Palmieri *et al.*, 2005). Mutations associated with adPEO are found primarily at the cytoplasmic membrane interface. Equivalent mutations introduced into yeast Aac2p lead to a reduced transport rate in liposomes (Fontanesi *et al.*, 2004). Recently, a reduced transport rate was measured for the same set of aforementioned disease associated mutations to human AAC1 expressed in *E. coli* (Ravaud *et al.*, 2012). In all cases, the decrease in or abolition of transport caused by mutations to human

AAC1 suggests that cytoplasmic cavity residues, including those in the vicinity of the proposed common substrate binding site, are crucial components of the carrier transport mechanism.

Phosphate carrier deficiency, carnitine/acylcarnitine carrier deficiency, Hyperornithinemia-hyperammonemia-homocitullinuria syndrome, aspartate/glutamate carrier isoform 2 deficiency, Amish microcephaly and neonatal myoclonic epilepsy are associated with mutations to the mitochondrial phosphate carrier, carnitine/acylcarnitine carrier, ornithine carrier, aspartate/glutamate carrier, thiamine pyrophosphate carrier and glutamate carrier, respectively (F. Palmieri, 2004; F. Palmieri, 2008). The missense mutations are clustered in the various regions of the cytoplasmic cavity, including the cytoplasmic and matrix salt bridge networks, and the common substrate binding site (Figure 1.10). All of these mutations adversely affect substrate transport. Consequently, disease models of mitochondrial carriers support the mechanism of transport based on symmetry analysis (Figure 1.17) (Robinson *et al.*, 2008) and the existence of a common substrate binding site (Kunji & Robinson, 2006; Robinson & Kunji, 2006).

1.8 Expression of mitochondrial carriers

1.8.1 Expression in *Lactococcus lactis* versus other systems

The *S. cerevisiae* ADP/ATP carrier can be expressed in native yeast mitochondria, but there are several disadvantages to using this expression system for characterisations. First, there are ~35 mitochondrial carriers expressed in yeast (Kunji, 2004), including carriers that transport ADP, such as isoforms of the ADP/ATP carrier (Lawson & Douglas, 1988; Kolarov *et al.*, 1990), Mg-ATP/P_i carrier (Fiermonte *et al.*, 2004), the coenzyme A transporter (Fiermonte *et al.*, 2009) and the thiamine pyrophosphate carrier (Lindhurst *et al.*, 2006). Second, yeast mitochondria need to be isolated, which may compromise their integrity for transport assays. Additionally, compromised membranes may allow membrane-impermeable probes, such as eosin-5-maleimide, to access both sides of the membrane. Finally, another potential

complication is that the outer membrane may prevent probes from accessing the inner membrane and the carriers therein.

An alternative expression system for mitochondrial carriers is *Escherichia coli* (*E. coli*), in which abundant expression levels of the ADP/ATP carrier and other mitochondrial carriers have been detected, but the proteins are found in inclusion bodies (Miroux & Walker, 1996). Alpha-helical proteins are especially problematic when expressed in inclusion bodies, because the proteins are often misfolded (Gordon *et al.*, 2008). In addition, proteins need to be isolated, refolded and reconstituted into membranes, and only a fraction of the reconstituted carriers are functional. Also, reconstitution scrambles the orientation of carriers in the membrane, so this system is not ideal for probing one surface of the protein with probes.

Another alternative is the *Lactococcus lactis* (*L. lactis*) expression system. *L. lactis* is a Gram-positive bacterium that can be used for expression of eukaryotic membrane proteins, including the ADP/ATP carrier, in a functional form in the cytoplasmic membrane without the production of inclusion bodies (Kunji *et al.*, 2003; Kunji *et al.*, 2005; Monné *et al.*, 2005). Protein expression is effectively regulated by a two-component Nisin A expression system (de Ruyter *et al.*, 1996). In addition, plant membrane proteins, which cannot be expressed in *E. coli*, insect or yeast cells, can be expressed in a functional form in *L. lactis* (Frelet-Barrand *et al.*, 2010). *L. lactis* has a single membrane, and thus the expressed ADP/ATP carrier and other mitochondrial carriers are directly accessible to substrates, inhibitors and probes for functional studies. Furthermore, mitochondrial carriers expressed in *L. lactis* are inserted into the cytoplasmic membrane in one orientation, with the cytoplasmic side to the outside of the cell and the matrix side facing the inside of the cell (Kunji *et al.*, 2003), as predicted by the positive-inside rule (Heijne, 1986; Heijne & Gavel, 1988; Heijne, 1989). A unique carrier orientation in the membrane is advantageous for probing water accessible residues with membrane-impermeable probes. The carrier can also be analysed functionally as transport studies can be carried out in whole cells if intracellular substrate is present. In summary, *L. lactis* is a highly suitable expression system and it was chosen here for functional and probing studies of the ADP/ATP carrier.

1.8.2 Truncation of yeast Aac2p

Although *L. lactis* is suitable for the expression of many mitochondrial carrier proteins, full length Aac2p was not well expressed in *L. lactis*, and its initial uptake rate was low (Figure 1.18) (Monné *et al.*, 2005). When the N-terminus was shortened to Δ2-19 Aac2p, the expression level increased and the initial uptake rate was the highest of the all of the truncation constructs tested. The requirement of the Δ2-19 truncation could be due to the differences in the orientation of insertion (Monné *et al.*, 2005). In mitochondria Aac2p is inserted from the cytosolic side of the membrane where it is produced, meaning that the N- and C-terminus do not traverse the mitochondrial inner membrane. During expression in *L. lactis* the protein is produced in the cytoplasm and the protein is inserted according to the positive-inside rule (Heijne, 1986; Heijne & Gavel, 1988; Heijne, 1989), meaning that the termini both have to traverse the cytoplasmic membrane. Aac2p has a long N-terminus, which may be an impediment to insertion, hence the need for the truncation to improve expression. Consequently, Δ2-19 truncated Aac2p will be used in this dissertation.

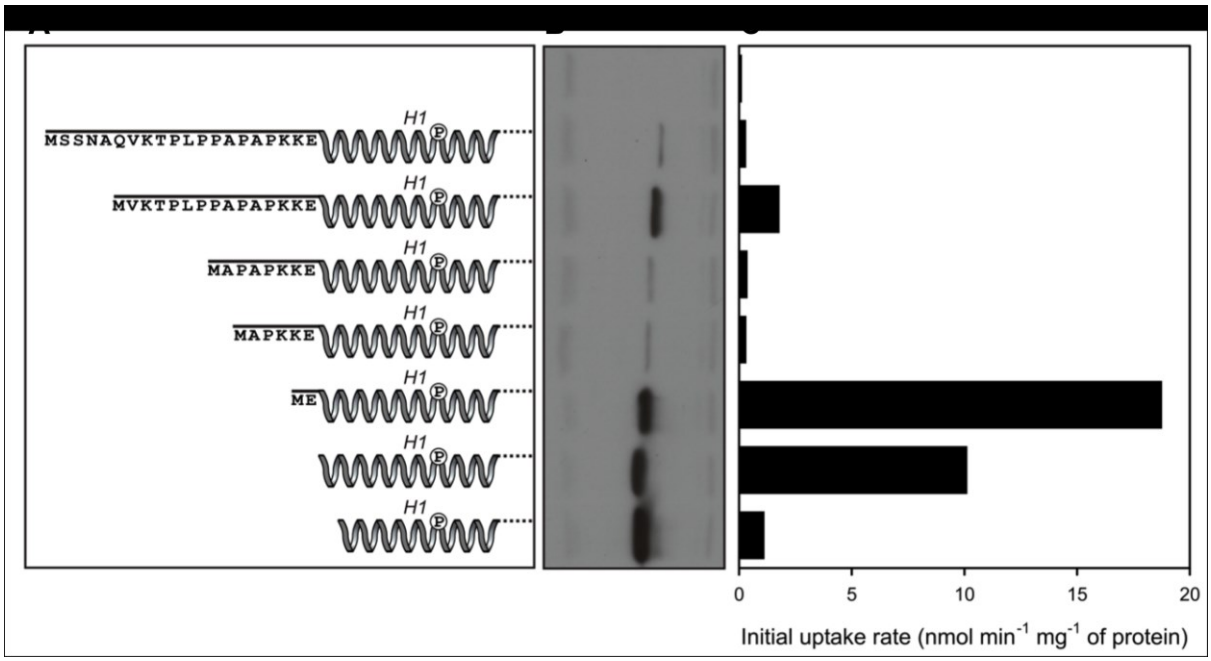

Figure 1.18 Truncation of the N-terminus of Aac2p in *L. lactis*. (A) This diagram depicts the systematic N-terminal truncation series. The secondary structure assignment is based on the bovine ADP/ATP carrier structure (Pebay-Peyroula *et al.*, 2003). The topmost image is full length Aac2p construct. Δ2-19 Aac2p is the third from the bottom, and the largest truncation Δ2-24 Aac2p is the bottommost. **(B)** Western blots of the corresponding full length and Aac2p truncation constructs **(C)** Initial uptake rates of the corresponding full length and Aac2p truncation constructs. The initial uptake rate was calculated three times from three time curves generated over 15 s. The data are represented by the average and standard error. This figure is modified from Monné *et al.* (2005).

1.9 Techniques for probing conformational changes

Many techniques have been developed to study protein conformational changes. Here they will be discussed, especially in relation to their application to mitochondrial carriers.

1.9.1 Accessibility of cysteine thiols to probes

Thiol groups, also known as sulphydryl groups, on cysteines are the most reactive of the 20 common amino acids found *in vivo*, so they are chemically amenable to specific modification by thiol-specific probes (Kenyon & Bruice, 1977); consequently, a plethora of thiol-specific probes are commercially available. Iodoacetamide and maleimide react with thiol groups on cysteines to form stable, irreversible thioether linkages (Figure 1.19). Iodoacetamide is more reactive than maleimide, but its

reaction is less specific for thiols (Whitehurst *et al.*, 2007). In order to prevent non-specific reactions with amines, tyrosines, histidines and methionines, iodoacetamide reagents must be kept limiting compared to the number of possible reaction sites with pH < 8.5 (Hermanson, 2008). Maleimides are less reactive than iodoacetamides, but they are highly specific for cysteine thiols from pH 6.5 to 7.5 (Gorin *et al.*, 1966; Smyth *et al.*, 1964). Both iodoacetamide and maleimide-based thiol-specific probes react quickly and irreversibly with cysteine thiols.

Iodoacetamide and maleimide groups can be conjugated to various groups to modify the chemical properties and to aid in the identification of modified cysteine thiols, if required. For instance, a charged group may be conjugated to iodoacetamide or maleimide to enable membrane-impermeability. Detectable conjugate groups may be radioactive, or they may be fluorescent compounds excited by UV or visible light.

Some thiol-specific probes are membrane-permeable whereas others are considered to be membrane-impermeable. Generally, the membrane-permeable reagents are uncharged, non-polar, and small. Some examples of thiol-specific, membrane-permeable probes are iodoacetamide (Whitehurst *et al.*, 2007), *N*-ethyl maleimide (Fonyó *et al.*, 1976), *N*-(N-acetyl-4-sulfamoyl-phenyl) maleimide (Houstěk & Pedersen, 1985) and carboxylated maleimides (Griffiths *et al.*, 1981). Iodoacetamide and *N*-ethyl maleimide are small and uncharged, allowing them to easily bypass membranes. *N*-(N-acetyl-4-sulfamoyl-phenyl) maleimide is uncharged and polar. Carboxylated maleimides contain carboxyl groups that are readily protonated, rendering them membrane-permeable. In physiological conditions, many thiol-specific probes will be membrane-permeable to some extent.

Thiol-specific, membrane-impermeable probes often are charged, polar and large. Lucifer yellow iodoacetamide (Hermanson, 2008), fluorescein-5-maleimide (Poelarends & Konings, 2002), eosin-5-maleimide (Schopfer & Salhany, 1998) and the alexa fluor series of probes (S. Liu *et al.*, 2010) have all been identified as being membrane-impermeable. Lucifer yellow iodoacetamide and fluorescein-5-maleimide are large and polar. Eosin-5-maleimide is polar because of its brominated xanthene ring. Alexa fluor probes contain two negatively charged sulphate groups. Overall, large, polar and charged probes have the potential to be membrane-impermeable.

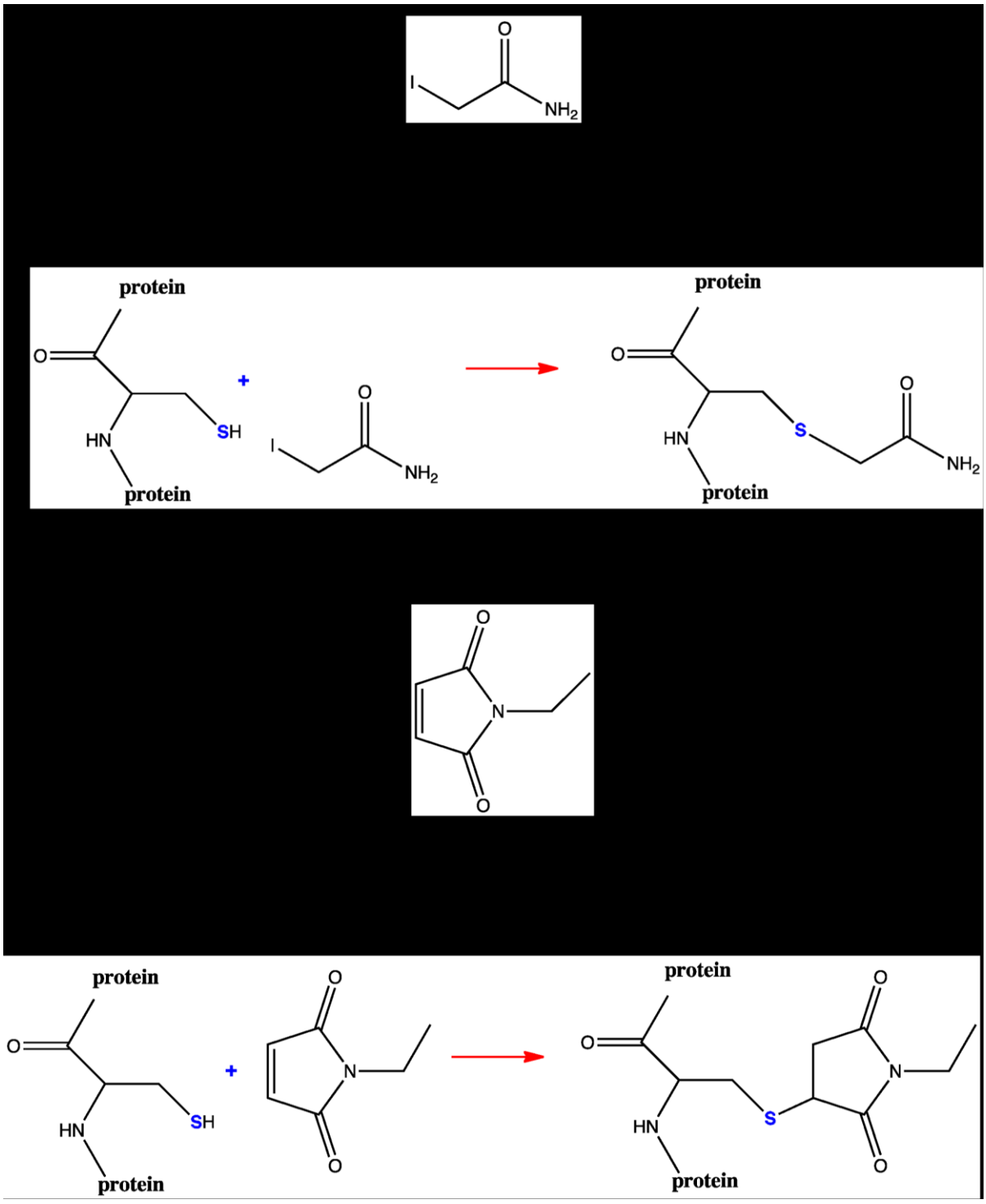

Figure 1.19 Chemical reaction of cysteine thiols with sulphydryl reagents. The chemical reactions of a cysteine thiol with **(A)** iodoacetamide and **(B)** *N*-ethyl maleimide are shown. The reactive sulphur is coloured blue.

Thiol-specific, membrane-impermeable fluorescent probes have been used extensively for probing membrane proteins (Figure 1.20). One such probe, eosin-5-maleimide (Figure 4.3 A), was first used to probe the rotational diffusion of the wild type ADP/ATP carrier (M. Müller *et al.*, 1982; M. Müller *et al.*, 1984). It was also demonstrated that cysteines of ADP/ATP carrier were labelled in bovine heart submitochondrial particles, but not in intact bovine heart mitochondria (Houstěk & Pedersen, 1985). It was also shown that the addition of CATR occluded labelling of the ADP/ATP carrier in submitochondrial particles. This was some of the first evidence suggesting that the native cysteines of the ADP/ATP carrier are located on the matrix side.

Following initial studies with eosin-5-maleimide, the native cysteines of the ADP/ATP carrier were probed more extensively. Of the four cysteines in the bovine ADP/ATP carrier, only C159 was labelled rapidly in submitochondrial particles by eosin-5-maleimide, leading to the idea that C159 is involved in nucleotide transport (Majima *et al.*, 1993). However, this conclusion is likely to be incorrect as C159 is now known to be found in matrix α-helix h34 (Pebay-Peyroula *et al.*, 2003), distant from the common substrate binding site (Kunji & Robinson, 2006; Robinson & Kunji, 2006). It has been shown that the residue becomes available as part of the transport cycle (Bamber, Harding, *et al.*, 2007a). An alternative attempt to characterise the substrate binding site of the ADP/ATP carrier was made by measuring substrate transport rate inhibition by eosin Y, a compound chemically identical to eosin-5-maleimide except that it lacks the maleimide moiety (Majima *et al.*, 1998).

In a follow-up study, the conformational dependency of cysteine labelling by eosin-5-maleimide was probed in the presence of CATR or BKA (Majima *et al.*, 1994). BKA-inhibited C159 labelling, and it was suggested that BKA binds near C159 on the matrix side of the ADP/ATP carrier. Additionally, methyl methanthiosulphonate labelling of C56, also located in matrix α-helix h12, abolished conversion between the m- and c-states, demonstrating that the matrix α-helix h12 undergoes conformational changes (Hashimoto *et al.*, 2000). The CATR-inhibited bovine ADP/ATP carrier structure has since shown that the gating mechanism on the matrix side of the carrier is the matrix salt bridge network (Pebay-Peyroula *et al.*, 2003).

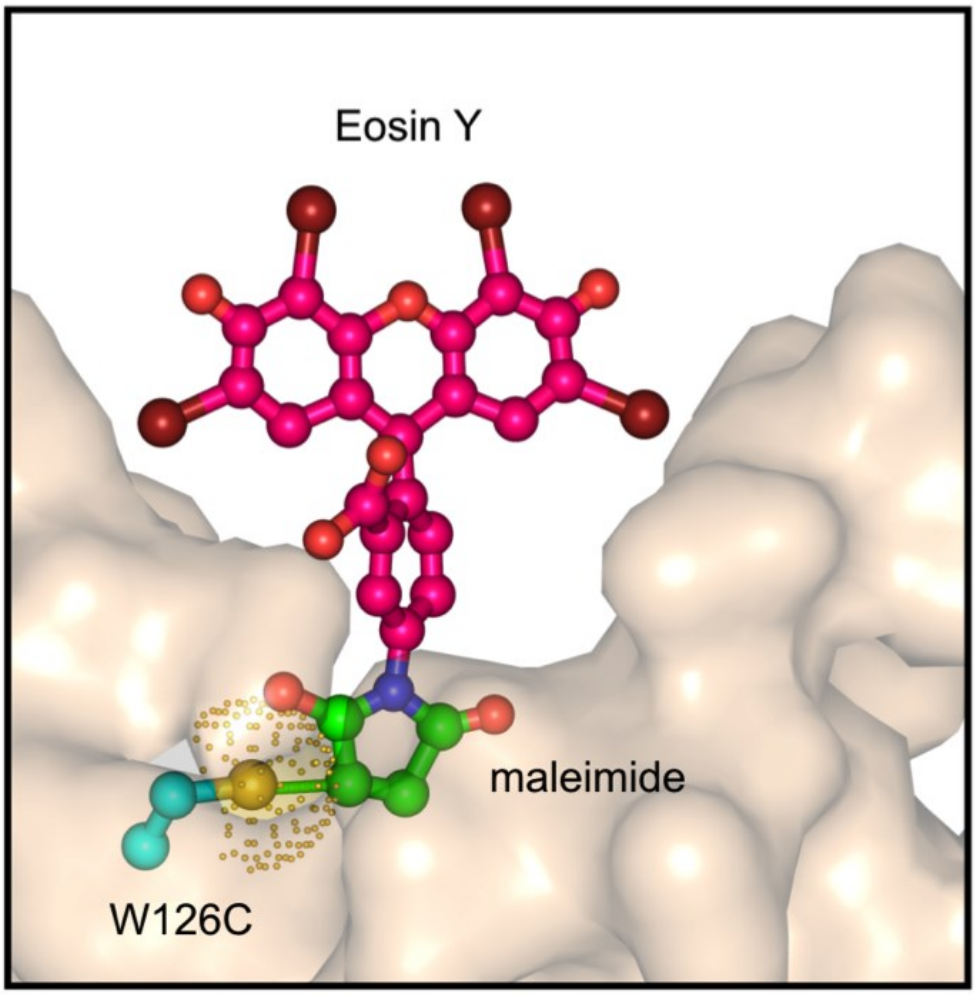

Figure 1.20 Thiol-specific, membrane-impermeable fluorescent probe eosin-5-malemide bound to W126C Aac2p. This Aac2p model is based on the CATR-inhibited bovine AAC1 structure (PDB code 1OKC) (Pebay-Peyroula *et al.*, 2003). The sequence alignment and comparative model were generated by Dr Alan Robinson. Aac2p is coloured wheat. The W126C residue has a yellow sulphur atom and turquoise carbon atoms. The W126C is shown reacted with eosin-5-maleimide. The maleimide is composed of green carbons, peach oxygens and a violet nitrogen. The maleimide is conjugated to an Eosin Y moiety to form eosin-5-maleimide. The Eosin Y carbons are pink, the oxygens are red and bromines are dark red. This figure was created by Dr Edmund R.S. Kunji.

To investigate conformational changes in the cytoplasmic loops of the ADP/ATP carrier, single cysteine mutants of Aac2p were generated and expressed in yeast (Hatanaka *et al.*, 2001; Kihira *et al.*, 2004; Kihira *et al.*, 2005; Iwahashi *et al.*, 2006; Iwahashi *et al.*, 2008). The mutant carriers were inhibited with BKA or CATR, and the accessibility of cysteine residues was probed with eosin-5-maleimide. By comparing BKA and CATR inhibition data, it was inferred that conformational changes occur in the cytoplasmic loops, but not at the C-terminus; the N-terminus

was not probed. It was concluded that only the loops change conformation in the m- and c-states, whereas the C-terminus does not. Additionally, α-helix H2 was shown to twist during transition from the m- and c-states, and in the m-state, the loops were proposed to gate the closure of the cavity. Based on studies of the C-terminus, it was concluded that the cytoplasmic side of the carrier was not fully closed in the m-state. Considering that the loop regions of the ADP/ATP carrier are not well conserved in length and composition (Figure 1.16) (Robinson *et al.*, 2008), it is unlikely that they form the cytoplasmic gate. Additionally, as the cytoplasmic and matrix gates are essential for preventing leakage of ions across the membrane, it would be inconsistent with the maintenance of a proton motive force that the gate should be left partially open in the m-state, as suggested (Iwahashi *et al.*, 2008).

Other mitochondrial carriers, the 2-oxoglutarate carrier (Zara & F. Palmieri, 1988) and uncoupling protein (Jezek, 1987) have been probed using eosin-5-maleimide. Additionally, pyruvate dehydrogenase (Scouten *et al.*, 1980), the $Na^{2+}K^{+}$-ATPase (Skou & Esmann, 1980), the *E. coli* D-galactose-H^{+} symport protein (McDonald & Henderson, 2001) and the erythrocyte band 3 anion-exchange protein (Cherry & Nigg, 1981; Macara & Cantley, 1981; Macara *et al.*, 1983) are other membrane proteins that have been probed in membranes using eosin-5-maleimide. In addition, fluorescein-5-maleimide was used to probe the orientation of the *L. lactis* multidrug transporter LmrA in its native membrane (Poelarends & Konings, 2002). In the past three decades, thiol-specific, membrane-impermeable fluorescent probes have facilitated studies of membrane protein topology, accessibility, substrate specificity and conformational dynamics.

1.9.2 Thiol-specific cross-linking

Cross-linking studies are often used to assess changes in the distances between residues that occur as a consequence of protein conformational changes. Thiol-specific cross-linking probes form intramolecular or intermolecular protein connections linking one cysteine thiol to a second cysteine thiol. Some examples of irreversible thiol-specific cross-linking probes are bibromobimane, bismaleimidoethane and bismaleimidohexane (Plessis *et al.*, 2009). Bibromobimane

reacts with a cysteine thiolate anion by displacement of its bromide ion, and only the fully reacted bibromobimane can be detected using ultraviolet light (Kim & Raines, 1995). Biobromobimane is rigid, with a 5 Å spacer arm. Bismaleimidoethane and bismaleimidohexane are maleimide-containing cross-linkers. The chemistry of maleimides is described in more detail in the previous section. Bismaleimidoethane is somewhat rigid, with an 8 Å spacer arm, whereas bismaleimidohexane is more flexible with a 13 Å spacer arm (Chen *et al.*, 1991; Plessis *et al.*, 2009).

Some examples of reversible thiol-specific cross-linking probes include copper-*o*-phenanthroline and 1,2-ethanediyl bismethanethiosulphonate (M-2-M). Copper-*o*-phenanthroline catalyses the formation of a disulphide bridge between two cysteines (Majima *et al.*, 2002). M-2-M contains two methanethiosulphonate groups that form reversible disulphide linkages with sulphydryl groups on cysteines (Figure 1.21). The copper-*o*-phenanthroline and M-2-M reactions are reversible because the disulphide bridges formed by both probes can be reduced by dithiothreitol (DTT) or β-mercaptoethanol (Kenyon & Bruice, 1977). In addition, M-2-M reacts rapidly and selectively with cysteines, and it introduces a short 5.2 Å spacer arm (Kenyon & Bruice, 1977; Loo & Clarke, 2001).

Irreversible and reversible thiol-specific cross-linking probes have been used to determine membrane protein conformational changes. Intermolecular and intramolecular cross-linking of cysteines by copper-*o*-phenanthroline and dimaleimides suggested that the matrix α-helices of Aac2p are highly flexible loops that function as a gating mechanism on the matrix side of the carrier (Majima *et al.*, 1995; Terada & Majima, 1997; Hashimoto *et al.*, 1999; Majima *et al.*, 2002). The CATR-inhibited bovine ADP/ATP carrier structure has since shown that the gating mechanism on the matrix side of the carrier is the matrix salt bridge network (Pebay-Peyroula *et al.*, 2003). In addition, bibromobimane, bismaleimidoethane and bismaleimidohexane were used to determine that the lateral gate of the SecYEG translocon opens during protein translocation (Plessis *et al.*, 2009). M-2-M and other methanethiosulphonate reagents with various spacer arm lengths were employed to measure the dimensions of the drug binding domain of human P-glycoprotein (Loo & Clarke, 2001). In another report, cross-linking of methanethiosulphonate reagents

was used to probe the conformational dynamics of G- and F-actin (Shvetsov *et al.*, 2006).

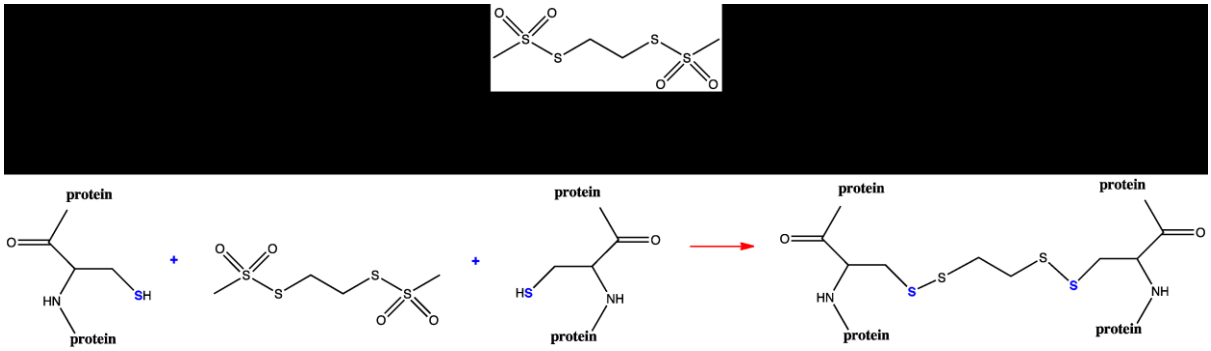

Figure 1.21 Chemical reaction of cysteine thiols with 1,2-bismethanethiosulphonate. The reactive sulphur is coloured blue.

1.9.3 Site-directed spin labelling for electron paramagnetic resonance spectroscopy

Site-directed spin labelling is a technique whereby one or more thiol-specific spin labels modify cysteine thiols in order to facilitate studies of protein conformational dynamics (Hubbell *et al.*, 2000). Thiol-specific spin labels introduce a paramagnetic unpaired electron on a protein for use in detection by electron paramagnetic resonance (EPR) spectroscopy. The thiol-specific moiety can be a methanethiosulphonate (Figure 1.21) or a maleimide (Figure 1.19 B), and this is covalently attached to a free radical-containing moiety, often a nitroxide. Nitroxide is a stable and unreactive paramagnetic free radical which can be detected by EPR spectroscopy (Wilson & Walker, 2010). Some examples of thiol-specific spin labels are (1-Oxyl-2,2,5,5-tetramethyl-Δ3-pyrroline-3-methyl) methanethiosulphonate (MTSL) and (1-Oxyl-2,2,6,6-tetramethyl-4-piperidinyl) maleimide (MAL-6). Both MTSL and MAL-6 react specifically and rapidly with cysteine thiols (Figure 1.22) (Kenyon & Bruice, 1977; Berliner, 1983).

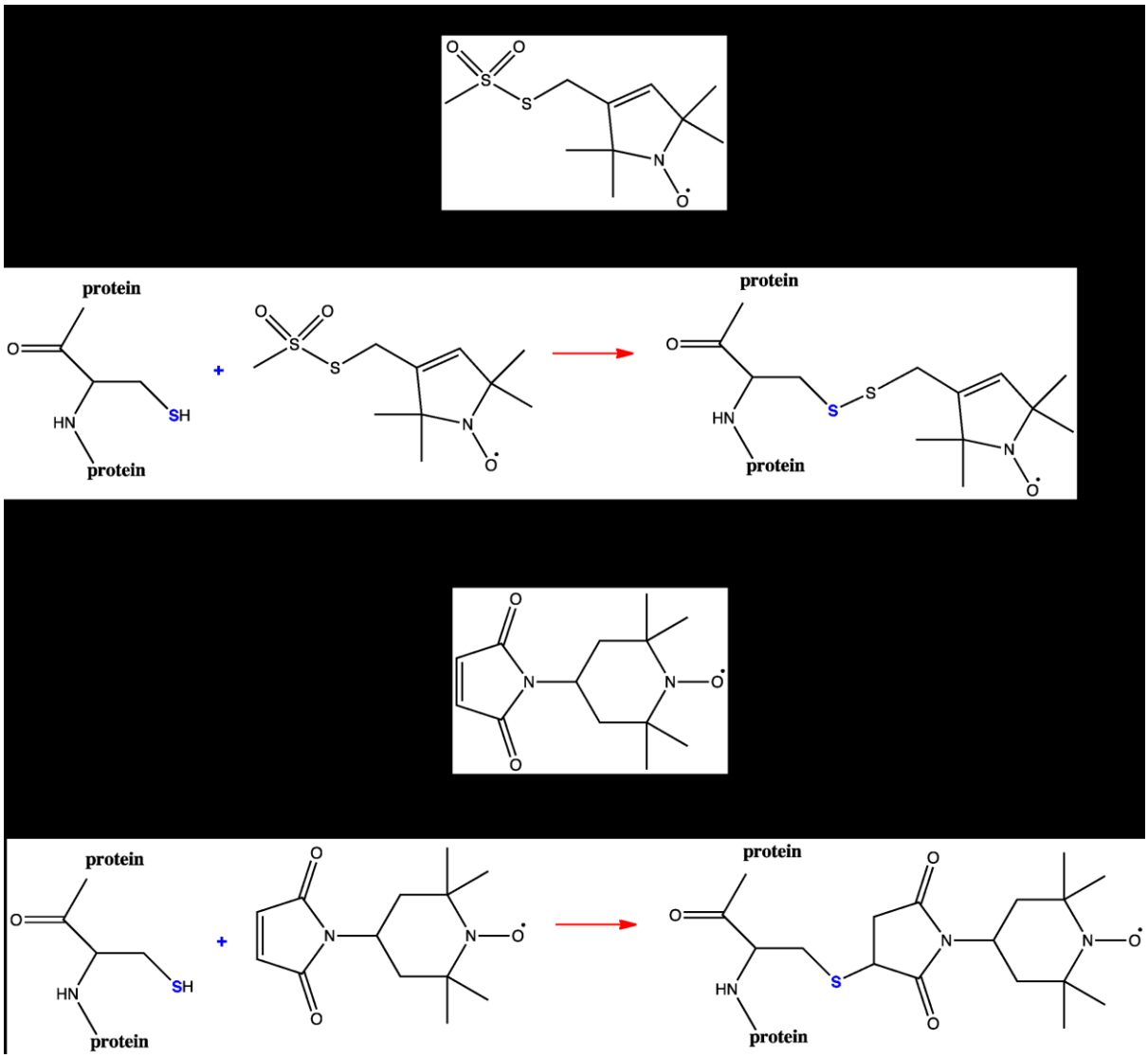

Figure 1.22 Chemical reactions of cysteine thiols with spin labels.

The chemical reactions of a cysteine thiol with **(A)** (1-Oxyl-2,2,5,5-tetramethyl-Δ3-pyrroline-3-methyl) methanethiosulphonate (MTSL) and **(B)** (1-Oxyl-2,2,6,6-tetramethyl-4-piperidinyl) maleimide (MAL-6) are depicted. The reactive sulphur is coloured blue.

EPR spectroscopy is used to detect site-directed spin-labelled protein (Weil *et al.*, 1994). An EPR sample is exposed to a constant microwave frequency while the magnetic field is concomitantly increased (Figure 1.23); if this increase in the strength of the magnetic field is continuous, then this type of EPR is termed continuous wave (cw). Initially, the population of spins of the paramagnetic species is randomly aligned parallel or anti-parallel to the magnetic field. As the magnetic field strength increases, the spin populations separate, with half the population in the parallel orientation and the other half in the anti-parallel orientation. At this point the energy difference of the spins in the magnetic field is equal to the microwave radiation

energy, and resonance is achieved. At resonance the maximum absorption of microwave radiation occurs, and the first derivative of the absorption peak is the resulting EPR spectrum (for an example, see Figure 6.10).

The cw-EPR spectrum can be used to determine the concentration, ligand geometry or oxidation state of a paramagnetic species (Prisner *et al.*, 2001). In pulsed EPR, short pulses of magnetic field can be applied to a sample to determine additional properties of the paramagnetic species. For instance, pulsed double electron resonance (PELDOR), may be used to determine distances between two unpaired electrons that are 15 to 80 Å apart (Reginsson & Schiemann, 2011). In PELDOR, pulsed microwave frequencies are applied at different intervals in a constant magnetic field, and the resulting spectrum derived from the interaction of the two electron spins is used to calculate the distance between the electrons. PELDOR can be used to determine intramolecular distances, such as the distance between α-helices that are greater than 15 Å apart.

Site-directed spin labelling combined with EPR has been used to probe conformational studies of membrane proteins. Labelling by MTSL and PELDOR EPR were used to probe the conformational changes of bacteriorhodopsin in purified purple bacterial membranes (Mollaaghababa *et al.*, 2000). In another study, MTSL helped map the location of residues of the *Escherichia coli* ferric enterobactin receptor, FepA, in liposomes (Klug *et al.*, 1997). MAL-6 was used to monitor drug interactions in erythrocyte membranes (Hornblow *et al.*, 1985). Synaposomal and mitochondrial membranes were labeled with MAL-6 to measure protein conformational changes due to succinate oxidation (Gabbita *et al.*, 1998). In addition, thiol-specific spin labels have been used to study the interactions of AAC with phospholipids and CATR (Devaux *et al.*, 1975; Munding *et al.*, 1983; Munding *et al.*, 1987; Drees & Beyer, 1988; Horváth *et al.*, 1989; Horváth *et al.*, 1990).

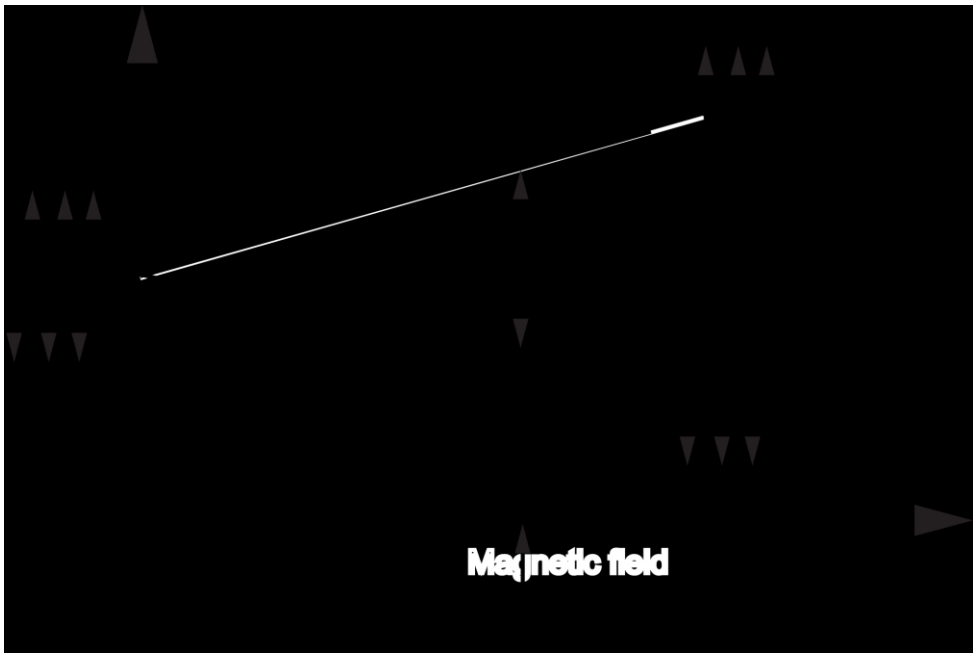

Figure 1.23 Energy level separation of paramagnetic spin populations in a magnetic field. The applied magnetic field (B) is increasing from left to right while the microwave frequency (v) is held constant. The paramagnetic resonance point is labelled and indicated with an arrow. ΔE is energy difference, h is Planck's constant (6.626 x 10^{-34} J s), v is microwave frequency (Hz), g is the g-value (dimensionless), β is the Bohr magneton (9.274 x 10^{-24} J T^{-1}) and B is the magnetic field (G).

1.9.4 Antibody accessibility studies

Antibodies can be raised against specific peptide sequences to probe accessibility of specific protein regions. The two inhibited states of bovine AAC1 purified in Triton X-100 were probed using antibodies. The two states could be discriminated with two specific antibodies, one specific for the inhibited c-state, but not for the m-state, and one for the inhibited m-state, but not for the c-state (Buchanan *et al.*, 1976). The antibody analysis provided direct evidence for the existence of two distinct conformational states of the ADP/ATP carrier. Additionally, the increase in BKA binding to mitochondrial membranes by ADP was interpreted as evidence that BKA binds to the matrix side of the ADP/ATP carrier (Erdelt *et al.*, 1972). Further evidence for conformational changes of the carrier in the m- and c-states was that the accessibility of the N-terminus of bovine AAC1 to an N-terminal antibody changed in BKA- and CATR-inhibited freeze-thawed mitochondria and mitoplasts (Brandolin *et al.*, 1989).

1.9.5 Lysine accessibility studies

Pyridoxal-5-phosphate is a hydrophilic membrane-impermeable reagent used to probe lysine accessibility. The conformational state of the BKA- or CATR-inhibited AAC1 from bovine mitochondria was probed in mitochondria and submitochondrial particles by pyridoxal-5-phosphate (Bogner *et al.*, 1986). In the CATR-inhibited state, lysine residues K106 and K198, which are located in the cytoplasmic loop and upper sections of the cavity, were labelled by pyridoxal-5-phosphate. In the BKA-inhibited state, lysines K22, K48, K91, K93, K95, K162, K198 and K205 were labelled. These lysines are located throughout the cavity and on the cytoplasmic side and matrix side of the carrier. The differential labelling of the m- and c-states was interpreted as indicative of the ADP/ATP carrier undergoing large conformational changes or that the residues are part of the substrate translocation channel. In retrospect, The CATR-inhibited structure of the ADP/ATP carrier has confirmed that bound CATR may block access to the central binding site of the cavity, where many of the lysines are located (Figure 1.9) (Pebay-Peyroula *et al.*, 2003), but not to all of them. Another caveat of the study was that lysines on the matrix side were probed in the inhibited m-state in mitochondria, indicating that the probe was either membrane-permeable or that the mitochondria were not intact. Overall, the lysine probing study provided evidence for the CATR binding site, but did not provide evidence of conformational changes between the inhibited m- and c-states.

1.9.6 Hydrogen/deuterium exchange coupled to mass spectrometry

Purified proteins can exchange hydrogen for deuterium atoms, and the extent of exchange is an indicator of protein accessibility. To detect the extent of exchange, the deuterium levels of peptide fragments are analysed by mass spectrometry. By this method, the conformational changes of inhibited and purified bovine AAC1 and yeast Aac2p in Triton X-100 were probed (Rey *et al.*, 2010; Clémençon *et al.*, 2011). The top of the cytoplasmic cavity of bovine AAC1 was weakly deuterated in the inhibited m-state, but was highly deuterated in the inhibited c-state, whereas the middle of the cytoplasmic cavity was highly deuterated in the inhibited m-state, but was weakly deuterated in the inhibited c-state (Rey *et al.*, 2010), suggesting that the

inhibited c-state is more water accessible compared to the m-state. The bovine studies demonstrated that the m- to the c-state transition is highly dynamic and it was speculated that α-helix H1, H3 and H5 associate upon closure of the cytoplasmic side of the carrier (Rey *et al.*, 2010), not α-helix H2, H4 and H6 as proposed by symmetry analysis. A BKA-inhibited structure would discriminate between these different models.

In contrast, the deuteration of the top of the cytoplasmic cavity of Aac2p was poor in comparison to AAC1, independent of the inhibited state (Clémençon *et al.*, 2011). Surprisingly, the top of the cavity was weakly labelled in the presence of CATR and moderately labelled in the presence of BKA, contradicting the bovine results. It was suggested that the yeast and bovine carriers have different conformational dynamics. More likely, the discrepancy could have occurred because the experiments were carried out in Triton X-100, which may lead to different accessibility as water can often penetrate micelles. No control experiments were done to confirm that the inhibited state was maintained in the micelles; this is especially important for the BKA-inhibited state as BKA does not confer stability in detergent micelles (Marilyn Harding, unpublished data).

1.10 Aims and objectives

The ultimate aim of this dissertation is to probe the conformational changes of the yeast ADP/ATP carrier Aac2p during the transport cycle.

In chapter 3, the aim was to determine whether mutant carriers were competent in transport when expressed in the cytoplasmic membrane of *L. lactis.* The first objective was to introduce single cysteine mutations at the cytoplasmic side of a truncated and cysteine-less Aac2p, which was fully functional. The second objective was to determine the expression levels and transport activity of mutant carriers. For mutants capable of ADP transport, the third objective was to determine the inhibition of transport by BKA and CATR, as it was necessary to ascertain that the carriers could be inhibited in the matrix or cytoplasmic state.

In chapter 4, the aim was to determine the orientation of the mutant carriers in the *L. lactis* cytoplasmic membrane. Thus the objective was to determine whether the labelling of single cysteine mutants was consistent with the carriers being oriented with the cytoplasmic side to the outside of the cell by using two approaches: (i) labelling of the single cysteines with the thiol-specific membrane-impermeable probe, eosin-5-maleimide; and (ii) assaying for complete inhibition by the membrane-impermeable CATR.

In chapter 5, the aim was to probe the accessibility of single cysteines in different transport states. The first objective was to determine whether the accessibility of single cysteines is different in the inhibited c-state and m-state by locking the carriers with CATR and BKA and by labelling the single cysteines of these carriers with eosin-5-maleimide. The second objective was to demonstrate that the accessibility of single cysteines changes in the absence or presence of substrate, indicating that the carrier cycles through different stages of the transport cycle only in the presence of substrate.

In chapter 6, the aim was to determine whether the residues of the cytoplasmic salt bridge network interact in the m-state. For this purpose the first objective was to replace the two residues of the salt bridge with cysteines and to use bi-reactive cross-linkers to see if they could be linked in the aborted m-state but not in the aborted c-state. In another approach the second objective was to introduce paramagnetic probes to cysteine replacements adjacent to the cytoplasmic salt bridge to determine their distance by electron paramagnetic resonance spectroscopy as a function of the inhibited state.

In chapter 7, results from chapters 3-6 are discussed.

Chapter 2 Materials and Methods

2.1 Chemicals

Laboratory chemicals were supplied by Sigma-Aldrich Chemicals (St. Louis, MO, USA), unless otherwise stated. KOD hot start polymerase, KOD buffer, deoxyribonucleotide triphosphate and magnesium sulphate for polymerase chain reactions (PCR) were supplied by Novagen (San Diego, CA, USA). Oligonucleotide primers for PCR were produced by Eurofins MWG Operon (Ebersberg, Germany). Restriction enzymes, including *DpnI*, were supplied by New England Biolabs (Ipswich, MA, USA). Pellet Paint Co-Precipitant was supplied by Novagen (San Diego, CA, USA). QIA prep Spin Miniprep Kits were supplied by Qiagen (Hilden, Germany). Chloramphenicol was supplied by BDH Laboratory Supplies (Poole, UK). Thiol-specific probes were supplied by Toronto Research Chemicals Inc. (North York, ON, Canada), unless declared otherwise. Eosin-5-maleimide, fluorescein-5-maleimide and lucifer yellow iodoacetamide were supplied by Invitrogen (Eugene, OR, USA). Radionucleotides were supplied by Perkin Elmer (Waltham, MA, USA). *Escherichia coli (E. coli)* polar lipids and egg phosphatidylcholine (PC) were supplied by Avanti Polar Lipids Inc. (Alabaster, AL, USA). Lysozyme for cell lysis was supplied by BDH Laboratory Supplies (Poole, UK).

2.2 Growth media and plasmid strains

Yeast extract, agar, sucrose, 2xTY broth, SOC broth, TYE broth, and M17 broth were supplied by ForMedium (Hunstanton, UK). Tryptone was supplied by Merck and Co., Inc. (Whitehouse Station, NK, UKA). All growth media was handled and autoclaved by the MRC/Wellcome Trust media kitchen (Cambridge, UK).

2.2.1 Growth media for *Escherichia coli*

E. coli DH5α cells were cultured in a 30 ml flask containing 5 ml of 2xTY broth, pH 7.0, containing 1.6% (w/v) tryptone, 1% (w/v) yeast extract and 0.1 mM NaCl, with

100 µg ml^{-1} chloramphenicol added. Electroporated *E. coli* were recovered in SOC, pH 7.0, containing 2% (w/v) tryptone, 0.5% (w/v) yeast extract, 20 mM glucose, 10 mM NaCl, 10 mM $MgCl_2$ 6 H_2O, 2.5 mM KCl. *E. coli* were plated on TYE+chloramphenicol plates, pH 7.4, contained 1.5% (w/v) agar, 1% (w/v) tryptone, 0.5% (w/v) yeast extract, 0.14 M NaCl and 100 µg ml^{-1} chloramphenicol.

2.2.2 *Escherichia coli* strains and vectors

E.coli DH5α (Genotype: F– Φ80*lac*ZΔM15 Δ(*lac*ZYA-*arg*F) U169 *rec*A1 *end*A1 *hsd*R17 (rK–, mK+) *pho*A *sup*E44 λ– *thi*-1 *gyr*A96 *rel*A1) (Invitrogen, Eugene, OR, USA)) was transformed with pNZ8048 (de Ruyter *et al.*, 1996) containing a modified *Saccharomyces cerevisiae (S. cerevisiae) aac2* gene. First, the wild type *S. cerevisiae aac2* gene was made cysteine-less in the pYES3/CT vector by replacing the four cysteine codons with alanine codons. The modified *S. cerevisiae aac2* gene had amino acids 1-19 deleted by copying the gene via PCR in the presence of a primer that anneals to the gene (Appendix I). A methionine codon was added back into the *aac2* gene product during PCR, giving a gene, *Δ2-19 cys-less aac2*, which encodes for the protein Δ2-19 cys-less Aac2p. Finally, *Δ2-19 cys-less aac2,* engineered by Dr Lisa Bamber, was cloned into an empty *Lactococcus lactis* (*L. lactis*) pNZ8048 vector (plasmid generated by Dr K. W. Chan) (Figure 2.1) by Dr Alex Hellawell. Gene expression of the pNZ8048 vector can be induced by the activation of its inducible promoter with Nisin A.

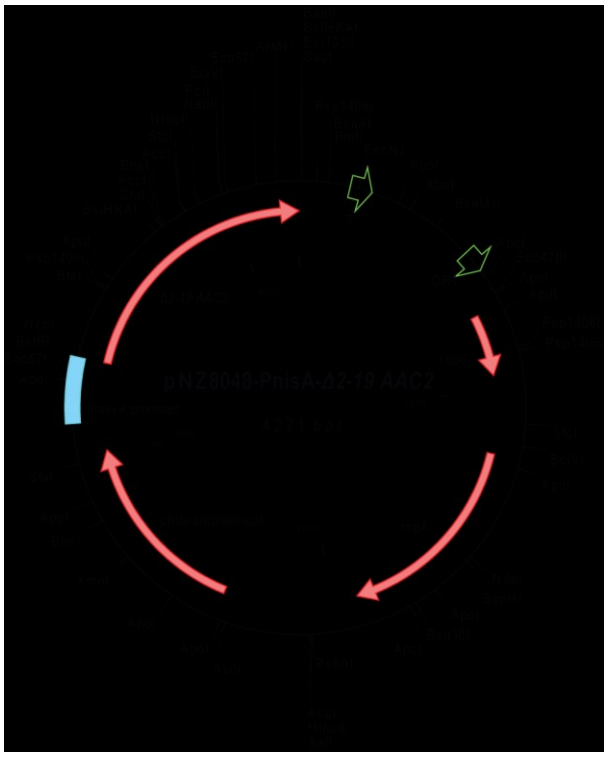

Figure 2.1 ***Lactococcus lactis*** **pNZ8048 plasmid vector map depicting the Nisin A promotor preceding the** ***Δ2-19 cys-less aac2 gene*** The Nisin A promotor is depicted as a blue bar, genes are shown as red arrows, and green arrows shown additional functional elements, such as the terminator and origin of replication. Restriction enzyme sites are named and their sites shown by black bars. Image courtesy of Dr Alex Hellawell.

2.2.3 Growth media for *Lactococcus lactis*

Lactococcus lactis were cultured in M17 broth containing 19% (w/v) disodium-β-glycerophosphate, 5% (w/v) soya peptone, 5% (w/v) digested casein, 5% (w/v) beef extract, 2.5% (w/v) yeast extract, 0.5% (w/v) ascorbic acid, and 0.25% (w/v) magnesium sulphate, with 5 μg ml^{-1} chloramphenicol and 1% (w/v) glucose added. Electroporated *L. lactis* (see below) were recovered in SM17 broth, which consists of M17 broth with 0.5 M sucrose added, and 1% (w/v) glucose, 20 mM $MgCl_2$ and 2 mM $CaCl_2$. *L. lactis* were plated on SM17 plates, containing SM17 broth, 1.5% (w/v) agar, 1% (w/v) glucose, and 5 μg ml^{-1} chloramphenicol. When required, gene expression was induced with the spent M17 broth from strain NZ9700, a strain that secretes Nisin A.

2.2.4 *Lactococcus lactis* strains and vectors

L. lactis strain NZ9000 (donated by Dr O. P. Kuipers, Department of Biophysical Chemistry, Netherlands Institute for Dairy Research, Ede, The Netherlands) was transformed with the pNZ8048 vector containing the *Δ2-19 cys-less aac2* gene (Section 2.2.2) by Dr Alex M. Hellawell. Site-directed single cysteine mutations were engineered into the *Δ2-19 cys-less aac2* gene (Section 2.3.3).

2.3 DNA methods

The pNZ8048 vector containing the *Δ2-19 cys-less aac2* gene was isolated from *L. lactis*. The vector was transformed into *E. coli* cells by electroporation, and isolated by a Qiagen plasmid purification kit (Hilden, Germany) for use as a PCR template to create site-directed single or double cysteine mutations (Figure 2.2A-B).

2.3.1 Electroporation competent *Escherichia coli* and *Lactococcus lactis* cells

Competent cells used in electroporation are termed electrocompetent cells. *E.coli* DH5α electrocompetent cells were prepared by Dr Anna Ludovico.

L. lactis electrocompetent cells were produced by inoculating SM17 medium containing 2% (w/v) glycine with the NZ9000 strain, and were incubated at 30°C overnight without shaking. The following day, the pre-cultures were diluted 20-fold in SM17 medium, usually 1-2 litres, containing 2% (w/v) glycine and were incubated at 30°C without shaking until A_{600} nm was 0.5-0.7. The cells were harvested by centrifugation for 5 min at 7430 *g* at 4°C, and the pellet was resuspended in 0.5 M sucrose containing 10% (w/v) glycerol. The centrifugation and resuspension steps were repeated four times. The final pellet was resuspended, and individual aliquots of cells were flash frozen and kept at -80°C.

2.3.2 Agarose gel electrophoresis

Agarose gels contained 1% (w/v) agarose (BioGene Ltd., Kimbolton, UK) in TBE buffer (8.9 M tris-borate, 8.9 mM boric acid, 0.2 mM EDTA), and 1.25 μg ml^{-1} ethidium bromide. DNA samples were prepared by adding 1 μl of the PCR product to a 6:1 dilution of loading dye consisting of 30% (w/v) glycerol and 0.25% (w/v) bromophenol blue, and TBE buffer. The DNA fragments were separated in an agarose gel submerged in TBE using a 100 mA current. A transilluminator (Syngene, Frederick, MD, USA) radiating ultraviolet light was used to visualise the separated DNA fragment bands.

2.3.3 Polymerase chain reaction

Amplified genes were generated by PCR (Figure 2.2 B-D) using a modified QuikChange II methodology-based protocol kindly provided by Dr Christopher Tate (Stratagene, San Diego, CA, USA and MRC Laboratory of Molecular Biology, UK). PCR reactions were carried out according to the *KOD Hot Start polymerase* handbook (Novagen, San Diego, CA, USA) and were programmed in the following manner.

(a)

Component	Volume (µl)	Stock conc	Final conc
$MgSO_4$	7.0	7.0 mM	3.5 mM
Deoxyribonucleotide triphosphates	28.5	2.0 mM	1.1 mM
10 x KOD reaction buffer	5.0	n/a	n/a
Dimethyl sulphoxide	1.5	n/a	n/a
KOD HotStart Polymerase	1.0	n/a	n/a
Template harvested from *E. coli*	1.0	< 10 ng	n/a
Forward primer	3.0	5.0 µM	0.3 µM
Reverse primer	3.0	5.0 µM	0.3 µM

(b)

Programme	Temperature (°C)	Time (s)	Cycles
Starting denaturation	98	30	1
Denaturation	98	30	
Annealing	80	60	5
Elongation	68	240	
Denaturation	98	30	
Annealing	75	60	5
Elongation	68	240	
Denaturation	98	30	
Annealing	70	60	5
Elongation	68	240	
Denaturation	98	30	
Annealing	65	60	5
Elongation	68	240	
Denaturation	98	30	
Annealing	80	60	5
Elongation	68	240	
Final hold	4	N/A	

Table 2.1 PCR (a) Typical components of a 50 µl reaction (b) Touchdown temperature cycling programme

The utilised temperature cycling programme is termed touchdown PCR (Don *et al.*, 1991). The touchdown programme cycles through a range of annealing temperatures until the optimal temperature for a particular set of mutagenic oligonucleotide primers is found, and the gene is amplified. The mutagenic oligonucleotide PCR primers were designed by Dr Chris Tate (MRC Laboratory of Molecular Biology, UK). The forward and reverse primers were designed to overlap partially and to introduce single cysteine mutations. See Appendix I for a list of the primers used. For the initial reactions, the PCR products were visualised by agarose gel electrophoresis stained with ethidium bromide. Most of the later reactions were not analysed by agarose gel electrophoresis, as it was found that an observed gel band did not always guarantee the identification of a desirable DNA sequence.

Single cysteine mutants of Aac2p L50C, Q101C, N104C, N130C, S147C and Y211C were generated by Lisa Görs. D109C, D212C and D306C were generated by Dr Alex Hellawell.

Legend of Figure 2.2 Site-directed mutagenesis procedure adapted for use with *Lactococcus lactis* Site-directed mutagenesis was used to introduce single cysteine mutations into the *Δ2-19 cys-less aac2* gene. (**A-B**) The isolated pNZ8048 vector containing *Δ2-19 cys-less aac2* gene from *L. lactis* is transformed into *E. coli*, because introduction into *E. coli* will lead to methylation of the plasmid. The double-stranded plasmid is shown as an orange strand annealed to a green strand. The asterisks depict methylation, and the *DpnI* restriction sites are labelled. (**B-C**) The plasmid is isolated from *E. coli*, denatured to form two separate strands, and primers bind to the strands. The primers, shown as red or blue arrows, contain a mismatched segment, depicted as a black cross, which introduces the mutation into the daughter plasmid. (**C-D**) The mutated plasmid is amplified by PCR. (**D-E**) *DpnI* cleaves the methylated parental plasmid, leaving only the mutated daughter plasmid. (**E-F**) The mutated plasmid is transformed directly into *L. lactis*.

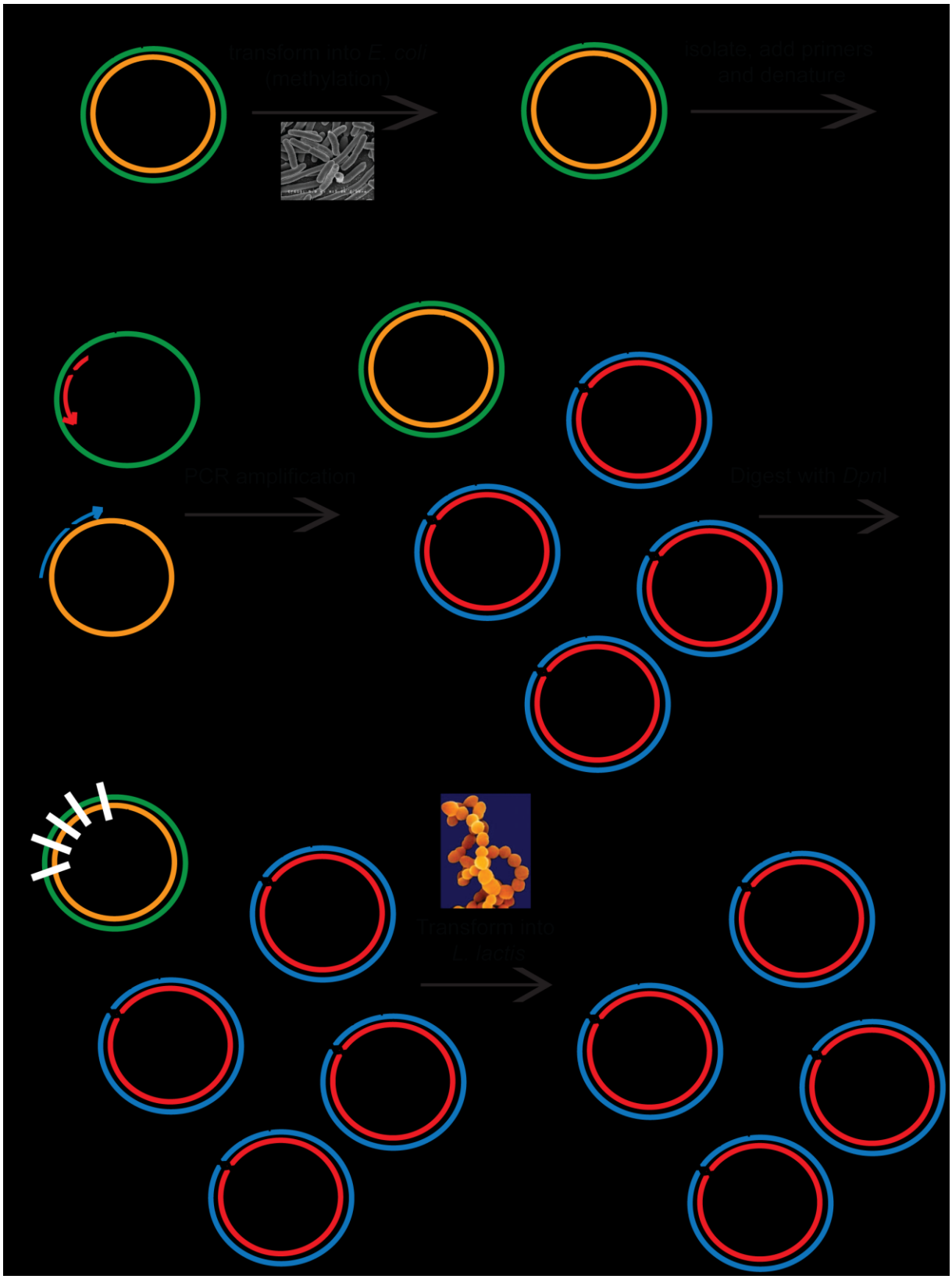

Figure 2.2 Site-directed mutagenesis procedure adapted for use with *L. lactis* For description, see previous page.

2.3.4 Restriction endonuclease digestion

Following temperature cycling, each PCR reaction mixture was treated with 40 Units of *Dpn*1 restriction endonuclease at 30°C overnight to digest the methylated parental plasmid DNA (Figure 2.2 D-E).

2.3.5 DNA precipitation

Following endonuclease digestion, Pellet Paint Co-precipitant was used to precipitate the DNA, according to the manufacturer's instructions with some modifications: 3 µl of pellet paint was added to the PCR product instead of 2 µl. Also, after 2 volumes of 100% ethanol were added, the samples were incubated for 5 min, not 2 min. The microcentrifuge spins were for 10 min instead of 5 min. Finally, the precipitated DNA was left at ambient temperature for 40 min to allow any residual ethanol to evaporate. The DNA pellet was resuspended in 10 µl of deionised water.

2.3.6 Electroporation

80 µl *E. coli* electrocompetent cells were added to 10 µl DNA and electroporated with a GenePulser II (Bio-Rad, Hercules, CA, USA) at 25 µF capacitance, resistance greater than 200 Ω, and voltage set to 2.5 kV. The cells were recovered in SOC broth for 1 h at 37°C, and then plated onto TYE+chloramphenicol plates and incubated overnight at 37°C.

50 µl of *L. lactis* electrocompetent cells were added to 10 µl DNA and electroporated with a GenePulser II as explained in the previous paragraph (Figure 2.2 E-F). 800 µl SM17 recovery broth was added to the *L. lactis* cells, and the mixture was incubated at for 2 h at 30°C. The cells were plated onto SM17+chloramphenicol+glucose plates and incubated for 2 days at 30°C.

2.3.7 Plasmid DNA extraction and cell preservation in glycerol

Individual *E. coli* colonies were isolated by using a sterile cocktail stick and added to 5 ml of 2x TY + 5 µg ml^{-1} chloramphenicol. The cultures were grown overnight at 37°C whilst shaking. The cells were preserved by mixing 500 µl cells with 500 µl 30% (v/v) glycerol and freezing in a cryotube vial (Nunc, Roskilde, Denmark) at -80°C. The remaining cells were pelleted and their plasmid DNA was extracted with a QIAprep Spin Miniprep Kit (Qiagen, Hilden, Germany) by following the manufacturer's instructions. A spectrophotometer (Nanodrop, Wilmington, DE, USA) was used to determine the plasmid DNA concentration.

Individual *L. lactis* colonies were isolated using a sterile cocktail stick and added to 5 ml of M17 + 5 µg ml^{-1} chloramphenicol + 1% (w/v) glucose. The cultures were grown overnight at 30°C. The cells were preserved by mixing 500 µl cells with 500 µl 30% (v/v) glycerol and freezing in a cryotube vial (Nunc, Roskilde, Denmark) at -80°C. The remaining cells were pelleted and their plasmid DNA was extracted with a QIAprep Spin Miniprep Kit (Qiagen, Hilden, Germany) by following the manufacturer's instructions with modifications. The cells were initially resuspended in Buffer P1 with 10 mg ml^{-1} lysozyme added and heated at 55°C for 10 min. A spectrophotometer (Nanodrop, Wilmington, DE, USA) was used to measure the plasmid DNA concentration.

2.3.8 DNA sequencing

Each plasmid was sequenced to check for the desired gene sequence (GeneService, Cambridge, UK) by alignments generated by Clustalw2 (http://www.ebi.ac.uk/Tools/clustalw2/) (Larkin *et al.*, 2007).

2.4 *Lactococcus lactis* cultures and harvesting

M17 + 5 µg ml^{-1} chloramphenicol + 1% (w/v) glucose pre-cultures were inoculated with *Lactococcus lactis* from a glycerol stock. The pre-cultures were incubated

overnight at 30°C without aeration. The confluent cells were diluted to an $A_{600\ nm}$ of 0.1 in M17 + 5 μg ml^{-1} chloramphenicol + 1% (w/v) glucose. The A_{600} nm was monitored every hour. Gene expression of Aac2p was induced at A_{600} nm of 0.4-0.6 by adding 1:10,000 spent M17 broth from strain NZ9700, a strain that secretes Nisin A. The cells were grown for 4 hr following Nisin A induction, and incubated at 20°C overnight. The next day, the cells were harvested by centrifugation at 5857 *g* for 3 min at 4°C. The cell pellets were re-suspended in phosphate-buffered saline (PBS) containing 140 mM sodium chloride, 2.7 mM potassium chloride, 8.1 mM disodium hydrogen phosphate and 1.8 mM potassium dihydrogen phosphate, pH 7.4 (Formedium Ltd., Hunstanton, UK). All PBS was prepared and autoclaved by the MRC/Wellcome Trust media kitchen (Cambridge, UK). The re-suspended cells were washed by centrifugation at 5857 *g* for 3 min at 4°C. The pellets were re-suspended in PBS to A_{600} nm of 40.0 ± 5.0, equivalent to 8.0 mg/ml total protein. The cells were used immediately or were pelleted and frozen in liquid N_2 for later use.

2.5 Labelling methods

2.5.1 Labelling of whole *Lactococcus lactis* cells with eosin-5-maleimide

If required, 200 μM bongkrekic acid (BKA) and 80 μM ADP or 200 μM carboxy-atractyloside (CATR) and 80 μM ADP were added to the cell suspension 30 min or 10 min prior to the labelling reaction, respectively. If required, AMP, ADP or ATP was added 1 min prior to the labelling reaction. The cells were incubated with 25 μM eosin-5-maleimide (Invitrogen, Eugene, OR, USA) in 1% (v/v) dimethylformamide for 10 min, whilst rolling, in the dark and at ambient temperature. Excess eosin-5-maleimide was reduced by adding 2.5 mM freshly prepared dithiothreitol (DTT) (Thermo Scientific, Rockford, IL, USA) in PBS for 30 s whilst rolling at ambient temperature. The cells were washed within 6 min by centrifugation at 16300 *g* for 1 min at ambient temperature and the pellets were resuspended in PBS containing 2.5 mM DTT. The cells were washed three more times with PBS containing 2.5 mM DTT. The cell pellets were frozen at -20°C.

2.5.2 Labelling of whole *Lactococcus lactis* cells with 1,2-ethanediyl bismethanethiosulphonate

If required, 10 µM BKA or 10 µM CATR was added to the cell suspension 30 min or 10 min prior to the further the labelling reaction, respectively. Cells were incubated with 200 µM 1,2-ethanediyl bismethanethiosulphonate (M-2-M) (Toronto Research Chemicals Inc., North York, ON, Canada) in 1% (v/v) dimethyl sulphoxide for 30 min whilst rolling at ambient temperature. Excess M-2-M was reduced by adding 10 mM *N*-ethylmaleimide (NEM) in PBS for 10 min, whilst rolling and at ambient temperature. The cells were collected by centrifugation at 3362 *g* for 5 min at 4°C, and the pellets were resuspended in PBS. The cells were washed twice more and the cell pellets were frozen at -20°C.

2.5.3 Labelling of whole *Lactococcus lactis* cells with eosin-5-maleimide and (1-Oxyl-2,2,6,6-tetramethyl-4-piperidinyl) maleimide

The cells were incubated with 25 µM (1-Oxyl-2,2,6,6-tetramethyl-4-piperidinyl) maleimide (MAL-6) (Toronto Research Chemicals Inc., North York, ON, Canada) in 0.25% (v/v) dimethyl sulphide for 10 min, whilst rolling at ambient temperature, if required. The cells were subsequently incubated with 25 µM eosin-5-maleimide in 1% (v/v) dimethylformamide for 10 min whilst rolling in the dark at ambient temperature. Excess maleimide containing compounds were reduced by adding 1 mM DTT in PBS for 30 s, whilst rolling at ambient temperature. The cells were collected by centrifugation at 16300 *g* for 1 min at ambient temperature and the pellets were resuspended in PBS containing 1 mM DTT. The cells were washed twice more and the cell pellets were frozen at -20°C.

2.6 General protein methods

2.6.1 Lysis of whole cells of *Lactococcus lactis*

Whole cells of *L. lactis* at A_{600} nm of 40.0 ± 5.0 were treated with 5 mg ml^{-1} lysozyme (BDH Laboratory Supplies, Poole, U.K.) and 5 mM ethylediaminetetraacetic acid for 10 min at 55°C. The cells were treated with 2% (w/v) *N*-lauroylsarcosine sodium salt (sarkosyl) and 2.5 mM DTT for 5 min at ambient temperature. The cells were put on ice and then subjected to 3, 10 s sonication pulses at power level 3.0, followed by 10 s breaks on a Sonicator 3000 (Misonix, Inc., Farmingdale, NY, USA). The lysed cells were mixed with 4% (w/v) sodium dodecyl sulphate (SDS) and 1.25 x sample buffer (5 x sample buffer contains 250 mM Tris HCl pH 6.8, 50% (v/v) glycerol, 10% (w/v) SDS, 10% (w/v) DTT, and 0.05% (w/v) bromophenol blue), aliquoted and frozen at -20°C.

2.6.2 Isolation of *Lactococcus lactis* membranes

The membranes of whole cells of *L. lactis* were isolated by mechanical disruption with a 2.2 kilowatt Z+ cell disrupter at 30000 psi (Constant Systems Ltd., Daventry, UK). The flow-through was centrifuged at 10800 *g* for 10 min at 4°C to separate debris and whole cells in the pellet from the broken cells in the supernatant. This step was repeated for large-scale preparations. Membranes from the supernatant were harvested by centrifugation at 138000 *g* for 30 min at 4°C. The membrane pellets were resuspended in PBS, and the centrifugation step was repeated. The pellets were resuspended in PBS to a total protein concentration of approximately 2 mg ml^{-1} and frozen at -20°C for later use in sodium dodecyl-sulphate polyacrylamide gel electrophoresis, fluorescence imaging and Western blotting. Alternatively, for large-scale preparations for use in transport assays, the isolated membranes were resuspended in PBS to a total protein concentration of approximately 5 mg ml^{-1} and stored in liquid nitrogen.

2.6.3 Estimation of protein concentration

A bicinchoninic acid (BCA) assay kit (Thermo Scientific, Rockford, IL, USA) was used to estimate the total protein concentration of each isolated membrane sample. The manufacturer's guidelines were followed. Each sample was diluted to less than 1 mg ml^{-1} and compared to a standard range of 0 to 1 mg ml^{-1} bovine serum albumin. The samples and standards were incubated on a multi-well plate in the presence of BCA and Cu^{2+}-containing reagents for 30 min at 37°C. The absorbance of Cu^{+} chelated to peptide bonds was measured at 562 nm on a Spectra max Plus spectrometer (Molecular Devices, Sunnyvale, CA, USA).

Total protein concentration of whole cells of *L. lactis* was determined by measuring A_{600} nm (A_{600} nm of 40.0 = 8.0 mg/ml total cellular protein).

2.6.4 Gel electrophoresis

Proteins were separated by sodium dodecyl sulphate-polyacrylamide gel electrophoresis (SDS-PAGE) on 15% (w/v) polyacrylamide gels. The 15% separating gels were composed of a mixture of 5 ml 30% (w/v) polyacrylamide (Severn Biotech Ltd., Kidderminster, UK), 4.8 ml 1.5 M Tris pH 8.8, 100 µl 20% (w/v) SDS, 100 µl 10% (w/v) ammonium peroxodisulphate (APS), and 10 µl N, N, N', N'-tetramethulethylene-diamine (TEMED). The 5% stacking gels were composed of a mixture of 1.7 ml 30% (w/v) polyacrylamide, 4 ml 0.5 M Tris pH 6.8, 100 µl 20% (w/v) SDS, 100 µl 10% (w/v) APS, and 10 µl TEMED. If not already pre-prepared, each lysed cell or isolated membrane protein-containing sample was mixed with sample buffer. Samples run on non-reducing gels were mixed with sample buffer lacking DTT. The proteins were separated on gels for 90 min at 30 mA in electrophoresis buffer (190 mM glycine, 25 mM Tris HCl, 0.1% (w/v) SDS).

2.6.5 Fluorescence imaging and quantification

Eosin-5-maleimide treated proteins separated on SDS-PAGE gels were analysed using a Typhoon 9410 Variable Mode Imager (Amersham Biosciences, Little

Chalfont, UK). The gel was scanned in the fluorescence mode with excitation at 532 nm and an emission filter at 560 nm, 600-740 V, 50 microns. After scanning, the same gel was used for Western blotting, if required. Densitometry estimates were measured using ImageQuant version 5.2 (Amersham Biosciences, Little Chalfont, UK).

2.6.6 Western blotting and quantification

Lysed cell and isolated membrane protein-containing samples separated on SDS-PAGE gels were blotted to determine Aac2p expression. Chromatography paper (Whatman, Maidstone, UK) was soaked in transfer buffer (192 mM glycine, 25 mM Tris HCl pH 8.3, 10% (v/v) methanol). Immobilon-P polyvinylidene fluoride (PVDF) membranes (Millipore, Bedford, MA, USA) were activated in methanol for 30 s and rinsed in transfer buffer before use. The PVDF membranes and SDS-PAGE gels were stacked between chromatography paper. The protein samples were transferred from the SDS-PAGE gels to the PVDF membranes in an ECL Semi-dry Transfer Unit (Amersham Biosciences, Piscataway, NJ, USA) at 120 mA at a maximum voltage at 16 V. The membranes were washed twice for 30 s in 25 ml Tris-buffered saline (TBS) (25 mM Tris HCl at pH 8.0, 145 mM NaCl, 16 mM KCl). The membranes were incubated for 1 hr at ambient temperature in 25 ml blocking buffer (1x TBS, 5% (w/v) Marvell skimmed milk powder, 0.4% (v/v) Tween 20). Chick α-AAC primary antibody (AgriSera, Vännäs, Sweden) with a sequence specificity of CYPLDTVRRRMMMT was added at a 1:25000 dilution in blocking buffer for 1 hr at ambient temperature. The membranes were washed twice for 30 s in 25 ml blocking buffer, and then twice for 10 min in 25 ml blocking buffer. A rabbit α-chick IgY horseradish peroxidase conjugate was added at a 1:25000 dilution in blocking buffer for 1 hr. This step was followed by the wash step described previously. The membranes were kept in 1x TBS. Each membrane was exposed to 10 ml Enhanced Chemiluminescence (ECL) Western blotting and detection reagents (GE Healthcare, Little Chalfont, UK) for 1 min, or to 5 ml ECL Prime Western blotting and detection reagents (GE Healthcare, Little Chalfont, UK). Chemiluminescent light was detected with a Photon Imaging Systems x-ray film processor (Swindon, UK), or alternatively, with a Bio-rad molecular imager Chemidoc XRS+ Imaging System (Bio-rad Laboratories, Inc.,

Hemel Hempstead, UK). Bands were quantified using Image Lab, version 3.0 (Bio-rad Laboratories, Inc., Hemel Hempstead, UK).

2.6.7 Coomassie gel staining

SDS-PAGE separated proteins were visualised on gels stained in Coomassie Brilliant Blue (50% (v/v) methanol, 10% (v/v) acetic acid, 0.1% (w/v) Coomassie Brilliant Blue R250) for 1 hr. The gels were destained with 2, 30 min incubations with 15% (v/v) methanol, 10% (v/v) acetic acid.

2.7 Transport Assays

2.7.1 Fused *Lactococcus lactis* membrane preparation

Liposomes were prepared as a 3:1 mass ratio of *E. coli* polar lipid extract (20 mg ml^{-1} in chloroform) and egg yolk phosphatidylcholine (20 mg ml^{-1} in chloroform). The lipids were warmed to ambient temperature, mixed in glass and shaken over N_2 gas to aid in chloroform evaporation. The lipids were resuspended in PBS at 20 mg ml^{-1} and homogenised before being stored in liquid nitrogen.

Liposomes and isolated *L. lactis* membranes were thawed to ambient temperature. The fused *L. lactis* membranes were prepared from 5 mg liposomes, 1 mg isolated *L. lactis* membranes, 5 mM ADP at pH 7.0, 10 µM BKA (if required), 10 µM CATR (if required) and PBS, to get a total volume of 1 ml. The *L. lactis* membranes were fused by freezing in liquid N_2 and thawing at ambient temperature for six cycles, and then stored in liquid N_2.

The fused *L. lactis* membranes were thawed to ambient temperature and extruded 11 times through a 1.0 µm polycarbonate filter (Avanti Polar Lipids Inc., Alabaster, AL, USA). The fused membranes were centrifuged at 300000 *g* for 30 min, 4°C. The pellet was resuspended in PBS containing 5 mM ADP at pH 7.0 and 10 µM BKA or CATR (if required). The solution was added to a poly-prep chromatography column

(Bio-Rad, Hercules, CA, USA) containing sephadex G-75 (Sigma-Aldrich, Steinheim, Germany), eluted and used immediately.

2.7.2 Fused *Lactococcus lactis* membrane transport assays

Transport assays were performed on a Hamilton Microlab Star robot (Bonaduz, GR, Switzerland) at ambient temperature. Fused *L. lactis* membranes were pipetted into individual wells on a 0.45 µm mixed cellulose ester filter plate (Millipore, Carrigtwohill, Ireland) before the assay. To inhibit the carrier 15 µM BKA or 15 µM CATR was added to 100 µl fused *L. lactis* membranes 30 min and 10 min, respectively, before 100 µl [^{14}C]-ADP at a final concentration of 1.34 µM (60 mCi mmol^{-1} = 2.22 GBq mmol^{-1}) was added. The transport assay was terminated at 5, 15, 30, 65, 125, 245 and 485 s by vacuum filtration, and then the addition of 200 µl cold PBS. 200 µl Microscint 20 (PerkinElmer, Shelton, CT, USA) was added to each well of the filter plate. After each filter was dissolved, the radioactivity was measured in a TopCount NXT Microplate Scintillation & Luminescence Counter (PerkinElmer, Shelton, CT, USA).

2.7.3 Whole cells of *Lactococcus lactis* transport assays

Transport assays were performed on a Hamilton Microlab Star robot (Bonaduz, GR, Switzerland) at ambient temperature. 50 µl of whole cells of *L. lactis* at A_{600} nm of 2.0 were pipetted into individual wells on a 0.45 µm mixed cellulose ester filter plate (Millipore, Carrigtwohill, Ireland) before the assay. If required, 10 µM BKA or 10 µM CATR was added to cells 30 min or 10 min, respectively, prior to the start of uptake. If required, 25 µM eosin-5-maleimide was added to cells 10 min prior to the start of uptake. To commence uptake, 200 µl [^{14}C]-ADP at a final concentration of 4.0 µM (60 mCi mmol^{-1} = 2.22 GBq mmol^{-1}) was added. The transport assay was terminated at 10, 20, 30, 60, 180 and 300 s by vacuum filtration, and then the addition of 2 washes of 200 µl cold PBS. 200 µl Microscint 20 (PerkinElmer, Shelton, CT, USA) was added to each well of the filter plate. After each filter was dissolved overnight, the radioactivity was measured in a TopCount NXT Microplate Scintillation &

Luminescence Counter (PerkinElmer, Shelton, CT, USA). Unless indicated otherwise, transport assays were conducted in whole cells as in Section 2.7.3.

Whole cells of *L. lactis* at $A_{600\ nm}$ of 1.0 were used for manual transport assays. To inhibit the carrier, 10 µM BKA or 10 µM CATR was added to 500 µl cells 30 min or 10 min, respectively, before 500 µl 1.34 µM [^{14}C]-ADP (60 mCi mmol^{-1} = 2.22 GBq mmol^{-1}) was added. The transport assay was terminated at 20 s, 1 min, 2 min, 3 min and 5 min by addition of 2 ml cold PBS and filtering of cells by a 0.45 µm cellulose nitrate filter using a vaccuum manifold with a second 2 ml cold PBS wash. 2 ml Ultima Gold AB liquid scintillant (Packard Biosciences, Perkin Elmer, Waltham, MA, USA) was added to each filter. After each filter was dissolved overnight, the radioactivity was measured in a Tri-Carb 2800TR Liquid Scintillation Analyser (PerkinElmer, Downers Grove, IL, USA).

2.8 Mass spectrometry

AAC bands from Coomassie-stained SDS-PAGE gels were excised. The proteins were digested with trypsin and the resulting peptide digests were analysed using a 4800 matrix-assisted laser desorption/ionization – time of flight – time of flight (MALDI-TOF-TOF) mass spectrometer (Applied Biosystems, Carlsbad, CA, USA) by Dr Kamburapola Jayawardena. The peptide masses and fragment ion masses from tandem mass spectrometry were compared with the Swis-Prot sequence database. Potential cross-linked peptides' masses were calculated using MassLynx (Waters, Ltd., Elstree, UK).

2.9 Electron paramagnetic resonance spectroscopy

Electron paramagnetic resonance (EPR) spectroscopy was performed by Dr Jessica van Wonderen (Centre for Molecular and Structural Biochemistry, School of Biological Sciences, University of East Anglia, Norwich, UK). Whole cells of *L. lactis* were labelled with (1-Oxyl-2,2,5,5-tetramethyl-Δ3-pyrroline-3-methyl) methanethiosulphonate (MTSL) or (1-Oxyl-2,2,6,6-tetramethyl-4-piperidinyl) maleimide (MAL-6). The labelled cells were washed several times in PBS, and then

oxidised with potassium ferricyanide. The samples were analysed with X-band (9.6 GHz) continuous wave EPR at ambient temperature. The spectra were collected on a Bruker EleXsys 500 spectrometer fitted with a ER4123D loop-gas resonator, and the individual samples were housed in 0.6 mm id x 0.84 mm od quartz. The parameters were set to 2 mW microwave power, 1 Gauss modulation amplitude, 100 kHz modulation frequency and 8-32 scans.

Chapter 3 Transport activity of single cysteine mutants of the ADP/ATP carrier

3.1 General introduction

The final aim of this thesis is to probe conformational changes of the mitochondrial ADP/ATP carrier by probing single cysteines with thiol-specific fluorescent probes (Chapter 5). The reasoning for the selection of particular mutations is first given by revisiting the main functional features of mitochondrial carriers. Mitochondrial carriers contain three repeats of approximately 100 amino acids in length (Saraste & Walker, 1982; Walker & Runswick, 1993). They have a conserved signature motif of acidic and basic residues on α-helixes H1, H3 and H5, PX[DE]XX[KR] (Figure 1.14). The charged residues of the motif were shown to form a salt bridge network closing off the matrix side of the carrier by selection of second-site revertants and by the structure of the CATR-inhibited ADP/ATP carrier (Nelson *et al.*, 1998; Pebay-Peyroula *et al.*, 2003). By comparing symmetry-related residues, a conserved salt bridge network has been identified on α-helices H2, H4 and H6 with the sequence [FY][DE]XX[KR] (Robinson *et al.*, 2008) (Figure 1.15). The cytoplasmic motif is believed to function similarly to the matrix motif, since both are both highly conserved and contain positively and negatively charged residues with the ability to form ionic pairs (Robinson *et al.*, 2008). As a structure of the inhibited c-state is available, it would be worthwhile to probe the residues of the putative cytoplasmic salt bridge network in different inhibited states to see if their accessibility changes. To gain a more thorough understanding, symmetry-related residues were chosen either side of the cytoplasmic network on the even-numbered helices too (Figure 1.15). Another central question is what happens to the residues on the odd-numbered α-helices on the cytoplasmic side when the carrier changes transport state and thus they were selected, too, taking symmetry into account (Figure 1.14). In this chapter, the transport activity of single cysteine mutants of Aac2p will be assessed in whole cells of *L. lactis*.

3.2 Expression of Δ2-19 cysteine-less Aac2p

To introduce single cysteine mutations, a suitable *L. lactis* host strain needed to be engineered to express functional yeast Aac2p to high levels. First, residues 2-19 were removed using PCR to form Δ2-19 Aac2p, which is known to increase the expression level and transport rate of Aac2p (Monné *et al.*, 2005) (Section 1.8.2 and Figure 1.18). Wild type Aac2p has four cysteines; C73 and C271 found in matrix loops h12 and h56, and C244 and C288 found in in α-helix H5 and H6 (Figure 3.1). These were mutated to alanine to remove non-specific sites for thiol-specific probes (see Chapter 5). The final Δ2-19 cys-less Aac2p is 300 amino acids long and has a molecular mass of 32.5 kDa. As a control, Δ2-19 Aac2p was also expressed in the membranes of *L. lactis.*

The expression level of Δ2-19 Aac2p was 1.4-fold greater than Δ2-19 cys-less Aac2p (Figure 3.2 A), as determined by Western blot quantification, but the specific initial [^{14}C]-ADP uptake rate in whole cells was similar within error (Figure 3.2 B). The ADP uptake for both Δ2-19 Aac2p and Δ2-19 cys-less Aac2p was fully inhibited by 10 μM CATR and to ~85% by 10 μM BKA (Figure 3.14 and Figure 3.16). Taken together, the expression and transport data show that cysteines are not required for ADP transport, and that the function of the Δ2-19 cys-less Aac2p carrier is not compromised by the truncation and replacement of the native cysteines with alanines. The activity of cys-less Aac2p expressed in yeast mitochondria has been previously shown to be comparable to the wild type protein (Hatanaka *et al.*, 2001; Bamber, Harding, *et al.*, 2007a).

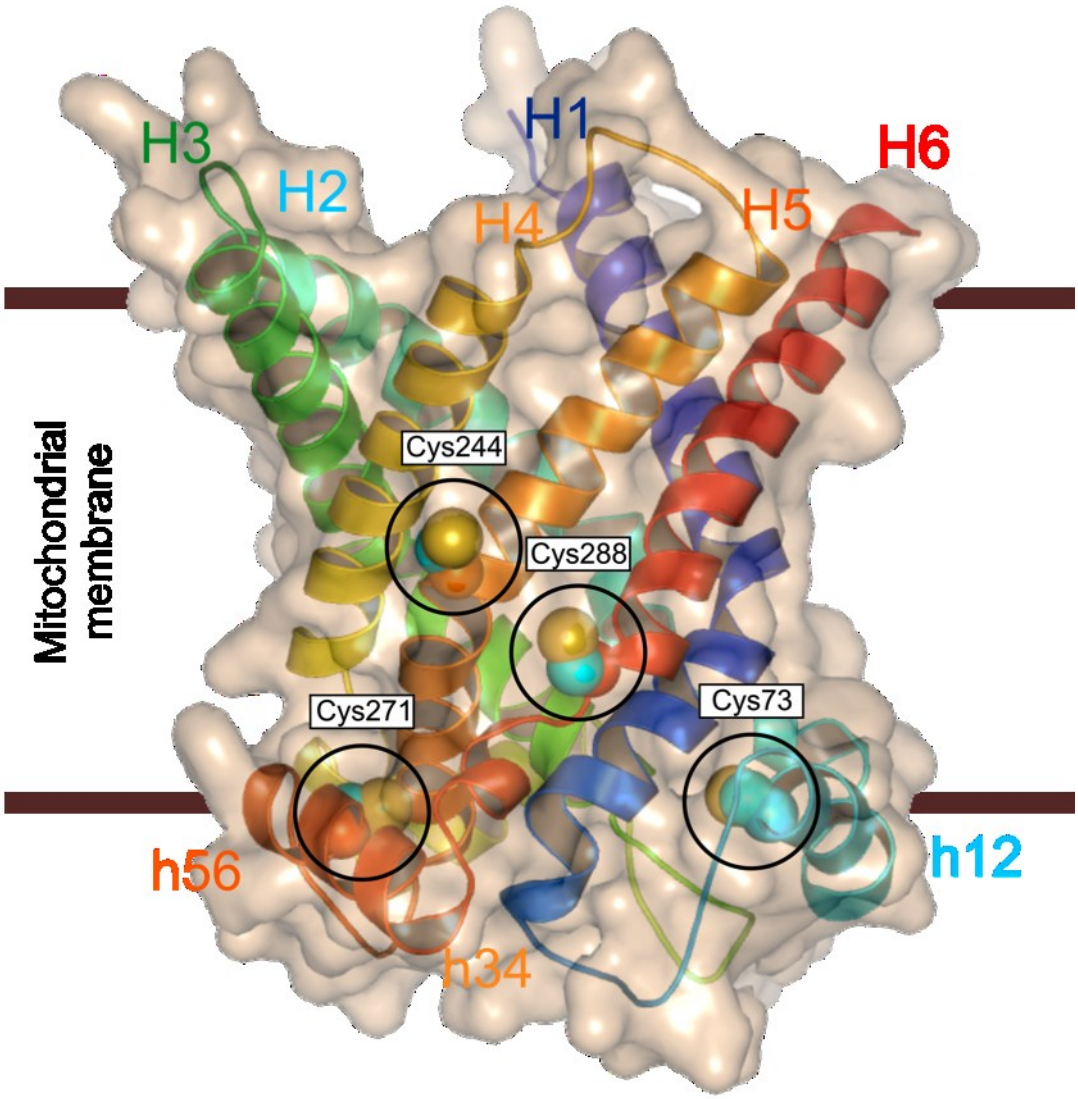

Figure 3.1 Cysteines in Aac2p. This Aac2p model is based on the CATR-inhibited bovine AAC1 structure (PDB code 1OKC) (Pebay-Peyroula *et al.*, 2003). The sequence alignment and comparative model were generated by Dr Alan Robinson. α-helix 1 (H1) is dark blue, α-helix 2 (H2) is teal, α-helix 3 (H3) is dark green, α-helix 4 (H4) is yellow, α-helix 5 (H5) is orange and α-helix 6 (H6) is red. Matrix helix 12 (h12) is light blue, matrix helix 34 (h34) is pea green and matrix helix 56 is orange-red. Cysteines are shown as spheres and are highlighted with a black circle. This figure was created by Dr Edmund R.S. Kunji.

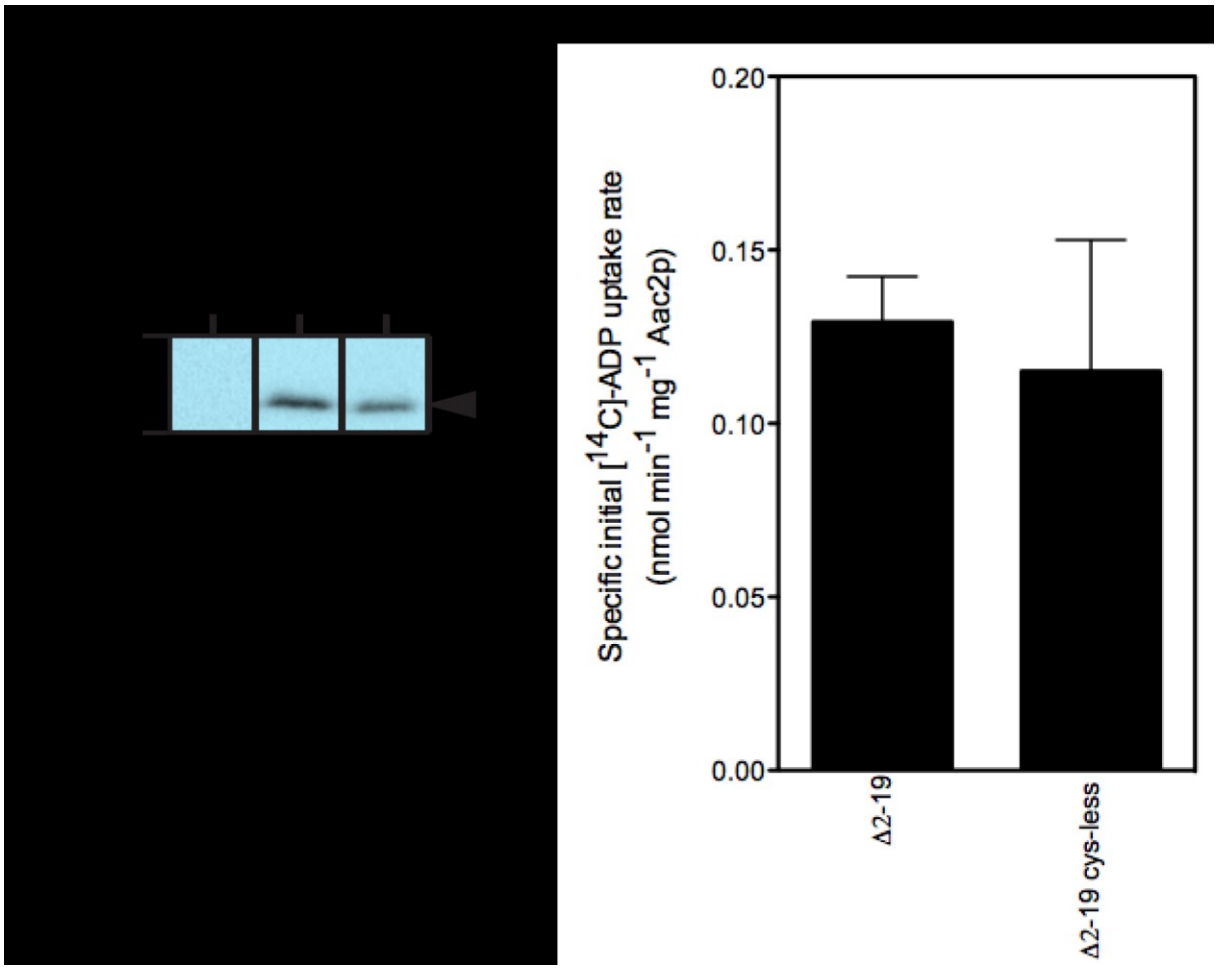

Figure 3.2 Expression and transport activity of Δ2-19 Aac2p and Δ2-19 cys-less Aac2p in *L. lactis*. (A) Western blot analysis of Δ2-19 and Δ2-19 cys-less Aac2p expressed in whole cells of *L. lactis* and lysed by lysosyme. A representative blot segment in shown. See Figure 3.8 for legend details. **(B)** Specific initial [^{14}C]-ADP uptake rate for Δ2-19 and Δ2-19 cys-less Aac2p into whole cells. The rates were calculated using linear regression from 0 to 300 s, including subtraction of the empty vector. The average and standard deviation (*n*=3) are shown.

3.3 Site-directed mutagenesis for the generation of single cysteine mutants of Aac2p

To study the involvement of particular residues in transport, single cysteine replacements were introduced at chosen sites in the *S. cerevisiae* ADP/ATP carrier isoform 2 (Aac2p). A novel site-directed mutagenesis procedure was employed to introduce the mutations into the plasmid vector for *L. lactis* (Figure 2.2). In the typical site-directed mutagenesis procedure, a mutation is introduced by PCR amplifying a mutation-containing DNA primer using a parental plasmid template. Following PCR

amplification, the parental plasmid is digested by *DpnI*, a restriction enzyme that specifically cleaves methylated DNA, leaving only the mutated DNA for transformation into a bacterial host. To maintain plasmid selectivity, the parental plasmid must be methylated before PCR amplification. Here, the parental plasmid was extracted from *L. lactis*, which lacks specific DNA methyltransferases (Dr Edmund R. S. Kunji, personal communication). To overcome this, the parental plasmid was transformed into and extracted from *E. coli* to obtain a methylated parental plasmid, which could be readily digested following the generation of single cysteine mutations.

It was necessary to establish the ability of the restriction enzyme, *DpnI*, to digest the 4275 base pair (bp) pNZ8048 vector containing the *Δ2-19 cys-less aac2* gene. Figure 3.3 shows that the untreated vector migrated the same distance (single band equivalent to 4275 bp) by agarose gel electrophoresis, regardless of which bacterium (*L. lactis* or *E. coli*) the vector was extracted from. When *L. lactis* and *E. coli*-extracted vector was digested with *NcoI* and *SacI,* restriction enzymes that cut DNA regardless of methylation status, both vector fragments were the same size. *NcoI* and *SacI* digest at either end of the *Δ2-19 cys-less aac2* gene, resulting in two bands of approximately 3306 bp (corresponding to the empty vector) and 969 bp (*Δ2-19 cys-less aac2* gene). The *DpnI* digestion of *L. lactis* and *E. coli*-extracted vector resulted in different migration distances and number of bands. For *L. lactis* +*DpnI,* a single band of 4275 bp is visible, suggesting that *DpnI* does not digest the vector. For *E. coli* +*DpnI*, five bands of 3144, 411, 351, 189 and 180 bp are visible, proving that *DpnI* did digest the vector extracted from *E. coli*. All of these bands can be viewed on the agarose gel, but the 189 and 180 bp bands cannot be distinguished because they are too similar in size. The control established that *E. coli* methylates its DNA, but that *L. lactis* does not significantly. Consequently, the parental plasmid was extracted from *E. coli* prior to use in the mutagenesis procedure.

With this modification of the site-directed mutagenesis procedure, 38 single cysteine mutants of *S. cerevisiae* Aac2p were generated. The numbering used is identical for the wild type Aac2p; the Δ2-19 truncation was not taken into account. Each mutant is named by the single-letter amino acid code of the residue prior to mutation, followed by the residue number, followed by the amino acid mutation. For example,

glutamate 120 mutated to cysteine is E120C. Symmetry-related residues predicted to be located on the cytoplasmic side of the cavity were mutated (Table 3.1). The Triplet ID is listed for each triplet in the table, and they correspond to the Triplet IDs in Figures 1.14 and 1.15. Q101C, N104C, N130C and Y211C Aac2p were generated by Lisa Görs. D109C, D212C and D306C Aac2p were generated previously by Dr Alex Hellawell.

The mutant proteins of the cytoplasmic side of the cavity are shown (Figure 3.4). A sub-set of mutant proteins of the cytoplasmic side of the cavity is highlighted as these are predicted to be important for function. The proposed cytoplasmic salt bridge was also mutated (Figure 3.5 A and B), as was the part of the CATR binding-site (Figure 3.5 C and D).

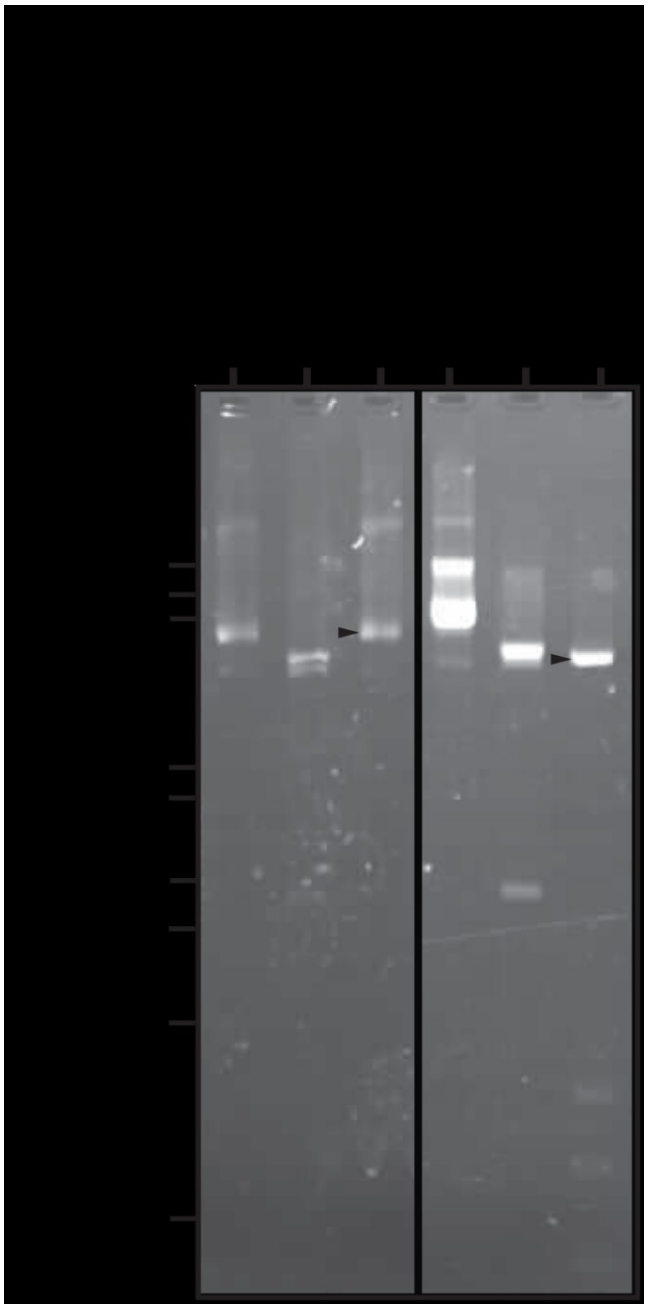

Figure 3.3 Comparison, by agarose gel electrophoresis, of plasmid DNA after extraction from *L. lactis* and *E. coli* and digestion by *DpnI*. pNZ8048 vector containing the *Δ2-19 cys-less aac2* gene was electroporated into *L. lactis* and *E. coli*, and then extracted by miniprep. The labels *L. lactis* or *E.coli,* respectively, indicate that the pNZ8048 vector was extracted from *L. lactis* or *E. coli*. The plasmid was not treated, digested with *NcoI* and *SacI*, or digested with *DpnI*. DNA was separated on a 1.0% agarose gel. DNA bands were visualised by ultraviolet light detection of ethidium bromide. The bands indicated with arrowheads highlight the different migration distances of pNZ8048 vector extracted from *L. lactis* (4275 bp fragment) or *E. coli* (3144 bp fragment, also, no arrowheads shown for 411, 351, 189 and 180 bp fragments), and digested with *DpnI*. The vertical line represents an excised portion of the gel.

Table 3.1 Mutations introduced into the odd and even α-helices in the cavity of Aac2p.

Triplet ID	α-helix H1	α-helix H3	α-helix H5	predicted topology
	N22C	W126C	S226C	adjacent to cytoplasmic salt bridge
10	D26C	N130C	S230C	cavity
14	G30C	G134C	G234C	cavity
18	A34C	G138C	T238C	cavity

Triplet ID	α-helix H2	α-helix H4	α-helix H6	predicted topology
83	T100C	Y203C	G298C	cavity
84	Q101C	R204C	A299C	cavity
87	N104C	Y207C	V301C	cavity
88	F105C	F208C	I302C	cavity
91	K108C	Y211C	Y305C	cavity
92	D109C[a]	D212C[a]	D306C[a]	cavity, cytoplasmic salt bridge
95	K112C	K215C	Q309C	cavity, cytoplasmic salt bridge
96	A113C	P216C		inter-helical
97	M114C	L217C	I311C	lipid bilayer

[a]Gifts of Dr Alex Hellawell.

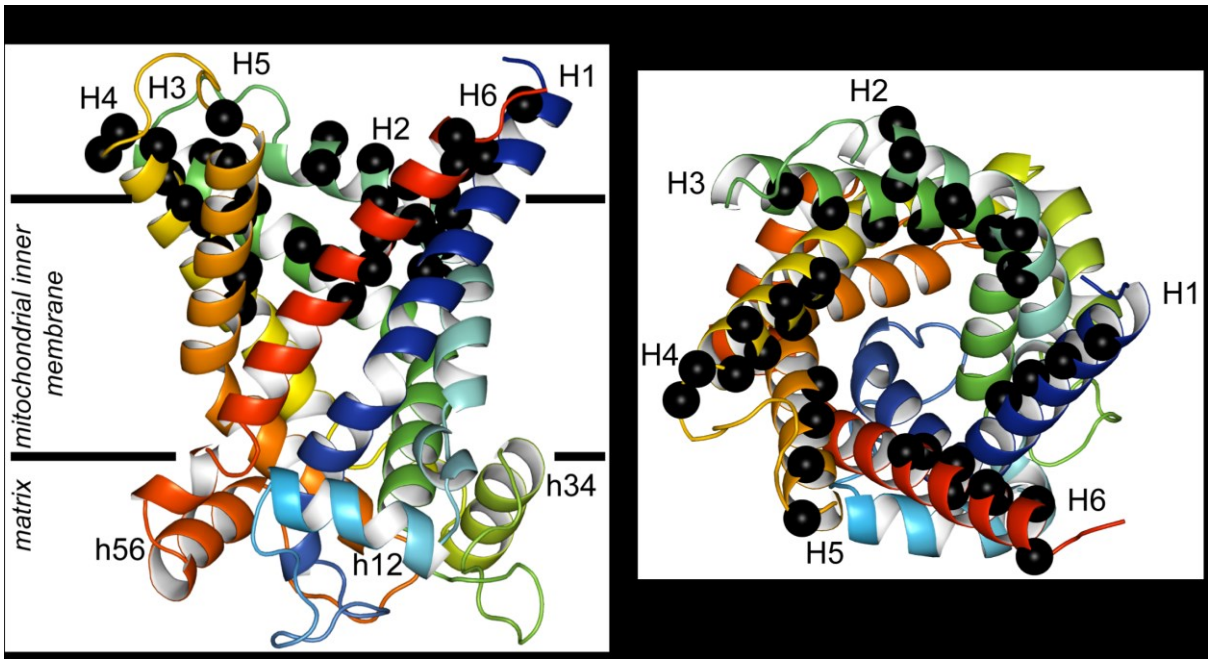

Figure 3.4 Single cysteine mutations in the cavity of Aac2p. This Aac2p model is based on the CATR-inhibited bovine AAC1 structure (PDB code 1OKC) (Pebay-Peyroula *et al.*, 2003). The sequence alignment and comparative model was created by Dr Alan Robinson, and subsequently modified by the addition of two residues to the C-terminus. α-helix 1 (H1) is dark blue, α-helix 2 (H2) is teal, α-helix 3 (H3) is dark green, α-helix 4 (H4) is yellow, α-helix 5 (H5) is orange and α-helix 6 (H6) is red. Matrix helix 12 (h12) is light blue, matrix helix 34 (h34) is pea green and matrix helix 56 is orange-red. The parallel black bars represent the approximate boundaries of the membrane. Each cysteine mutation is shown as a single black sphere centred on its α-carbon. See Table 3.1 for a list of the individual mutations. **(A)** The lateral view and **(B)** the cytoplasmic view of the cavity.

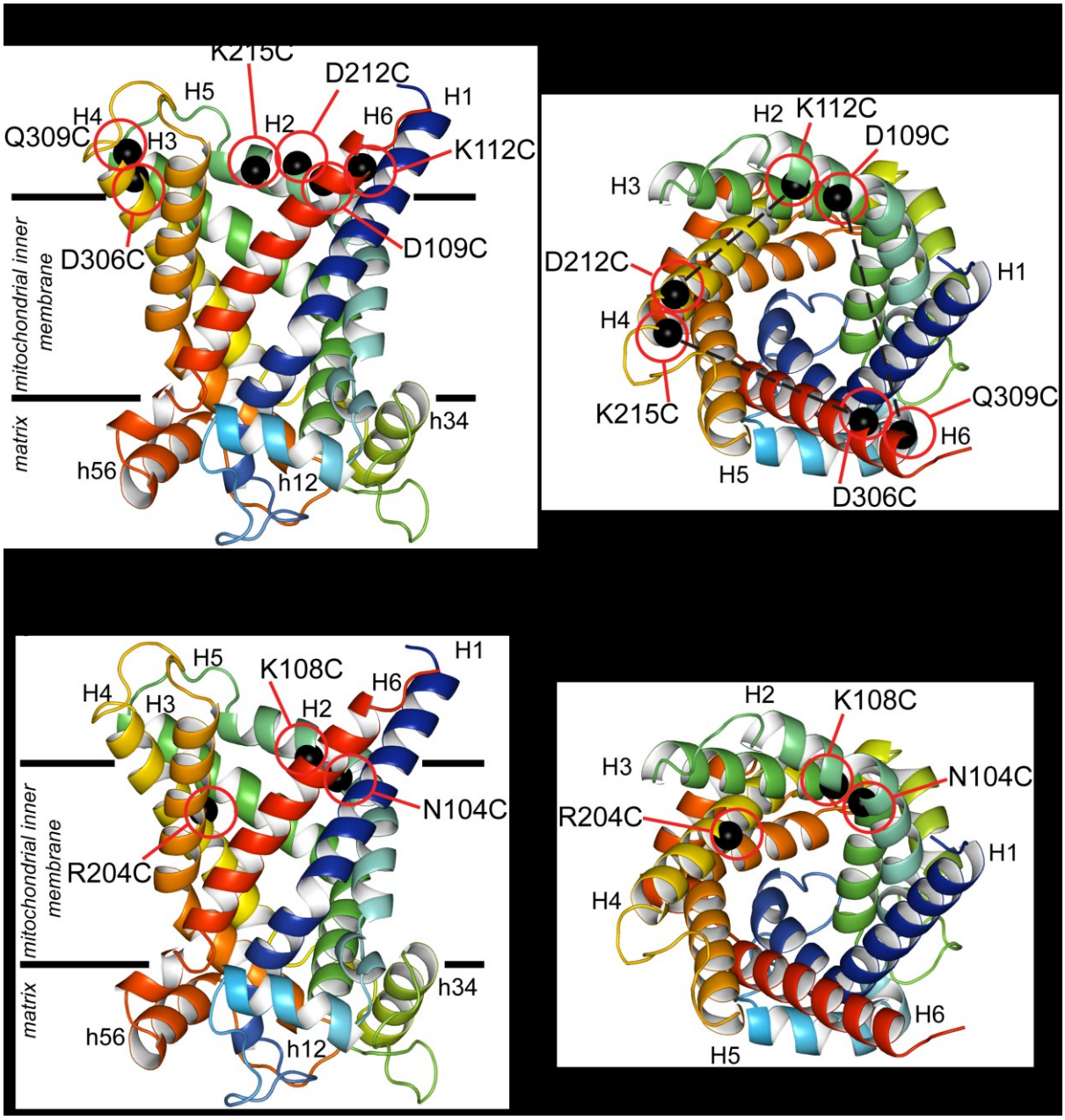

Figure 3.5 Sub-set of single cysteine mutations in the cavity of Aac2p. For details, see Figure 3.4. Each cysteine mutation is shown as a single black sphere centred on the α-carbon, and highlighted by a red circle. Individual mutations are labelled. **(A)** The lateral view of mutations to the cytoplasmic salt bridge and **(B)** the cytoplasmic view of the cavity depicting mutations to the cytoplasmic salt bridge. The dashed black lines depict predicted electrostatic salt bridge or ionic interactions. **(C)** The lateral view of mutations to the CATR binding site and **(D)** the cytoplasmic view of the cavity depicting mutations to the CATR binding site.

3.4 Expression level of single cysteine mutants

The single cysteine mutants of Δ2-19 cys-less Aac2p were expressed in whole cells of *L. lactis*. To determine the expression levels of the mutant proteins, membranes need to be isolated by disruption and centrifugation, but this is a lengthy procedure. Isolation of membranes is normally required as *L. lactis* has a thick peptidoglycan layer that prevents lysis by detergents, such as SDS. A new technique to lyse whole cells was developed from a procedure originally pioneered by Dr John Mifsud. *L. lactis* cells were concentrated to an A_{600} nm of 40 (8.0 mg/ml protein) to concentrate the expressed Aac2p. The cells were treated with 10 mg/ml lysozyme to hydrolyse the peptidoglycan cell wall. Finally, the cells were treated with one of the three procedures outlined in Figure 3.6. First, sonication was used to make the samples more homogeneous for loading accurately onto SDS-PAGE gels. The sonication treatment did not completely lyse the cells, as evinced by the diffused Aac2p bands on the Western blot (Figure 3.6). Second, sarkosyl addition followed by sonication and DNAase addition was tested. Sarkosyl is a detergent often used to lyse *E. coli* and DNAse lyses released DNA following cell lysis, which makes the sample viscous, and thus it should help to homogenise the samples. Both the combined treatments with and without DNAse worked well; the samples were homogeneous, easier to pipette and resulted in sharper bands on a Western blot (Figure 3.6). Consequently, the combined treatment without DNAase was used for all subsequent cell lysis because it was the minimal procedure.

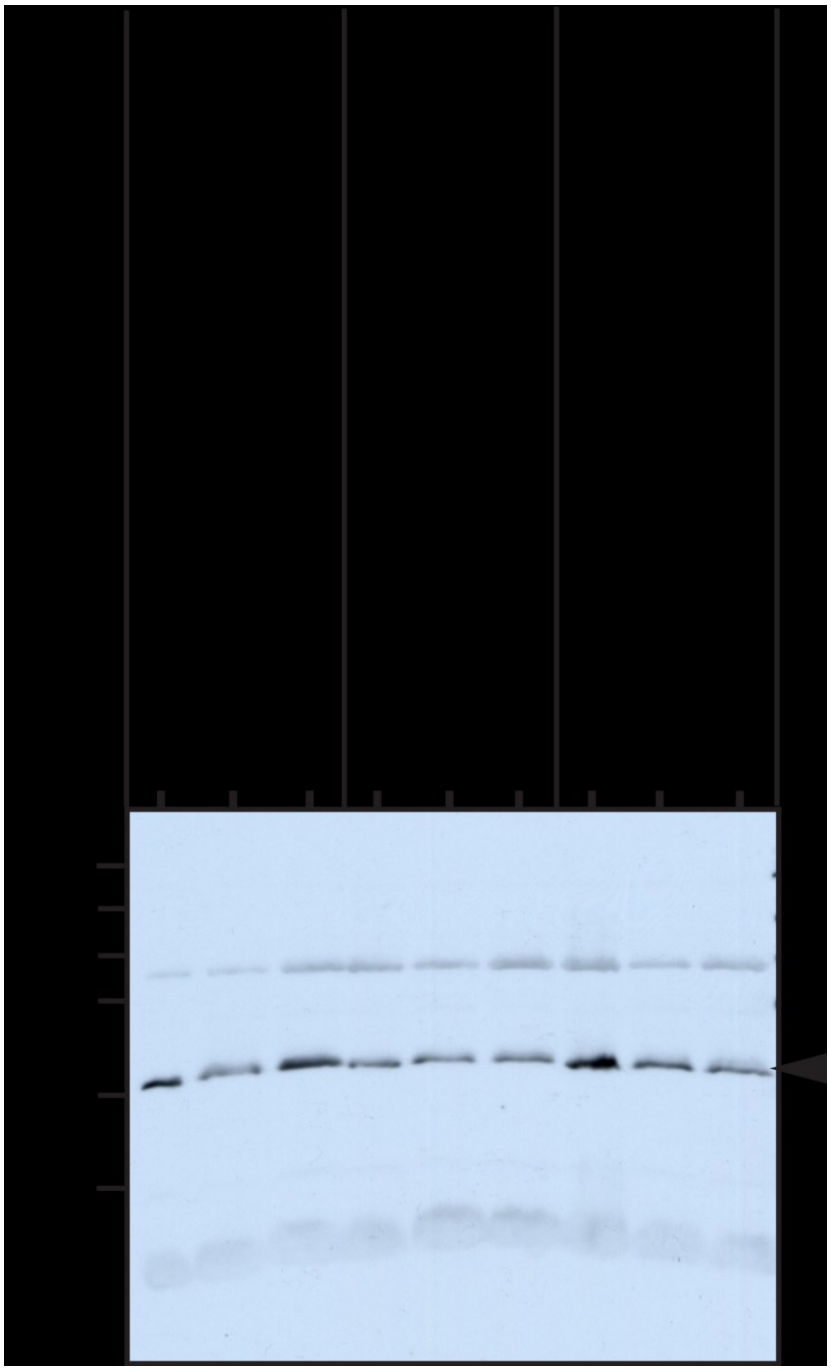

Figure 3.6 Western blot analysis of Δ2-19 cys-less, M114C and T243C Aac2p to optimise cell lysis. The antibody used to probe expression is directed against α-helix H5 of Aac2p. *L. lactis* expressing mutant Aac2p was treated with 10 mg/ml lysozyme at 55°C followed by sonication, or by sonication and sarkosyl treatment with or without DNAse treatment. The band for Aac2p is indicated by a black arrowhead. 30 µg total cellular protein was loaded per lane. Imaged on X-ray film.

Following the lysis of *L. lactis* cells expressing single cysteine mutants of Aac2p, the samples were separated by SDS-PAGE and the signals quantified using Western blotting. The primary antibody used to target Aac2p was raised in chickens against the peptide sequence CYPLDTVRRRMMMT, which is found on α-helix H5. This peptide includes the RRRMMM AAC signature motif, found in the bottom of the cavity in Aac2p. As there are no mutations that affect this site (Table 3.1), the antibody is suitable for accurately quantifying protein yields using densitometry.

An example Western blot and quantification are depicted in Figure 3.7. The bands for Aac2p have a molecular mass of 32.5 kDa (Figure 3.7 A). There is only one background band (~40 kDa), and there is no evidence of protein degradation, suggesting the antibody is specific and the protein is not degraded.

To quantify Aac2p expression levels in whole cells, a dilution series of standards was employed (Figure 3.7 A). Purified *S. cerevisiae* Aac2p was kindly donated by Dr Jonathan Ruprecht, and its concentration was accurately determined by amino acid composition analysis (Protein & Nucleic Acid Chemistry Facility, Department of Biochemistry, Cambridge, UK). Four different amounts of Aac2p standards were loaded per gel and a standard curve (Figure 3.7 B) was generated by densitometry. These data were subsequently used to estimate the expression levels of single cysteine mutants of Aac2p. An example of the quantification of the expression levels is shown in Table 3.2 for the data in Figure 3.7 A and the standard curve in Figure 3.7 B.

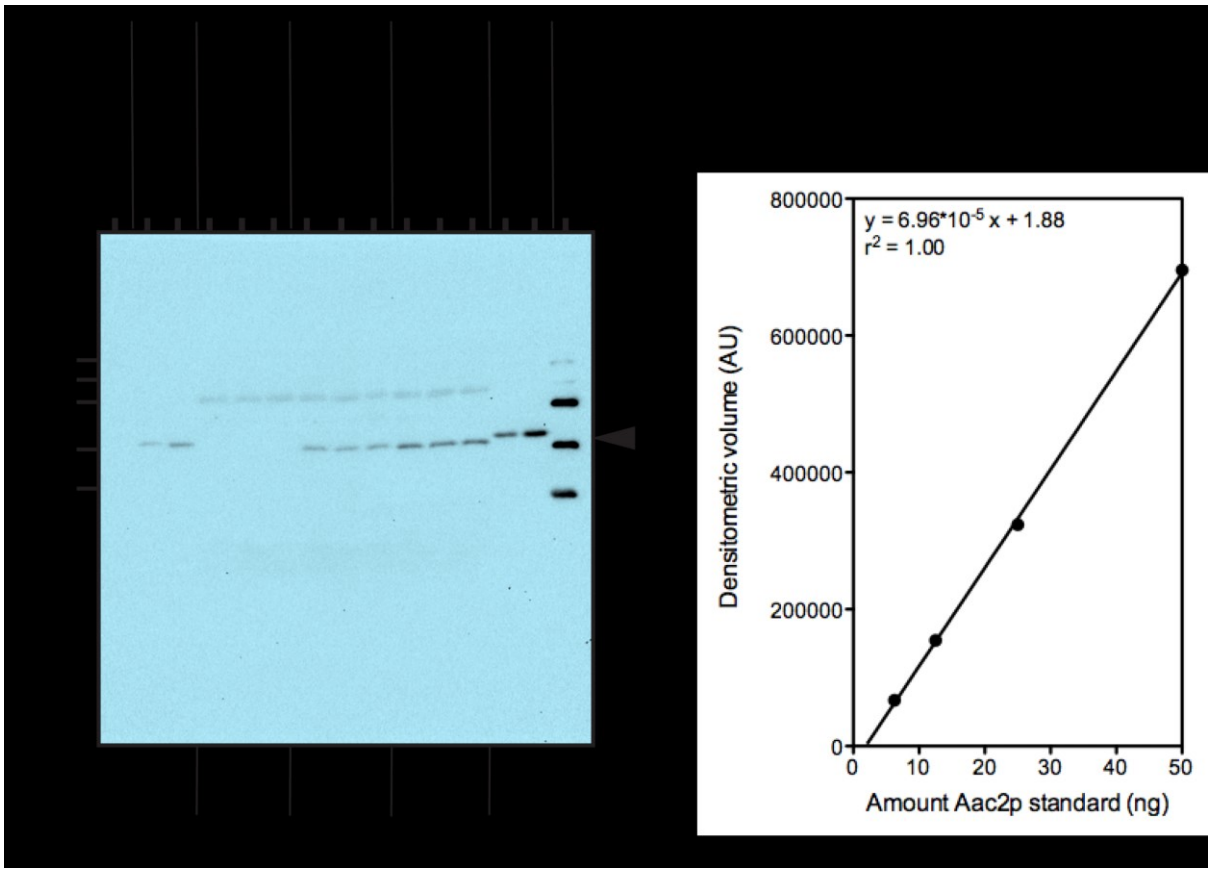

Figure 3.7 Expression and quantification of empty vector, A113C and P216C Aac2p. (A) Western blot analysis of A113C and P216C mutants expressed in *L. lactis* and lysed by lysozyme. The antibody used to probe expression is directed against α-helix H5 of Aac2p. Quantified amounts of purified *S. cerevisiae* Aac2p are used as standards. The bands for Aac2p are indicated by a black arrowhead. 22.5 µg total cellular protein was loaded per lane. Imaged using Chemi-doc XRS+. The total signals were quantified using Image Lab (*n*=3). The amount of Aac2p was calculated using the standard curve shown in (B). **(B)** Linear regression of the 6.25, 12.5, 25.0 and 50.0 ng purified Aac2p standards shown in (A).

Table 3.2 The quantification of Aac2p mutants and the empty vector background.

Aac2p	Densitometric volume (AU)	Calculated amount Aac2p (ng)
Empty vector	3575	2.13
Empty vector	7200	2.38
Empty vector	8875	2.50
A113C	133300	11.2
A113C	119275	10.2
A113C	136150	11.4
P216C	264940	20.3
P216C	251264	19.4
P216C	290948	22.1

All 38 mutant Aac2p Western blot signals and signals from the empty vector, Δ2-19 and Δ2-19 cys-less Aac2p were imaged and quantified in triplicate (Figure 3.8). Although all single cysteine mutants of Aac2p were expressed, it was found that the levels of expression varied, most more than two-fold lower than the Δ2-19 cys-less Aac2p. The introduction of mutations may have had an impact on membrane targeting and insertion by the Sec translocase system. D26C and A34C Aac2p were exceptions, as they expressed 1.6-fold higher or similar to Δ2-19 cys-less Aac2p, respectively (Figure 3.8). Also, they were the only mutant proteins that led to growth defects upon induction of expression (data not shown). The mutations were to cavity residues on α-helix H1 and they might have improved the recognition and insertion of transmembrane α-helix H1 by the Sec translocase. For a more detailed discussion, see Section 4.4.

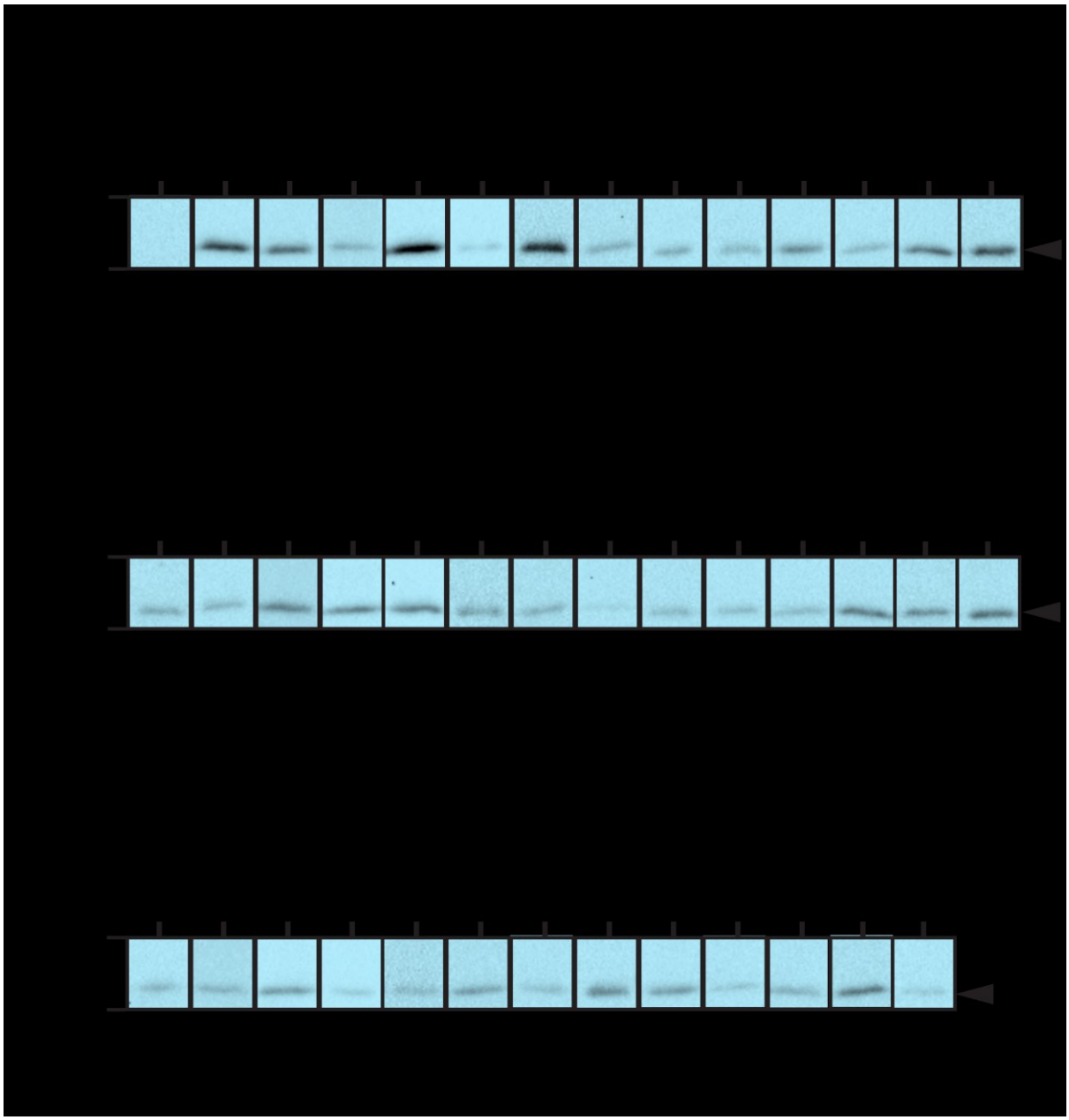

Figure 3.8 Expression and quantification of single cysteine mutants of Aac2p. Western blot analysis of Δ2-19 cys-less mutants expressed in whole cells of *L. lactis* and lysed by lysozyme. The primary antibody is directed against α-helix H5 of Aac2p. The bands for Aac2p are indicated by a black arrowhead. 22.5 µg total cellular protein was loaded per lane, prepared as described in Section 2.6.1. Imaged for 360-600 s using Chemi-doc XRS+. The total amounts were quantified by Image Lab after subtraction of the empty vector background. The data are represented by the average and standard deviation (*n*=3). A representative blot segment in shown. An example of an intact Western blot is shown in Figure 3.7.

3.5 Specific initial uptake rates of single cysteine mutants in *Lactococcus lactis*

3.5.1 Effect of single cysteine mutations on transport

The transport of ADP catalysed by single cysteine mutants of Aac2p was measured in whole cells of *L. lactis*, whose intracellular pools of adenine nucleotides can be exchanged with externally added [^{14}C]-ADP. A Hamilton microlab star robot was programmed to assay the time-dependent uptake of [^{14}C]-ADP. First, cells were added to a filter plate and the uptake was started by the addition of [^{14}C]-ADP after defined periods of time. After the last addition the filtration started, which corresponded approximately to the zero time point. However, it was clear that uptake had still occurred, as the filtration step was too slow in separating the cells from the externally added [^{14}C]-ADP (data not shown). To shorten the filtration step, the vacuum was improved by optimising the filtration pump and vacuum tubing plus the filtration was started 2 s prior to the last addition. The uptake of [^{14}C]-ADP by Δ2-19 cys-less and S222C Aac2p was linear over the measured time period with an apparent start at -30 s instead of -60 s (Figure 3.9), and thus provided a better estimate of the initial rate.

Using the improved uptake protocols, ADP uptake by mutant Aac2p was measured. It was found that most of the mutants containing single cysteines at the top of the cavity transported at higher specific initial uptake rates than Δ2-19 cys-less Aac2p (Figure 3.10), but not consistently. Mutants containing single cysteines close to the centre of the cavity transported at rates lower than Δ2-19 cys-less Aac2p or not at all. In general, mutations introduced to residues close to the entrance of the cavity, near the cytoplasmic loops, had a less detrimental effect on the transport rate than those close to the centre of the cavity (Figure 3.10 B-C). The mutations nearer the centre of the cavity are closer to the proposed substrate binding site also found there, and many of these residues are functionally important. Residues close to the cytoplasmic loops may be less important for the function of the carrier than residues close to the centre of the cavity.

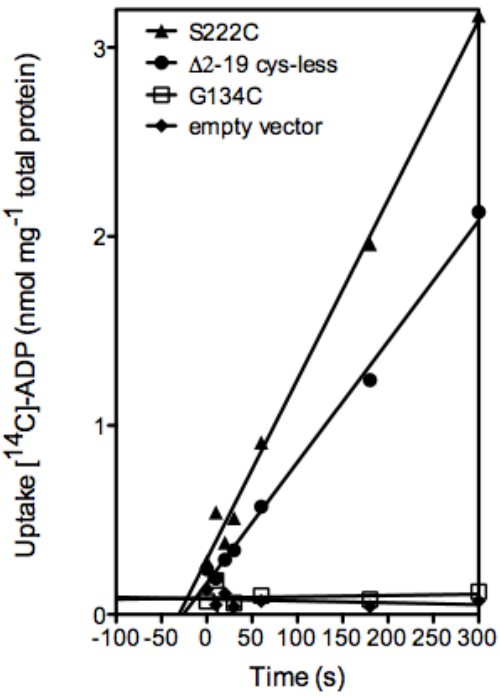

Figure 3.9 Activity of Aac2p assayed by robot. Time curves of [^{14}C]-ADP uptake into whole cells of *L. lactis* by S222C Aac2p (filled triangles), Δ2-19 cys-less Aac2p (filled circles), G134C Aac2p (open squares) and empty vector (filled diamonds). The time points were fitted using linear regression.

It was unexpected that many of the mutant Aac2p containing single cysteines near the entrance to the cavity would have a higher specific initial uptake rate compared to Δ2-19 cys-less Aac2p, as one would expect mutations to interfere with the structure and decrease transport efficiency. The specific activity takes into account the amount of expressed Aac2p (Figure 3.8), but not the insertion or folding efficiency for each mutant. It is possible that certain mutations improve the insertion and folding properties of the expressed protein. It is not possible to discriminated between misfolded and folded protein, but this caveat is always an issue with mutagenesis work. Here, expression in whole cells was monitored, but it might have been more advantageous to measure expression in isolated membranes because only proteins inserted into the membrane are isolated. Furthermore, it is possible that different mutant Aac2p have different intracellular adenine nucleotide levels, which could have affected the overall rate of transport.

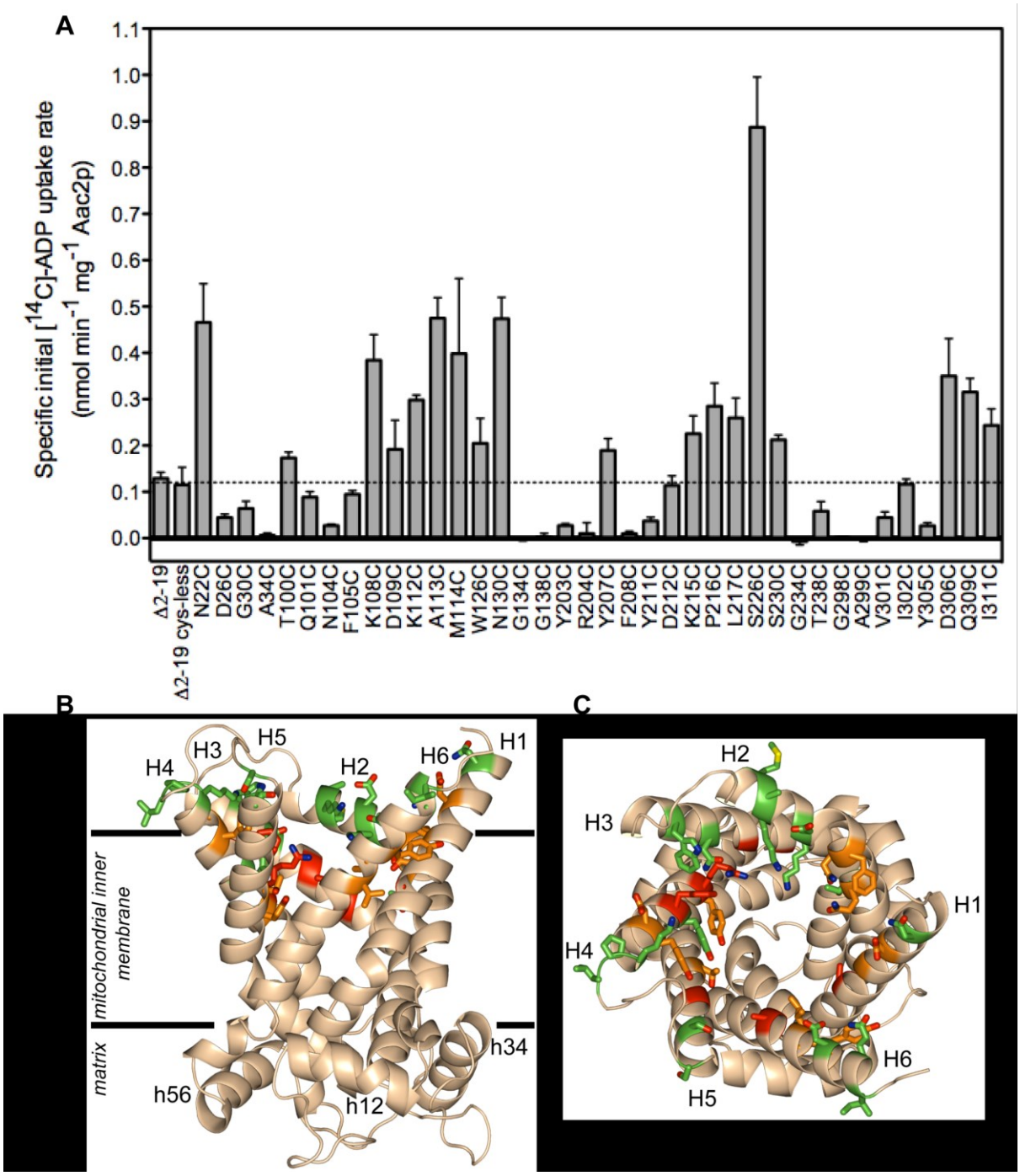

Figure 3.10 Specific initial ADP uptake rates of mutant Aac2p containing single cysteines introduced in the cavity. For legend, see next page.

Legend of Figure 3.10 Specific initial [^{14}C]-ADP uptake rates of mutant Aac2p containing single cysteines introduced in the cavity. (A) The data are represented by the average and standard deviation (*n*=3). **(B)** The lateral view of Aac2p is a visual representation of the data for mutant Aac2p shown in (A). The comparative model was generated by Dr Alan Robinson based on the AAC1 structure (PDB code 1OKC) (Pebay-Peyroula *et al.*, 2003), and modified by the addition of two residues to the C-terminus. The parallel black bars represent the boundaries of the membrane. Each residue that was mutated to a cysteine is shown in stick representation. Mutant Aac2p transporting at an average rate higher than Δ2-19 cys-less Aac2p are coloured green, those transporting at an average rate lower than Δ2-19 cys-less Aac2p are coloured orange and those that do not transport significantly above background (Student's *t*-test, unequal variance, $P<0.05$) are coloured red. See Table 3.1 for a list of individual mutations and Appendix II for individual mutant statistics. **(C)** As B, but viewed toward the cavity from the cytoplasmic side.

One intriguing outcome was that single mutations of the cytoplasmic salt bridge or ionic pair residues D109C, K112C, D212C, K215C, D306C and Q309C did not affect the transport capability as their mutant Aac2p had equal or higher transport rates than Δ2-19 cys-less Aac2p (Figure 3.11). This possibility had been anticipated when the cytoplasmic salt bridge network was discovered on the basis of symmetry analysis (Robinson *et al.*, 2008). With a single mutation, two out of three salt bridges or ionic pairs can still form and thus it should not have a significant effect on the function. The only aspect that might be affected is the exchange ratio of imported and exported nucleotide, as a weaker network may allow net import of adenine nucleotides, but this aspect was not studied. Another effect might have been on the integrity of the proton motive force, as the mutation may have caused a leak, leading to a lower energy barrier for uptake of charged nucleotides.

Of those mutated residues predicted to be involved in CATR binding, R204C Aac2p did not transport at rates significantly above the background and N104C Aac2p transported at a rate lower than the Δ2-19 cys-less Aac2p (Figure 3.12), whereas K108C Aac2p transported at a higher rate than Δ2-19 cys-less Aac2p. In Section 3.5.2, the level of inhibition by CATR for N104C and K108C Aac2p will be discussed.

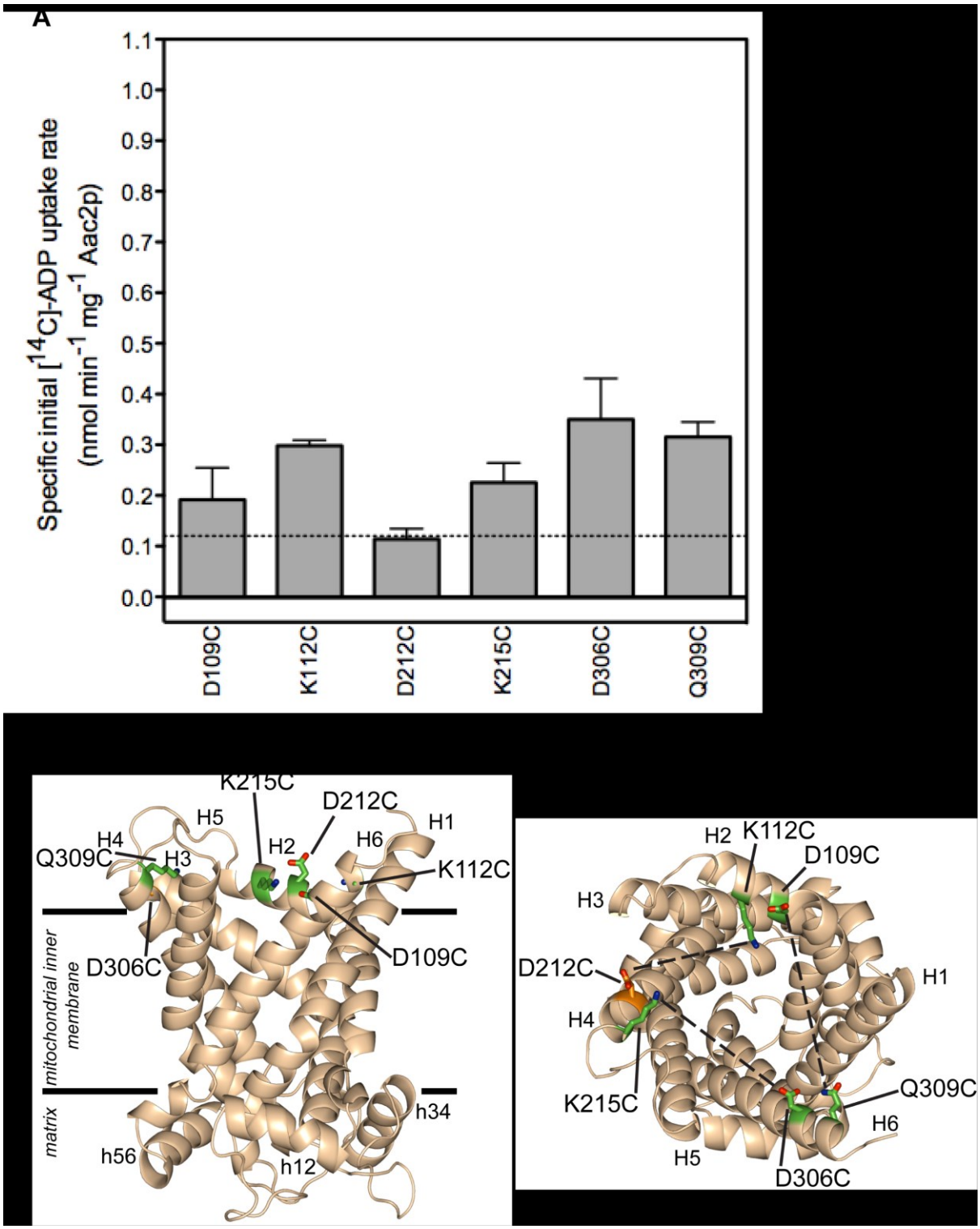

Figure 3.11 Specific initial ADP uptake rates of Aac2p with single cysteine mutations of the cytoplasmic salt bridge residues. See Figure 3.10 for legend details. In **(B and C)** individual mutations are labelled. In (C), the dashed lines show the electrostatic and hydrogen bonding interactions of the proposed cytoplasmic salt bridge network and ionic pair hydrogen bonding interactions if they were to form in the m-state.

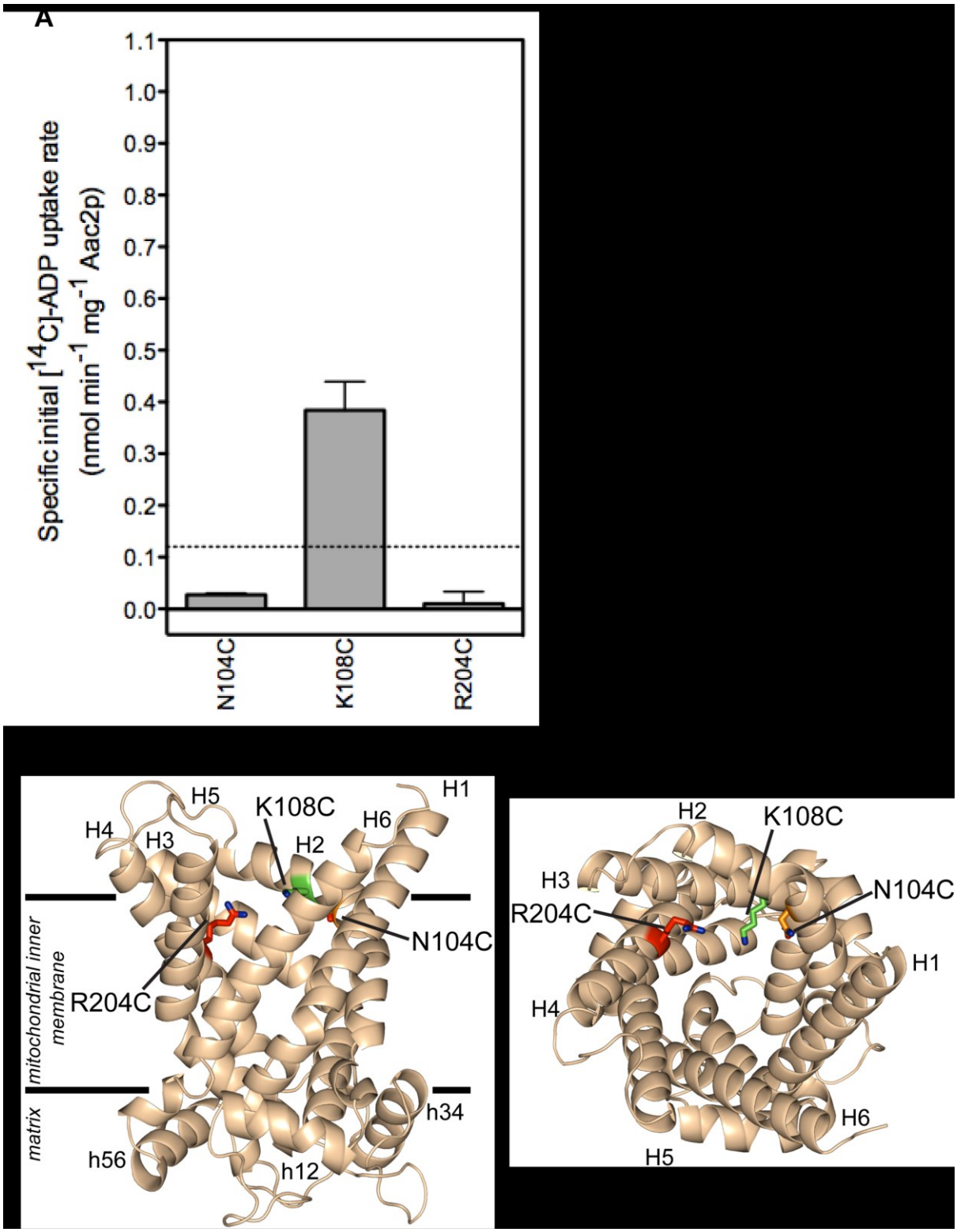

Figure 3.12 Specific initial ADP uptake rates of Aac2p with single cysteine mutations of residues involved in carboxy-atractyloside binding. See Figure 3.10 for legend details. In **(B and C)** individual mutations are labelled.

The single cysteine mutant Y203C Aac2p had a specific initial uptake rate that was ~20% of the specific initial uptake rate of Δ2-19 cys-less Aac2p and its uptake was significantly above background (Figure 3.10 and Appendix II). Y203 is located toward the centre of the cavity on α-helix H4, and based on sequence analysis (Robinson & Kunji, 2006; Robinson *et al.*, 2008) and molecular dynamics simulations (Dehez *et al.*, 2008; Wang & Tajkhorshid, 2008), it has been proposed to be part of contact point II for the adenine moiety together with G199 and I200 (Section 1.6 and Figure 1.10). The observation that the transport activity was severely compromised supports this theory.

Of the mutations introduced to residues in the cavity, A34C, G134C, G138C, R204C, F208C, G234C, G298C and A299C Aac2p did not transport at rates significantly above background levels (Figure 3.13), based on a one-tailed and unpaired Student's *t*-test, correcting for unequal variance ($P<0.05$) (Appendix II). Of all the glycine to cysteine mutants, only G30C Aac2p was competent in transport (Figure 3.10 A), although this was only 40% inhibited by BKA (see below) (Figure 3.16). G30, G134, G138 and G234 are highly conserved residues of the mitochondrial carrier family (Figure 1.14 and Table 3.1, triplet IDs 14 and 18) forming a GXXXG motif, which is thought to facilitate inter-helical interactions during the transport cycle (Y. Liu *et al.*, 2002; Schneider & Engelman, 2004; Robinson *et al.*, 2008). Similarly, alanine to cysteine mutations also led to the abolishment of transport as A34C and A299C Aac2p did not transport significantly (Figure 3.13 A), which may be for the same structural and functional reasons.

Of all the mutations to aromatic residues (F105C, W126C, Y203C, Y207C, F208C, Y211C, Y305C), only the F208C mutation caused transport abolition (Figures 3.10 A and 3.13 A). Bulky aromatic residues can close large areas efficiently, for example during the closure of the carrier, but they can also be important for folding and structural stability (Lanzarotti *et al.*, 2011). The only critical aromatic residue F208 is located on α-helix H4 (Figure 3.13 C) and it might be involved in the closure of the cytoplasmic side of the carrier in the m-state.

Finally, the R204C mutation on α-helix H4 of Aac2p abolished transport (Figure 3.13). This positively charged residue is located close to the binding site, so it may be crucial for binding the negatively charged phosphates of ADP and ATP during the transport cycle, but not in the c-state (Dehez *et al.*, 2008; Wang & Tajkhorshid, 2008). Alternatively, the very low expression levels (~10% of Δ2-19 cys-less Aac2p, Figure 3.8) could have precluded the accurate measurement of transport.

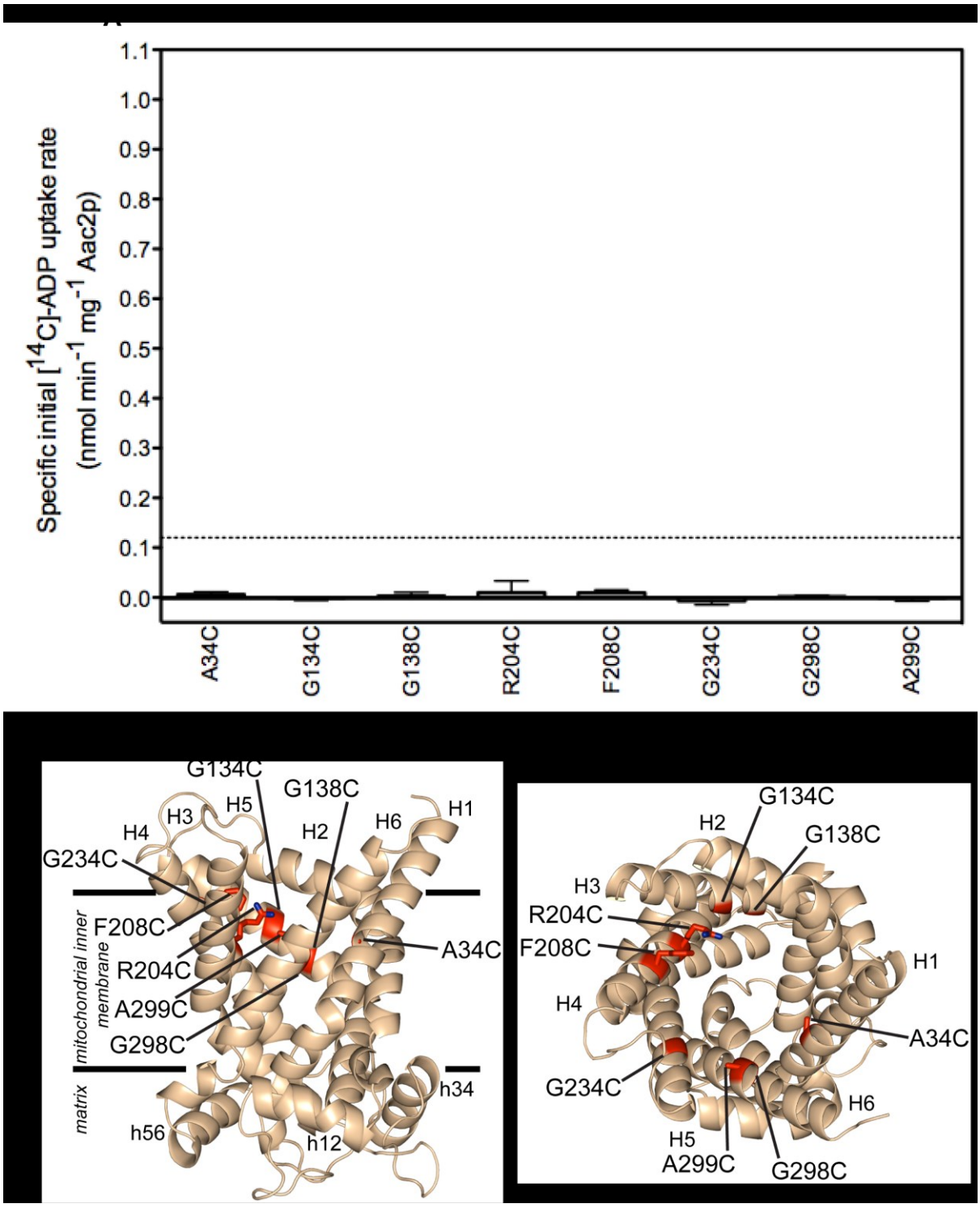

Figure 3.13 Specific initial ADP uptake rates by single cysteine mutants that do not transport significantly above background. See Figure 3.10 for legend details.

3.5.2 Effect of carboxy-atractyloside and bongkrekic acid

Both CATR and BKA are specific inhibitors of the ADP/ATP carrier that lock the carrier protein in the c-state and m-state, respectively (Buchanan *et al.*, 1976). The transport activity was determined for all the single cysteine replacement mutants in the presence of the two inhibitors. Both inhibitors should fully inhibit the activity of single cysteine mutants of Aac2p if the mutations do not interfere with inhibition. The effects of the two inhibitors could not be determined for mutant Aac2p that did not transport significantly above background.

The specific initial [^{14}C]-ADP uptake rate by Δ2-19 cys-less Aac2p in *L. lactis* was completely inhibited by CATR (Figure 3.14). Inhibition that was not significantly different than or was significantly greater the inhibition of Δ2-19 cys-less Aac2p was observed for all mutants that are competent in transport, and for the Δ2-19 Aac2p control. These results show that all of the single cysteine mutants of Aac2p can be locked in the inhibited c-state. Since the inhibition by CATR was complete, all of the transport activity could be attributed to the Aac2p mutant carriers.

The transport of N104C and K108C Aac2p, the mutations of which are located near the top of the CATR binding site, were both significantly inhibited by CATR (Figure 3.12 and Figure 3.14). This was unexpected because N104 and K108 are two of the three residues that are thought to bind to the sulphate moieties of the glycosidic ring of CATR (Section 1.4.2 and Figure 1.9). Although inhibition is not significantly different than Δ2-19 cys-less Aac2p, the average inhibition of N104C is ~88 % (Figure 3.14). CATR binds to many other residues, including R96, K108, R204 and R252 with polar interactions and these residues seem to be sufficient for CATR potency.

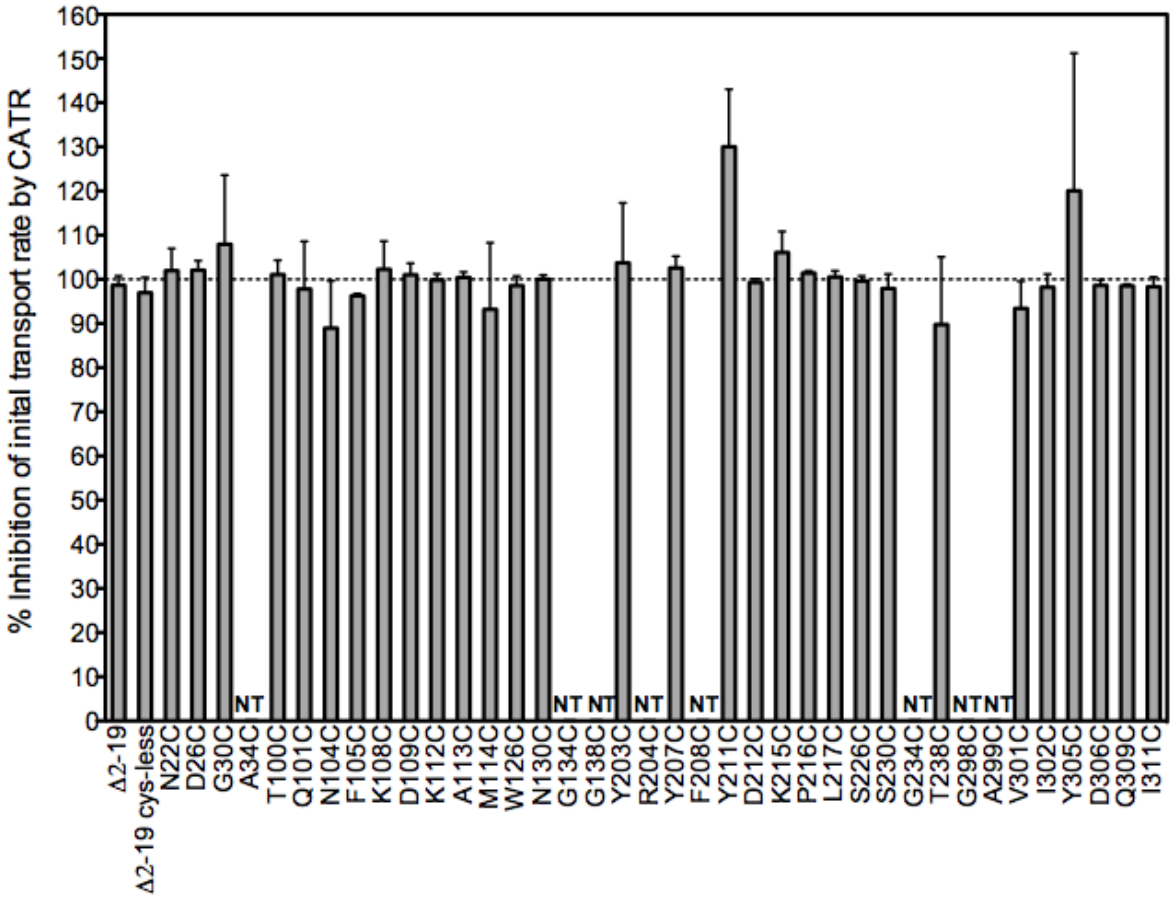

Figure 3.14 Percentage of inhibition of the specific initial ADP uptake rate by carboxyatractyloside of single cysteine mutants of Aac2p. The percentage of inhibition in the presence of CATR is relative to the specific initial uptake rate in the absence of inhibitor (Figure 3.10). Mutant proteins that did not transport significantly above background (A34C, G134C, G138C, F208C, G234C, G298C and A299C Aac2p) are labelled with NT for 'not transporting' (Figure 3.13). 10 μM CATR was added 10 min before the start of the uptakes. The data are represented by the average and standard deviation (n=3). An unpaired, two-tailed Student's t-test assuming unequal variance (P<0.05) was used to determine that none of the mutant Aac2p were inhibited significantly lower than Δ2-19 cys-less Aac2p (see Appendix II for individual mutant statistics).

Unlike CATR inhibition, BKA inhibition is dependent on various factors, such as temperature, pH, timing of addition and amount of addition (Henderson & Lardy, 1970; Henderson *et al.*, 1970; Kemp *et al.*, 1970; Klingenberg *et al.*, 1970). BKA needs to be protonated to cross the membrane, and then needs to be deprotonated in order to bind to the matrix side of Aac2p, locking it in the m-state. It was therefore necessary to optimise BKA inhibition conditions for the transport assays. The *L. lactis* cells were treated with BKA at ambient temperature and the pH of the cells in PBS buffer was 7.1. It was demonstrated that BKA inhibited Δ2-19 cys-less Aac2p transport to different degrees, depending on the concentration of BKA and when it was added (Figure 3.15). The initial transport rate of Δ2-19 cys-less Aac2p was ~90% inhibited when the cells were pre-incubated with 10 μM BKA for 30 min and when 10 μM BKA was also present during transport (Figure 3.15 B). When BKA was added only during the pre-incubation step or during transport, the percentage of inhibition was ~60-70%. Interestingly, inhibition was further improved when 50 μM BKA was added instead of 10 μM BKA, but the same trends were observed for the timing of the addition (Figure 3.15 B). Therefore, BKA inhibits ADP transport in *L. lactis* most efficiently when it is present during the pre-incubation step and the transport assay. The 30 min incubation time may be necessary to give BKA time to protonate to cross the membrane and then to deprotonate to bind to Aac2p. A high BKA concentration might be required because the dissociation rate of BKA is high. It is also clear that BKA requires time to inhibit fully, necessitating the need for a pre-incubation step. This is best demonstrated by the observation that when BKA is added only at the start of the transport assay (open diamonds, Figure 3.15), inactivation is achieved after three min.

With the optimised inhibition conditions (10 μM BKA pre-incubation and 10 μM BKA during transport), BKA was found to inhibit the specific transport of single cysteine mutants of Aac2p to varying extents (Figure 3.16). Inhibition ranged from ~40% to 100% of the specific initial uptake rate, whereas Δ2-19 cys-less Aac2p was inhibited to ~85%. This percentage inhibition agrees well with the ~90% inhibition of Δ2-19 cys-less Aac2p by 20 μM BKA reported by Dr Alex Hellawell (PhD dissertation, 2010). Most of the single cysteine mutants of Aac2p were not inhibited significantly different than the Δ2-19 cys-less Aac2p, suggesting that the single cysteine

mutations did not interfere with inhibition (Student's *t*-test (P<0.05)) (Figure 3.16 and Appendix II).

These results confirm that most of these mutant carriers can be locked in the inhibited m-state, however, Aac2p mutants N104C, Y203C and D212C were inhibited significantly lower than Δ2-19 cys-less Aac2p (Figure 3.14), denoted by asterisk, P<0.05). In addition, G30C Aac2p was inhibited less than 50% and Y211C, T238C and Y305C Aac2p were inhibited less than 75% (Figure 3.14). For all of these mutants, it is not clear that they can be locked in the m-state by the addition of BKA. In support of this observation, it was noted that the single cysteines of these mutant proteins had a different accessibility to thiol-specific fluorescent probes in the presence of BKA than those that can be inhibited well (data not shown). It is currently unclear why some of these mutants are less susceptible to BKA inhibition than others. They may partially prevent the binding of BKA by direct interactions or by interfering with the formation of the m-state to which BKA can bind well.

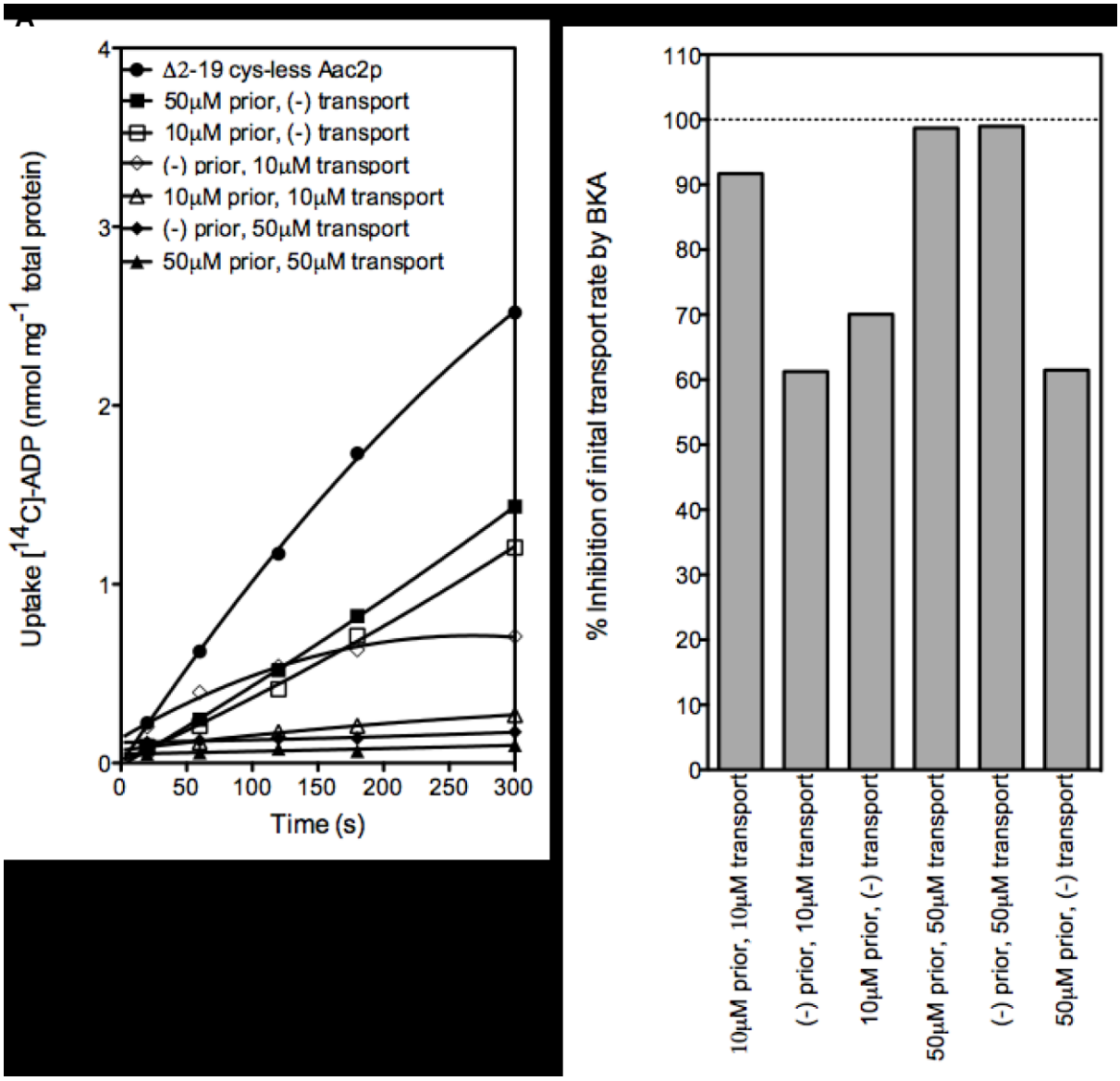

Figure 3.15 Transport activity of Δ2-19 cys-less Aac2p in the absence and presence of different concentrations of BKA added prior or during the transport assay. (A) Time curves of [^{14}C]-ADP uptake for Δ2-19 cys-less Aac2p at various concentrations of BKA added prior and/or during transport, as indicated in the figure. All pre-incubations lasted 30 min and the transport assay was done manually using whole cells. The curves were fitted to a second order polynomial equation. **(B)** The percentage inhibition of initial [^{14}C]-ADP uptake rate by BKA, shown as percentage of the initial transport rate of Δ2-19 cys-less Aac2p. The initial rates were calculated from the slope of the curves.

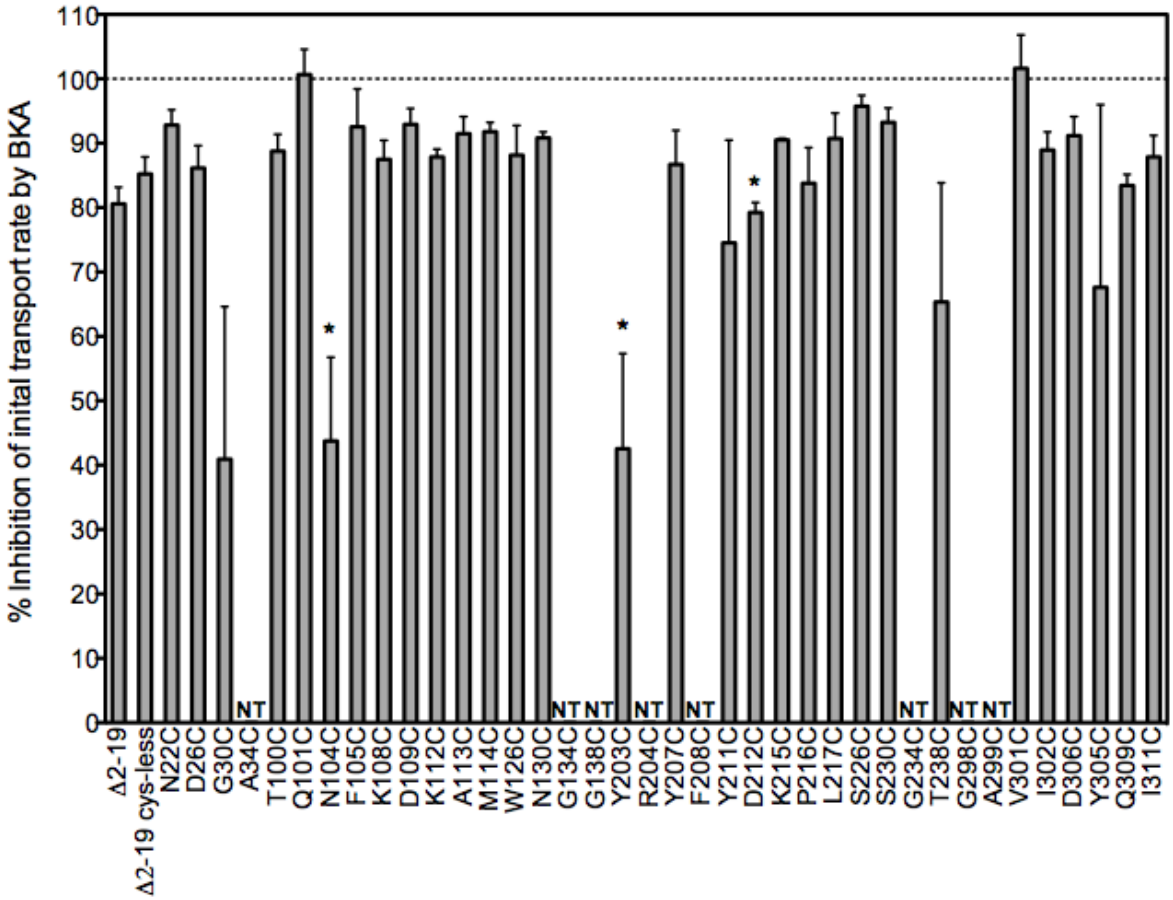

Figure 3.16 Percentage of inhibition of the specific initial ADP uptake rate by bongkrekic acid of single cysteine mutants of Aac2p. The percentage of inhibition in the presence of BKA is relative to the specific initial uptake rate in the absence of inhibitor (Figure 3.10). Mutant proteins that did not transport significantly above background (A34C, G134C, G138C, F208C, G234C, G298C and A299C Aac2p) are labelled NT for 'not transporting' (Figure 3.13). 10 µM BKA was added 30 min prior to the start of uptake, and 10 µM BKA was added during transport. The data represent the average and the standard deviation (*n*=3). The average values that show significantly less inhibition than the Δ2-19 cys-less Aac2p are denoted by an asterisk (unpaired, two-tailed Student's *t*-test assuming unequal variance ($P<0.05$) (see Appendix II for individual mutant statistics)).

Chapter 4 Orientation of single cysteine mutants of the ADP/ATP carrier in *Lactococcus lactis* membranes

4.1 Introduction

The aim of this chapter is to probe the orientation of single cysteine mutants of Aac2p in *L. lactis* membranes. It was hypothesised that the mutant Aac2p expressed in *L. lactis* would be oriented with their cytoplasmic sides facing outside the cell, just as Δ2-19 cys-less Aac2p is predicted to based on the positive-inside rule (Heijne & Gavel, 1988; Heijne, 1986; Heijne, 1989). This hypothesis was tested by two methods; first, by determining the accessibility of single cysteines to the thiol-specific, membrane-impermeable probe eosin-5-maleimide and second, by determining the degree of transport inhibition of the single cysteine mutants in the presence of the membrane-impermeable inhibitor, CATR.

4.2 Selection of a thiol-specific, membrane-impermeable probe

A series of thiol-specific, membrane-impermeable probes were tested to find one suitable for labelling single cysteines of mutant Aac2p expressed in the cytoplasmic membrane of whole cells of *L. lactis*. Several criteria have to be fulfilled for a particular probe to be useful; first, the probe has to be membrane-impermeable so that only cysteines that are on the water-accessible extracellular surface are labelled. Second, the probe needs to react with a cysteine thiol in an irreversible manner to prevent signal loss during sample preparation. Finally, it needs to be fluorescent to aid in safe and easy detection. For a more detailed discussion of thiol-specific, membrane-impermeable probes, see Section 1.9.1.

To select a detectable, thiol-specific, membrane-impermeable probe, Δ2-19 cys-less Aac2p and the single cysteine mutants E120C and A262C Aac2p were expressed and exposed to different probes. As the reaction is specific only to cysteines, Δ2-19 cys-less Aac2p was expected to remain unlabelled. The residue E120C is located in the cytoplasmic loop between transmembrane α-helices 2 and 3 on the cytoplasmic side of the carrier (Figure 4.1). When expressed in the cytoplasmic membrane of *L. lactis*, E120C is predicted to be water-accessible and on the outside of the cell and thus it should be labelled well by any of the tested probes. In contrast, the residue A262C is located in a flexible loop region between α-helix 5 (H5) and matrix helix 56 (h56) on the matrix side of the carrier, so when expressed it is predicted to be on the inside of the cell (Figure 4.1). Thus, A262C Aac2p should not be labelled because the probe should not be able to cross the membrane.

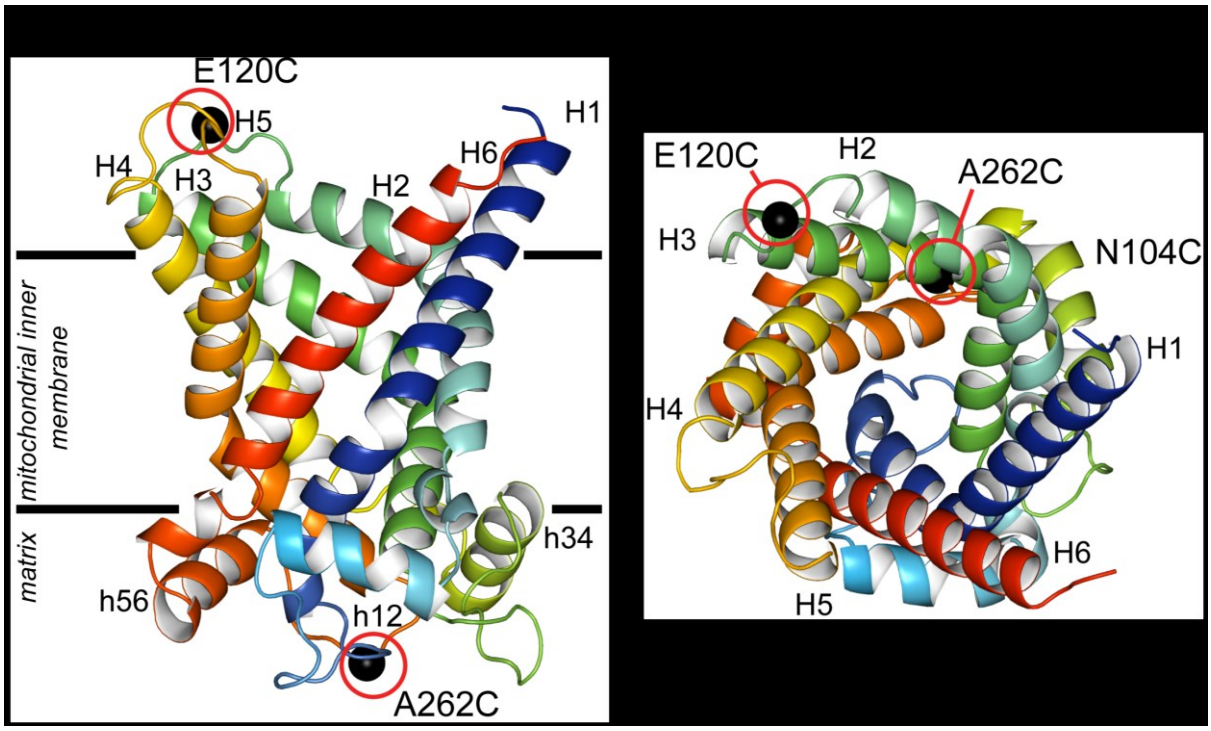

Figure 4.1 Single cysteine mutantions used for sulphydryl reagent screening. This Aac2p model is based on the CATR-inhibited bovine AAC1 structure (PDB code 1OKC) (Pebay-Peyroula *et al.*, 2003) (built by Dr Alan Robinson). α-helix 1 (H1) is dark blue, α-helix 2 (H2) is teal, α-helix 3 (H3) is dark green, α-helix 4 (H4) is yellow, α-helix 5 (H5) is orange and α-helix 6 (H6) is red. Matrix helix 12 (h12) is light blue, matrix helix 34 (h34) is pea green and matrix helix 56 (h56) is orange-red. The parallel black bars represent the boundaries of the membrane. The single cysteine replacements used for fluorescent probe screening (see Figure 4.2 and 4.3) are shown as single black spheres centred on α-carbons. **(A)** The lateral view and **(B)** the cytoplasmic view of the cavity.

L. lactis cells expressing Δ2-19 cys-less, E120C and A262C Aac2p were treated with four different fluorescent probes predicted to be thiol-specific and membrane-impermeable. These are lucifer yellow iodoacetamide (Figure 4.2 A), alexa fluor 488 (Figure 4.2 B), eosin-5-maleimide (Figure 4.3 A) and fluorescein-5-maleimide (Figure 4.3 B). The fluorescent signal from protein-bound lucifer yellow iodoacetamide could not be detected (Figure 4.2 E) as there are no bands visible for any of the mutants. A possible reason may be that the absorbance and emission maxima are 426-428 nm and 530-535 nm, respectively, whereas the laser and emission filter could only be set to the non-optimal 457 and 555 nm wavelengths, respectively. Thus, the excitation wavelength of 457 nm is at the far end of the excitation spectrum for lucifer yellow iodoacetamide. Alternatively, the 20 min incubation period may have been insufficient, as lucifer yellow iodoacetamide may require a longer reaction time period than maleimide-based probes.

In contrast, mutant Aac2p was fluorescently labelled with alexa fluor 488 (Figure 4.2 F). A fluorescent signal for Δ2-19 cys-less Aac2p was not visible, as expected, demonstrating that the probe is thiol-specific. A strong signal was detected for E120C Aac2p and no signal was detected for A262C Aac2p, demonstrating that the single cysteine of E120C Aac2p is accessible to alexa fluor 488 in agreement with the extracellular cytoplasmic loop location of the residue. Provided that single cysteine A262C, which is predicted to be on the inside of the cell, is reactive (see below), the absence of signal may indicate that the probe is membrane-impermeable. Alexa fluor 488 may therefore be a suitable candidate for a fluorescent probe.

Two other maleimide-conjugated fluorescent probes, eosin-5-maleimide and fluorescein-5-maleimide, were also tested (Figure 4.3). Eosin-5-maleimide labelled single cysteines on mutant Aac2p similarly to alexa fluor 488 (Figure 4.3 E), suggesting that eosin-5-maleimide is also thiol-specific and membrane-impermeable. Fluorescein-5-maleimide, however, failed to label the single cysteine mutants in a similar way (Figure 4.3 F). Fluorescein-5-maleimide did not label Δ2-19 cys-less Aac2p, as expected, but it did label both E120C and A262C Aac2p. The accessibility of residue A262C to fluorescein-5-malemide suggests that it is membrane-permeable under the conditions tested and it also demonstrates that A262C Aac2p can be

labelled. Fluorescein-5-maleimide (Figure 4.3 B) may be able to penetrate the membrane of *L. lactis* as it is much more non-polar.

Alexa fluor 488 and eosin-5-maleimide were both found to be suitable for probing the water-accessible surfaces of Aac2p. Eosin-5-maleimide was chosen for subsequent studies because it is much more affordable than alexa fluor 488.

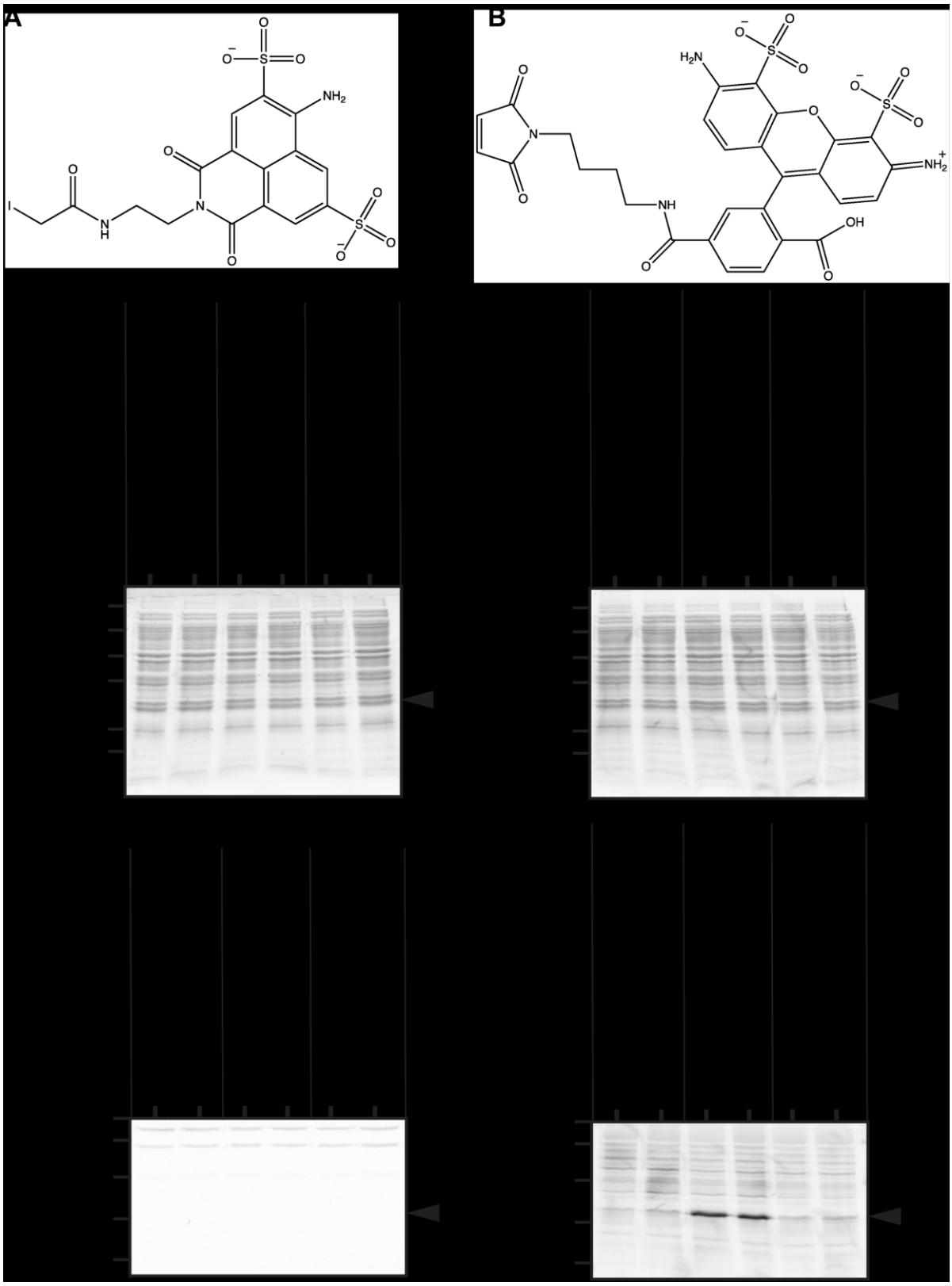

Figure 4.2 Chemical structure of lucifer yellow iodoacetamide and alexa fluor 488, and the expression levels and fluorescent scans of Δ2-19 cys-less, E120C and A262C Aac2p treated with lucifer yellow iodoacetamide and alexa fluor 488. For legend, see next page.

Legend of Figure 4.2 (A) Structure of the thiol-specific probes lucifer yellow iodoacetamide and **(B)** alexa fluor 488. **(C) and (D)** Expression levels of Δ2-19 cys-less, E120C and A262C Aac2p. Whole cells of *L. lactis* were treated with either 50 μM or 200 μM lucifer yellow iodoacetamide (LY) in (C) or 25 μM or 50 μM Alexa 488 (Alexa) in (D). Membranes were isolated and the expression levels were analysed by SDS-PAGE followed by Coomassie staining. **(E) and (F)** The fluorescent scans of Δ2-19 cys-less, E120C and A262C Aac2p as in (C) and (D). The fluorescent scans were imaged by using a Typhoon imager set at 475 PMT Volts with the excitation/emission wavelengths set at 457/555 nm for (E) and 488/526 nm for (F). The band for Aac2p is indicated by a solid black arrowhead. 28.8 μg total protein was loaded per lane.

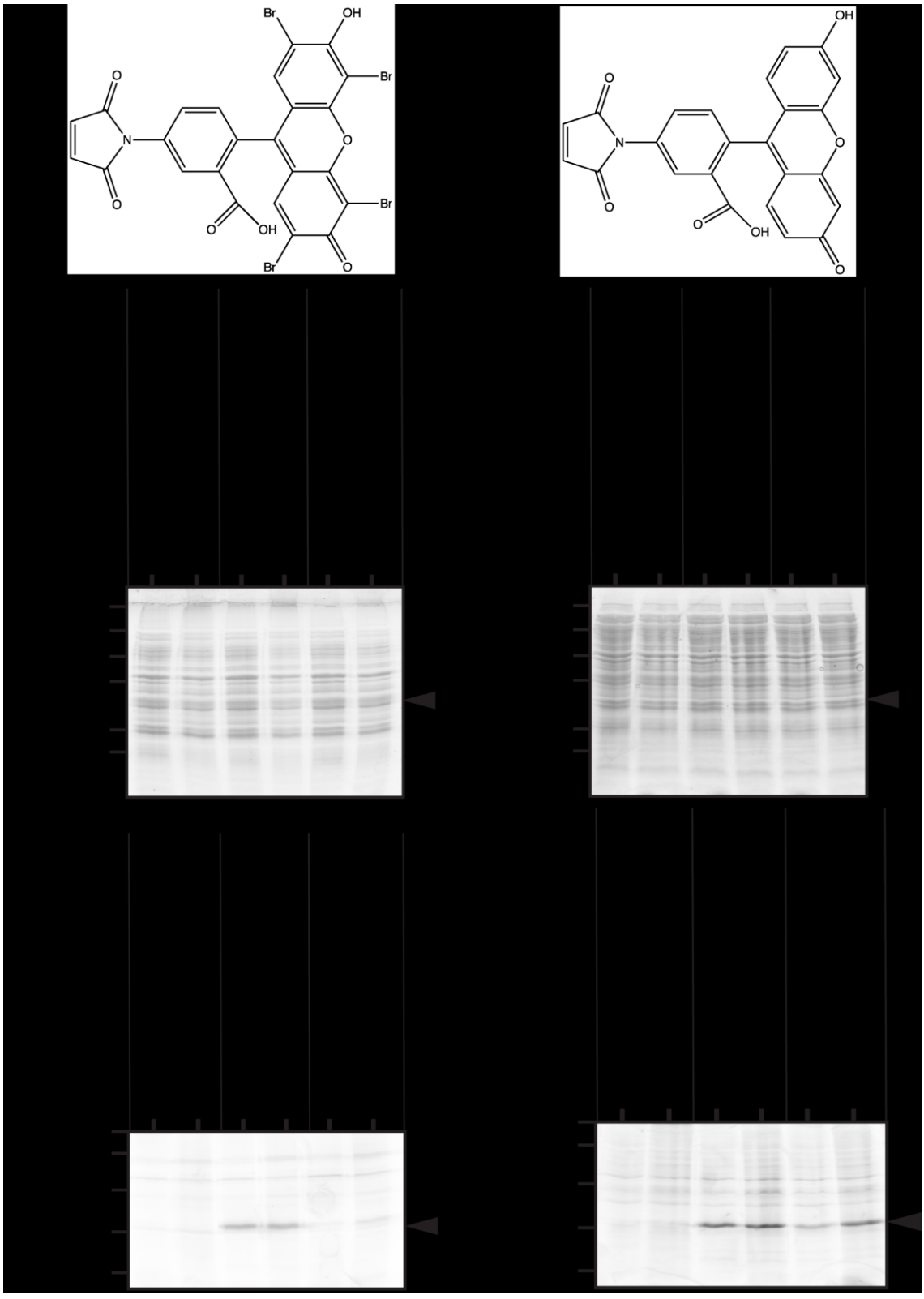

Figure 4.3 Chemical structure of eosin-5-maleimide and fluorescein-5-maleimide, and the expression levels and fluorescent scans of Δ2-19 cys-less, E120C and A262C Aac2p treated with eosin-5-maleimide and fluorescein-5-maleimide. Legend as Figure 4.2 except with 50 μM or 200 μM eosin-5-maleimide (EMA), or 50 μM or 200 μM fluorescein-5-maleimide (FMA). The excitation/emission wavelengths were 532/560 nm for EMA and 488/526 nm for FMA.

4.3 Selection of mutants

Single cysteine mutants of Aac2p were generated using the novel *L. lactis* site-directed mutagenesis procedure, as described previously (Section 3.3). Fifteen control mutants were also generated to determine the orientation of the mutants in the lactococcal cytoplasmic membrane (Table 4.1). The selected mutations represent all of the major surface areas of Aac2p, as they are located on membrane-facing or inter-helical sides of the transmembrane α-helices (Figure 4.4 A), or on the matrix (Figure 4.4 B) and cytoplasmic loops (Figure 4.4 C). The introduced cysteines on the water-accessible surfaces of the cytoplasmic side of Aac2p are expected to be accessible to eosin-5-maleimide, whereas those that are on the matrix side or in the membrane-facing or inter-helical areas are not. In total, 15 controls were chosen to probe these different surfaces of Aac2p. The initial transport rate of ADP was above background for all 15 controls (Appendix III, Figure A.1) (unpaired, one-tailed Student's *t*-test, unequal variance ($P<0.05$)), which showed that they were functional and inserted correctly.

Table 4.1 Single cysteine mutations to probe different surfaces of Aac2p.

single cysteine mutation	location
L50C[a]	helix 1, inter-helical
T79C	helix 12, water-phase of the mitochondrial matrix
E120C	helix 23, cytoplasmic loop
A124C	helix 23, cytoplasmic loop
A136C	helix 3, lipid bilayer
S147C[a]	helix 3, lipid bilayer
K179C	helix 34, water-phase of the mitochondrial matrix
A187C	helix 34, water-phase of the mitochondrial matrix
S222C	helix 45, cytoplasmic loop
E224C	helix 45, cytoplasmic loop
T243C	helix 5, lipid bilayer
R273C	helix 56, water-phase of the mitochondrial matrix
A278C	helix 56, water-phase of the mitochondrial matrix
A297C	helix 6, lipid bilayer
G314C	C-terminus, cytoplasmic side

[a]L50C and S147C were generated by Lisa Görs.

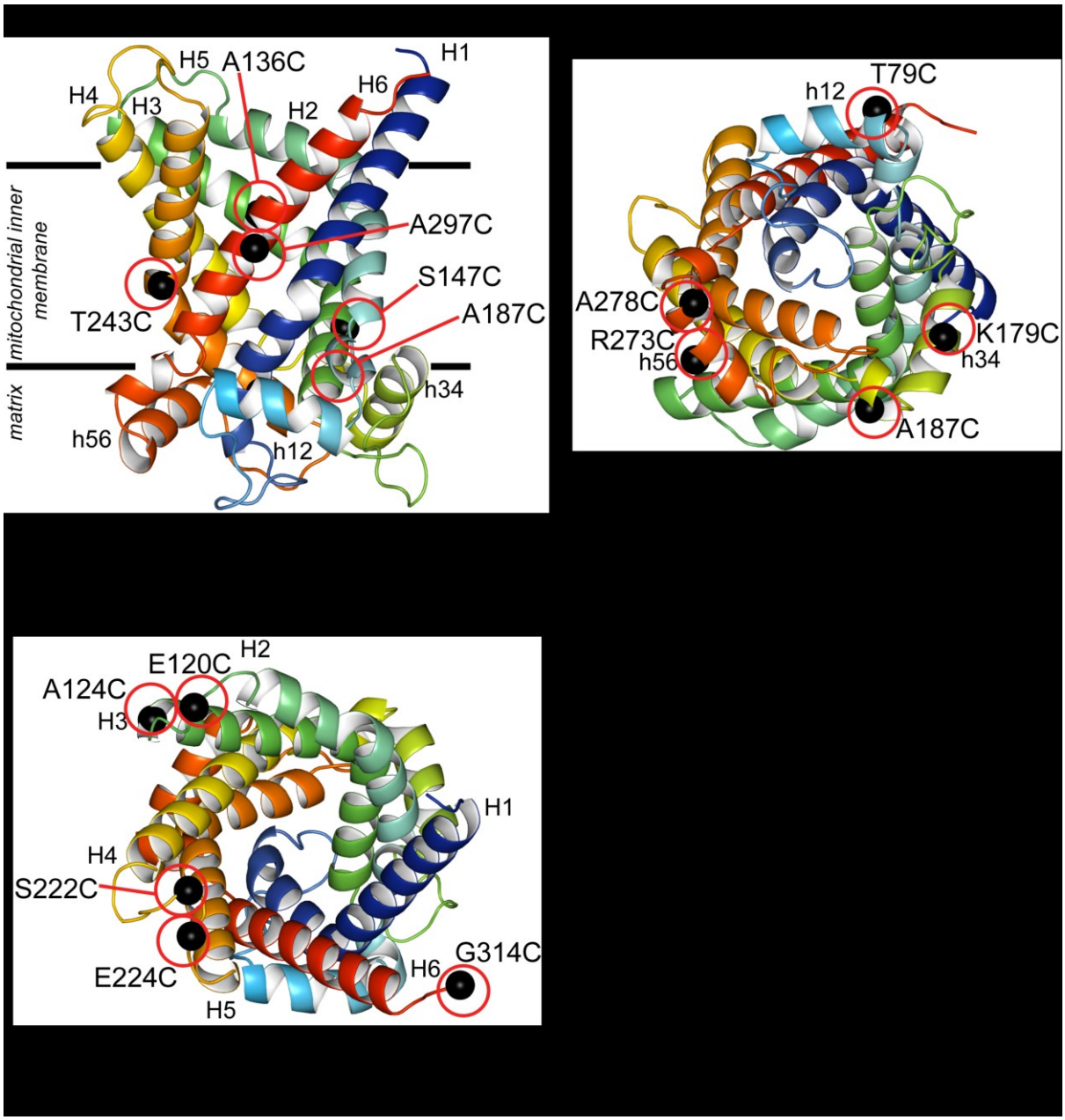

Figure 4.4 Location of single cysteine mutations to probe the accessibility of different surfaces of Aac2p. For legend details, see Figure 4.1. The cysteine mutations are shown as a single black spheres centred on their α-carbons and highlighted by a red circle. Individual mutants are labelled. For a list of mutations, see Table 4.1. **(A)** Lateral view from the membrane showing the cysteine mutations that are membrane-facing or inter-helical. **(B)** View from the mitochondrial matrix depicting the cysteine mutations that are on the matrix side. **(C)** View from the cytoplasm/intermembrane region depicting cysteine mutations on the cytoplasmic side.

In addition, single cysteine mutations located in the upper cytoplasmic cavity of Aac2p were also selected to test whether the orientation in the lactococcal membrane was consistent for each mutant carrier (Figure 4.5). The chosen single cysteine mutations needed to satisfy two criteria. First, the selected mutant carriers must be able to transport ADP at initial rates significantly above background, as determined by a Student's *t*-test to ensure that the expressed protein is active (Figure 3.10 and 3.13 and Appendix II). Second, the single cysteines should be accessible to the probe and be labelled significantly above background (Figure 5.3 and Appendix II). Some single cysteines at the cytoplasmic side may be more accessible, for instance, than residues lower in the cavity because the cavity is too narrow for the probe to enter. Thus, single cysteine mutations were selected from all of the surface areas of Aac2p, including the cytoplasmic loops, the upper areas of the cavity, the membrane or inter-helical surface and the matrix loops/helices.

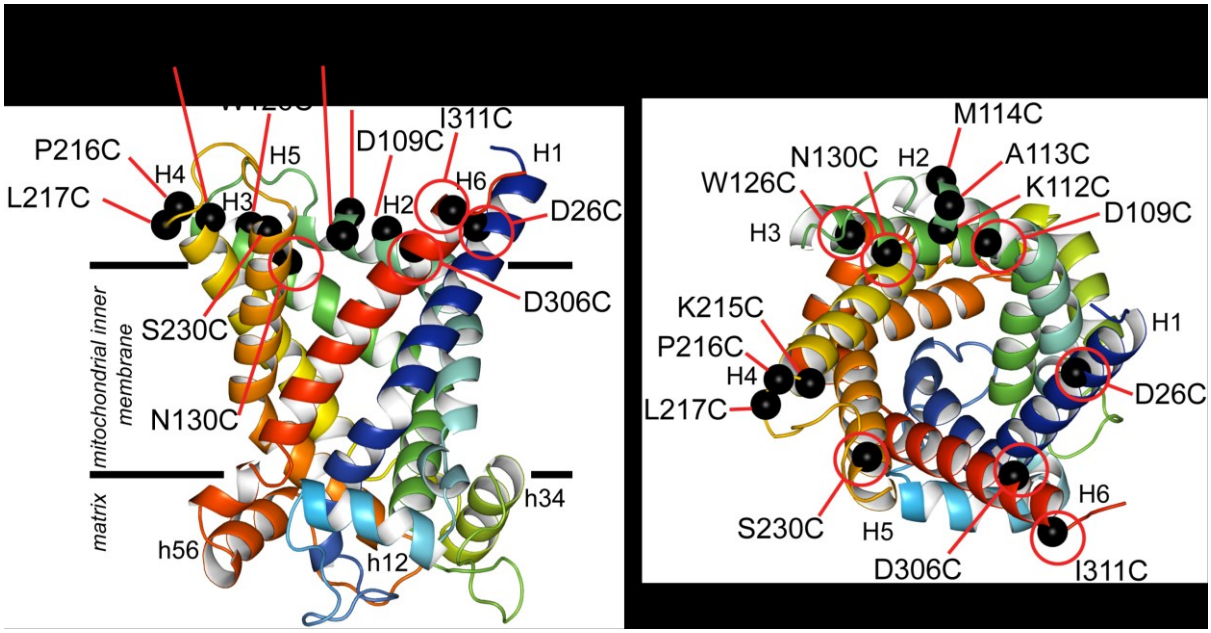

Figure 4.5 Location of single cysteine mutations to probe the accessibility of residues in the upper cytoplasmic cavity of Aac2p. For legend details, see Figure 4.1. The cysteine mutations are shown as single black spheres centred on their α-carbons and highlighted by red circles. Individual mutations are labelled. For a list of mutations, see Table 3.1. **(A)** Lateral view from the membrane and **(B)** the view into the cavity from the cytoplasmic side.

4.4 Expression level of single cysteine mutants

Single cysteine mutants of Aac2p were expressed in the cytoplasmic membrane of *L. lactis*. The whole cell lysates were separated by SDS-PAGE and the amounts of Aac2p were quantified on Western blots (for details, see Section 3.4); an example Western blot is shown in Figure 4.6. The bands for Aac2p have a molecular mass of 32.5 kDa. There are only two bands visible; one unknown protein at ~40 kDa and lysozyme at ~15 kDa, which is known to react with the antibody (personal communication, Dr Edmund R.S. Kunji).

The quantification of W126C Aac2p, which was used as a standard, is shown in Figure 4.6. Different amounts of purified Aac2p (Section 3.4) were loaded alongside an eosin-5-maleimide labelled W126C standard, loaded in triplicate (Figure 4.6 A). Using the standard curve shown in Figure 4.6 B, the amount of loaded W126C standard was determined. The W126C standard was loaded onto every gel and was used as an internal standard to determine the amount of Aac2p mutant carriers (Table 3.2 and Figure 4.6 C).

The Western blot signals for the BKA- or CATR-inhibited, eosin-5-maleimide labelled single cysteine mutants of Aac2p (described in Section 4.2), and for the empty vector, Δ2-19 and Δ2-19 cys-less Aac2p were imaged and quantified (Appendix IV Figure A.2). As noted previously in Section 3.4 for the transport mutants, the eosin-5-maleimide labelled mutants varied in expression, ranging from levels similar to Δ2-19 cys-less Aac2p to 6.8-fold higher. The difference was much higher than observed when the expression levels were quantified for transport assays (Figure 3.8). A possible reason could be that protein transfer varied or was less efficient due to the time lag between imaging fluorescent scans and protein transfer (see below). Nevertheless, all of the eosin-5-maleimide labelled mutant Aac2p could be detected and quantified in this way.

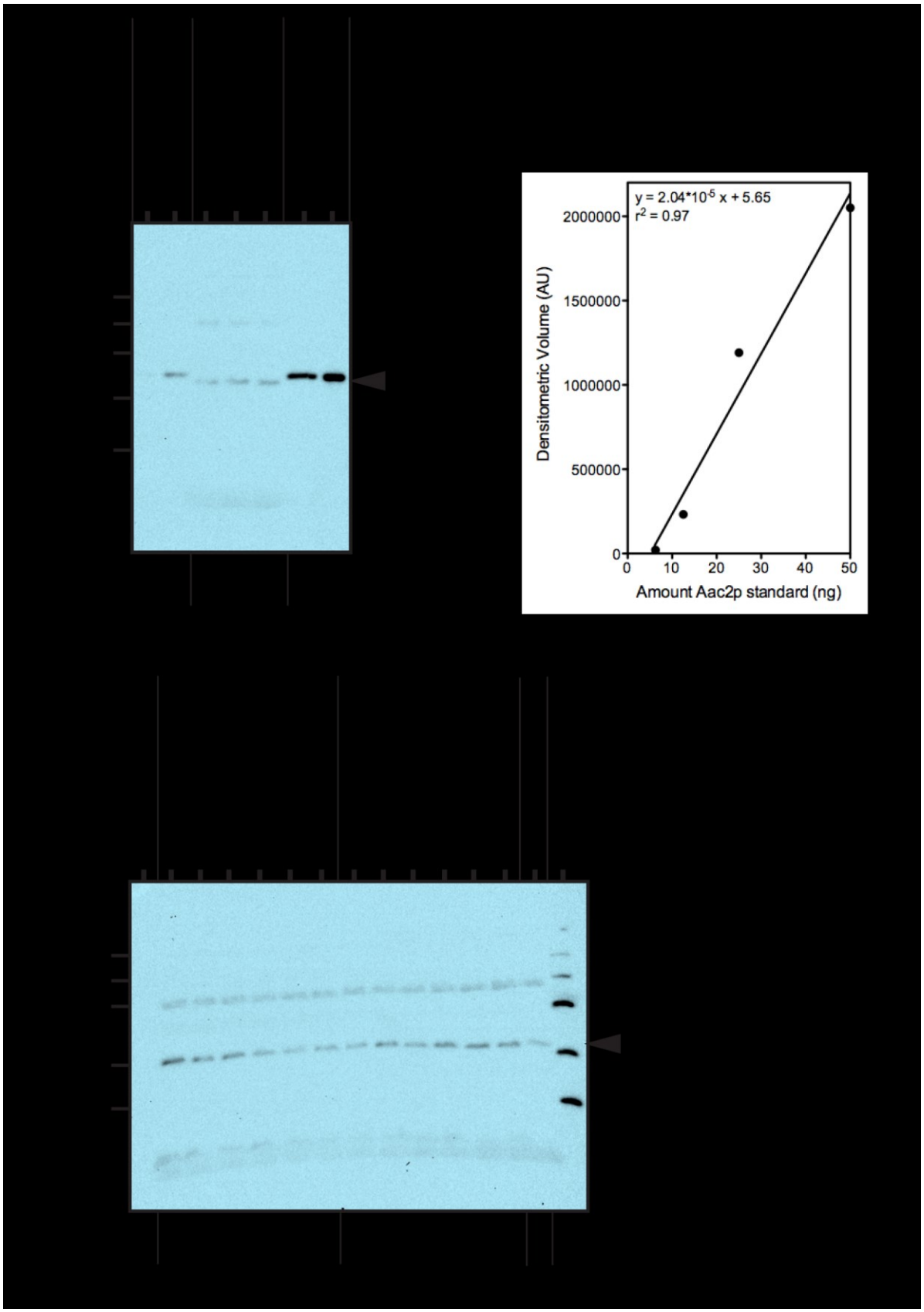

Figure 4.6 Expression and quantification of A113C and P216C Aac2p. For legend, see next page.

Legend of Figure 4.6 **(A)** Western blot analysis of the eosin-5-maleimide labelled W126C Aac2p reference standard expressed in whole cells of *L. lactis*. The antibody is directed against α-helix H5 of Aac2p. Known amounts of purified *S. cerevisiae* Aac2p (determined by Protein & Nucleic Acid Chemistry Facility, Department of Biochemistry, Cambridge, UK) and 30 µg of total lysozyme-lysed cellular protein were loaded in the other lanes. The blots were imaged using a Chemi-doc XRS+ and the total signals were quantified with Image Lab (*n*=3). **(B)** The amount of eosin-5-maleimide labelled W126C was determined by generating a standard curve with 6.25, 12.5, 25.0 and 50.0 ng purified Aac2p standards and linear regression. **(C)** Western blot analysis of BKA- or CATR-inhibited, eosin-5-maleimide labelled A113C and P216C Aac2p. See Table 4.2 for the quantifications.

Table 4.2 The quantification of labelled Aac2p mutants under different conditions by using W126C as a reference.

Aac2p	Densitometric volume (AU)	Relative volume	Calculated amount Aac2p (ng)
A113C +BKA	447104	3.58	2.13
A113C +BKA	238710	1.91	2.38
A113C +BKA	263850	2.11	2.50
A113C +CATR	153420	1.23	11.2
A113C +CATR	107070	0.86	10.2
A113C +CATR	144420	1.16	11.4
P216C +BKA	126150	1.01	20.3
P216C +BKA	226720	1.81	19.4
P216C +BKA	154260	1.23	19.4
P216C +CATR	274500	2.20	19.4
P216C +CATR	290760	2.33	19.4
P216C +CATR	241290	1.93	22.1
W126C standard	124980	1	8.47

The Western blot signals (Appendix IV, Figure A.3) for the single cysteine mutants of Aac2p used to quantify the specific initial uptake rate in the presence of CATR (Section 4.7) were quantified as described previously (Section 3.4, Figure 3.7 and Table 3.2). Similar to Figure 3.8, most of the mutants are expressed at levels more than two-fold lower than Δ2-19 cys-less Aac2p. The exceptions, D26C and A34C Aac2p, were previously described as being expressed 1.6-fold higher or similar to Δ2-19 cys-less, respectively (Section 3.4). Mutants A124C and G314C Aac2p also were exceptions, being expressed between 2.2-fold higher than, or similar to, Δ2-19 cys-less, respectively (Appendix IV, Figure A.3). These residues are located on α-helix H1, on the N-terminal side of transmembrane α-helix 3 or on the C-terminus. Hydrophobic single cysteine mutations to the cytoplasmic side of the Aac2p could possibly aid in protein targeting or insertion by the Sec translocase machinery of *L. lactis*, which recognises hydrophobic 'signal sequence' regions, and this could explain the higher expression levels of these mutants (Facey & Kuhn, 2004; Plessis *et al.*, 2011).

The absolute expression levels of mutant Aac2p, as determined for labelling studies (Appendix IV, Figure A.2) and transport studies (Appendix IV, Figure A.3) are roughly similar when protein loading amounts are taken into account (30 μg, Figure A.2 versus 22.5 μg, Figure A.3 per lane). This observation confirms that the expression levels are reproducible in independent experiments.

4.5 Optimisation of labelling

The specific eosin-5-maleimide labelling of single cysteines of Aac2p in whole cells was optimised. First, the minimal concentration required to label an accessible single cysteine of mutant Aac2p was determined. W126C is accessible at the top of the cavity (Figure 4.7), whereas Δ2-19 cys-less Aac2p functioned as a control. Four different concentrations of eosin-5-maleimide, 3 μM, 10 μM, 30 μM and 90 μM were added to whole cells expressing Δ2-19 cys-less and W126C Aac2p. The experiment was carried out only once, but the results indicate that the labelling of W126C was saturated at 30 μM eosin-5-maleimide (Figure 4.8 B and C). In addition, a time course experiment using 25 μM eosin-5-maleimide demonstrated that all W126C

sites were saturated with label after 2 min (data not shown). For subsequent experiments, a 10 min incubation with 25 μM eosin-5-maleimide was selected as the standard condition.

β-mercaptoethanol and dithiothreitol (DTT) were both tested as compounds to terminate the labelling reaction, as they are known to react with excess eosin-5-maleimide. It was shown that the background labelling of proteins was higher when β-mercaptoethanol was used (data not shown) and thus DTT was selected to quench the eosin-5-maleimide reaction.

It was found that it was not sufficient to add DTT to halt the eosin-5-maleimide reaction, as the background labelling was still high. The cells also needed to be washed several times to remove excess eosin-5-maleimide. It was observed that when the cells expressing M114C (see Figure 4.7 for mutation location) were washed up to three times with buffer that the non-specific background labelling decreased (Figure 4.9 A) whilst the specific labelling of residue M114C remained constant. Thus, washing the cells after DTT addition is important for preventing non-specific labelling.

In addition, wash timing was optimised (Figure 4.9 B-C). When cells expressing N130C Aac2p (see Figure 4.7 for mutation location) were treated with DTT immediately after the addition of eosin-5-maleimide, and then left on ice for 50 min, the reaction was not quenched and the background labelling of proteins is high (0 min, Figure 4.9 B). However, when the cells were washed immediately following the addition of DTT, the background labelling is almost negligible (0 min, Figure 4.9 C). Taken together, it was decided to reduce the background by washing the cells three times in the presence of DTT, immediately following the initial addition of DTT.

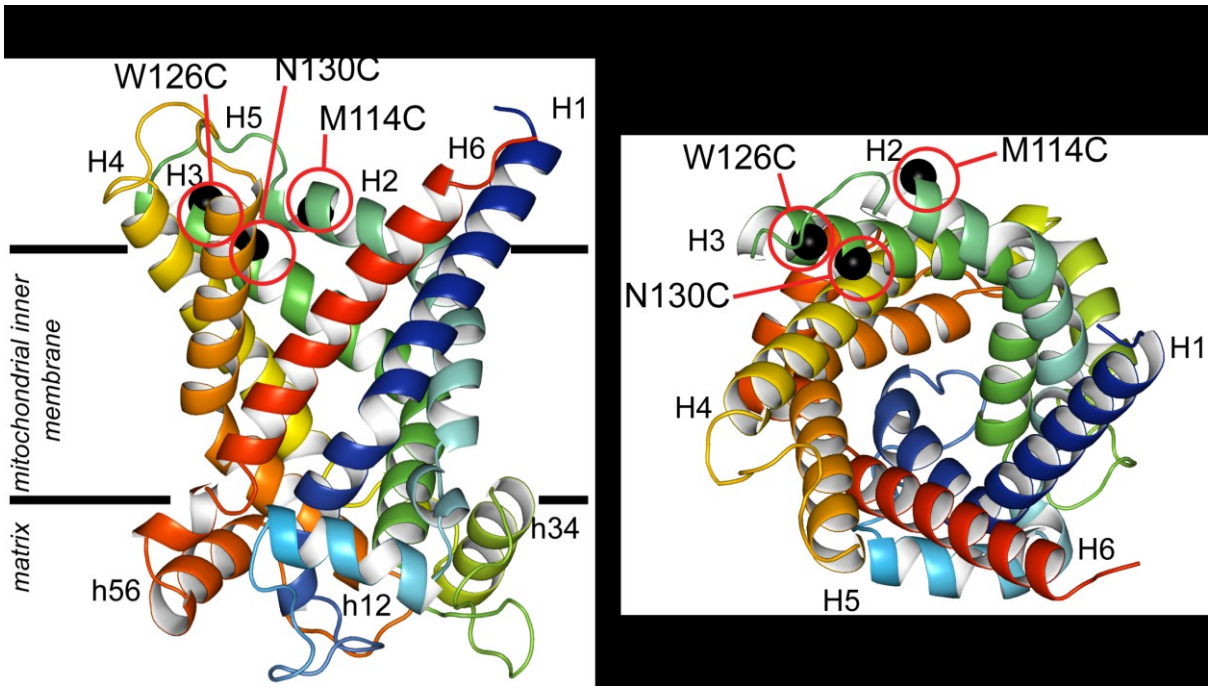

Figure 4.7 Location of single cysteine mutations used for labelling optimisation. For legend details, see Figure 4.1. The cysteine mutations are shown as single black spheres centred on their α-carbons and highlighted by red circles. Individual mutations are labelled. For a list of mutations, see Table 3.1. **(A)** Lateral view from the membrane and **(B)** the view into the cavity from the cytoplasmic side.

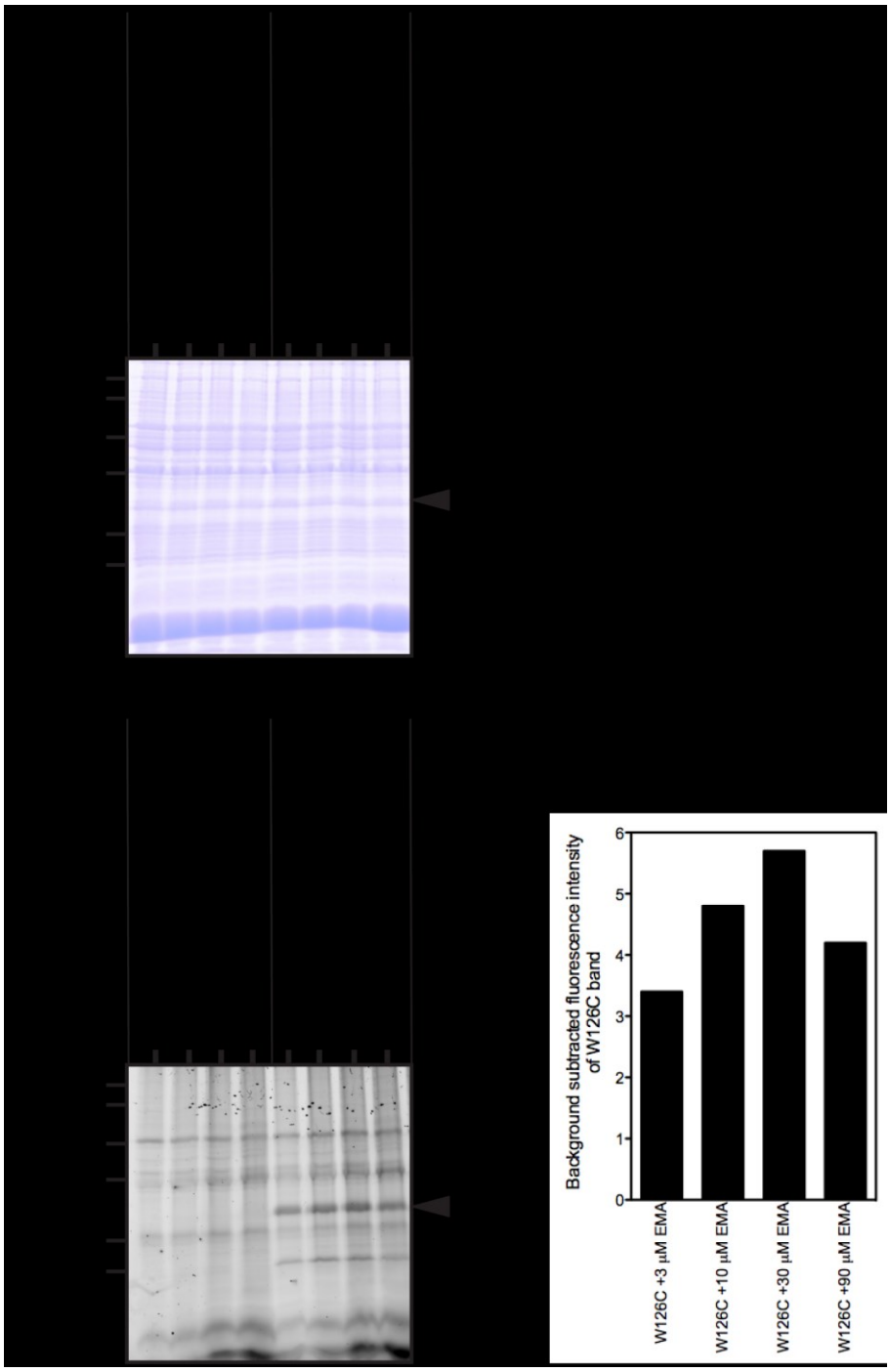

Figure 4.8 Labelling levels of Δ2-19 cys-less and W126C Aac2p as a consequence of different concentrations of eosin-5-maleimide. (A) Levels of Δ2-19 cys-less and W126C Aac2p expressed in *L. lactis*. Whole cells were treated with 3 µM, 10 µM, 30 µM or 90 µM eosin-5-maleimide, followed by cell lysis. **(B)** The fluorescent scan of Δ2-19 cys-less and W126C Aac2p. The fluorescent scan was imaged using a Typhoon imager set at 650 PMT Volts and excitation/emission wavelengths at 532/560 nm, respectively. The band for Aac2p is indicated by a solid black arrowhead. 30 µg total protein was loaded in each lane. **(C)** Graph of the intensity of the W126C Aac2p bands, as quantified by ImageQuant, in which the background was subtracted.

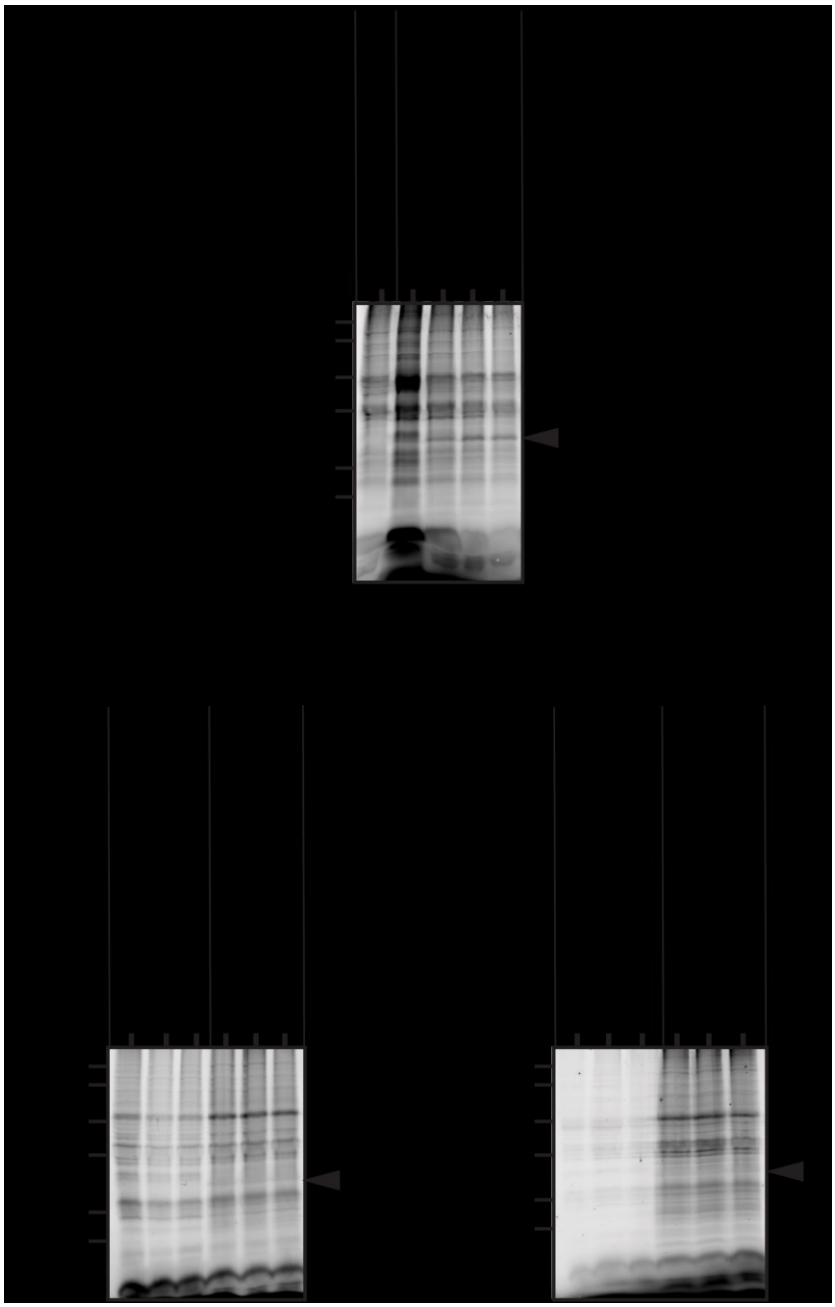

Figure 4.9 Labelling levels of Δ2-19 cys-less, M114C and W126C Aac2p with different wash conditions with DTT following the eosin-5-maleimide addition. (A) The fluorescent scan of Δ2-19 cys-less and M114C Aac2p. Following a 10 min 25 μM eosin-5-maleimide treatment, the samples were washed 0, 1, 2 or 3 times before cell lysis. The fluorescent scan was imaged using a Typhoon imager set at 730 PMT Volts. **(B) and (C)** Fluorescent scans of N130C Aac2p. Following a 0 or 10 min 25 μM eosin-5-maleimide incubation period, DTT was added and the samples were left on ice for 50 minutes before washing (B), or the samples were washed immediately (C). The fluorescent scans were imaged using a Typhoon imager set at 650 PMT Volts. For (A-C), the excitation/emission wavelengths were 532/560 nm, respectively. The band for Aac2p is indicated by a solid black arrowhead. 30 μg total protein was loaded per lane.

In addition, BKA inhibition was optimised. It was found that labelling of N130C Aac2p was occluded in the presence of BKA and ADP, but was labelled in the presence of BKA only (Figure 4.10). This result indicates that BKA only fully inhibits, and thus occludes labelling of single cysteines, in the presence of ADP, as previously noted (Henderson & Lardy, 1970; Kemp *et al.*, 1970). Consequently, this condition was adopted for all labelling of BKA-inhibited samples.

Figure 4.10 Labelling levels of BKA-inhibited N130C Aac2p in the presence or absence of ADP. 200 µM BKA was added in the presence or absence of 80 µM ADP 30 min before the addition of eosin-5-maleimide. 30 µg lysozyme-lysed cellular protein was loaded per lane. The fluorescent scan was imaged using a Typhoon imager at 650 PMT Volts. The band for Aac2p is indicated by a solid black arrowhead. The data are *n*=3.

4.6 Specific labelling in the presence of bongkrekic acid and carboxy-atractyloside

Single cysteine mutants of Aac2p (Section 4.3) were inhibited with BKA or CATR, and labelled with eosin-5-maleimide using the optimised conditions to probe the water accessibility of the mutations in the two inhibited states. The fluorescence level of the Aac2p bands was corrected for the background in the gel (Figure 4.11) for each lane to account for lane-to-lane and gel-to-gel background variation. The corrected fluorescence intensity was subsequently normalised to an eosin-5-maleimide labelled W126C standard to account for variations in fluorescence detection (Table 4.3). The fluorescence intensity for all of the BKA- and CATR-inhibited single cysteine mutants of Aac2p is shown relative to the W126C standard (Figure 4.12).

The labelling of the single cysteine mutants is distinguishable above the background (Figure 4.12). As expected, for the empty vector and Δ2-19 cys-less Aac2p, there was no discernible band. In addition, Δ2-19 Aac2p is not labelled, as its cysteines are inaccessible from the cytoplasmic side (Houstěk & Pedersen, 1985). The single cysteine mutants were labelled only in the c-state, in both the m- and c-states or in neither state.

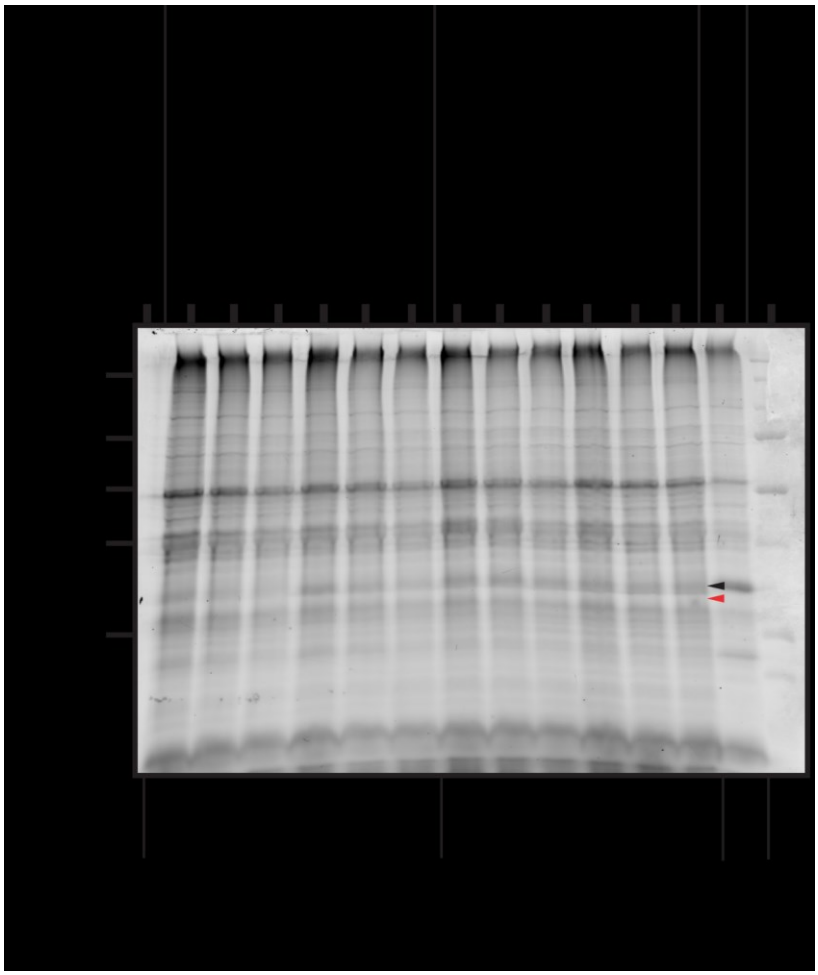

Figure 4.11 Fluorescence quantification of bongkrekic acid or carboxy-atractyloside inhibited, eosin-5-maleimide labelled, A113C and P216C Aac2p. The fluorescent scans were imaged using a Typhoon imager set at 675 PMT Volts. The excitation/emission wavelengths were 532/560 nm, respectively. 30 µg lysozyme-lysed cellular protein was loaded per lane. Fluorescence was quantified using ImageQuant. The fluorescence of the Aac2p band (black arrow head) was corrected for by the subtraction of the background (red arrow head), and then normalised to the W126C reference (see Table 4.3).

Table 4.3 Background correction of the fluorescence intensity of eosin-5-maleimide labelled Aac2p and normalisation to the eosin-5-maleimide labelled W126C standard for the Aac2p bands in Figure 4.11

Aac2p	Background subtracted fluorescence intensity of Aac2p	Normalisation factor of W126C standard	Normalised fluorescence intensity of Aac2p
A113C +BKA	7.09	1.56	11.1
A113C +BKA	5.74	1.56	8.95
A113C +BKA	3.01	1.56	4.70
A113C +CATR	12.1	1.56	18.9
A113C +CATR	8.39	1.56	13.1
A113C +CATR	6.70	1.56	10.5
P216C +BKA	11.8	1.56	18.4
P216C +BKA	13.5	1.56	21.1
P216C +BKA	13.1	1.56	20.4
P216C +CATR	11.7	1.56	18.3
P216C +CATR	14.1	1.56	22.0
P216C +CATR	12.8	1.56	20.0

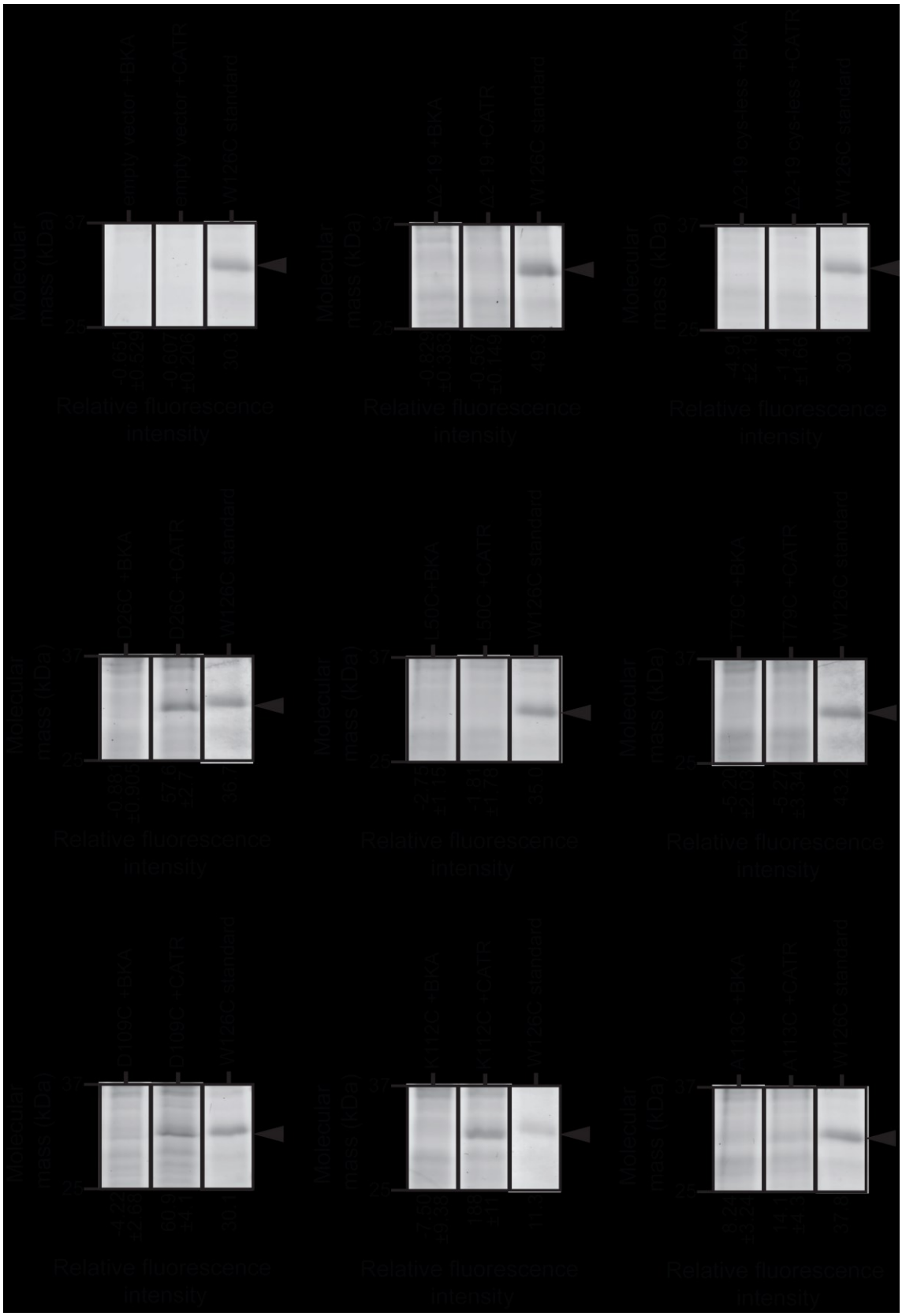

Figure 4.12 Relative fluorescence intensity of eosin-5-maleimide labelled, single cysteine mutants of Aac2p inhibited by bongkrekic acid or carboxy-atractyloside. For legend details, see the last page of the figure.

Figure 4.12 continued Relative fluorescence intensity of eosin-5-maleimide labelled, single cysteine mutants of Aac2p inhibited by bongkrekic acid or carboxy-atractyloside. For legend details, see the last page of the figure.

Figure 4.12 continued Relative fluorescence intensity of eosin-5-maleimide labelled, single cysteine mutants of Aac2p inhibited by bongkrekic acid or carboxy-atractyloside. For legend details, see the next page.

Figure 4.12 continued Relative fluorescence intensity of eosin-5-maleimide labelled, single cysteine mutants of Aac2p inhibited by bongkrekic acid or carboxy-atractyloside. The fluorescent scans were imaged using a Typhoon imager. The PMT Voltage used is listed in the top left-hand corner of each fluorescent scan. The excitation/emission wavelengths were 532/560 nm, respectively. The band for Aac2p is indicated by the solid black arrowhead. 30 µg lysozyme-lysed cellular protein was loaded per lane. Fluorescence was quantified using ImageQuant and the background correction and normalisation were calculated as explained above (see Figure 4.11 and Table 4.3 for an example). The normalised relative fluorescence intensities are indicated below (average and standard deviation (*n*=3)).

The specific fluorescence intensity (Figure 4.12) mg^{-1} Aac2p (Figure A.2) is shown (Figures 4.13 and 4.14). The average fluorescence labelling of the single cysteine mutations in the upper parts of the cavity (Figure 4.13 A) and in the cytoplasmic loops (Figure 4.13 B) was significantly above background (P<0.05) (Appendix II). These results are consistent with these cysteines being accessible and hence with an orientation in which the cytoplasmic side of Aac2p is oriented to the outside of the cell.

The labelling of single cysteines in the cytoplasmic loops or the C-terminus in the CATR- or BKA-inhibited state was within error not significantly different (unpaired, two-tailed Student's *t*-test (P<0.05)(Appendix II), except for A124C (Figure 4.13 B). Thus the cysteines were equally accessible to eosin-5-maleimide in both of the inhibited m- and c-states, which is consistent with the loops and C-terminus facing outside of the cell irrespective of the inhibited states. The exception, A124C, which is labelled in the CATR-inhibited state but not the BKA-inhibited state, is located on the N-terminal side of transmembrane α-helix 3 rather than in the middle of a cytoplasmic loop. The result shows that the cysteine is accessible to the outside in the CATR-inhibited state, but becomes occluded in the BKA-inhibited state, however, this result is still consistent with a cytoplasmic side-out orientation.

None of the cysteines that were membrane-facing or inter-helical (Figure 4.14 A) or were on the matrix side (Figure 4.14 B) were labelled significantly above background (P<0.05), irrespective of whether they were in the CATR- or BKA-inhibited state. These results are consistent with the mutant Aac2p being oriented with their cytoplasmic sides to the outside of the cell.

In summary, all of the labelling data are consistent with the single cysteine mutants of Aac2p being oriented with their cytoplasmic side to the outside of the *L. lactis* cell in agreement with the positive-inside rule and previous observations (Kunji *et al.*, 2003).

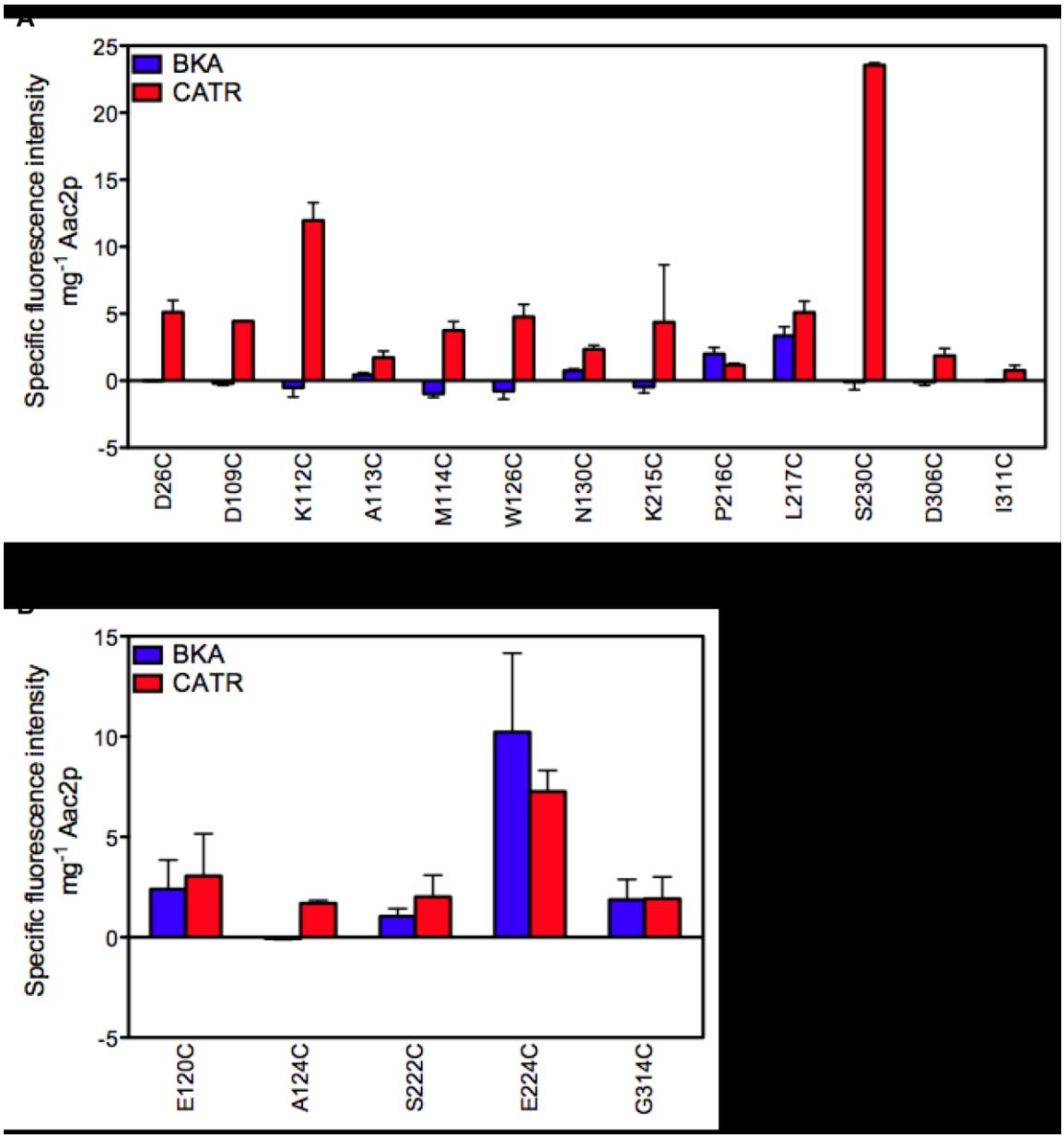

Figure 4.13 Specific eosin-5-maleimide labelling of single cysteines on the cytoplasmic side of mutant Aac2p inhibited with bongkrekic acid or carboxy-atractyloside. The specific fluorescence intensity (Figure 4.12) for single cysteine mutations in the **(A)** upper parts of the cavity on the cytoplasmic side (Figure 4.5) and **(B)** cytoplasmic loops and termini (Table 4.1 and Figure 4.4 C). BKA plus ADP (blue bars) were added 30 min and CATR plus ADP (red bars) were added 10 min prior to a 10 min incubation with eosin-5-maleimide. The fluorescence intensity was corrected for background and the data are presented as the average and the standard deviation (n=3). An unpaired, one-tailed Student's t-test assuming unequal variance (P<0.05) was used to determine whether the average fluorescence intensity of the CATR-inhibited mutants was significantly above background. All of the average fluorescence intensities of the CATR-inhibited Aac2p shown are significantly above background. Please see Appendix II for individual mutant statistics.

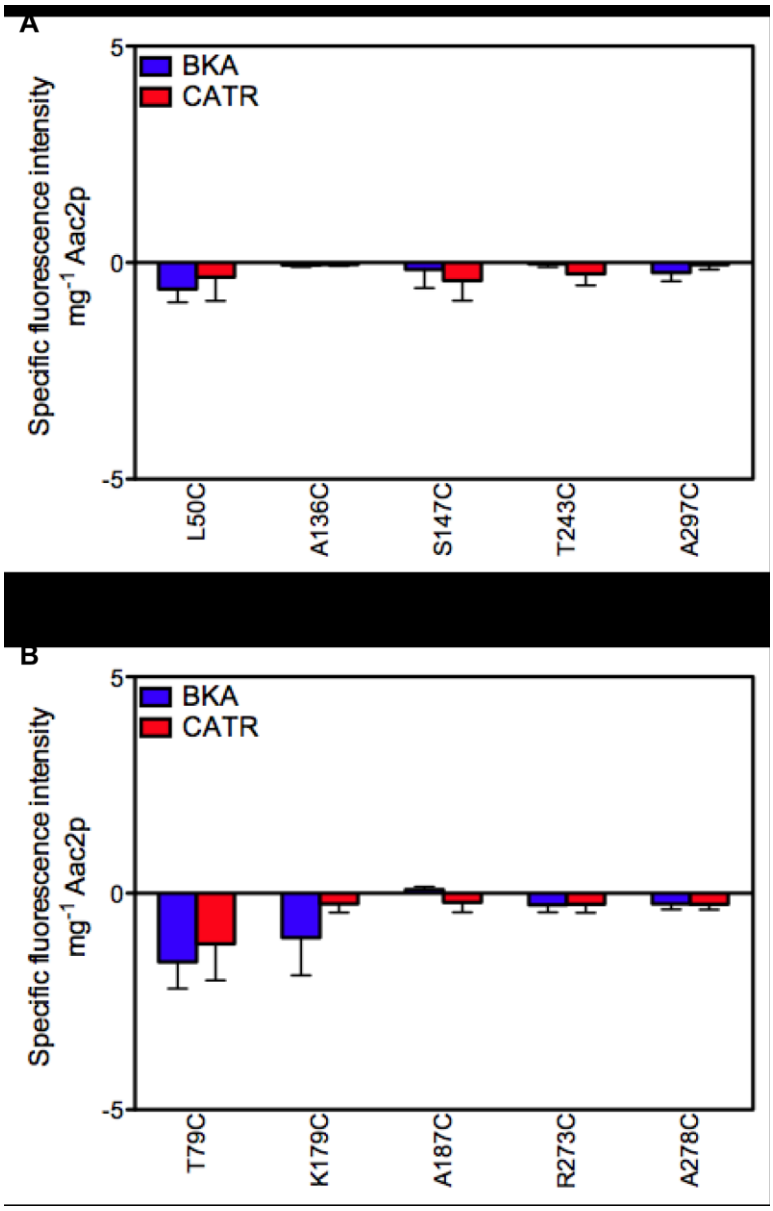

Figure 4.14 Specific eosin-5-maleimide labelling of single cysteines on the cytoplasmic side of mutant Aac2p inhibited with bongkrekic acid or carboxy-atractyloside. For legend details, see Figure 4.13. The specific fluorescence intensity (Figure 4.12) for single cysteine mutations that are **(A)** membrane facing or inter-helical (Table 4.1 and Figure 4.4 A) and **(B)** on the matrix side (Table 4.1 and Figure 4.4 B). All of the average fluorescence intensities of the CATR-inhibited Aac2p shown are not significantly higher than the background. Please see Appendix II for individual mutant statistics.

4.7 Specific initial uptake rates in the presence of carboxy-atractyloside

CATR only inhibits the c-state of the carrier when the binding site is open to the cytoplasm. CATR cannot diffuse passively across the membrane because it has two negatively charged sulphate groups, two negatively charges and other polar properties (Figure 1.6 A and 1.9) (Fiore *et al.*, 1998). These two properties can be exploited to determine the orientation of the single cysteine mutants of Aac2p in the cytoplasmic membrane of *L. lactis*.

The percentage inhibition of ADP uptake in the presence of CATR was measured in *L. lactis* cells expressing single cysteine mutants of Aac2p, as described previously (Section 3.5.2 and Figure 3.14). The specific initial ADP uptake rate was completely inhibited by CATR for all single cysteine mutants that were used as controls (Section 4.3) and they were not significantly different from Δ2-19 cys-less Aac2p in this respect (P<0.05) (Figure 4.15). These data are consistent with all single cysteine mutants of Aac2p being oriented with their cytoplasmic sides to the outside of the *L. lactis* cell, as also observed for the *Neocallimastix patriciarum* ADP/ATP carrier (Kunji *et al.*, 2003).

Thus, the labelling (Section 4.6) and CATR inhibition data (Section 4.7) are consistent with every mutant Aac2p tested being oriented with the cytoplasmic side to the outside of the cell.

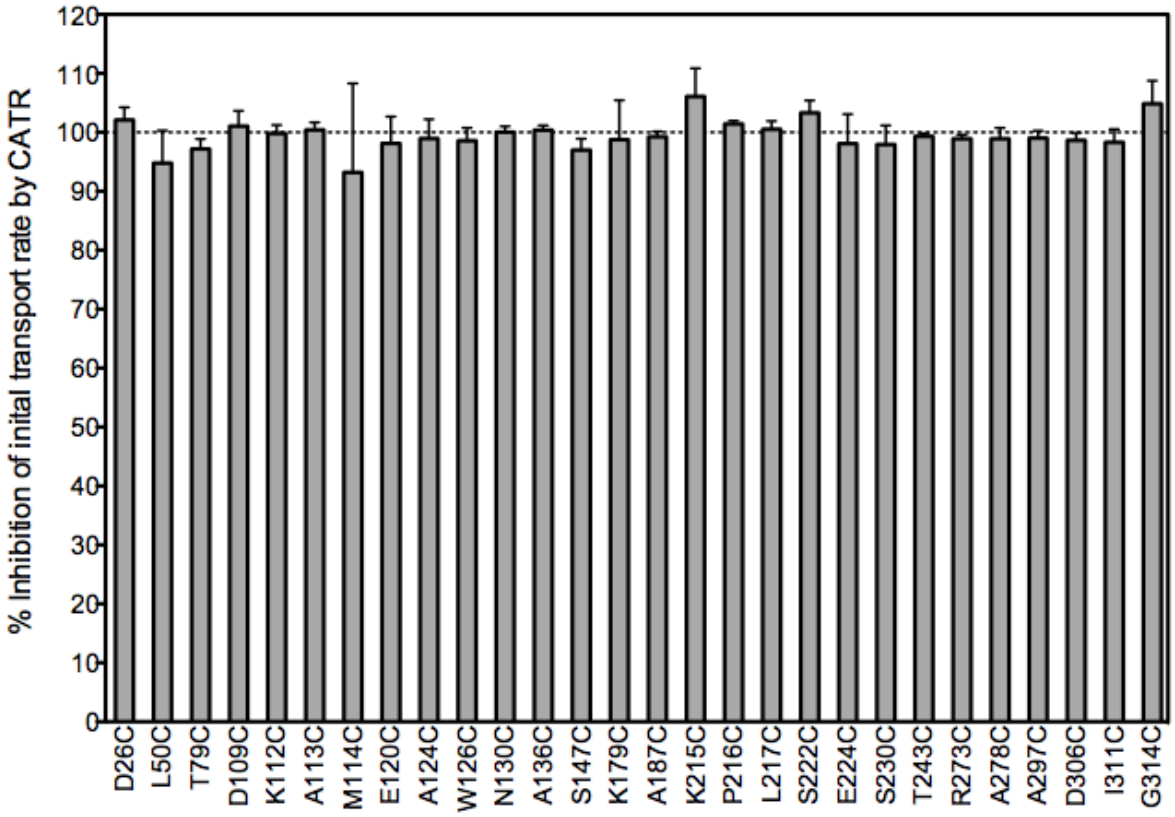

Figure 4.15 Percentage of inhibition of the specific initial ADP uptake rate by carboxy-atractyloside of single cysteine mutants of Aac2p. For details, see legend of Figure 3.14. The selection of mutants is described in Section 4.3. An unpaired, two-tailed Student's *t*-test assuming unequal variance ($P<0.05$) was used to determine that the average inhibition levels were not significantly different than Δ2-19 cys-less Aac2p. See Appendix II for individual mutant statistics.

Chapter 5 Accessibility of single cysteine mutants of the ADP/ATP carrier in different transport states

5.1 Introduction

The aim of this chapter is to determine the accessibility of single cysteines of mutant Aac2p in different transport states. It was predicted that mutations targeted in the water-filled cavity on the cytoplasmic side of the membrane would be labelled well by eosin-5-maleimide in the presence of CATR, when the cavity is open, but would be blocked in the presence of BKA, when the cavity is thought to be closed. These conformational changes should be indicative of the cytoplasmic side of the carrier opening and closing during transport. [Here and throughout this chapter and dissertation 'cytoplasmic side' refers orientation in the original mitochondrion, not to orientation after expression in *L. lactis*.]

5.2 Selection of mutants

Of the initial 38 single cysteine mutants selected (Table 3.1, Figure 3.4), a sub-set were selected for accessibility studies. The inactive A34C, G134C, G138C, R204C, F208C, G234C, G298C and A299C Aac2p were excluded because they did not transport ADP above background levels, as determined by a Student's *t*-test ($P<0.05$) (Section 3.5.1 and Figure 3.13). It is possible that these mutations resulted in a non-functional carrier, or had deleterious effects on protein folding or membrane insertion. As their transport state could not be determined with certainty, they were not used to probe the accessibility of single cysteines in different states. The poorly inhibited G30C, N104C, Y203C, Y211C, D212C, T238C and Y305C Aac2p were also excluded, as they were not inhibited by BKA as efficiently as the Δ2-19 cys-less Aac2p, and thus could not be locked completely in the m-state (Section 3.5.2 and Figure 3.16).

The remaining single cysteine mutants N22C, D26C, T100C, Q101C, F105C, K108C, D109C, K112C, A113C, M114C, W126C, N130C, Y207C, K215C, P216C, L217C,

S226C, S230C, V301C, I302C, D306C, Q309C and I311C Aac2p were considered suitable for accessibility studies. The single cysteines of these Aac2p are located at the entrance to the cavity on the cytoplasmic side in mitochondria (outside *L. lactis*) and should in principle be accessible to the thiol-specific and membrane-impermeable eosin-5-maleimide (Figure 5.1).

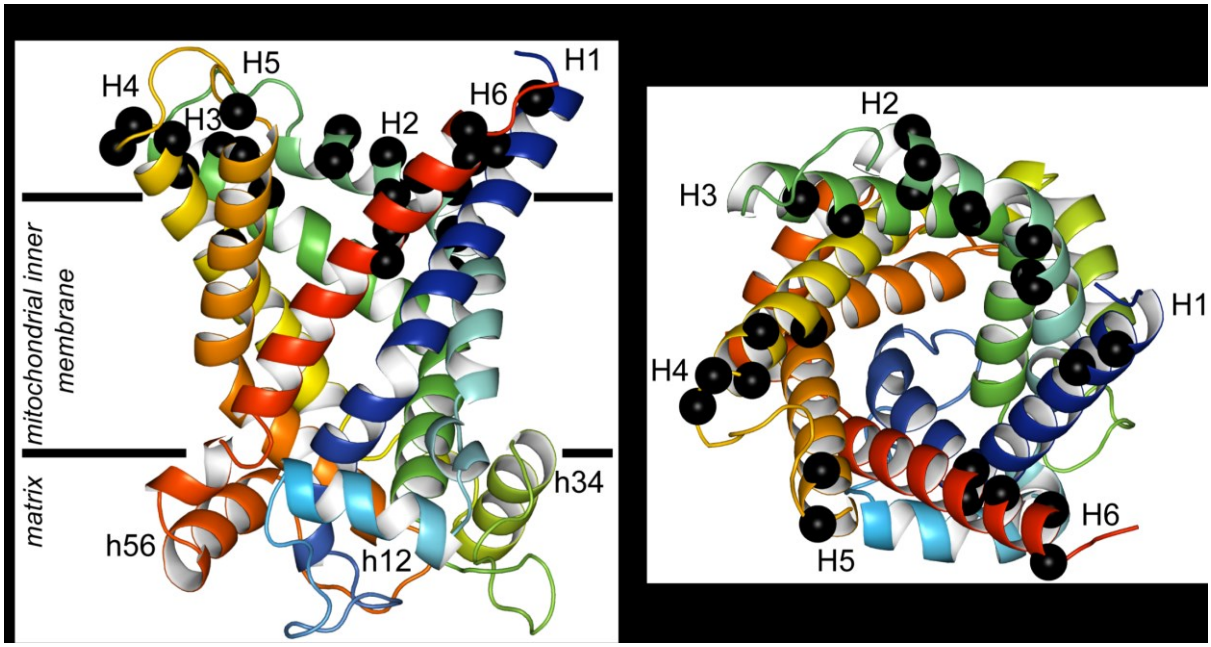

Figure 5.1 Single cysteine mutations used for accessibility studies. For details, see Figure 4.1. The cysteine mutations used are shown as a single black spheres centred on their α-carbons. The mutations shown are N22C, D26C, T100C, Q101C, F105C, K108C, D109C, K112C, A113C, M114C, W126C, N130C, Y207C, K215C, P216C, L217C, S226C, S230C, V301C, I302C, D306C, Q309C and I311C. For a description of the mutations, see Table 3.1. **(A)** The lateral view and **(B)** the view into the cavity from the cytoplasm (outside *L. lactis*).

5.3 Expression level of single cysteine mutants

Single cysteine mutants of Aac2p were expressed in membranes of *L. lactis*, inhibited with BKA or CATR and labelled with eosin-5-maleimide. The mutants varied in their levels of expression; all were expressed at levels ranging from similar to 5.1-fold higher compared to Δ2-19 cys-less Aac2p (Appendix IV, Figure A.4), and the levels are consistent with those reported in Section 4.4. Importantly, all of the single cysteine mutants of Aac2p were expressed, and thus it is possible to carry out labelling studies.

5.4 Eosin-5-maleimide labelling of single cysteine mutants in the presence of bongkrekic acid or carboxy-atractyloside

5.4.1 Specific labelling

Single cysteine mutants of Aac2p were inhibited with BKA or CATR, and subsequently their cysteine thiols were labelled with eosin-5-maleimide to probe the water accessibility of the introduced cysteines in the two inhibited states (mutants described in Section 5.2). The specific fluorescence intensities of the mutants are shown in Figure 5.2. The labelling of the single cysteines is distinguishable above background and is thiol-specific. Some of the single cysteines were not labelled at all, some were labelled preferentially in the CATR-inhibited c-state, one was labelled preferentially in the BKA-inhibited m-state, and some were labelled in both inhibited states.

The specific fluorescence intensity (mg^{-1} Aac2p) (determined using data in Figure 5.2 and Appendix IV, Figure A.4) was determined for all of the single cysteine mutations on the cytoplasmic side. The mutants that were labelled significantly above background ($P<0.05$) in either the inhibited c- or m-state or both, are shown in Figure 5.3, whereas those that are not significantly different than, or lower than, background, irrespective of the inhibited state, are shown in Figure 5.4.

The residues in the cavity that were labelled significantly above background in the CATR-inhibited state are D26C, D109C, K112C, A113C, M114C, W126C, N130C, K215C, P216C, L217C, S230C, I302C and I311C (Figure 5.3). In the presence of BKA, however, D26C, D109C, K112C, M114C, W126C, K215C, S230C and I311C were not labelled significantly, indicating they had become occluded because the cytoplasmic side closed, creating a 'barrier' to eosin-5-maleimide labelling.

Some mutants, namely A113C, N130C, P216C, L217C and I302C Aac2p, were labelled in both states, indicating that these residues had not become fully occluded

and are possibly outside the region in Aac2p that closes in the inhibited m-state. Very low levels of labelling still occurred in the m-state, which is possibly because complete inhibition by BKA cannot be achieved (Figure 3.16). Some mutations, such as A113C and P216C at the top of α-helix H2 and H4, respectively, could be in the dynamic areas of Aac2p that have variable accessibility due to movements at the helix-loop interface.

In the BKA-inhibited state the single cysteines of mutant Aac2p were consistently poorly labelled whereas in the CATR-inhibited state the level of labelling varied widely, from moderate to high (Figure 5.3 B-C and D-E). These data suggest that most of the single cysteines on the cytoplasmic side are accessible in the inhibited c-state, but not in the m-state.

Δ2-19 Aac2p was expected to remain unlabelled because its four endogenous cysteines are inaccessible from the cytoplasmic side (Houstěk & Pedersen, 1985) whereas Δ2-19 cys-less Aac2p lacks cysteines. As expected, both were not labelled (Figure 5.4). The single cysteines that were within error labelled not significantly different than or lower than the background in both states were N22C, T100C, Q101C, F105C, K108C, Y207C, S226C, V301C and Q309C (Figure 5.4). Most of these are located further down the cavity (Figure 5.4 B-C), which may be too narrow for eosin-5-maleimide to access. N22C, S226C and Q309C are located near the top of the cavity, but they are not labelled. A large number of the unlabelled cysteine thiols are located along α-helix H2, including T100C, Q101C, F105C and K108C. CATR binding may block eosin-5-maleimide from accessing these sites. They will not be used in further analysis as there is no significant labelling irrespective of the inhibited state.

Of the mutant Aac2p with single cysteine replacements of the CATR binding site, namely N104C, K108C and R204C Aac2p (Figure 3.5 C-D), only the labelling of residue K108C could be determined because N104C Aac2p was not significantly inhibited by BKA (Figure 3.16), and R204C Aac2p transport was not significantly different than the background (Figure 3.12). There was no significant labelling of K108C in the c-state, most likely because CATR binding occludes the single cysteine (Figure 5.4).

Of the cytoplasmic salt bridge or ionic pair mutants, D109C, K112C, D212C, K215C, D306C and Q309C Aac2p (Figure 3.5 A-B), D212C Aac2p was the only mutant that could not be analysed by fluorescent labelling, as transport activity of D212C Aac2p was not significantly inhibited by BKA (Figure 3.16). Four of the five salt bridge or ionic pair mutations tested, D109C, K112C, K215C and D306C, were labelled significantly in the CATR-inhibited state, and three of the five (D109C, K215C and D306C) were labelled differently in the two inhibited states (Figure 5.5), indicating that these residues become occluded. Q309C was not labelled in either state (Figure 5.4), indicating that this residue is not accessible for labelling. In summary, the labelling results are consistent with the theory that a cytoplasmic salt bridge is formed in the m-state.

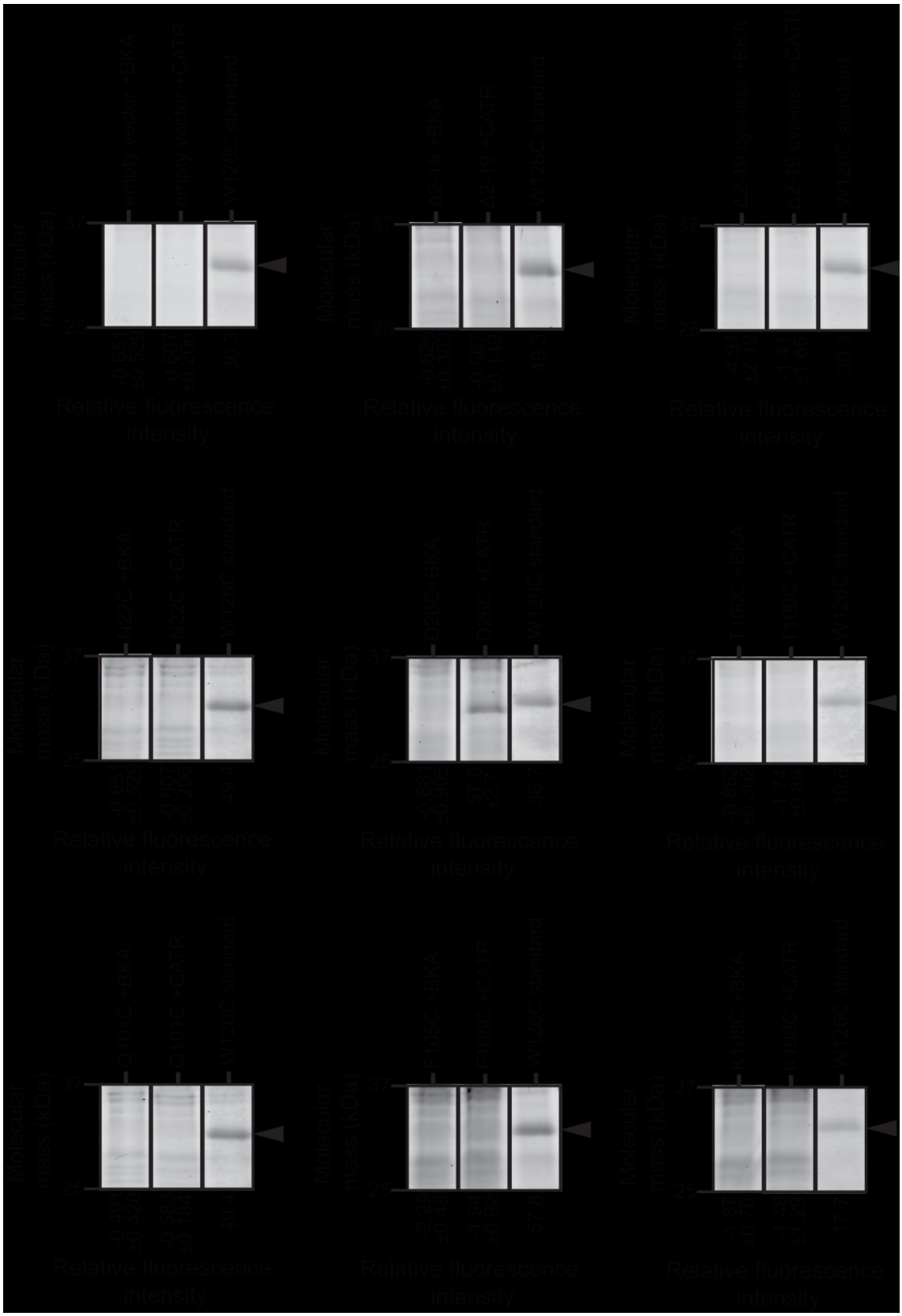

Figure 5.2 Relative fluorescence intensity of eosin-5-maleimide labelled, single cysteine mutants of Aac2p inhibited by bongkrekic acid or carboxy-atractyloside. For details, see legend of Figure 4.12.

Figure 5.2 continued Relative fluorescence intensity of eosin-5-maleimide labelled, single cysteine mutants of Aac2p inhibited by bongkrekic acid or carboxy-atractyloside. For details, see Figure 4.12.

Figure 5.2 continued Relative fluorescence intensity of eosin-5-maleimide labelled, single cysteine mutants of Aac2p inhibited by bongkrekic acid or carboxy-atractyloside. For details, see legend of Figure 4.12.

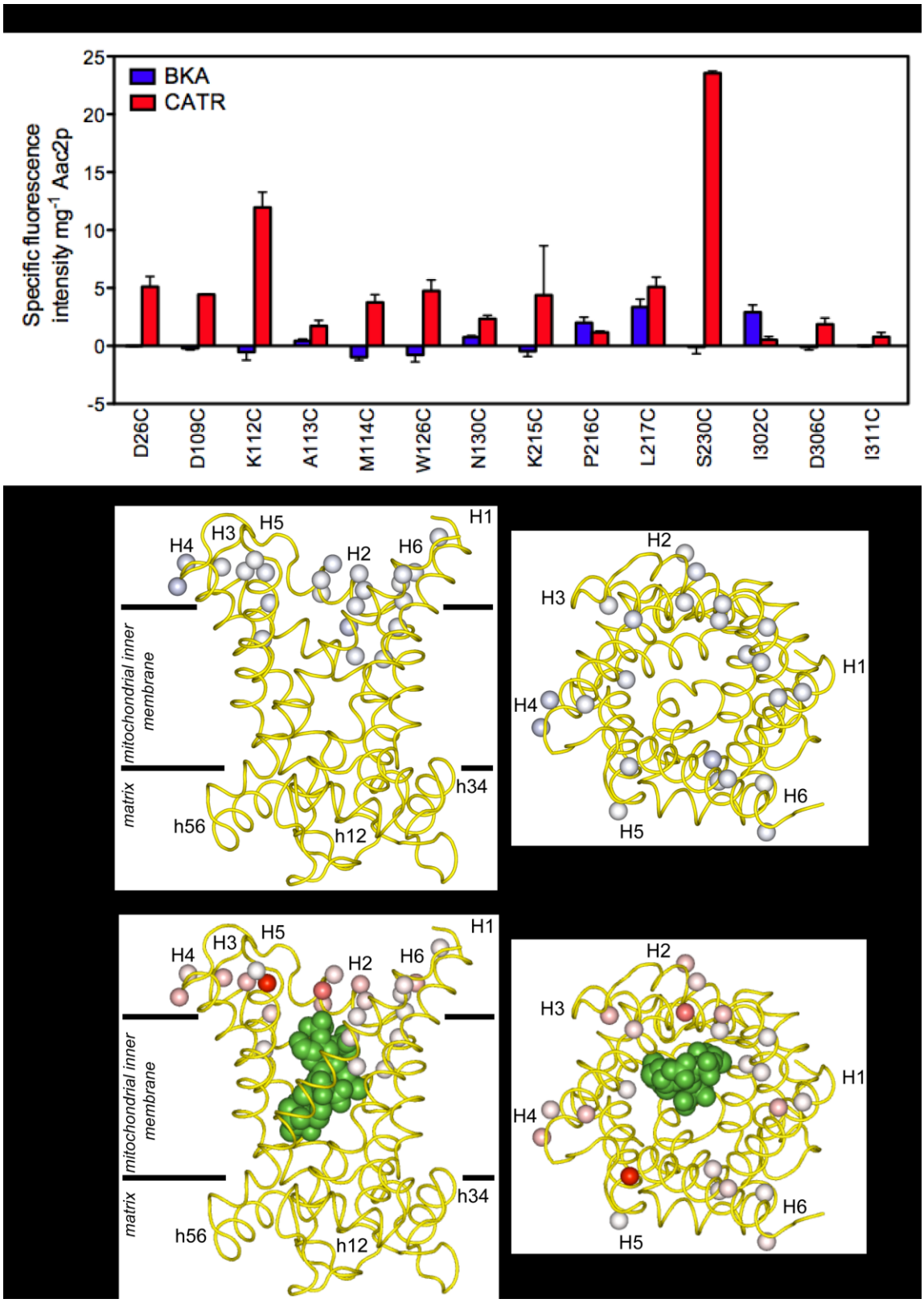

Figure 5.3 Specific fluorescence intensity of eosin-5-maleimide labelled single cysteine mutants of Aac2p that are labelled above background in the carboxy-atractyloside- or bongkrekic acid-inhibited state. For legend, see next page.

Legend of Figure 5.3 Specific fluorescence intensity of eosin-5-maleimide labelled single cysteine mutants of Aac2p that are labelled above background in the carboxy-atractyloside- or bongkrekic acid-inhibited state. (A) The specific fluorescence intensities for the active and inhibited sub-set of mutant Aac2p with single cysteines on the cytoplasmic side (Figure 5.1) that labelled significantly above background. BKA and ADP (blue bars) were added 30 min prior and CATR and ADP were added 10 min prior to the 10 min incubation with eosin-5-maleimide. The fluorescence intensity was corrected for background and the data are the average and the standard deviation (n=3). An unpaired, one-tailed Student's t-test assuming unequal variance (P<0.05) was used to determine whether the CATR- or BKA-inhibited mutant Aac2p were labelled significantly above background. For individual mutant statistics, see Appendix II. **(B) and (C)** Model depicting the specific fluorescence intensities for the BKA-inhibited Aac2p shown on a scale from blue (highly labelled) to white. **(D) and (E)** The CATR-inhibited Aac2p on a scale from red (highly labelled) to white. Aac2p is shown as a yellow wire and CATR is shown in green. Each single cysteine mutation is shown as a sphere centred on the C_α atom. (B) and (D) The lateral view from the membrane and (C) and (E) the view from the cytoplasm.

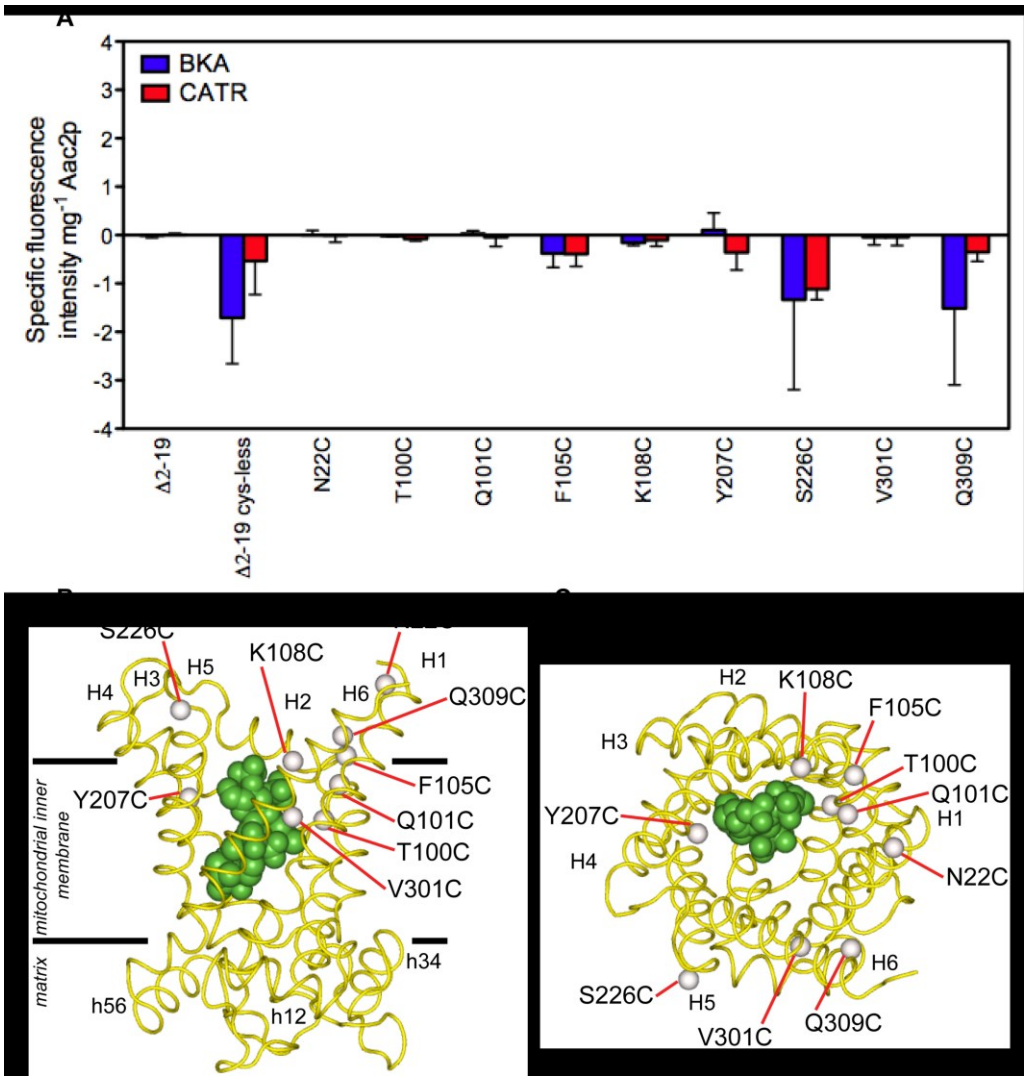

Figure 5.4 Specific fluorescence intensity of eosin-5-maleimide labelled single cysteine mutants of Aac2p that are within error labelled not significantly different than or lower than background in the carboxy-atractyloside- and bongkrekic acid-inhibited state. Legend as for Figure 5.2 except that an unpaired, one-tailed Student's *t*-test assuming unequal variance ($P<0.05$) was used to determine whether the CATR- or BKA-inhibited mutants of Aac2p were within error labelled not significantly different or significantly lower than background. Specific labelling of F105C in the presence of BKA, and specific labelling of S226C and Q309C in the presence of CATR was significantly lower than background.

5.4.1 Difference in labelling

The average difference in fluorescence intensity between the CATR- and BKA-inhibited states was calculated for those mutants competent in transport (Figure 3.10), for those that were well inhibited (Figure 3.14 and 3.16) and for those that were significantly labelled in either or both inhibited states. The mutants with significant differences in labelling of single cysteines between the two inhibited states are shown in Figure 5.5 and the mutants with no significant differences are shown in Figure 5.6.

The mutations with significantly higher labelling in the inhibited c-state were D26C, D109C, K112C, A113C, M114C, W126C, N130C, S230C and D306C (Figure 5.5). All of these mutations are located at the top of the cavity on the cytoplasmic side of the carrier (Figure 5.5 B-C). These data show that these residues become occluded in the m-state, which is consistent with the closure of the cytoplasmic side of the cavity.

The only exception, I302C was labelled marginally higher in the inhibited m-state compared to the c-state. I302C is located further in the cavity on α-helix H6 (Figure 5.5 B). The average difference in labelling was -2.4, compared to 23.6 for S230C, which had the highest difference in labelling between the inhibited c- and m-states (Figure 5.5 A). Oddly, I302C was labelled in both the inhibited m- and c-states, indicating the labelling was state independent. Importantly, subsequent work by Janina Tiedemann showed that eosin-5-maleimide labelling of untreated I302C is similar to that of the BKA-inhibited I302C (Figure 5.7). These data show that the uninhibited c-state can be labelled, whereas the CATR-inhibited state cannot, suggesting that CATR blocks the accessibility of this residue to eosin-5-malemide. The specific initial uptake rate of I302C Aac2p was inhibited to ~90% by BKA (Figure 3.16), and thus the result is not a consequence of the failure of BKA to lock I302C Aac2p in the m-state. Considering all the evidence, it is likely that weaker labelling in the CATR-inhibited state is due to interference by CATR rather than stronger labelling in the BKA-inhibited state.

No significant difference in labelling was observed for residues K215C, P216C, L217C and I311C (Figure 5.6). These single cysteines are located at the very top of the cavity where the accessibility might not change much depending on the state (Figure 5.6 B-C). However, the labelling levels were low (Figure 5.3 and 5.6), indicating that they are mostly inaccessible, even though some of them were predicted to be located on water-accessible surfaces.

In conclusion, the data are consistent with the inhibited c-state being open on the cytoplasmic side and the inhibited m-state being closed on the cytoplasmic side.

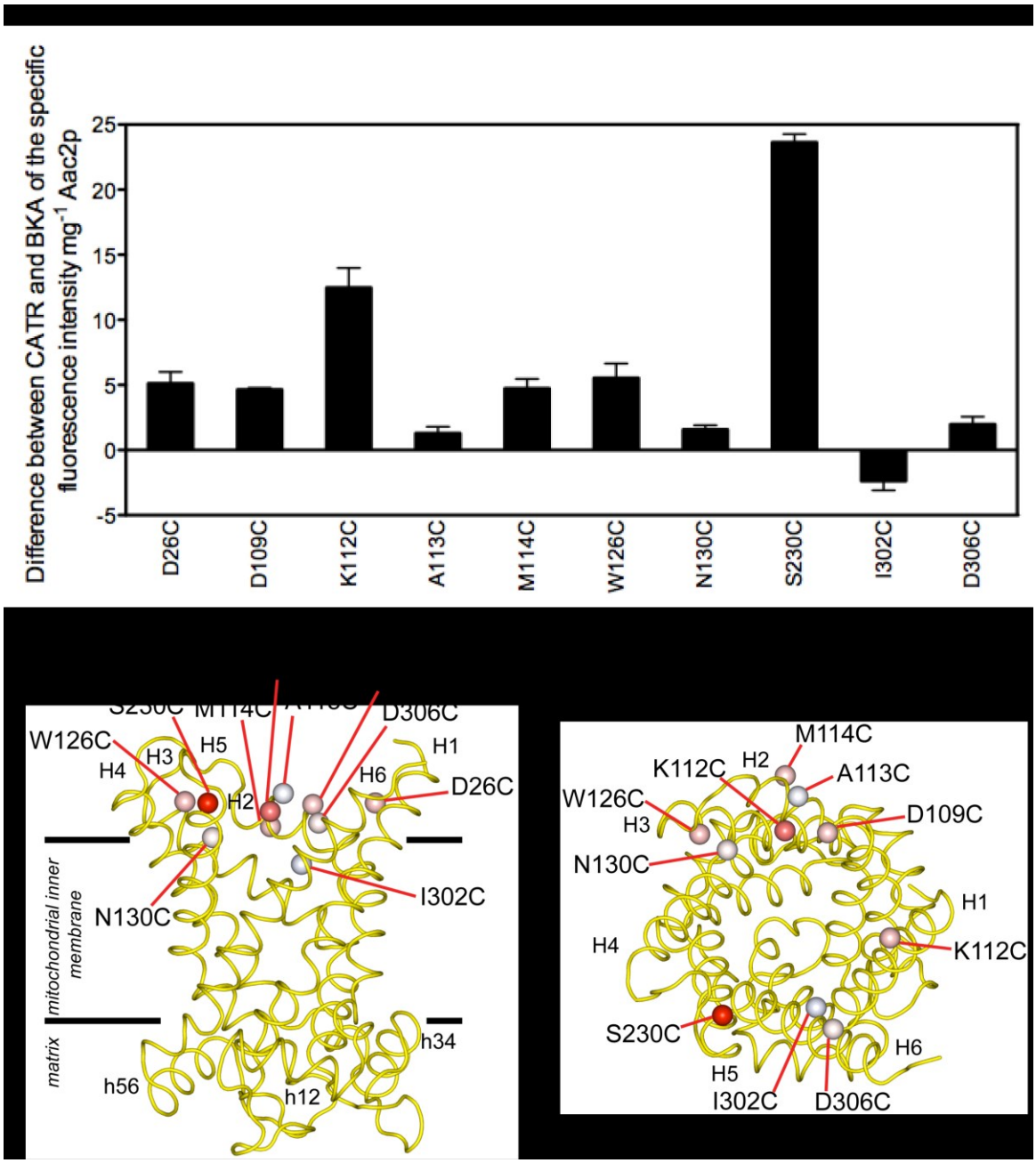

Figure 5.5 Significant differences of the specific eosin-5-maleimide labelling intensities between carboxy-atractyloside- and bongkrekic acid-inhibited states of single cysteine mutants of Aac2p (A) The calculated difference between the specific fluorescence intensities of the CATR-inhibited state minus the BKA-inhibited state. The data show the average and the standard deviation (n=3). An unpaired, two-tailed Student's t-test assuming unequal variance (P<0.05) was used to determine that the differences were significant (Appendix II). **(B) and (C)** Model depicting the data shown in (A) on a colour scale from the highest difference (red) to no difference (white). Only in the case of I302C is the difference negative, which is indicated with a light blue sphere. The Aac2p is shown as a yellow wire. (B) The lateral view from the membrane and (C) the view from the cytoplasmic side.

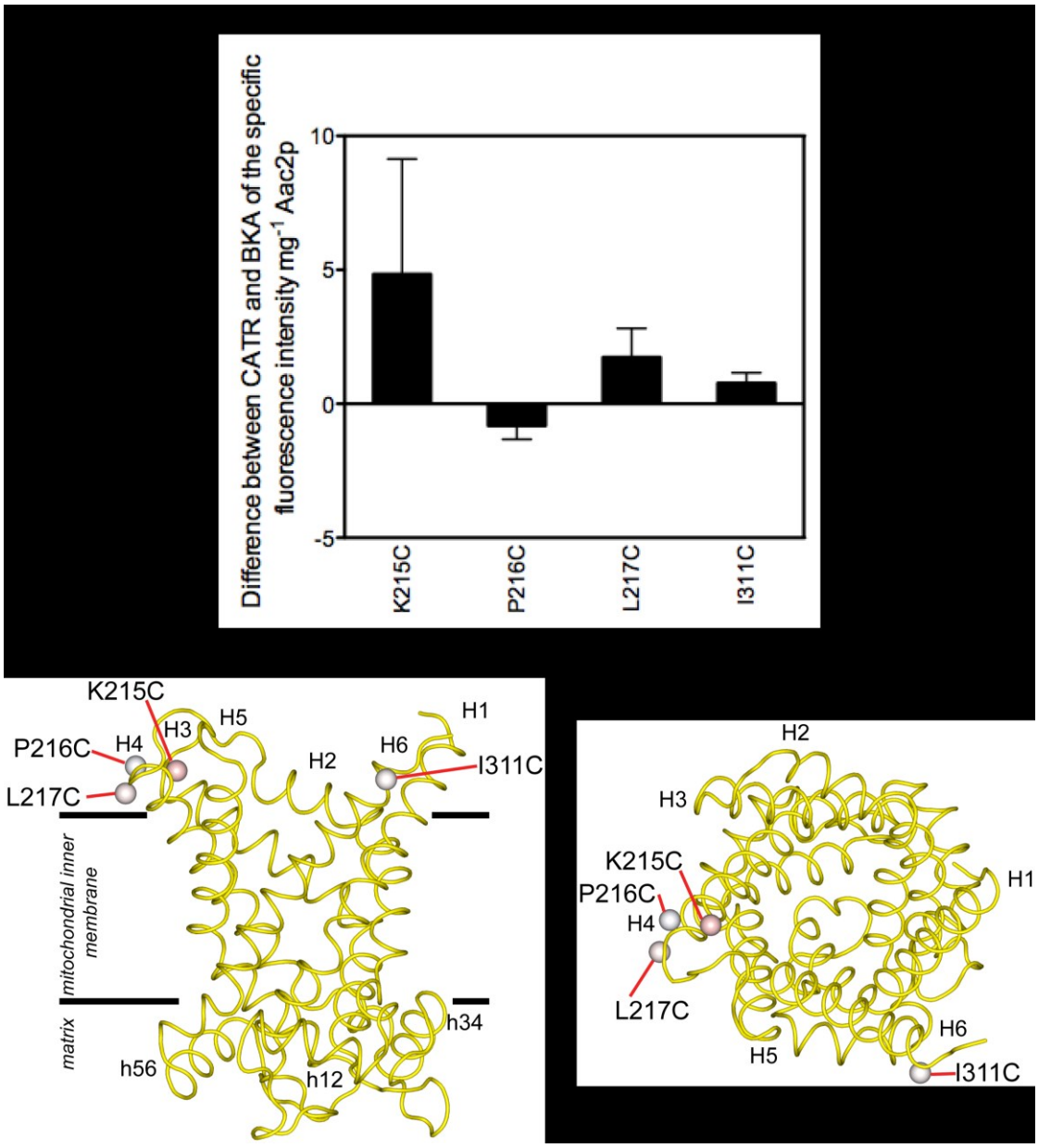

Figure 5.6 Non-significant differences in the specific eosin-5-maleimide labelling intensities between carboxy-atractyloside- and bongkrekic acid-inhibited states of single cysteine mutants of Aac2p. Legend as in Figure 5.5.

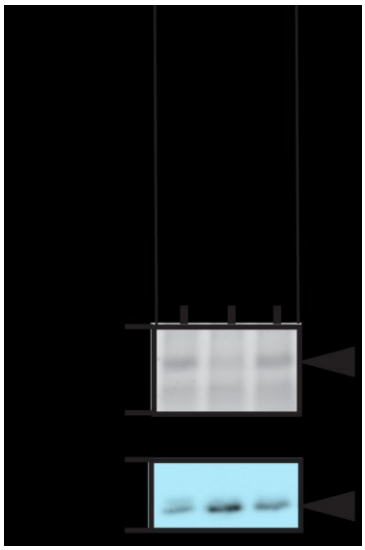

Figure 5.7 Fluorescence intensity and expression of eosin-5-maleimide labelled I302C Aac2p in the presence and absence of inhibitors. Fluorescence labelling intensity (above) and Western blot analysis (below) of I302C Aac2p treated with BKA or CATR, or untreated. The fluorescent scan was imaged at 675 V and the Western blot was analysed as described previously, except that ECL Prime was substituted for standard ECL (*n*=3).

5.5 Effect of eosin-5-maleimide on the specific initial uptake rates of single cysteine mutants

To explore the effect of nucleotide substrates on eosin-5-maleimide labelling, the specific initial uptake rate was measured for single cysteine mutants in the presence and absence of eosin-5-maleimide and the percentage of inhibition was calculated (Figure 5.8). The uptake rates of both Δ2-19 and Δ2-19 cys-less Aac2p were, within error, unaffected by eosin-5-maleimide labelling (P<0.05). These data are in agreement with the theory that the endogenous cysteines are not accessible to eosin-5-maleimide from the outside of the cell. However, many of the single cysteine mutants of Aac2p were significantly affected by eosin-5-maleimide (unpaired, two-tailed Student's *t*-test assuming unequal variance (P<0.05))(marked by asterisk in Figure 5.8). It is possible that eosin-5-maleimide may block access to the substrate binding site or that labelling interferes with conformational changes in the transport cycle.

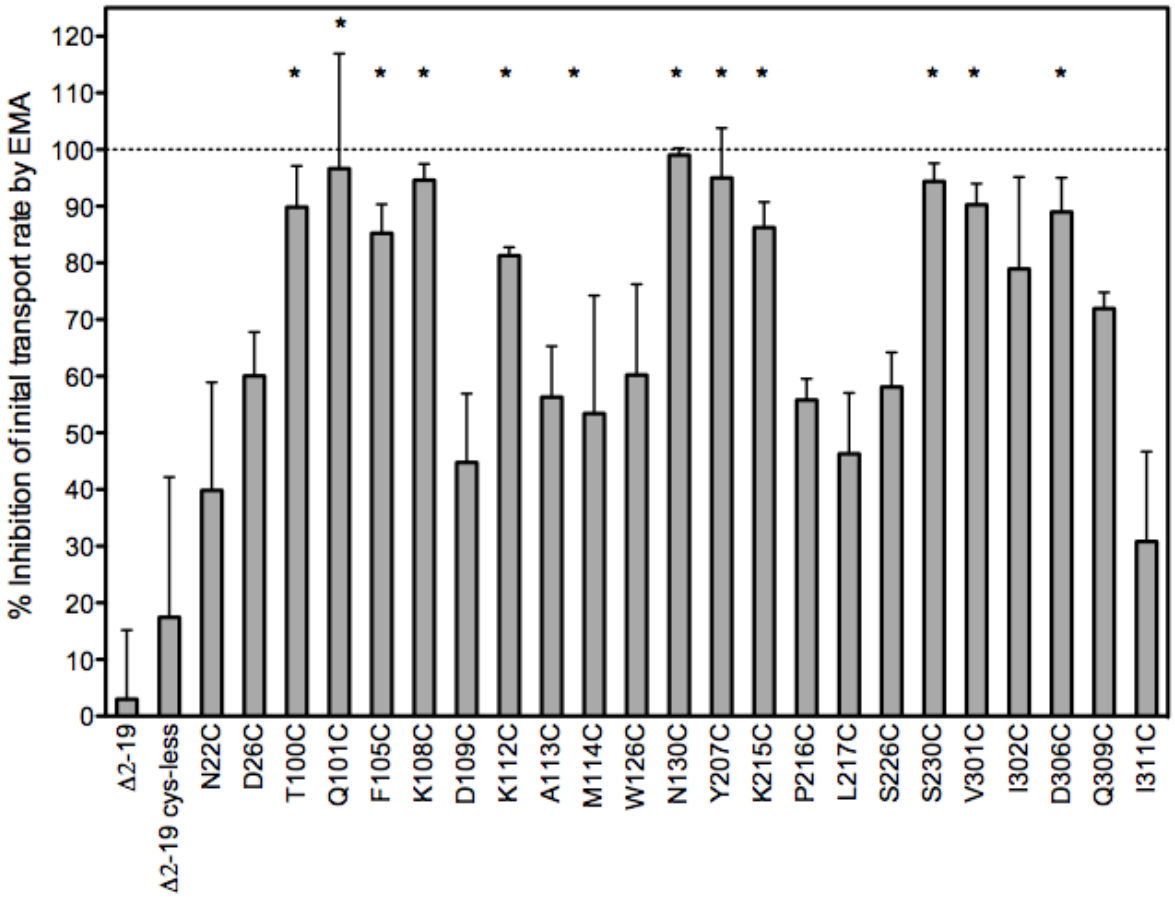

Figure 5.8 Percentage inhibition of the specific initial ADP uptake rate by eosin-5-maleimide labelling of single cysteine mutants of Aac2p. The percentage inhibition is calculated from the specific initial uptake rate in the presence and absence of eosin-5-maleimde (Figure 3.10). The mutants of Aac2p that were not transporting or were not inhibited significantly were excluded from the analysis. The data show the average and the standard deviation (*n*=3). The average of Δ2-19 and Δ2-19 cys-less Aac2p is not significantly different from the empty vector, as determined using an unpaired, one-tailed Student's *t*-test assuming unequal variance (*P*<0.05). Average inhibition values that are significantly higher than Δ2-19 cys-less Aac2p are indicated by an asterisk (unpaired, two-tailed Student's *t*-test assuming unequal variance (*P*<0.05)).

5.6 Effect of nucleotides on eosin-5-maleimide labelling of single cysteine mutants

The effect of nucleotides on eosin-5-maleimide labelling of single cysteines of mutant Aac2p was determined to understand how accessibility of single cysteines changes during transport. Ten single cysteine mutants of Aac2p that were competent in transport (Figure 3.10), were inhibited well (Figure 3.14 and 3.16) and showed significant differences in labelling between the two inhibited states (Figure 5.5) were studied. The experimental work was done by Janina Tiedemann.

Single cysteines of mutant Aac2p were labelled in the absence or presence of ADP (Figure 5.9 and A.5), and specific labelling was determined (Figure 5.10). It was found that single cysteines were labelled to levels well above background in the absence of ADP, similarly to levels in the presence of CATR (Figure 5.3). For instance, the specific labelling of W126C Aac2p in the absence of nucleotide (2.77 ± 0.70 mg^{-1} W126C) was not significantly different from that of CATR-inhibited W126C Aac2p (2.14 ± 0.74) (unpaired, two-tailed Student's *t*-test assuming unequal variance (P<0.05, n=9)). These results show that in the absence of substrate the carriers are in the c-state, which is consistent with the current transport mechanism. In the absence of substrate on the outside, the carrier is fixed in the c-state by the matrix salt bridge network, which forms an energy barrier preventing a spontaneous change to the m-state. Only the binding of substrate will provide sufficient energy to overcome the energy barrier leading to a conversion to the m-state.

Specific labelling in the absence of ADP was higher than in the presence of ADP for seven of the ten single cysteine mutants of Aac2p (P<0.05) (Figure 5.10, significant differences indicated by an asterisk). In the presence of high concentrations of ADP, the transporter cycles rapidly through the transport states and consequently the introduced cysteines become less available for labelling. The exceptions, D109C, I302C and D306C Aac2p were not within error labelled differently in the absence or presence of ADP, indicating that the labelling is not affected by cycling through the transport states. In D109C and D306C Aac2p, the single cysteine replacements are in the cytoplasmic network, which could still be accessible even when the network

forms, indicating that the closure occurs adjacent to the network. I302C Aac2p is an exceptional case in many respects. The results here show that the labelling is higher in the absence of substrate than in the presence of CATR (Figure 5.7), which indicates that CATR prevents labelling through accessibility, but only marginally. This observation could also explain why the labelling in the presence of BKA was slightly higher than in the presence of CATR. The result here shows that the labelling of I302C is independent of substrate, which may indicate that it reflects mostly background labelling rather than a specific state dependent labelling.

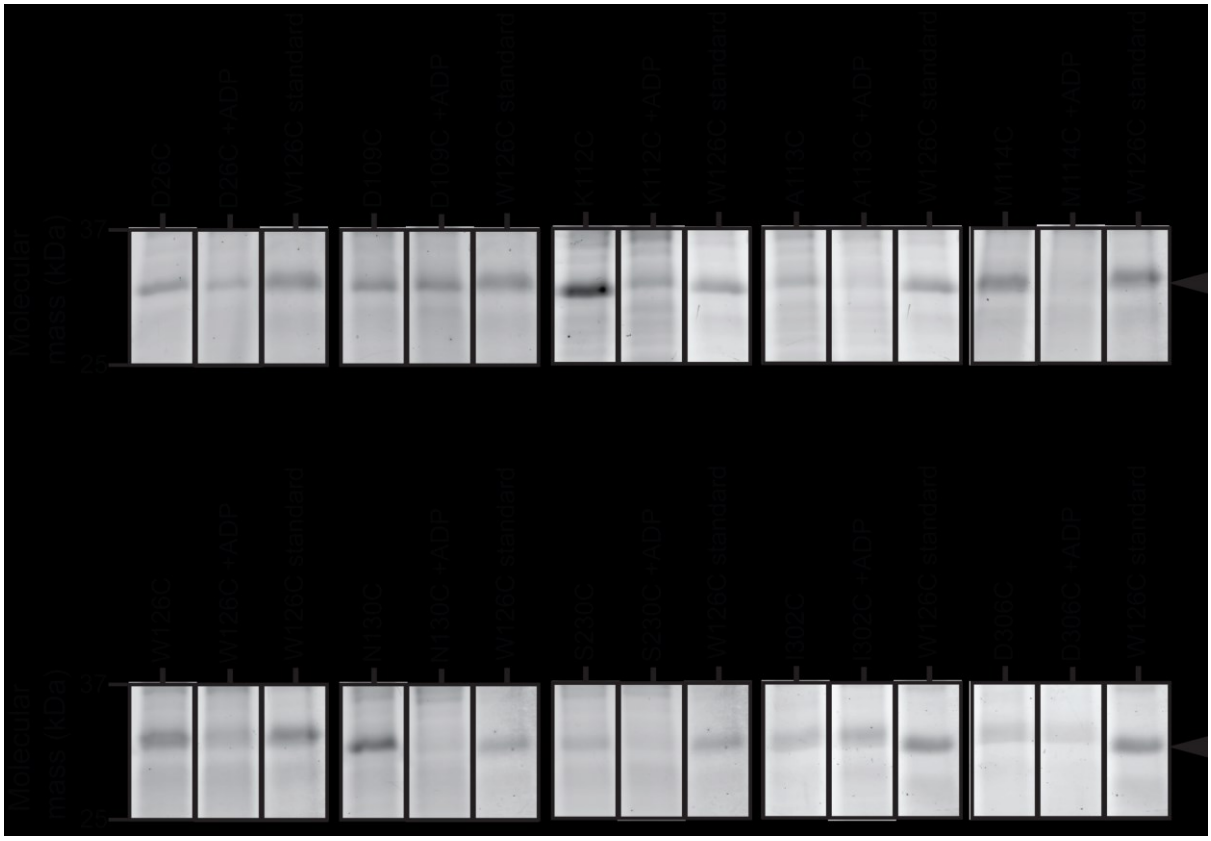

Figure 5.9 Fluorescence intensity of single cysteine mutants of Aac2p labelled with eosin-5-maleimide in the absence or presence of ADP. (A) Fluorescence labelling in the absence or presence of 2.5 mM ADP of those mutant Aac2p that showed significant differences in labelling between the BKA- and CATR-inhibited states (Figure 5.5 and Section 5.4.2). The fluorescent scans were imaged at 675 V, except for those of K112C and A113C, which were at 635 V. The Western blots are shown in Appendix IV (Figure A.5). The labelling studies were repeated three times and a representative example is shown.

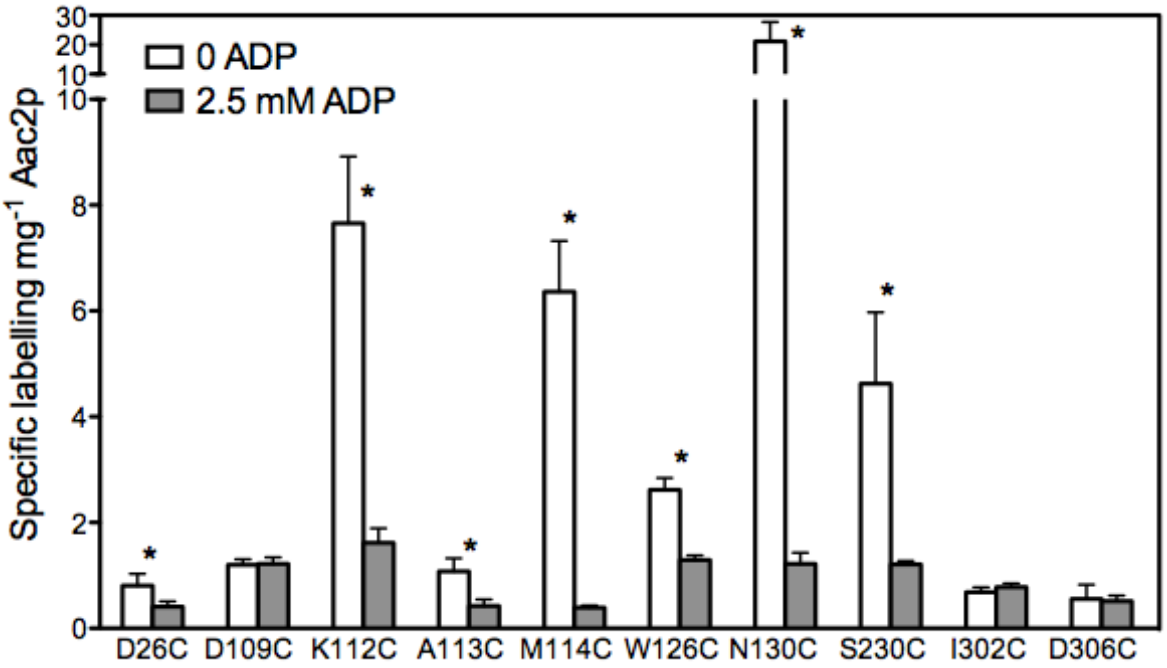

Figure 5.10 Specific fluorescence labelling of single cysteine mutants of Aac2p with eosin-5-maleimide in the absence or presence of ADP. The specific labelling of mutant Aac2p in the absence or presence of 2.5 mM ADP (determined using data from Figure 5.9 and A.5). Mutants that showed significant differences in labelling are marked by an asterisk (unpaired, one-tailed Student's *t*-test assuming unequal variance (P<0.05)). The data are presented as the average and the standard deviation (n=3).

To test whether the differences in labelling were a consequence of ADP being a specific substrate of Aac2p, the effect of different nucleotides on the labelling of W126C Aac2p was determined. W126C Aac2p was chosen for two reasons; first, transport of W126C Aac2p was only ~60% inhibited by an 80-fold excess of eosin-5-maleimide, indicating that labelling does not affect the uptake activity to a large extent (Figure 5.8). Second, W126C Aac2p was labelled significantly differently by eosin-5-maleimide in the absence and presence of ADP (Figure 5.10). The nucleotides chosen were AMP, ADP, ATP, deoxyadenosine 5'-diphosphate (dADP), deoxyadenosine 5'-triphosphate (dATP), guanosine 5'-monophosphate (GMP), guanosine 5'-diphosphate (GDP), guanosine 5'-triphosphate (GTP), cytidine 5'-diphosphate (CDP) and uridine 5'-diphosphate (UDP).

In the presence of ADP, ATP, dADP and ATP the labelling was significantly lower than in the absence of substrate (P<0.0.5) (Figure 5.11, significant differences indicated by asterisk). In the presence of AMP, GMP, GDP, GTP, CDP and TDP the

labelling was not significantly different. This result agrees with the known substrate specificity of Aac2p and would agree with the properties of the substrate binding site (Brierley & O'Brien, 1965; Duee & Vignais, 1969; Pfaff & Klingenberg, 1968; Kunji & Robinson, 2006; Robinson & Kunji, 2006; Dehez *et al.*, 2008; Robinson *et al.*, 2008; Wang & Tajkhorshid, 2008). Thus, the labelling of W126C can be used as an indicator of the substrate specificity of Aac2p.

Finally, the effect of different concentrations of ADP and ATP on eosin-5-maleimide labelling of single cysteine W126C was investigated. High concentrations of ADP and ATP led to the significant occlusion of the residue W126C ($P<0.05$), (Figure 5.12), as previously observed for one concentration (Figure 5.10 and 5.11). The occlusion of W126C exhibited saturation kinetics in the presence of ADP and ATP, suggesting that the transport rate in the presence of high substrate concentrations is so high that W126C cannot by labelled by eosin-5-maleimide. Thus, the maximal occlusion does not just represent the maximal transport rates but also the limiting concentration of eosin-5-maleimide, which might have been too low to reflect transport rates accurately. To improve this, higher eosin-5-maleimide concentrations were tested, but the increase in background labelling prevented the accurate measurement of the specific labelling of W126C (data not shown). These results demonstrate that the external addition of the substrates ADP and ATP leads to a change in the accessibility of residues on the cytoplasmic side of the cavity. The most likely interpretation is that the cytoplasmic side of Aac2p opens and closes as part of the transport cycle.

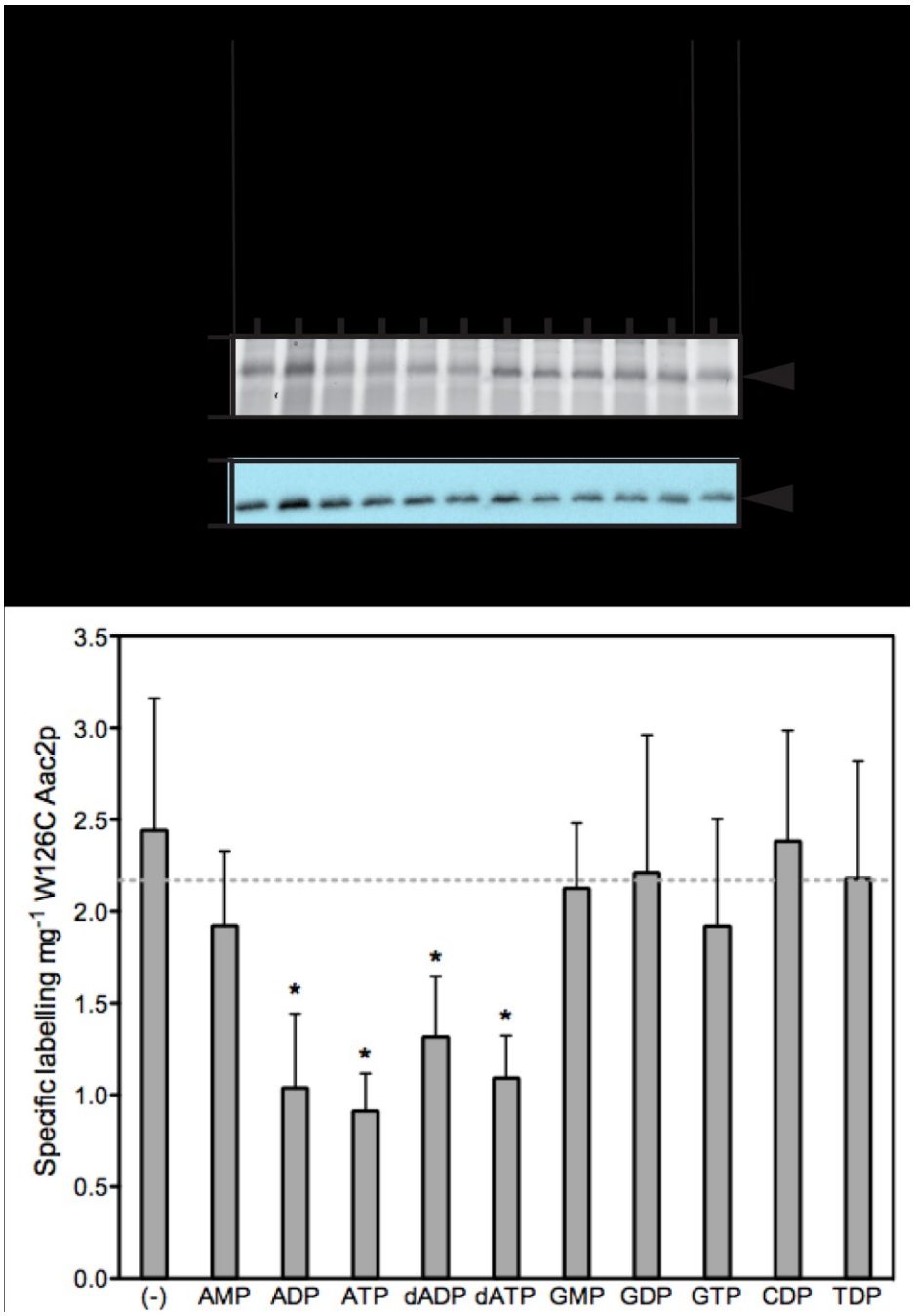

Figure 5.11 Nucleotide specificity of eosin-5-maleimide labelling of W126C. (A) Fluorescence intensity (above) and Western blot analysis (below) of W126C Aac2p in the presence of various nucleotides at a concentration of 2.5 mM. The fluorescent scans were imaged at 675 V. The Western blots were analysed as described, except that ECL prime was substituted for standard ECL. The labelling and Western blots were repeated three times and a representative example is shown. **(B)** The specific labelling of W126C Aac2p in the presence and absence of nucleotide was compared (unpaired, one-tailed Student's *t*-test assuming unequal variance (P<0.05)). Significant differences are indicated (asterisk). The data show the average and the standard deviation (n=3).

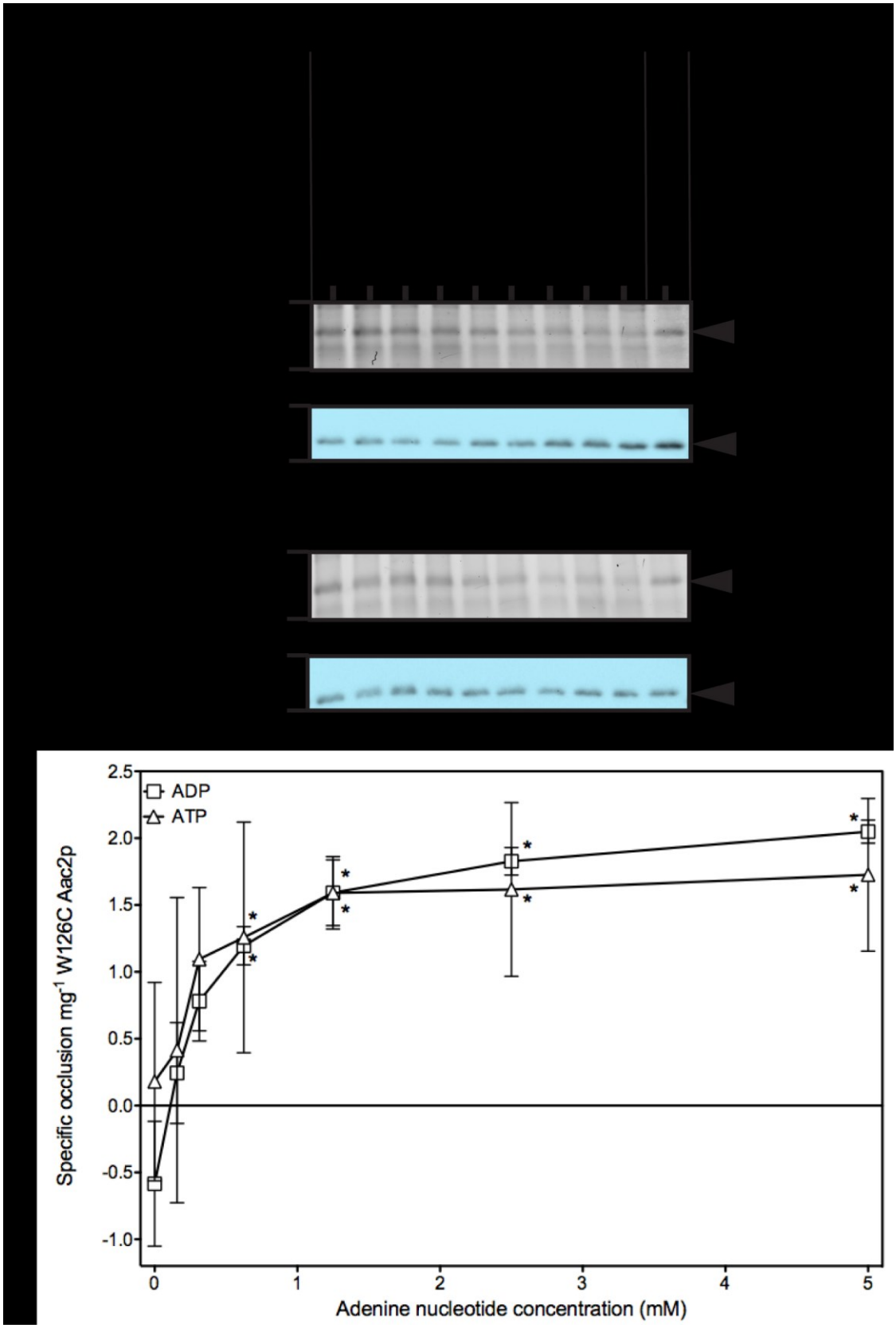

Figure 5.12 Dependency of eosin-5-maleimide labelling of W126C on the concentration of ADP or ATP. For legend details, see next page.

Legend of Figure 5.12 Dependency of eosin-5-maleimide labelling of W126C on the concentration of ADP or ATP. **(A)** Fluorescence labelling intensity (above) and Western blot analysis (below) of W126C Aac2p in the presence of various concentrations of ADP or ATP, as indicated. The fluorescent scans were imaged at 675 V. The Western blots were analysed as described, except that ECL prime was substituted for standard ECL. The experiments were repeated three times and a representative example is shown. The average specific fluorescence intensity of labelled W126C in the absence of substrate was 2.77 ± 0.70 mg^{-1} W126C Aac2p (*n*=9). **(B)** The specific occlusion of W126C Aac2p eosin-5-maleimide labelling as a function of adenine nucleotide concentration. The average value for each concentration was subtracted from the average in the absence of substrate to calculate the specific occlusion mg^{-1} W126C Aac2p. The specific occlusion in the presence of ADP or ATP was compared to the specific occlusion in the absence of substrate for each concentration by using an unpaired, one-tailed Student's *t*-test assuming unequal variance ($P<0.05$). The Student's *t*-test showed that the addition of 0.625, 1.25, 2.50 and 5.00 mM ADP or ATP led to a significant change in occlusion (marked by asterisk).

Chapter 6 Probing the formation of the cytoplasmic salt bridge network

6.1 Introduction

The aim of this chapter is to demonstrate that the putative cytoplasmic salt bridge network, first identified by symmetry analysis (Robinson *et al.*, 2008), closes in the m-state. This was explored using two methods. First, cross-linking of double cysteine replacement mutant Aac2p coupled to mass spectrometry and second, probing spin-labelling of single cysteine mutant Aac2p close to the cytoplasmic salt bridge network using EPR spectroscopy with the later aim to detect the closure of its α-helices in the m-state.

6.2 Probing the putative cytoplasmic salt bridge network

6.2.1 Selection of a thiol-specific cross-linking probe

The primary aim of this section is to demonstrate that the positively and negatively charged residues of the cytoplasmic salt bridge network form an ionic bond in the m-state. For this purpose, both residues were mutated to cysteine and a bi-reactive probe was selected to determine whether the two could be cross-linked in a conformation dependent manner. A salt bridge bond comprises an acidic and basic residue with each residue's side chain having a centroid to centroid distance of less than 4.0 Å apart (Kumar & Nussinov, 2002). Consequently, a cross-linker with a short spacer arm was chosen to probe cross-linking between double cysteine replacement mutants of Aac2p. As M-2-M has a 5.2 Å spacer arm, it is ideal for this purpose (Loo & Clarke, 2001). Moreover, M-2-M bond formation is fully reversible because it forms disulphide bonds that can be reduced (Section 1.9.3 and Figure 1.21). The ability to reverse M-2-M modifications of Aac2p is advantageous because any changes in protein activity or other properties due to M-2-M treatment should be fully reversible if the initial cross-linking reaction is specific and truly responsible for the M-2-M induced changes.

6.2.2 Selection of single and double cysteine mutants

The residues of the putative cytoplasmic salt bridge network have been identified previously by symmetry analysis (Robinson *et al.*, 2008) (Figure 1.15). Single cysteine mutants of the cytoplasmic salt bridge were chosen as controls (Figure 3.10 A-B). D109C, K112C, D212C, K215C, D306C and Q309C Aac2p were generated by site-directed mutagenesis (Section 3.1.2 and 3.2.2). Acidic D109 on α-helix H2 is predicted to hydrogen bond with polar Q309 on α-helix H6, basic K112 on α-helix H2 is predicted to form a salt bridge with acidic D212 on α-helix H4 and basic K215 on α-helix H4 is predicted to form a salt bridge with acidic D306 on α-helix H6 (Figure 1.16 C). Thus the ionic pairs K112-D212, K215-D306 and Q309-D109 of Aac2p were targeted for double cysteine replacements by site-directed mutagenesis (Section 3.3 and Figure 3.5 B). Single cysteine mutants of the cytoplasmic salt bridge residues were also generated as controls (Figure 3.5 A-B).

6.2.3 Expression and cross-linking of single and double cysteine mutants in the presence or absence of bongkrekic acid and carboxy-atractyloside

The expression levels of the single and double cysteine mutants of Aac2p in *L. lactis* membranes were determined (Figure 6.1). All of the single and double cysteine mutants of Aac2p were expressed to roughly similar levels as the Δ2-19 cys-less Aac2p (Figure 6.1 C-D). For unknown reasons, the double cysteine mutants D109C/Q309C and K112C/D212C were expressed to twice the level of K215C/D306C.

In the presence or absence of ADP, the single and double cytoplasmic salt bridge mutants were treated with M-2-M (Figure 6.1). In the absence of ADP, single bands of ~32.5 kDa were visible for Δ2-19 cys-less Aac2p and the single cysteine mutants (Figure 6.1 C-D). In contrast, double bands at ~32.5 kDa and ~30 kDa were visible for D109C/Q309C and K112C/D212C Aac2p, whereas only a ~30 kDa band was visible for K215C/D306C Aac2p. Thus a shift in migration only occurred in the case

of the double cysteine mutants of Aac2p, but not for Δ2-19 cys-less or single cysteine mutants of Aac2p. However, as the addition of ADP did not alter the migration behaviour for any of the mutants, the appearance of a migration band at ~30 kDa may indicate the formation of a cross-link between two cysteines, although one would expect it to be promoted by the addition of ADP as the cytoplasmic salt bridge should form more often during substrate translocation. One possible explanation for the results is that the cross-linking occurred after the wash steps in a non-specific manner when the proteins were unfolded. To try and prevent this, the M-2-M reaction was quenched by the addition of *N*-ethyl maleimide (NEM), preventing any further non-specific reactions (Figure 1.19 B). However, double bands were visible for K112C/D212C Aac2p both in the absence and presence of ADP, demonstrating that NEM cannot quench the reaction (Figure 6.2 B). One possible explanation is that NEM cannot penetrate the *L. lactis* peptidoglycan layer very well due its hydrophobicity, as also observed for both DTT (Section 4.5) and spin labels (Section 6.3.5).

The other issue was that the transport state was not fully defined. Therefore, the putative cross-linking of the cysteines of K112C/D212C in the BKA- and CATR-inhibited states was investigated (Figure 6.3 B). ~32.5 kDa and ~30 kDa bands were visible in both inhibited states, but the ~30 kDa band intensity was greater in the inhibited m-state than the c-state. These results suggest that more cross-linking occurred in the m-state compared to the c-state, but no cross-linking is expected in the c-state because CATR should prevent the residues of the cytoplasmic salt bridge network from engaging. It is possible that the residues of the cytoplasmic salt bridge are closer together than the structure of the bovine AAC1 suggests (Pebay-Peyroula *et al.*, 2003). More likely, the appearance of the two bands suggests that the reaction was not complete and thus more control experiments need to be completed before firm conclusions can be reached.

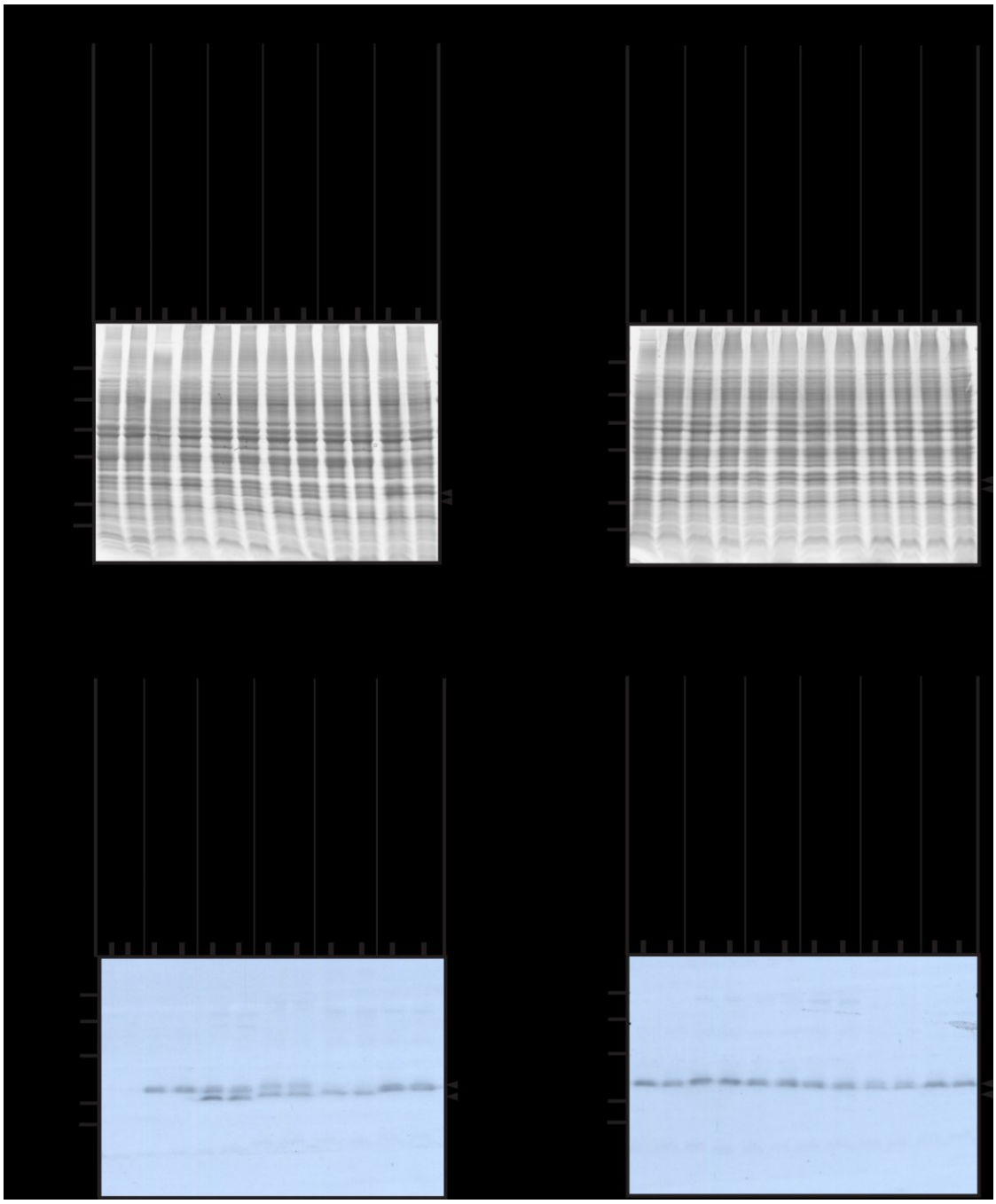

Figure 6.1 Gel migration of M-2-M treated single and double cysteine mutants of Aac2p in the absence and presence of ADP. Whole cells of *L. lactis* were incubated with 50 µM M-2-M for 5 min in the absence or presence of 1 mM ADP, which was added 1 min prior. The cells were washed twice to remove excess M-2-M. **(A) and (B)** SDS-PAGE analysis and **(C) and (D)** Western blot analysis of isolated membranes. The antibody is directed against α-helix H5 of Aac2p. The mutants are described in Section 6.2.2. 20 µg total protein was loaded per lane on non-reducing gels. The blots were imaged on x-ray film for 5 min. The bands of Aac2p are indicated by solid black arrowheads.

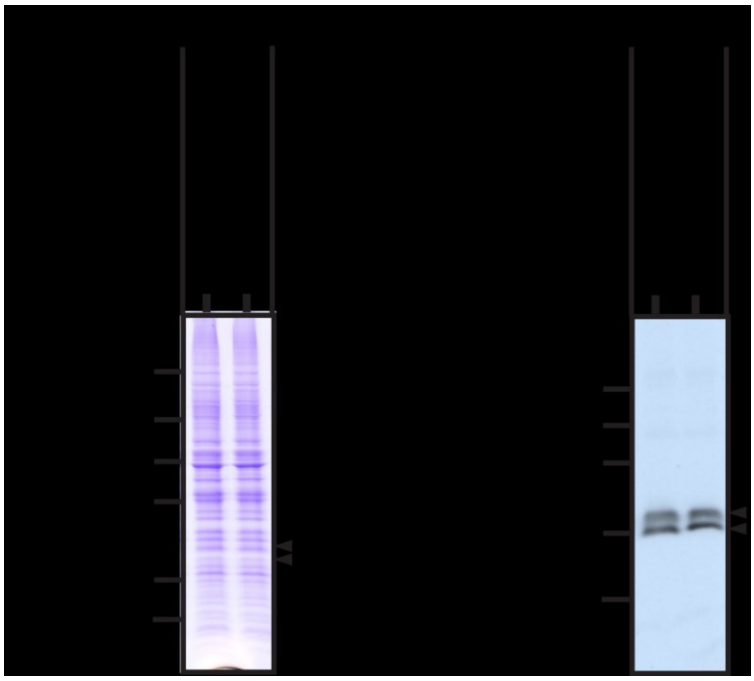

Figure 6.2 Gel migration of M-2-M treated K112C/D212C Aac2p in the absence and presence of ADP and quenched by NEM. Similar to Figure 6.1 except that the cells were incubated with M-2-M for 30 min, and the reaction was quenched with 5 mM NEM. **(A)** SDS-PAGE analysis and **(B)** Western blot analysis of isolated membranes. The antibody is directed against α-helix H5 of Aac2p. 20 µg total protein was loaded per lane on non-reducing gels. The blots were imaged on x-ray film for 1 min. The bands of Aac2p are indicated by solid black arrowheads.

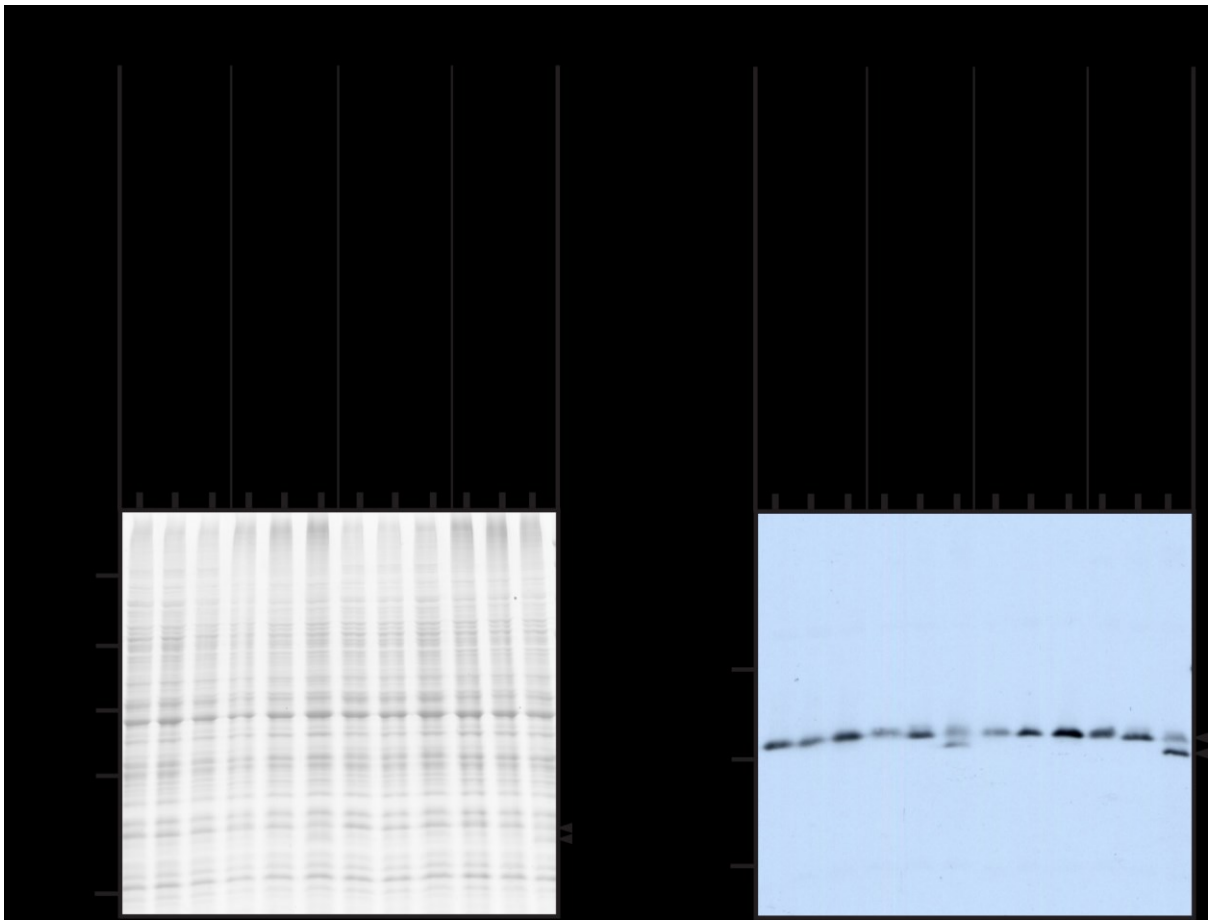

Figure 6.3 Gel migration of M-2-M treated or untreated single and double cysteine mutants of Aac2p inhibited with either bongkrekic acid or carboxy-atractyloside. Whole cells of *L. lactis* were treated with either 10 µM BKA or 10 µM CATR for 30 min before being treated with 200 µM M-2-M for 30 min. The reaction was quenched by the addition of 10 mM NEM followed by one washing step. **(A)** SDS-PAGE analysis and **(B)** Western blot analysis of isolated membranes. The antibody is directed against α-helix H5 of Aac2p. 10 µg total protein was loaded per lane on non-reducing gels. The blots were imaged on x-ray film for 15 s. The bands of Aac2p are indicated by solid black arrowheads.

6.2.4 Transport activity of cross-linked ADP/ATP carrier

The specific initial ADP uptake rates of the single cysteine mutants of Aac2p of the cytoplasmic salt bridge were determined (Figure 3.11). It was found that all of the single cysteine mutants transported significantly above background, between similar to and two-fold greater than Δ2-19 cys-less Aac2p. The initial ADP uptake rates of the double cysteine mutants were also determined (Figure 6.4). It was shown that D109C/Q309C and K112C/D212C Aac2p transported ADP at rates similar to those of Δ2-19 cys-less Aac2p, whereas K215C/D306C Aac2p did not transport at all (Figure 6.4 B). Thus, not only did K215C/D306C Aac2p transport poorly, but it also was expressed poorly and showed a different migration pattern on Western blots compared to D109C/Q309C and K112C/D212C Aac2p (Figure 6.1 C).

Having established that D109C/Q309C and K112C/D212C Aac2p are competent in transport, the effect of M-2-M on transport was explored in the presence or absence of the reducing agent DTT. The initial uptake rates of K112C/D212C Aac2p with and without DTT were similar, as expected since DTT should not affect Aac2p transport (Figure 6.5). The specific initial uptake rate of K112C/D212C Aac2p in the presence of M-2-M (K112C/D212C +M-2-M) was only 9.5% of the rate without M-2-M. However, when DTT was added subsequently, 65% of the K112C/D212C Aac2p transport activity was restored, as DTT reduces the disulphide bonds formed by M-2-M. Thus, M-2-M severely inhibited ADP transport in a thiol-specific manner, but the reason is not clear. One molecule of M-2-M could cross-link the two cysteines of K112C/D212C Aac2p, one M-2-M molecule could bind to either cysteine or two M-2-M molecules could bind to both cysteines without cross-linking.

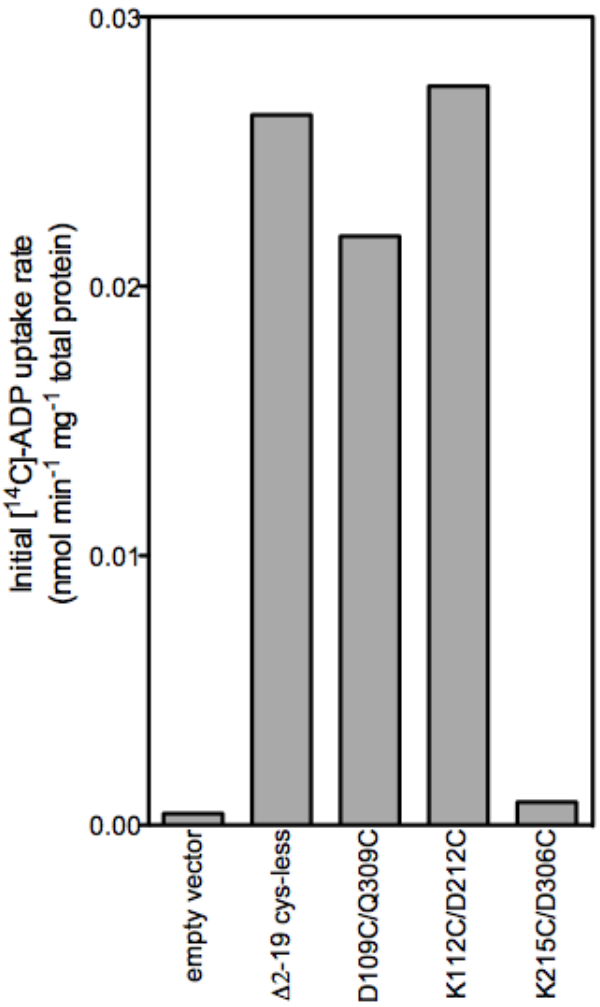

Figure 6.4 Transport activity of double cysteine mutants of Aac2p expressed in membranes of *L. lactis*. Initial uptake rate of ADP for empty vector, Δ2-19 cys-less, D109C/Q309C, K112C/D212C and K215C/D306C Aac2p. A Hamilton robot modified for transport assays was used. The rates were calculated using linear regression of uptake data in the time period 30-140 s.

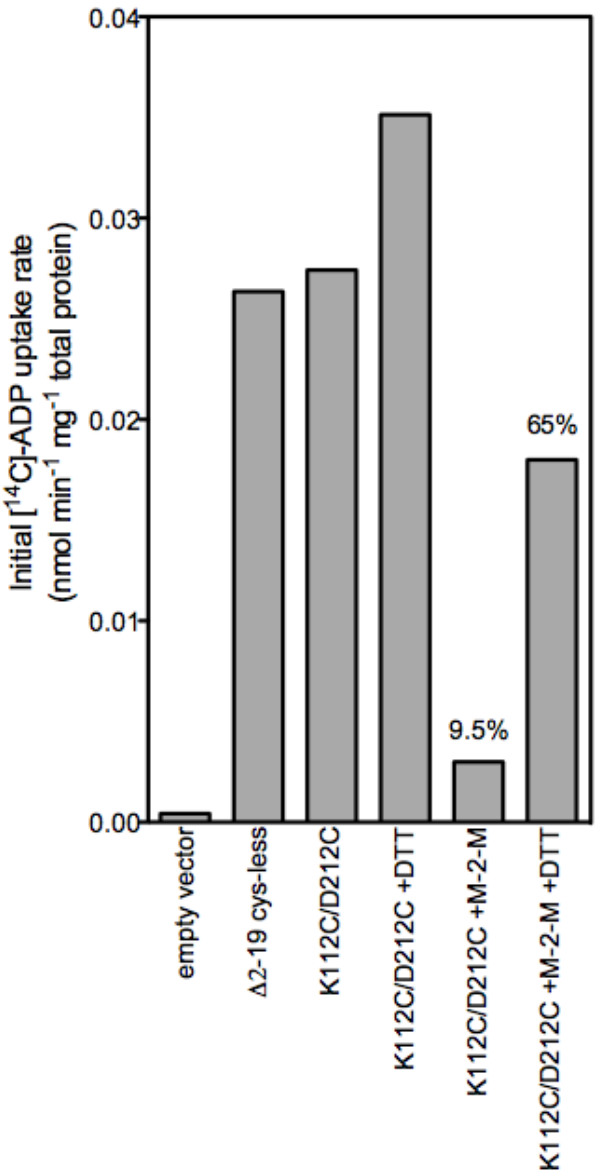

Figure 6.5 Effect of M-2-M on the transport activity of K112C/D212C Aac3p in the presence or absence of DTT. Initial uptake rate of ADP of empty vector, Δ2-19 cys-less Aac2p, K112C/D212C Aac2p, K112C/D212C Aac2p with 1 mM DTT, 50 μM M-2-M or 50 μM M-2-M plus 1 mM DTT. The remaining transport activity (%) is also shown. A Hamilton robot modified for transport assays was used. The rates were calculated using linear regression of uptake date in the time period 20-140 s.

6.2.5 Matrix-assisted laser desorption/ionisation time of flight mass spectrometry of cross-linked ADP/ATP carrier

To examine whether M-2-M was physically cross-linking the double cysteine mutants D109C/Q309C, K112C/D212C and K215C/D306C in *L. lactis* (Figure 6.1 C), samples were analysed by MALDI-TOF MS by Dr Kamburapola Jayawardena. The 30kDa and 32 kDa protein bands from a coomassie-stained SDS-PAGE gel (Figure 6.1 A) were excised, digested with trypsin and the resultant peptide digests analysed by MALDI-TOF MS. The peptide masses and fragment ion masses from tandem MS were compared with a SWISSPROT sequence database. One peptide ion, TATQEGVISFWR, was present in each of the two protein bands observed for all of the double cysteine mutants (data not shown). Additionally, the peptide ion GFLPSVVGIVVYR was present in the 30 kDa K215C/D306C sample (data not shown). The sequence coverage ranged from 3-27% for all of the double cysteine mutants, and was unexpectedly low. A sequence coverage approaching 50% was expected for trypsin-digested Aac2p (personal communication, Dr Ian Fearnley). The poor coverage could be due to complications arising from using an impure protein sample, or having low Aac2p expression.

In an attempt to avoid the complications of using an impure protein sample, *S. cerevisiae* purified Aac3p samples (donated by Dr Jonathan Ruprecht) were also digested and the resulting peptides were analysed by MALDI-TOF MS, similarly to the description in the previous paragraph. These experiments were proof of principle experiments, to learn whether cross-linked peptides could be identified in a cleaner system. Aac3p has four native cysteines. The amino acid sequences and theoretical masses of the tryptic cysteine-containing peptides are listed in Table 6.1. The C233 peptide has a mass >4000 Daltons, and is outside the mass range usually examined by MALDI-TOF MS. In Table 6.2, the theoretical monoisotopic peptide masses (calculated in MassLynx) together with the masses observed (Figure 6.6) for cysteine-modified peptides are listed. The observed masses in Table 6.2 were identified in the MALDI-TOF mass spectrometry spectra (Figure 6.6).

Table 6.1 Sequences and mass of cysteine-containing Aac3p tryptic peptides from Aac3p.

peptide name	peptide	amino acid sequence	theoretical monoisotopic mass (MH+)
C62	57-65	YSGIVD**C**FK	1031.4873
C233	195-254	GLYFGMFDSLKPLVLTGSLDGSFL-ASFLLGVVTTGAST**C**SYPLDTVR	6483.65
C260	255-263	YNGAID**C**LK	996.4825
C278	277-284	G**C**GANILR	803.4199

Table 6.2 Mass measurements of modified Aac3p peptides in Figure 6.6.

modified peptide	theoretical monoisotopic mass (MH^+)	observed mass (MH^+)	mass difference (ppm)
C62-alkyl	1088.5214	1088.4819	36
C260-alkyl	1053.5166	1053.4751	40
C278-alkyl	860.4540	860.4172	43
C62-M-2-M-C62	2151.9265	ND	ND
C62-M-2-M-C260	2116.9217	ND	ND
C62-M-2-M-C278	1923.8591	1924.9409	562
C260-M-2-M-C260	2081.9169	ND	ND
C260-M-2-M-C278	1888.8543	ND	ND
C278-M-2-M-C278	1695.7917	ND	ND

None of the peaks in the untreated Aac3p control sample match the theoretical masses of modified cysteine peptides (Figure 6.6 A-B and Table 6.2). Also, no peaks corresponding to unmodified cysteine were identified (Figure 6.6 A, some portions of the mass spectra are not shown). When Aac3p was alkylated by iodoacetamide, peaks corresponding to alkylated peptides C62, C260 and C278, with the masses, 1088.5214, 1053.5166 and 860.4540, respectively, were identified (Figure 6.6 C and Table 6.2). The mass differences of these peaks were 36 parts per million (ppm), 40 ppm and 43 ppm for alkylated peptides C62, C260 and C278, respectively. At best, the accuracies of measurements should be <10 ppm for MALDI-TOF MS, but <50 ppm is also considered to be reliable. Consequently, all three of the alkylated cysteine containing peptides were identified (Figure 6.6 C), but unmodified peptides with free cysteines (Figure 6.6 A) were not identified.

Samples of Aac3p cross-linked with M-2-M were examined as above. In the M-2-M treated Aac3p sample, only one peak, potentially corresponding to C62-M-2-M-C278, was identified in the spectrum as having a mass of 1924.9409 (Figure 6.6 F). The difference between the observed mass and the theoretical mass was 562 ppm (Table 6.2). The peptide ion corresponding to a mass of 1924.9409 was analysed by tandem MS, but the signal to noise ratio was too low to obtain useful fragment data (data not shown). As the ppm accuracy is much lower than expected, it is unlikely that the peak with a mass of 1924.9409 corresponds to the cross-linked peptide C62-M-2-M-C278.

Although alkylated cysteine peptides were identified, suggesting that the cysteine thiols were accessible for modification, M-2-M cross-linked peptides were not identified. There are several potential explanations. First, if the peptides were cross-linked, they could have been difficult to detect with mass spectrometry because they were larger. Second, the cross-linking efficiency may have been too low to enable detection of the cross-linked peptides. Finally, the cysteines may not have cross-linked because they were spatially separated. Singly or in combination, these factors could have contributed to a failure to detect cross-linked peptides.

Thus, despite observing specific effects of M-2-M on ADP transport and a shift in migration in gels, definitive proof of the cross-linking of two cysteines replacing a putative salt bridge has not been obtained.

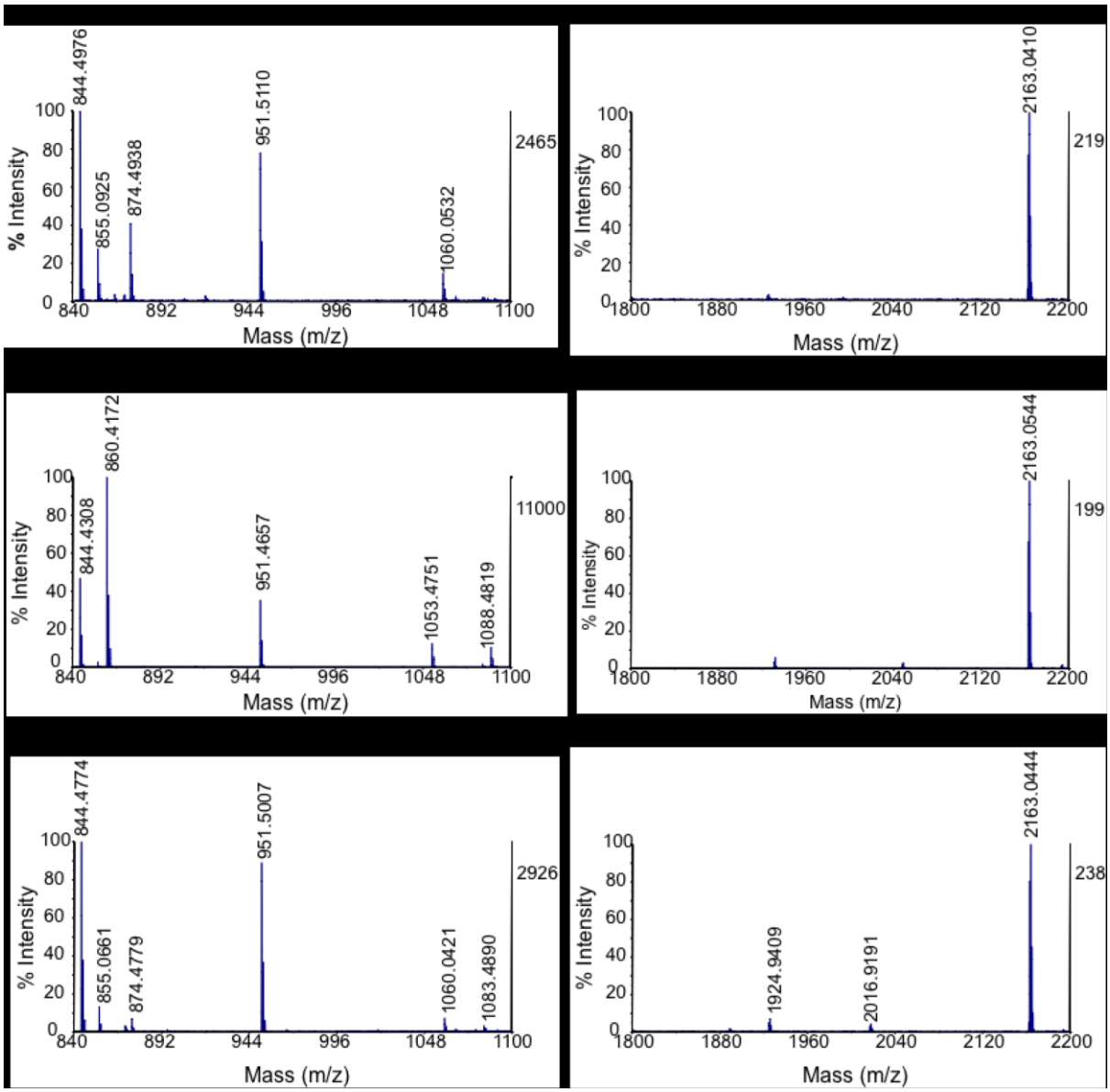

Figure 6.6 Matrix-assisted laser desorption/ionisation time of flight mass spectrometry spectra of purified *S. cerevisiae* Aac3p. N-terminus cleaved Aac3p purified from *S. cerevisiae* was analysed. **(A) and (B)** Aac3p without treatment, **(C) and (D)**, alkyated with 100 mM iodoacetamide for 10 min or **(E) and (F)** treated with 1 mM M-2-M for 10 min. The Aac3p samples were separated by non-reducing SDS-PAGE. The Aac3p bands were excised. Portions of the MALDI-TOF mass spectrometry spectra and labelled peptides are shown from (A), (C) and (E) 840-1100 m/z and (B), (D) and (F) 1800-2200 m/z. The peak at 2163.0 in (B), (D) and (F) is an autodigestion product of trypsin. The peak at 1060.0 in (A) and (C) originates from the matrix compound.

6.3 Probing the distance between alpha-helices adjacent to the putative cytoplasmic salt bridge network by pulsed double electron resonance

6.3.1 Selection of thiol-specific spin labels

Thiol-specific spin labels were required to probe the distance between α-helices adjacent to the putative cytoplasmic salt bridge network using PELDOR (Section 1.9.3). The spin labels need to be thiol-specific to bind to single and double cysteine mutants of Aac2p. Additionally, the spin labels need to contain a paramagnetic centre to enable detection by EPR. Two spin labels, MTSL and MAL-6, were selected for use in EPR (Figure 1.22). MTSL was chosen because it is considered to be an optimal thiol-specific spin label. MTSL contains the fewest number of flexible single bonds between the sulfhydryl and nitroxide ring, is stable and is specific for cysteines (Figure 1.22 A) (Berliner, 1983). MAL-6 was chosen because it also is stable and specific, like MTSL, but its nitroxide ring is covalently bound to a maleimide moiety (Figure 1.22 B). MAL-6 should behave similarly to eosin-5-maleimide, which was shown to react with single cysteines of mutant Aac2p (Chapters 4 and 5), because both MAL-6 and eosin-5-maleimide contain thiol-specific maleimide groups.

6.3.2 Selection of single and double cysteine mutants

The aim of this section is to determine the distances between α-helix H2 and H4, α-helix H2 and H6 and α-helix H4 and H6 of Aac2p in the BKA- and CATR-inhibited states. Alpha-helices H2, H4 and H6 contain the putative cytoplasmic salt bridge network, and they are predicted to close the cytoplasmic side of the cavity during the transport cycle. Thus, they should come close together in the m-state, and should be further apart in the c-state.

M114C and I311C were selected as sites for the introduction of cysteines in order to facilitate labelling with spin labels and to determine the distance between the cysteines in the inhibited m- and c-state. Thus, the single cysteine mutants M114C and I311C Aac2p, and the double mutant M114C/I311C Aac2p were generated (Figure 6.7). The mutation sites were chosen because they are two residues away from K112 and Q309, which are involved in the formation of the cytoplasmic salt bridge network. Therefore, M114C, I311C and M114C/I311C Aac2p were considered to be suitable indicators of conformational changes occurring near the cytoplasmic salt bridge, yet they are unlikely to interfere with function. In addition, M114C and I311C were significantly labelled above background by eosin-5-maleimide in the c-state (Figure 5.3), so they should be accessible to spin labels, too.

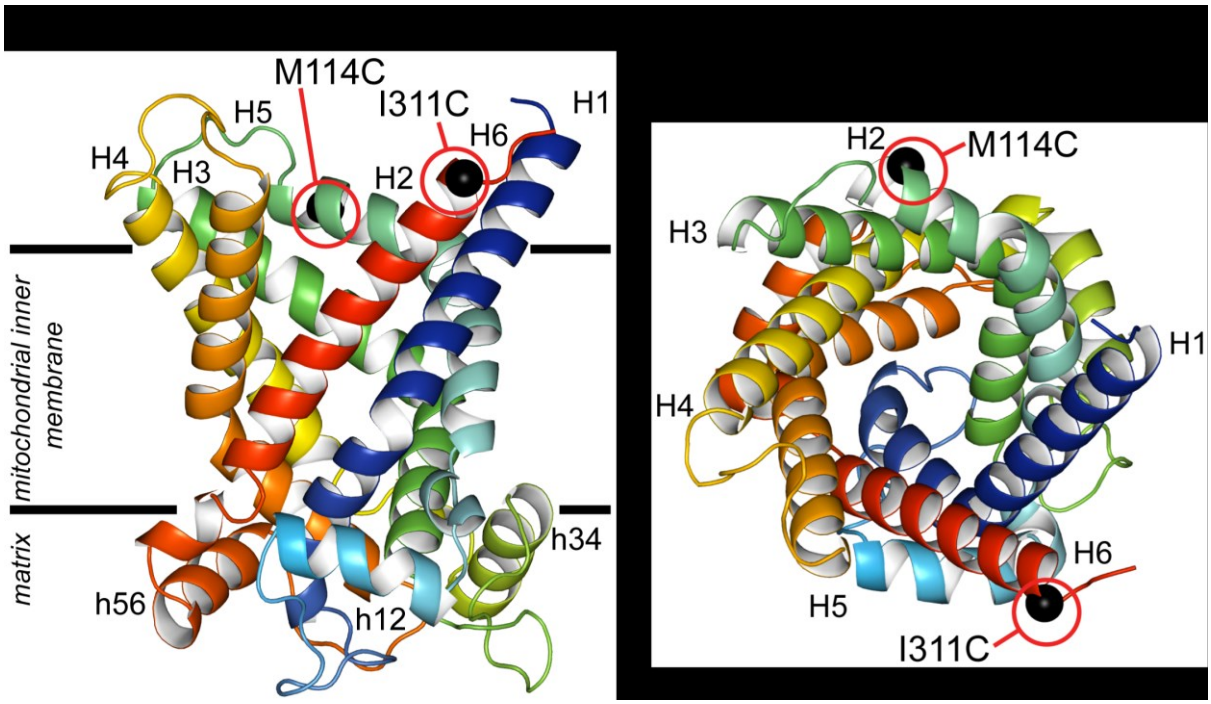

Figure 6.7 M114C, I311C and M114C/I311C Aac2p selected for EPR studies. For details, see legend of Figure 3.4. Each cysteine mutation site is shown as a black sphere centred on the α-carbon and is highlighted by a red circle. Individual mutation sites are labelled. **(A)** The lateral view from the membrane and **(B)** the view of the cavity from the cytoplasmic side.

6.3.3 Expression of single and double cysteine mutants

The expression levels of M114C, I311C and M114C/I311C Aac2p were determined relative to that of Δ2-19 cys-less Aac2p using Western blots (Figure 6.8). M114C Aac2p was expressed three-fold lower than Δ2-19 cys-less Aac2p (Figure 6.8 A). I311C Aac2p was expressed 1.5-fold higher than Δ2-19 cys-less Aac2p, and M114C/I311C Aac2p was expressed at slightly lower levels than Δ2-19 cys-less Aac2p, but at higher levels than M114C Aac2p (Figure 6.8 A and B). The M114C and I311C Aac2p levels of expression are comparable to the ones shown in Figure A.4, as I311C Aac2p was expressed ~2.7-fold higher than M114C. Thus, both the single as well as the double mutants of M114C and I311C Aac2p were expressed in *L. lactis*.

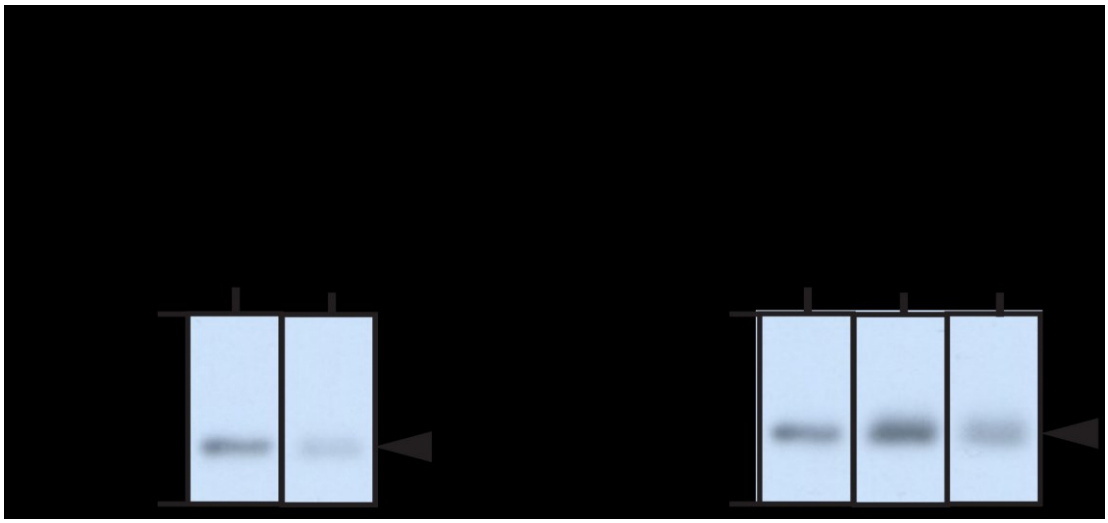

Figure 6.8 Expression of single and double cysteine mutants of Aac2p. Western blot analysis of isolated membranes. **(A)** Δ2-19 cys-less and M114C Aac2p and **(B)** Δ2-19 cys-less, I311C and M114C/I311C Aac2p. The antibody is directed against α-helix H5 of Aac2p. 10 µg total cellular protein was loaded per lane. Imaged for 1 min using an X-ray film processor. The band for Aac2p is indicated by a solid black arrowhead. Segments of a representative blot are shown (*n*=4).

6.3.4 Transport activity of single and double cysteine mutants in fused lactococcal membranes

The transport activities of M114C, I311C and M114C/I311C Aac2p were assessed by using fused lactococcal membranes loaded with ADP and when required, inhibitors (Figure 6.9). It was found that M114C, I311C and M114C/I311C Aac2p transported at lower specific initial uptake rates than Δ2-19 cys-less Aac2p. The difference could be due to the fact that in the fused membrane vesicles the ADP pool can be controlled, whereas this is an unknown in uptakes involving whole cells. Additionally, the error in transport rates was large, which could be a consequence of the robot transport assay not being fully optimised when the data were measured. Despite these limitations, all the mutants were found to be competent in transport.

The inhibition of the initial ADP uptake rate by BKA or CATR was determined for M114C, I311C and M114C/I311C Aac2p (Figure 6.9). Δ2-19 cys-less Aac2p was previously shown to be ~85% inhibited by BKA and ~100% by CATR in whole cells of *L. lactis* (Figure 3.14 and 3.16). It was found that both BKA and CATR completely abolished the transport activity of all three mutants of Aac2p (Figure 6.9). The inhibition levels by CATR were similar to those previously observed in whole cell uptakes by M114C and I311C Aac2p (Figure 3.14). The inhibition of transport by BKA was close to 100% in fused lactococcal membranes (Figure 6.9), but only ~92% and ~88% for M114C and I311C Aac2p, respectively, when the transport assays were carried out with whole cells (Figure 3.16). The difference in BKA inhibition levels could be partially due to the higher concentration of BKA added to lactococcal membranes; 15 μM for lactococcal membranes versus 10 μM for whole cells, but more likely the reason was that BKA was available on both sides of the membrane in the transport assay with fused membranes. In the whole cell uptake experiments, BKA was added externally, therefore, it had to cross the membrane before it could bind to the matrix side of the carrier, and thus was less readily available to bind to Aac2p.

To summarise, M114C, I311C and M114C/I311C Aac2p are competent in transport and are fully inhibited by BKA and CATR.

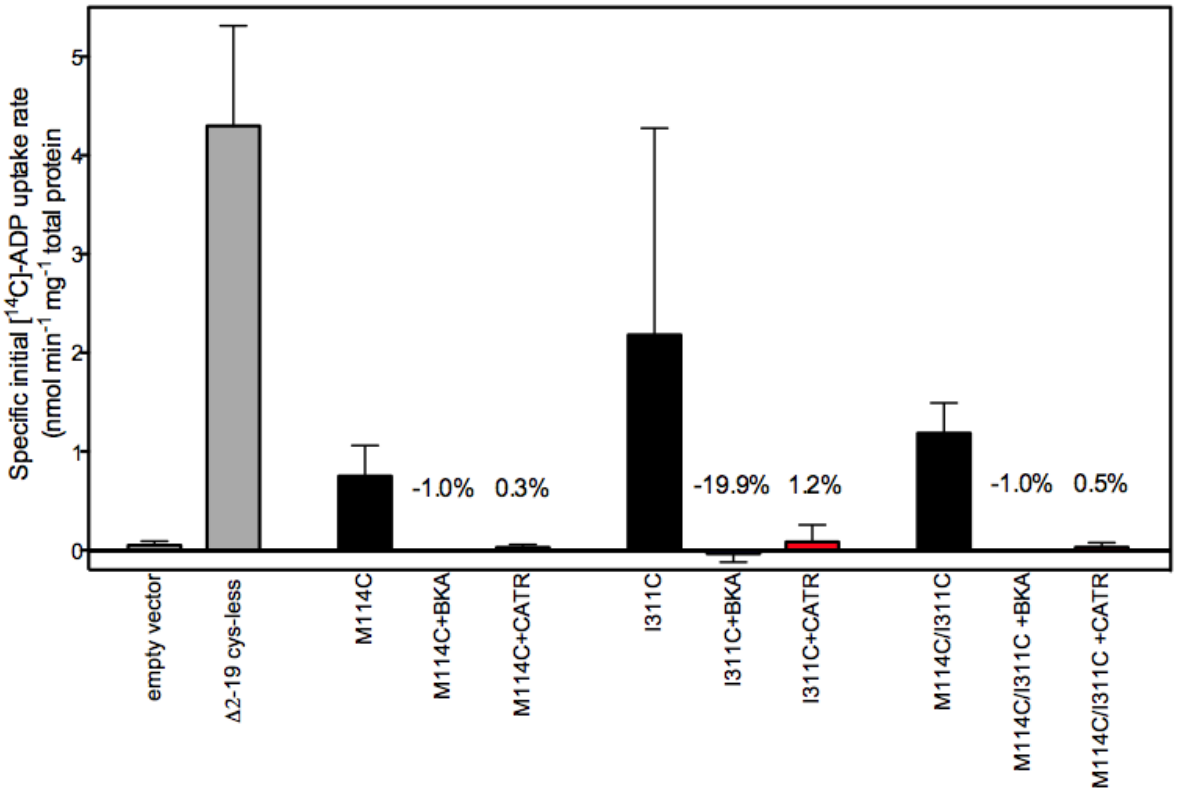

Figure 6.9 Transport activity of M114C, I311C and M114C/I311C Aac2p in fused lactococcal membranes. Time curves of [^{14}C]-ADP into lactococcal membranes fitted using linear regression were used to determine the initial ADP uptake rate for the empty vector, Δ2-19 cys-less Aac2p, and M114C, I311C and M114C/I311C Aac2p in the presence or absence of CATR or BKA. 5 mM ADP was loaded inside all fused membranes and 15 μM BKA or 15 μM CATR were also loaded, when required. The percentage activity remaining of the inhibited carrier is also shown. A Hamilton robot was used. The data were normalised against Δ2-19 cys-less Aac2p expression (determined using blots in Figure 6.8). The average and the standard deviation are shown (*n*=3).

6.3.5 Electron paramagnetic resonance of single and double cysteine mutants

6.3.5.1 Labelling with MTSL

Having established that M114C, I311C and M114C/I311C Aac2p were expressed, competent in transport and inhibited by BKA and CATR (see sections above), single cysteine mutants and Δ2-19 cys-less Aac2p were expressed in *L. lactis,* the cells were spin-labelled and cw-EPR was attempted with the aim later to measure the distance between M114C and I311C using PELDOR (Section 1.9.3). Immediately

before cw-EPR scans were collected, potassium ferricyanide, $(Fe(CN)_6)^3$, was added to the cells to oxidise the nitroxide moiety of the spin labels. This oxidation step was necessary because it was discovered that *L. lactis* cells cause reduction of the spin label that prohibits detection by cw-EPR (data not shown). Site-directed spin labelling and EPR spectroscopy were performed by Dr Jessica van Wonderen (Centre for Molecular and Structural Biochemistry, School of Biological Sciences, University of East Anglia, Norwich, UK).

Δ2-19 cys-less and M114C Aac2p were treated with MTSL (for MTSL reaction see Figure 1.22 A). Ambient temperature cw-EPR of the MTSL treated samples was performed to identify mobility changes in the bound versus unbound spin label. It was found that the first derivatives of the EPR spectra were the same for MTSL treated Δ2-19 cys-less and M114C Aac2p expressed in whole cells of *L. lactis* (Figure 6.10). This result was unexpected as MTSL should only bind to M114C, which contains a cysteine, and not to Δ2-19 cys-less Aac2p. Furthermore, it was established previously that there were few cysteine-containing proteins that reacted with eosin-5-maleimide, so it was anticipated that background MTSL labelling should also be minimal (Figure 6.14 B). Consequently, these results could be due to a low MTSL reaction efficiency. However, eosin-5-maleimide labelled M114C could be detected (Figure 5.3), and M-2-M cross-linked cysteines of K112C/D212C Aac2p in a state dependent manner (Figure 6.3), therefore it is unlikely that MTSL would have reacted inefficiently with M114C. Another possibility was that MTSL was ensnared in the *L. lactis* peptidoglycan layer, despite repeated cell washes, or was too hydrophobic to bypass the layer. Alternatively, MTSL could have bound non-specifically to other thiol-containing proteins of *L. lactis*.

MTSL labelling of Δ2-19 cys-less and M114C Aac2p was attempted with isolated *L. lactis* membranes, rather than whole cells. Differences between the MTSL labelled Δ2-19 cys-less and M114C Aac2p in *L. lactis* membranes were not significant, as detected by cw-EPR (data not shown).

In another experiment, whole cells expressing M114C/I311C Aac2p were labelled with MTSL, and a PELDOR spectrum was generated. However, distances between single cysteines M114C and I311C could not be determined (data not shown).

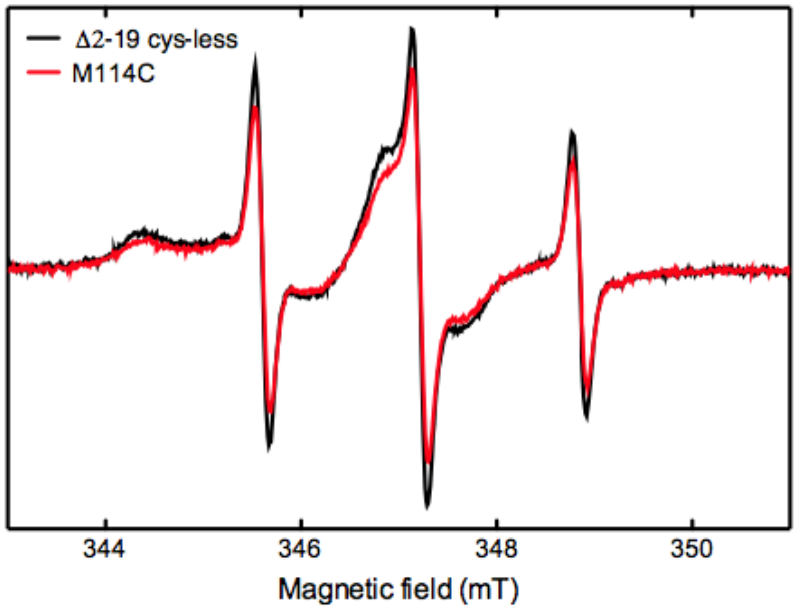

Figure 6.10 Continuous wave electron paramagnetic resonance spectra of MTSL-treated Δ2-19 cys-less and M114C Aac2p. Whole cells of *L. lactis* expressing Δ2-19 cys-less and M114C Aac2p were treated with 200 μM MTSL for 30 min. The cells were washed four times, and 10 mM $(Fe(CN)_6)^3$ was added in the final wash step. cw-EPR was performed at ambient temperature. The conditions were: 9.6 GHz (X-band), 1 G modulation amplitude, 100 kHz modulation frequency and 8-32 scans. The spectra are first derivatives. The spectra of Δ2-19 cys-less and M114C Aac2p are black and red, respectively.

6.3.5.2 Labelling with MAL-6

Having failed to identify a specific cw-EPR signal for MTSL-labelled M114C Aac2p, an alternative spin label, MAL-6, was tested (reaction shown in Figure 1.22). MAL-6 contains a maleimide moiety, so it was predicted that it would be more amenable to reacting with cysteine, similar to eosin-5-maleimide (Section 6.3.6 and Chapter 5). Additionally, unlike the MTSL reaction, the MAL-6 reaction is irreversible, so DTT could be added to the MAL-6 reaction to remove unreacted MAL-6 without reversing the binding of the already reacted MAL-6. MAL-6 was added to react with Δ2-19 cys-less and M114C Aac2p by using the same method described previously for MTSL (see above). Both the MTSL (Figure 6.10) and MAL-6 (Figure 6.11) data were collected on the same day, in the same conditions and with the same batch of cells. Similarly to the MTSL spectra, there was little difference between the Δ2-19 cys-less

and M114C Aac2p spectra (Figure 6.11). Possible reasons for this result were identified (see above).

The spectra corresponding to the MTSL and MAL-6 treated Aac2p are shaped differently due to the different mobilities of the nitroxide spin labels (Figure 5.12 and Figure 5.13). Each nitroxide is comprised of an electron spin (S = ½) and a nuclear spin (I = 1), which gives rise to three lines per absorption peak (number of hyperfine lines = 2I + 1). Three sharp lines are observed for unbound or highly mobile nitroxide spin labels because the anisotropy of the hyperfine splitting by the nuclear spin of the nitrogen (I =1) averages when the correlation time is fast. Broader, more featured lines are observed for some bound labels if the spin label is rigid (low mobility). In this case, the hyperfine is anisotropic, and separate hyperfine features are observed in each direction when they are not averaged. In the spectra depicted (Figure 6.10 and 6.11), there are two sets of spectral features for MTSL, but only one for MAL-6. Both the MTSL and MAL-6 spectra are typical for non-reacted spin label (sharp lines), so either the spin labels did not react with cysteine, or the spin labels were cysteine bound but highly mobile. The MTSL spectrum also had a set of broader lines as well as free/mobile spin label, signifying that some MTSL is also rigidly bound.

To investigate the idea that unreacted MAL-6 might be caught in the *L. lactis* peptidoglycan layer, thus obscuring the M114C-bound MAL-6 signal, the cells were washed multiple times following MAL-6 labelling. It was found that the EPR signal decreased drastically following the first wash, and incrementally so thereafter, both for the Δ2-19 cys-less and M114C Aac2p samples (Figure 6.12). This result suggests that MAL-6 was washed away from the cells in the conditions tested, and that it did not bind robustly to the single cysteine M114C.

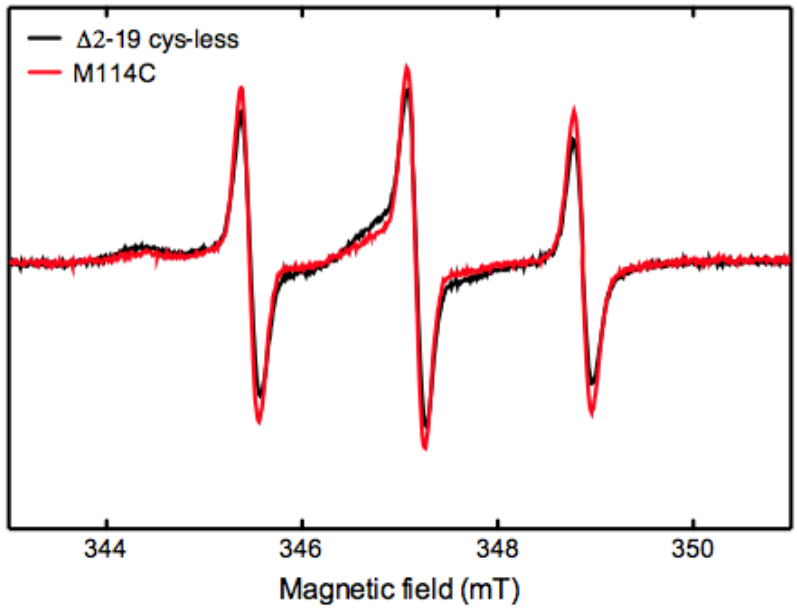

Figure 6.11 Continuous wave electron paramagnetic resonance spectra of MAL-6 treated Δ2-19 cys-less and M114C Aac2p. Legend identical to Figure 6.10, except that MAL-6 was used instead of MTSL. The spectra of Δ2-19 cys-less and M114C Aac2p are black and red, respectively.

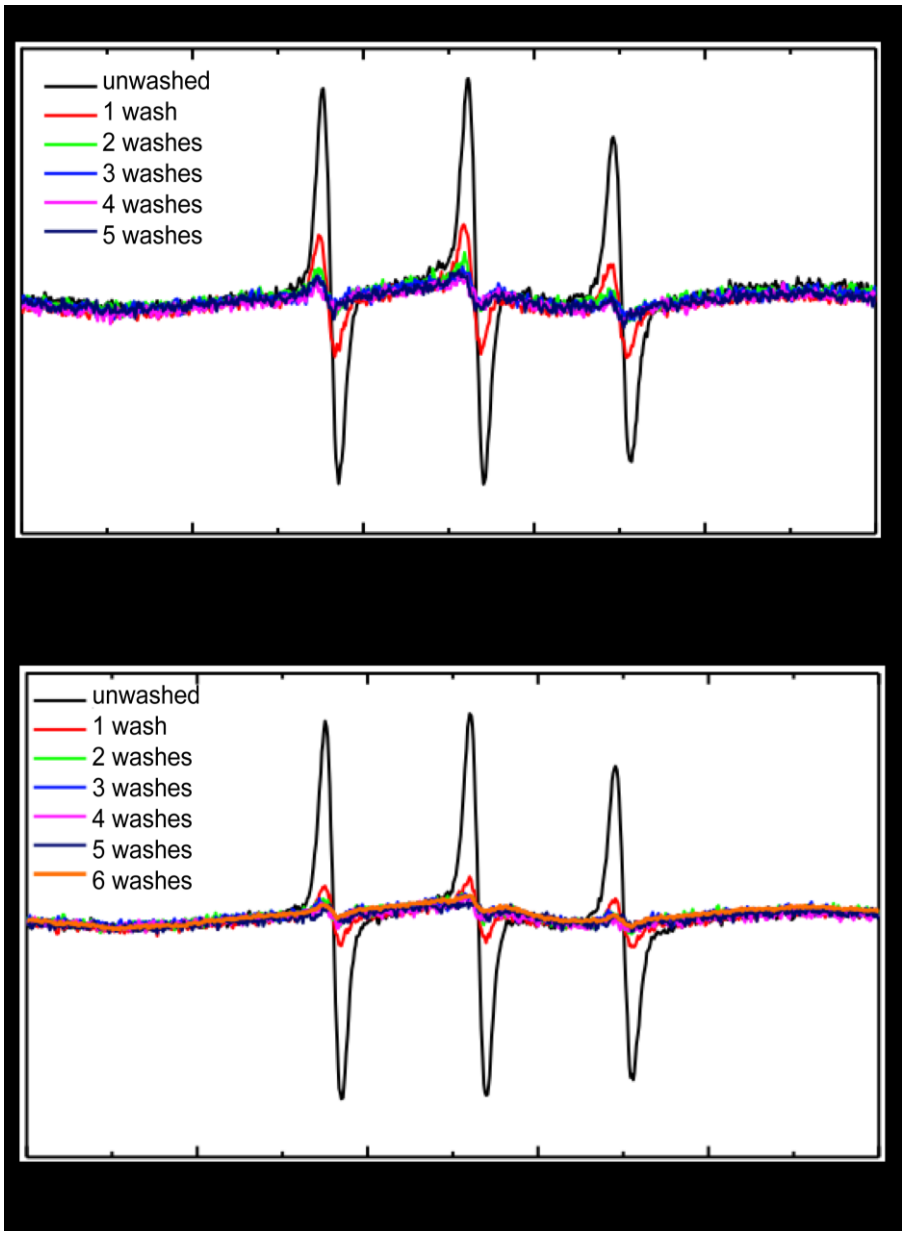

Figure 6.12 Continuous wave electron paramagnetic resonance spectra of MAL-6 treated and washed Δ2-19 cys-less and M114C Aac2p. Whole cells of *L. lactis* expressing **(A)** Δ2-19 cys-less Aac2p and **(B)** M114C Aac2p were treated with 25 μM MAL-6 for 10 min. The reaction was quenched with 1 mM DTT. The cells were left unwashed or were washed one to six times with PBS containing 1 mM DTT. Before collecting cw-EPR spectra, all of the samples were washed one additional time with PBS containing 10 mM $(Fe(CN)_6)^3$. cw-EPR was performed at ambient temperature. The conditions were: 9.6 GHz (X-band), 1 G modulation amplitude, 100 kHz modulation frequency and 8-32 scans. The spectra are first derivatives. The black spectra are for unwashed samples, the red were washed once, the green were washed twice, the blue were washed three times, the pink were washed four times, the violet were washed five times and the orange was washed six times.

Possible explanations for the poor labelling efficiency were a short incubation time (10 min) and a low spin label concentration (25 μM). To increase the efficiency of MAL-6 labelling, Δ2-19 cys-less and M114C Aac2p were incubated with 25 μM MAL-6 for 30 min, 1 hr, 4 hr or 24 hr. Following extensive washing, EPR signals for all of the samples remained undetected (data not shown), similar to previous observations (Figure 6.12). It was interpreted from the results that the concentration of label was likely too low, even when combined with a long incubation time. In contrast, when a long incubation (24 hr) and a high MAL-6 concentration (250 μM) were tested, three broad lines were observed for Δ2-19 cys-less and M114C Aac2p expressing cells (Figure 6.13, only M114C Aac2p shown). These broad lines are the signature of covalently bound spin label. As broad lines were observed for both Δ2-19 cys-less and M114C Aac2p, the spin label bound non-specifically to other cysteine-containing *L. lactis* proteins inside the cell, presumably due to the spin label being membrane-permeable.

In summary, it was not possible to label single cysteine M114C of Aac2p with the spin labels MTSL or MAL-6 specifically in the conditions tested.

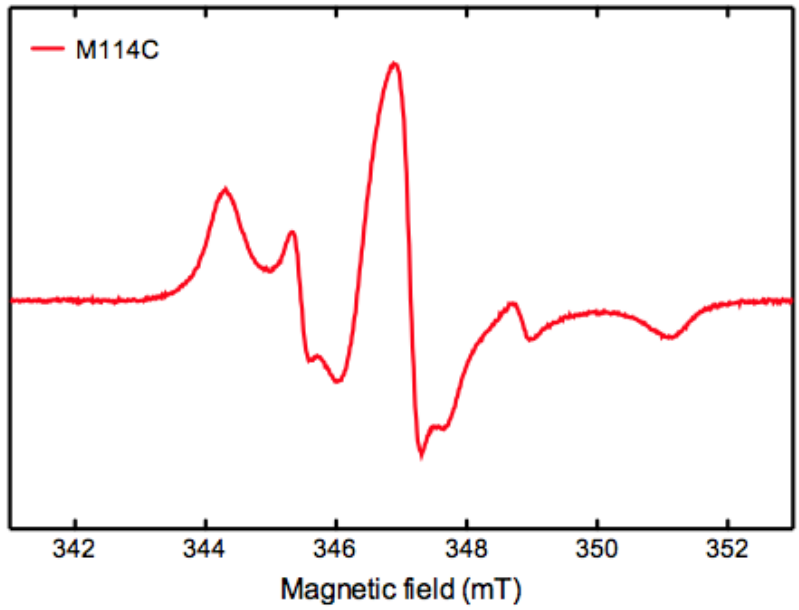

Figure 6.13 Continuous wave electron paramagnetic resonance spectrum of M114C Aac2p treated with MAL-6 for 24 hr. Whole cells of *L. lactis* expressing M114C Aac2p were treated with 250 μM MAL-6 for 24 hr. The reaction was quenched by 1 mM DTT and the cells were washed six times with PBS containing 1 mM DTT. Before collecting the cw-EPR spectrum, the sample was washed one additional time with PBS containing 10 mM $(Fe(CN)_6)^3$. cw-EPR was performed at ambient temperature. The conditions were: 9.6 GHz (X-band), 1 G modulation amplitude, 100 kHz modulation frequency and 8-32 scans. The spectrum is a first derivative.

6.3.6 Competition between MAL-6 and eosin-5-maleimide

An alternative approach to EPR was tested to determine the degree of MAL-6 labelling of single and double cysteines of mutant Aac2p. First, MAL-6 was added to react with specific cysteine thiols in the mutant Aac2p, after which eosin-5-maleimide was added to react with any remaining unreacted cysteine thiols. As expected, the Δ2-19 cys-less Aac2p control was not labelled by eosin-5-maleimide, as determined by a fluorescent scan (Figure 6.14 B top). Importantly, cysteines of M114C, I311C and M114C/I311C Aac2p were labelled equally by eosin-5-maleimide, regardless of whether MAL-6 was added prior to the addition of eosin-5-maleimide. These results, combined with the cw-EPR data (Figure 6.12), support the hypothesis that MAL-6 did not react with cysteines in the short 10 min time frame.

Eosin-5-maleimide labelled the cysteine of M114C Aac2p more robustly compared to I311C Aac2p, which was labelled very weakly (Figure 6.14 B top). This result was expected, because M114C was found to be more accessible compared to I311C in the inhibited c-state (Figure 5.3). The low labelling of I311C by eosin-5-maleimide indicates that this residue is not readily accessible to the probe.

Overall in this chapter two methods, cross-linking combined with MALDI MS and EPR spectroscopy, were used to probe the closure of the cytoplasmic salt bridge in the m-state, but definitive proof was not obtained.

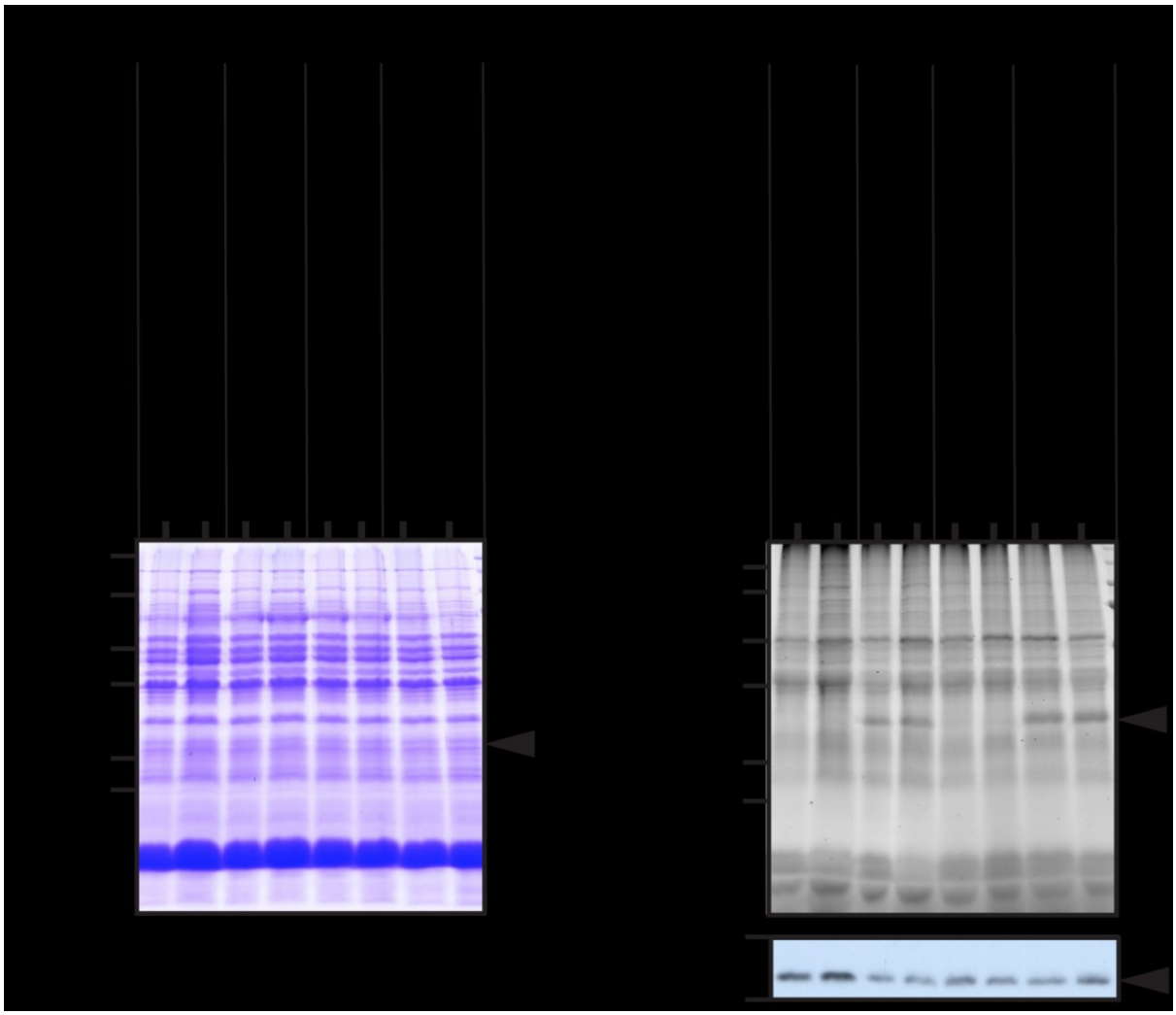

Figure 6.14 Expression levels and fluorescence intensity of single and double cysteine mutants of Aac2p labelled first with MAL-6 and then with eosin-5-maleimide. Whole cells of *L. lactis* expressing M114C, I311C or M114C/I311C Aac2p were treated with 25 µM MAL-6 for 10 min followed by 25 µM eosin-5-maleimide for 10 min, or were not treated with MAL-6 and then treated with 25 µM eosin-5-maleimide. **(A)** SDS-PAGE analysis and **(B)** fluorescent scan (above) and Western blot (below) of lysosome-lysed cells. 30 µg total cellular protein was loaded per lane. The fluorescent scans were imaged using a Typhoon imager. The PMT Voltage was 675 V. The excitation/emission wavelengths were 532/560 nm, respectively. The antibody for the Western blot was directed against α-helix H5 of Aac2p. The Western blot was exposed for 5 min on x-ray film. The band for Aac2p is indicated by a solid black arrowhead.

Chapter 7 General discussion

On the basis of symmetry analysis a new transport mechanism has been proposed (Robinson *et al.*, 2008). The main structural elements of the proposed mechanism are a single substrate binding site in the central cavity and two salt bridge networks on either side of the cavity. The networks regulate access to the binding site from either side of the membrane in an alternating way, satisfying the alternating access mechanism formulated for transporters in general (Jardetzky, 1966), or more particularly for mitochondrial carriers in the single-binding centre gated pore mechanism (Klingenberg, 1989; Klingenberg, 2005).

The central substrate binding site has been supported by sequence analysis (Kunji & Robinson, 2006; Robinson & Kunji, 2006; Robinson *et al.*, 2008) and by molecular dynamics simulations of ADP binding to the ADP/ATP carrier (Dehez *et al.*, 2008; Wang & Tajkhorshid, 2008). The substrate binding site is characterised by three contact points I, II and III, which are located on the even-numbered α-helices in the central part of the cavity. More recently, the substrate specificities of two isoforms of the human mitochondrial ornithine carrier were modified completely by swapping residues in the contact points of the substrate binding site (Monné *et al.*, 2012), providing the most convincing experimental evidence yet.

The formation of the salt bridge networks as part of the transport mechanism is based on several lines of evidence. First, the three motifs of the matrix salt bridge network PX[DE]XX[RK] are almost completely conserved throughout the mitochondrial carrier family (Robinson *et al.*, 2008). The formation of the matrix network as part of the transport cycle is supported by selection of second site revertants (Nelson *et al.*, 1998), structural data (Pebay-Peyroula *et al.*, 2003), mutagenesis and functional data (reviewed in (Robinson *et al.*, 2008)) and mutant carriers that cause human diseases (F. Palmieri, 2008). Second, the formation of the cytoplasmic salt bridge network consisting of the [FY][DE]XX[RK] motifs is based largely on the high level of symmetrical conservation throughout the family, although it is not as well conserved as the matrix network (Robinson *et al.*, 2008). Additional support arises from the observation that both networks are present at the water-

membrane interface, where they would function best as gates (Robinson *et al.*, 2008). Further supporting evidence was obtained from mutagenesis, in which residues in the cytoplasmic network were found to be critical or important for function of the mitochondrial oxoglutarate carrier (Stipani *et al.*, 2001; Cappello *et al.*, 2006). Consequently, to date there is no experimental evidence supporting the formation of cytoplasmic salt bridge network as part of the transport cycle in which the cytoplasmic side of the carrier closes.

In this dissertation, several different approaches have been explored to test this hypothesis. In the first approach, the water-accessible cytoplasmic side of the yeast mitochondrial ADP/ATP carrier was probed in different conformational states by targeting single cysteines with fluorescent probes. In the second approach, the positively and negatively charged residues of the cytoplasmic network were replaced by cysteines and attempts were made to cross-link them in different conformational states with M-2-M, which can react with two cysteine thiols at the same time. In the third approach, the plan was to determine the distances between α-helices on the cytoplasmic side by PELDOR EPR combined with site-directed spin labelling. Central to all of these approaches was the expression and functional characterisation of single and double cysteine mutants of Aac2p in the Gram-positive *Lactococcus lactis*, which will be discussed first.

7.1 Expression and transport activity of mutant Aac2p

In this dissertation, the lactococcal expression system was used to express and characterise single and double cysteine mutants of the yeast ADP/ATP carrier Aac2p. As noted previously, this system has many practical advantages over alternative systems, such as: (i) growth of lactococci proceeds to high cells densities without the need for aeration; (ii) DNA transformation and isolation protocols are available; (iii) a strongly and tightly regulated promoter system is available and protein expression at highly reproducible levels can be induced using Nisin A; (iv) there is no endogenous adenine nucleotide transport; (v) expressed membrane proteins are targeted exclusively to the single cytoplasmic membrane, allowing the direct application of substrates and inhibitors to study membrane protein activity in

whole cells; (vi) the bacterium has mild proteolytic activity, indicating that the expressed protein is likely to remain intact; and (vii) membrane proteins are readily solubilised from the membrane in a wide range of mild detergents (Kunji *et al.*, 2003). In this dissertation, additional advantages have been observed: (viii) a simplified and efficient system is now available for the introduction of mutations into structural genes, based on a methylation step in *E. coli* and PCR (Chapter 2 and 3); (ix) the topology of inserted mitochondrial carriers is strictly defined even when single or double cysteine mutations are introduced (Chapter 4); (x) *L. lactis* has a generally low cysteine codon usage, indicating that cysteines can be introduced for specific labelling without much background interference (Chapter 4 and 5); (xi) the surface of membrane proteins can be directly labelled with thiol-specific probes in whole cells, provided they are water soluble (Chapter 4 and 5); (xii) the expression levels of membrane proteins can be determined in whole cells without the need to isolate membranes.

In chapter 3, the expression levels and transport activity of 38 mutant carriers were determined in whole cells of *L. lactis*. All of the mutant carriers were expressed, but they had variable specific transport activities. Single cysteine replacements of Aac2p, A34C, G134C, G138C, R204C, F208C, G234C, G298C and A299C, which are located nearer the centre of the cavity, did not significantly transport ADP, whereas mutations in the upper cavity, termini and the cytoplasmic loops did not affect activity much or even improved the specific activity. The vast majority of mutants capable of ADP transport could also be inhibited with BKA and CATR to 85 and 100%, respectively, demonstrating that transport was specific.

Most previous mutation studies of the ADP/ATP carrier focused on probing charged residues, which was not the focus here. Competitive ELISA showed that R204L Aac2p was not expressed in yeast mitochondria (V. Müller *et al.*, 1996), and, as expected, R204L Aac2p did not exchange ADP for ATP in phospholipid vesicles (Heidkämper *et al.*, 1996). Although expressed in a different system and mutated to cysteine instead of leucine, R204C Aac2p was also one of the lowest expressed mutants, expressing at ~10% of Δ2-19 cys-less Aac2p levels (Figure 3.8) and also, R204C Aac2p was not active (Figure 3.13 A). Thus, in both studies R204 mutations had a severe effect on expression and, consequently, function of the carrier.

Residues Y203, Y207, F208 and Y211 of Aac2p have been proposed to form an aromatic ladder on α-helix H4 to guide the adenine moiety to the substrate binding site (Pebay-Peyroula *et al.*, 2003). These residues have been mutated to alanine and the kinetics of the mutant Aac2p have been analysed in yeast mitochondria (David *et al.*, 2008). The K_M^{ADP} for Y203A, Y207A, F208A and Y211A Aac2p were reported as 328 ± 61, 0.9 ± 0.1, not measurable and 8.5 ± 0.8 μM, respectively, with the wild type K_M^{ADP} being measured as 0.68 ± 0.08 μM. Here, it was found that F208C Aac2p did not transport significantly (Figure 3.13). Also, the specific initial transport rate of Y207C Aac2p was higher than that of Δ2-19 cys-less Aac2p (Figure 3.10), whereas Y203C and Y211C Aac2p were much lower than that of Δ2-19 cys-less Aac2p. Y207C, Y203C and Y211C Aac2p were well inhibited by CATR, but Y203C and Y211C Aac2p were only partially inhibited by BKA (~44% and ~75%, respectively, Figure 3.16). These two studies on the aromatic residues of Aac2p agree very well, but the results can be interpreted very differently. Residues F208 and Y211 are part of well-conserved [YF]XX[YF] motif that is adjacent to the charged residues of the cytoplasmic salt bridge and are symmetrically conserved in all mitochondrial carriers, whether or not the substrates are adenine nucleotides. Residue Y203 is part of the adenine nucleotide binding pocket (Kunji & Robinson, 2006; Robinson & Kunji, 2006; Robinson *et al.*, 2008; Dehez *et al.*, 2008; Robinson *et al.*, 2008; Wang & Tajkhorshid, 2008) and thus its sensitivity to mutation is well understood. Y207 is not important for function and thus it is highly unlikely that there is an aromatic ladder specific for adenine.

The expression and transport activity of single cysteine mutants of Aac2p was previously determined in yeast mitochondria. The expression levels of single cysteine mutants of Aac2p relative to cys-less Aac2p were found to vary between 0.5-fold and 1.25-fold of the cys-less Aac2p (Kihira *et al.*, 2004; Kihira *et al.*, 2005; Iwahashi *et al.*, 2006; Iwahashi *et al.*, 2008). Similarly, the expression levels of the 38 single cysteine mutants of Aac2p in *L. lactis* were found to vary (Figure 3.8, Appendix IV).

The initial rate of ADP transport was measured for mutant Aac2p containing single cysteine replacements on the cytosolic ends of α-helices H2 and H3, and on the

cytosolic loop h23 (Kihira *et al.*, 2005). The initial rate of ADP transport was measured using 100 μM ADP, compared to the 4.0 μM ADP used here (Chapter 3). At lower ADP concentrations the transport rates are lower because V_{max} has not been reached. With the exception of A113C Aac2p, all of the single cysteine mutants were competent in transport, but they transported at lower initial rates than cys-less Aac2p (Kihira *et al.*, 2005). The mutant Aac2p K108C, D109C, A113C, M114C, W126C and N130C were also characterised here, but the specific initial transport rates of this mutant sub-set were higher than those of Δ2-19 cys-less Aac2p, not lower. Also, A113C was found to transport well here, but not in yeast mitochondria (Kihira *et al.*, 2005). The expression and the transport rates of A113C Aac2p were both abnormally low in Kihira *et. al.,* so there could have been a genetic defect in that strain, or some other anomaly. None of these regions are well conserved in length and sequence with the exception of the C-terminal end of α-helix H2, which is involved in the formation of the cytoplasmic network, and thus they are unlikely to be critical for function, as both studies show. The observation that some mutations on the cytoplasmic side improve function of mutant Aac2p could be a consequence of improved protein insertion into the membrane. The carriers are synthesised in the cytoplasm of *L. lactis* and during insertion the cytoplasmic loops and termini must traverse the membrane, which might be easier when a polar residue is replaced by the more hydrophobic cysteine.

7.2 Orientation of single cysteine mutant carriers in the *Lactococcus lactis* membrane

The orientation of bovine AAC1 was shown to be with the N-terminus to the outside of the bovine mitochondrion when probed with N-terminus-specific antibodies (Brandolin *et al.*, 1989). The orientation of Aac2p in yeast mitochondrial membranes was confirmed by probing the accessibility of the single cysteine mutants from the intermembrane region with the membrane-impermeable probe eosin-5-maleimide (Hatanaka *et al.*, 2001). The accessibility of C73 (located on the matrix side, Figure 3.1) in the C244A/C271A/C288A mutant was found to be dependent on the preparation; in intact mitochondria it was inaccessible to the probe, but in solubilised samples it was accessible, providing evidence that C73 is on the matrix side.

Furthermore, eosin-5-maleimide labelled both solubilised and membrane embedded S21C, A124C, S222C and L312C single cysteine replacements of mutant Aac2p, suggesting that they are on the cytoplasmic side facing the intermembrane region. Other members of the mitochondrial carrier family are also oriented with the N- and C-termini to the intermembrane region. Phosphate and oxoglutarate carriers in the mitochondrial membrane were treated with proteolytic enzymes and peptide-specific antibodies to prove that they are oriented with their cytoplasmic termini to the outside (Capobianco *et al.*, 1991; F. Palmieri, Bisaccia, *et al.*, 1993a). The C-terminus of the mitochondrial phosphate carrier was targeted by a specific antibody, demonstrating that it faced the intermembrane region in rat liver mitochondria (Ferreira *et al.*, 1990).

In chapter 4, the orientation of single cysteine mutants of Aac2p that were competent in transport was determined in whole cells of *L. lactis*. This analysis was crucial for the interpretation of the fluorescent labelling studies presented later. It was predicted that the cytoplasmic side of the single cysteine mutants would face outside the lactococcal cell, similarly to the orientation of Δ2-19 and Δ2-19 cys-less Aac2p. Labelling of single cysteines with the membrane-impermeable probe eosin-5-maleimide confirmed that the topology of a selected sub-set of mutant Aac2p was consistent with this idea. The cysteine replacements in the cytoplasmic loops and termini, as well as the upper sections of the central cavity, were all labelled in the CATR-inhibited state, whereas the membrane facing or inter-helical replacements as well as those on the matrix side of the carrier were not in both inhibited states. Additional evidence was gained from the observation that the same sub-set plus an additional 18 single cysteine mutants were fully inhibited by CATR, a membrane-impermeable inhibitor that only binds from the cytoplasmic side of Aac2p. These results demonstrate that the orientation is the same irrespective of the original type and location of residue replaced by cysteine.

The positive-inside rule predicts that membrane proteins are oriented upon insertion into the membrane with the majority of their positively charged amino acids inside the bacterial cell (Heijne, 1986; Heijne & Gavel, 1988; Heijne, 1989). The rule predicted that ADP/ATP carrier and other mitochondrial carriers would be oriented with their cytoplasmic sides to the outside of *L. lactis.* Mitochondria and bacteria have a similar polarity of membrane potential, so the orientation of mitochondrial carriers in both is

also expected to be similar. For instance, the complete inhibition of ADP transport of the *Neocallimastix patriciarum* ADP/ATP carrier expressed in whole cells of *L. lactis* by CATR provided evidence that the carrier was oriented with its cytoplasmic side to the outside of the cell (Kunji *et al.*, 2003). All of these observations indicate that the positive-inside rule applies to the expression of mitochondrial carriers in *L. lactis*.

7.3 Accessibility of single cysteine mutants in different transport states

With the orientation of the single cysteine mutants of Aac2p in the *L. lactis* membrane established, it was possible to probe the accessibility of the cytoplasmic side of the single cysteine mutants of Aac2p which face outside the cell. Only those mutants that were competent in transport and were inhibited by BKA and CATR were considered for labelling with the membrane-impermeable probe eosin-5-maleimide. Single cysteines that were labelled within error not significantly different from background in both the inhibited m- and c-states also could not be used. The sub-set of mutants remaining were D26C, D109C, K112C, A113C, M114C, W126C, N130C, S230C, I302C and D306C Aac2p. With the exception of I302C, which will be discussed below, all of these mutants were labelled preferentially in the CATR-inhibited state compared to the BKA-inhibited state, and the sites of mutation were at the top of the cavity (Figure 7.1). These results demonstrated that these residues are accessible in the inhibited c-state but become occluded in the m-state. The most likely explanation is that the entrance of the cavity on the cytoplasmic side closes in the inhibited m-state (Figure 7.2). Subsequent experiments showed that in the absence of substrate the level of single cysteine labelling for the ten mutants was similar to that of the CATR-inhibited c-state, indicating that they are also in the c-state. When the substrate ADP was added, a decrease in labelling was observed for seven of the ten mutants of Aac2p, suggesting that the transporter cycles rapidly through the transport states making the introduced cysteines less available for labelling. It was also confirmed that the differences in labelling were a consequence of ADP being a specific substrate of Aac2p and that labelling of the single cysteine of W126C Aac2p was occluded by high ADP and ATP levels. Thus, the cytoplasmic side of the ADP/ATP carrier closes as part of the transport cycle.

All of these results are consistent with the cavity closing, except for the labelling of I302C. In this particular case, the labelling in the CATR-inhibited state is lower than in the BKA-inhibited state. The labelling of I302C was found to be independent of substrate, which may indicate that most of it is background labelling rather than specific state dependent labelling.

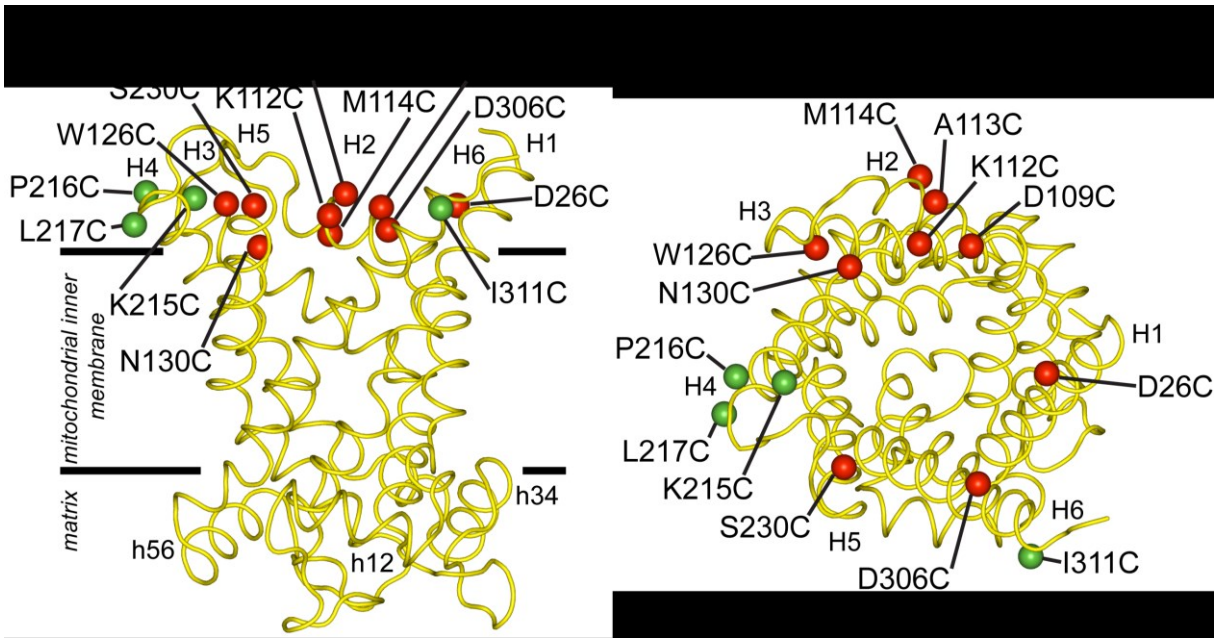

Figure 7.1 State-dependent accessibility of cytoplasmic side single cysteines demonstrates closure of the cavity. Summary of significant conformational changes between the CATR- and BKA-inhibited states. Residues that are significantly labelled in the inhibited c-state but not in the m-state (coloured red) and those that are significantly labelled in both inhibited states (coloured green) are named and shown. **(A)** Lateral and **(B)** cytoplasmic view of the cavity.

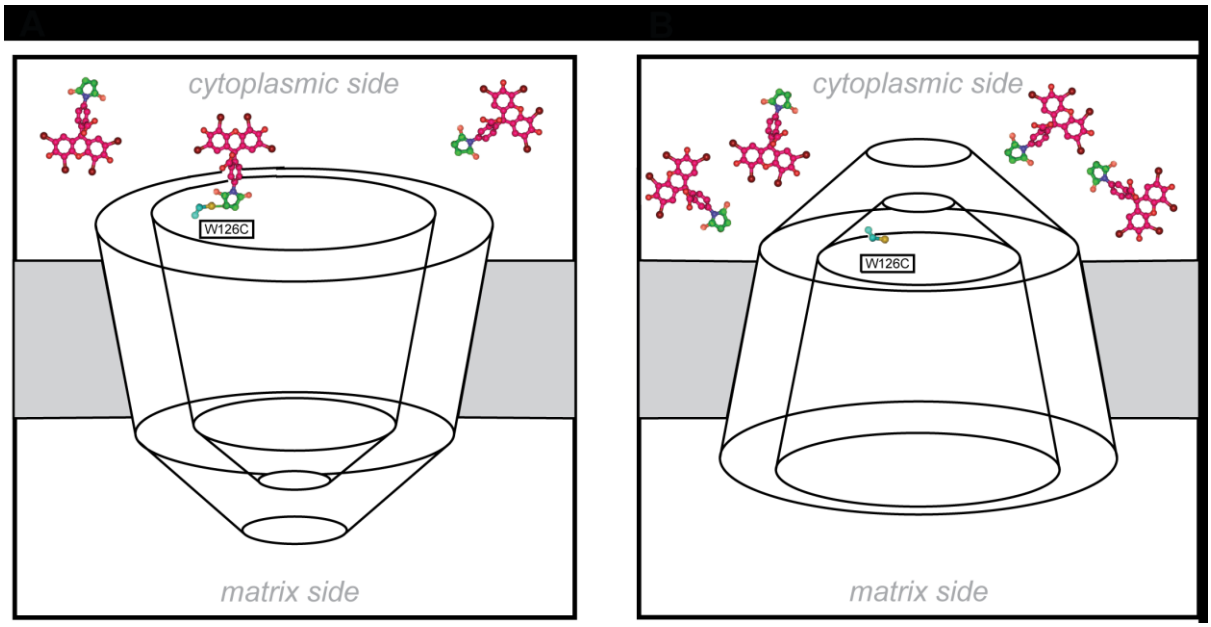

Figure 7.2 Conformation dependent accessibility of single cysteine mutants of Aac2p to the thiol-specific, membrane-impermeable probe eosin-5-maleimide. (A) Eosin-5-maleimide binds to residue W126C in the c-state when the cytoplasmic side in open but **(B)** cannot access the residue in the m-state, when the cytoplasmic side is closed. W126C is labelled and shown as turquoise and yellow sticks, and eosin-5-maleimides are shown as green, pink and violet sticks. Aac2p is shown as a transparent model surrounded by a gray-coloured membrane. The cytoplasmic and matrix sides are labelled.

Eosin-5-maleimide labelling of inhibited single cysteine mutants of Aac2p expressed in *S. cerevisiae* mitochondria has been done previously (Kihira *et al.*, 2004; Kihira *et al.*, 2005; Iwahashi *et al.*, 2006; Iwahashi *et al.*, 2008). The complete set of residues found in the cytoplasmic loops, the C-terminus and a portion of the cytoplasmic cavity was probed with eosin-5-maleimide in the presence of BKA and CATR in these studies too. The cysteine replacements of the cavity residues in T100C, Q101C, N104C, F105C, K108C, D109C, K112C, A113C, M114C, K215C, P216C, L217C, G298C, A299C, V301C, I302C, Y305C, D306C, Q309C and I311C mutant Aac2p were probed in both studies. As N104C, G298C, A299C and Y305C Aac2p did not transport ADP or were not well inhibited in *L. lactis*, only the labelling of T100C, Q101C, F105C, K108C, D109C, K112C, A113C, M114C, K215C, P216C, L217C, V301C, I302C, D306C, Q309C and I311C can be directly compared. When expressed in yeast mitochondria, cysteines D109C, K112C and A113C were labelled more in the inhibited c-state, M114C and N130C were labelled more in the inhibited

m-state, whereas W126C, K215C, P216C, L217C, I302C, D306C and I311C were labelled similarly in both inhibited states (Kihira *et al.*, 2004; Kihira *et al.*, 2005; Iwahashi *et al.*, 2006; Iwahashi *et al.*, 2008). When expressed in *L. lactis*, D109C, K112C, A113C, M114C, W126C, N130C and D306C were labelled more in the inhibited c-state, I302C was labelled more in the inhibited m-state, whereas K215C, P216C, L217C and I311C were labelled similarly in both inhibited states (Figure 5.5 and 5.6). Thus, in *L. lactis* the cysteines introduced in the upper cavity were labelled more in the inhibited c-state than in the inhibited m-state, except for I302C (discussed above). Little or no labelling occurred when these mutants of Aac2p were fixed in the inhibited m-state in *L. lactis*, but they were labelled in the yeast experiments.

Furthermore, in the yeast studies Q101C, V301C and Q309C were unlabelled in both the BKA- and CATR-inhibited states (Kihira *et al.*, 2004; Iwahashi *et al.*, 2008). In contrast, there was no significant labelling of T100C, Q101C, F105C, K108C, V301C and Q309C in the BKA- and CATR-inhibited states reported here (Figure 5.4 A). T100C, Q101C, F105C and K108C are located on α-helix H2, close to or in the CATR binding site. Thus, in the former yeast study, the labelling pattern was not consistent with CATR binding, whereas it was here.

Cysteine replacements of residues of the cytoplasmic loops and C-terminus, E120C, A124C, S222C, E224C and G314C were also tested in both studies, and the labelling was similar irrespective of the inhibited state, with the exception of A124C which was labelled significantly more in the presence of CATR than BKA in *L. lactis* (Kihira *et al.*, 2005; Iwahashi *et al.*, 2006; Iwahashi *et al.*, 2008).

The studies are in agreement with respect to the single cysteine replacements of residues of the cytoplasmic loops and C-terminus being labelled similarly in both states, but they differ with respect to residues in the upper parts of the cavity. In the *L. lactis* labelling studies, BKA blocked accessibility of eosin-5-maleimide to most of the upper parts of the cavity; in yeast studies a consistent difference in labelling did not emerge as both the inhibited m- and c-state mutants were labelled, often at equivalent levels.

Based on the yeast labelling studies, it was proposed that the cytoplasmic loops unfold in the inhibited c-state and fold into the cytoplasmic cavity in the inhibited m-state, and that the cytoplasmic loops do not entirely close off the cytoplasmic side of the carrier (Kihira *et al.*, 2004; Kihira *et al.*, 2005; Iwahashi *et al.*, 2006; Iwahashi *et al.*, 2008).

However, many crucial controls are lacking in the experiments of Terada and co-workers. First, of all of the mutants discussed above, only D109C, K112C, A113C and M114C Aac2p were tested for ADP transport in yeast mitochondria, and thus for the majority of these mutants it cannot be confirmed that they were active and could cycle through the transport states. Second, the inhibition of transport by BKA or CATR was not assessed for any of the single cysteine mutants of Aac2p expressed in yeast mitochondria. This is especially a concern for labelling studies in the presence of BKA, as the presence of ADP is required for efficient inhibition by BKA (Henderson & Lardy, 1970; Kemp *et al.*, 1970; Erdelt *et al.*, 1972). When both BKA and ADP were added to *L. lactis* expressing N130C Aac2p, labelling was not detected, but when BKA was added in the absence of ADP, labelling was detected (Figure 4.10), demonstrating that the addition of ADP was critical for locking Aac2p in the inhibited m-state. Thus, it cannot be confirmed that the mutants were locked in the required states prior to labelling, opening the possibility that they were in mixed states, which could explain labelling of cysteines in the presence of BKA in yeast. Third, the eosin-5-maleimide labelling conditions differed markedly between the two studies. The yeast studies were done at an 8-fold higher eosin-5-maleimide concentration (200 µM versus 25 µM eosin-5-maleimide for similar amounts of total protein) and incubation times were three-fold longer (30 min versus 10 min). It is possible that these different conditions could have facilitated more non-specific labelling. This idea is supported by the observation that cysteines that were introduced in the CATR binding site were not labelled in the presence of CATR in *L. lactis*, as expected, but were in yeast. Fourth, another critical factor is the addition of DTT to quench labelling. It was observed in the *L. lactis* studies that eosin-5-maleimide continued to label proteins non-specifically even after 100-fold excess DTT was added (Figure 4.9). To reduce the non-specific background it was also necessary to wash the samples several times to remove eosin-5-maleimide efficiently (Figure 4.9). These studies demonstrate that there is the potential for unreacted

eosin-5-maleimide to label protein non-specifically after the principal labelling steps are completed. No controls are shown to ascertain that this is not the case in the yeast studies, opening the possibility that some of the labelling is non-specific. Fifth, no controls were done to establish the orientation of each mutant Aac2p and the membrane impermeably of eosin-5-maleimide was not firmly established in yeast mitochondria. Both controls are necessary for a correct interpretation of the labelling studies.

In conclusion, the studies presented here show that the accessibility of residues in the upper sections of the cavity is different between the inhibited m- and c-states. More importantly, they show that substrates can induce the same changes in accessibility indicating that the labelling is probing conformational changes of the transport cycle.

7.4 The formation of the cytoplasmic salt bridge network

Only three cysteine replacements of residues of the cytoplasmic salt bridge network led to impaired transport of the mitochondrial oxoglutarate carrier (Stipani *et al.*, 2001; Cappello *et al.*, 2006), indicating that these residues are important for function, but the results do not prove that the residues form a network. Better experimental evidence for the formation of the cytoplasmic salt bridge network in Aac2p was obtained by Dr Alex Hellawell (PhD dissertation, 2010). The three basic residues of the cytoplasmic salt bridge network were mutated to acidic aspartate residues, resulting in an Aac2p mutant with only acidic residues in the network. Another mutant Aac2p was engineered in which the three acidic residues were mutated to basic lysine residues, resulting in a mutant containing only basic residues in the network. The initial ADP uptake rates of the all acidic and all basic Aac2p were approximately 5% of Δ2-19 cys-less Aac2p. When all of the residues of the network were replaced by residues of the opposite charge, essentially swapping the networks around, transport was restored to approximately 15% of Δ2-19 cys-less Aac2p. Despite containing six introduced mutations, the mutant Aac2p in which all of the charges of the salt bridge network had been swapped was more active than the mutant Aac2p in which the network was either all basic or all acidic through the

introduction of three mutations. Although not ideal, this is the most convincing evidence obtained for the formation of the cytoplasmic salt bridge during the transport cycle.

The eosin-5-maleimide labelling data are consistent with the cavity becoming occluded at or adjacent to the cytoplasmic salt bridge network during transport, but they do not prove that the network forms during transport. The single cysteine replacements of residues of the cytoplasmic network in Aac2p do not interfere with transport in a detrimental manner. At first, it could be argued that the network is not important for function of the carrier on the basis of these results. However, as only one mutation was introduced, two of the three salt bridges or ionic pairs in the network can still form, meaning that the interaction energy in the overall network is reduced by one-third, all other factors remaining equal. Mitochondrial carriers differ in the number of salt bridges in the network, as aromatic, polar and hydrophobic substitutions can be present, which can lead to the formation of cation-π interactions or hydrogen bonds, or to a complete loss of interaction. On the basis of biological function and efflux properties it has been argued that differences in interaction energies might determine whether carriers function as equimolar exchangers or as uniporters (Robinson *et al.*, 2008). The cytoplasmic salt bridge network functions as an energy barrier that prevents the change from the m-state to c-state in the absence of substrate. The introduction of a single cysteine might have lowered the energy barrier, changing the transporter from a strict exchanger to a transporter capable of uniport steps, but this aspect has not been investigated. Another important feature of the network could be the closure of the carriers to prevent an influx of protons. A mutation may compromise the integrity of the proton barrier, but this aspect has not been studied either. In any case it is likely that other residues than those belonging to the network are involved in the proton barrier, possibly the aromatic residues that are adjacent to the residues of the network. Consequently, the transport data are not inconsistent with the formation of the network.

The eosin-5-maleimide labelling of single cysteine replacements of the cytoplasmic salt bridge network residues showed that three of the six replacements were labelled significantly in the CATR-inhibited state but not in the BKA-inhibited state. Of the remaining three, one could not be locked in the m-state, one could not be labelled in

either state and one was labelled not significantly differently in the two inhibited states, but the error was very high and the overall labelling trend was consistent with labelling in the CATR-inhibited state but not the BKA-inhibited state. Thus, these results are consistent with the formation of the cytoplasmic salt bridge in the BKA-inhibited state, but do not prove that it forms.

In addition, attempts were made to cross-link double cysteine replacements of residues of the cytoplasmic salt bridge network that are predicted to interact, such as K112C and D212C of K112C/D212C Aac2p. It was shown that a lower molecular weight migration shift of the K112C/D212C Aac2p band occurred when the samples were treated with M-2-M, a bi-reactive cross-linker. The amount of this species was higher when BKA was present than when CATR was present, indicating that the cross-link occurred more readily in the inhibited m-state. The conditions for inhibition might not have been ideal. The addition of M-2-M also interfered with ADP uptake, indicating that the cross-link could have prevented carrier function. Mass spectrometry was used to identify the peptides that were cross-linked by M-2-M, but the cross-linking could not be confirmed. Also, an attempt was made to measure the distances between spin-labelled residues M114C and I311C that are close to the cytoplasmic salt bridge network using PELDOR. However, the spin label could not be introduced into M114C in whole cells, and thus this approach was unsuccessful.

In this dissertation, the conformational changes of the yeast mitochondrial ADP/ATP carrier were probed. Several observations have been made that substantiate a transport mechanism in which the carrier closes on the cytoplasmic side by the formation of the cytoplasmic salt bridge network, but more work is required to verify the mechanism.

Appendix I

Generation of mutants and list of primers

A1.1 Generation of mutants

All of the single cysteine mutants of *S. cerevisiae* Δ2-19 cys-less Aac2p were constructed in the *Δ2-19 cys-less aac2* gene for use in *L. lactis*.

Single cysteine mutants D109C, D212C and D306C Aac2p were generated using overlap extension PCR by Dr Alex Hellawell.

Single cysteine mutants L50C, Q101C, N104C, N130C, S147C and Y211C Aac2p were generated using a modified QuikChange II methodology-based PCR protocol by Lisa Görs.

All remaining mutants were generated using a modified QuikChange II methodology-based PCR protocol by Valerie Ashton.

A1.2 Primers

The mutagenic oligonucleotide PCR primers were designed by Dr Chris Tate (MRC Laboratory of Molecular Biology, UK). The forward and reverse primers were designed to overlap partially and to introduce single cysteine mutations. The primers for DNA sequencing were synthesised by Sigma-Genosys (St. Louis, MO, USA). All other primers were synthesised by Eurofins MWG Operon (Ebersberg, Germany).

Double cysteine mutants D109C/Q309C, K112C/D212C, M114C/I311C and K215C/D306C Aac2p were generated using identical primers to those used to generate their corresponding single cysteine mutants.

Table A.1 Oligonucleotide primers used for DNA sequencing. *For* is an abbreviation for forward and *rev* is an abbreviation for reverse.

Plasmid	Mutation	Primer name	Primer sequence (5'-3')
pNZ8048-*Δ2-19 cys-less aac2*	n/a	pNZ for	ATA TTA TTG TCG ATA ACG C
pNZ8048-*Δ2-19 cys-less aac2*	n/a	pNZ rev	TTG GCT ATC AAT CAA AGC

Table A.2 Oligonucleotide primers used to introduce mutations into the *Δ2-19 cys-less aac2* gene in *L. lactis*. *For* is an abbreviation for forward and *rev* is an abbreviation for reverse.

Plasmid	Mutation	Primer name	Primer sequence (5'-3')
pNZ8048-*Δ2-19 cys-less aac2*	N22C	N22C for	TGG AAT CTT GCT TTT TGA TTG ATT TCT TAA TGG GTG GTG TCA GTG CCG
pNZ8048-*Δ2-19 cys-less aac2*	N22C	N22C rev	CCA TTA AGA AAT CAA TCA AAA AGC AAG ATT CCA TGG TGA GTG CCT CC
pNZ8048-*Δ2-19 cys-less aac2*	D26C	D26C for	TTT TGA TTT GTT TCT TAA TGG GTG GTG TCA GTG CCG CTG TCG C
pNZ8048-*Δ2-19 cys-less aac2*	D26C	D26C rev	CCC ATT AAG AAA CAA ATC AAA AAG TTA GAT TCC ATG GTG AGT GCC TCC
pNZ8048-*Δ2-19 cys-less aac2*	G30C	G30C for	TCT TAA TGT GTG GTG TCA GTG CCG CTG TCG CC
pNZ8048-*Δ2-19 cys-less aac2*	G30C	G30C rev	CAC TGA CAC CAC ACA TTA AGA AAT CAA TCA AAA AGT TAG ATT CCA TGG
pNZ8048-*Δ2-19 cys-less aac2*	A34C	A34C for	GTG TCA GTT GCG CTG TCG CCA AAA CTG CTG CAT CTC
pNZ8048-*Δ2-19 cys-less aac2*	A34C	A34C rev	GGC GAC AGC GCA ACT GAC ACC ACC CAT TAA GAA ATC AAT C

Plasmid	Mutation	Primer name	Primer sequence (5'-3')
pNZ8048-*Δ2-19 cys-less aac2*	L50C	L50C for	TCG AAA GAG TTA AAC TTT GCA TCC AAA ACC AAG ATG AAA TGT TAA AAC AAG GTA C
pNZ8048-*Δ2-19 cys-less aac2*	L50C	L50C rev	GTT TTG GAT GCA AAG TTT AAC TCT TTC GAT GGG AGA TGC AGC AG
pNZ8048-*Δ2-19 cys-less aac2*	T79C	T79C for	GAA CCG CTT GTC AGG AAG GTG TTA TCT CAT TCT GGA GAG GTA ACA CTG
pNZ8048-*Δ2-19 cys-less aac2*	T79C	T79C rev	ACC TTC CTG ACA AGC GGT TCT CTT GAA AGC GTC TAA GAT ACC TGC G
pNZ8048-*Δ2-19 cys-less aac2*	T100C	T100C for	ATT TCC CCT GTC AAG CTT TGA ATT TCG CCT TCA AGG ACA AGA TCA AG
pNZ8048-*Δ2-19 cys-less aac2*	T100C	T100C rev	CAA AGC TTG ACA GGG GAA ATA ACG GAT AAC GTT AGC AGT GTT ACC
pNZ8048-*Δ2-19 cys-less aac2*	Q101C	Q101C for	TCC CCA CTT GCG CTT TGA ATT TCG CCT TCA AGG ACA AGA TCA AGG C
pNZ8048-*Δ2-19 cys-less aac2*	Q101C	Q101C rev	ATT CAA AGC GCA AGT GGG GAA ATA ACG GAT AAC GTT AGC AGT GTT ACC

Plasmid	Mutation	Primer name	Primer sequence (5'-3')
pNZ8048-*Δ2-19 cys-less aac2*	N104C	N104C for	AAG CTT TGT GTT TCG CCT TCA AGG ACA AGA TCA AGG CCA TGT TTG
pNZ8048-*Δ2-19 cys-less aac2*	N104C	N104C rev	GAA GGC GAA ACA CAA AGC TTG AGT GGG GAA ATA ACG GAT AAC G
pNZ8048-*Δ2-19 cys-less aac2*	F105C	F105C for	CTT TGA ATT GTG CCT TCA AGG ACA AGA TCA AGG CCA TGT TTG GTT TC
pNZ8048-*Δ2-19 cys-less aac2*	F105C	F105C rev	CTT GAA GGC ACA ATT CAA AGC TTG AGT GGG GAA ATA ACG GAT AAC G
pNZ8048-*Δ2-19 cys-less aac2*	K108C	K108C for	TCG CCT TCT GTG ACA AGA TCA AGG CCA TGT TTG GTT TCA AGA AGG AAG
pNZ8048-*Δ2-19 cys-less aac2*	K108C	K108C rev	GAT CTT GTC ACA GAA GGC GAA ATT CAA AGC TTG AGT GGG GAA ATA ACG
pNZ8048-*Δ2-19 cys-less aac2*	D109C	D109C for	CAA GCT TTG AAT TTC GCC TTC AAG TGT AAG ATC AAG GCC ATG TTT GGT TTC
pNZ8048-*Δ2-19 cys-less aac2*	D109C	D109C rev	GAA ACC AAA CAT GGC CTT GAT CTT ACA CTT GAA GGC GAA ATT CAA AGC TTG

Plasmid	Mutation	Primer name	Primer sequence (5'-3')
pNZ8048-*Δ2-19 cys-less aac2*	K112C	K112C for	ACA AGA TCT GCG CCA TGT TTG GTT TCA AGA AGG AAG AAG GTT ACG CC
pNZ8048-*Δ2-19 cys-less aac2*	K112C	K112C rev	AAA CAT GGC GCA GAT CTT GTC CTT GAA GGC GAA ATT CAA AGC TTG AG
pNZ8048-*Δ2-19 cys-less aac2*	A113C	A113C for	AGA TCA AGT GCA TGT TTG GTT TCA AGA AGG AAG AAG GTT ACG CC
pNZ8048-*Δ2-19 cys-less aac2*	A113C	A113C rev	ACC AAA CAT GCA CTT GAT CTT GTC CTT GAA GGC GAA ATT CAA AGC TTG
pNZ8048-*Δ2-19 cys-less aac2*	M114C	M114C for	TCA AGG CCT GTT TTG GTT TCA AGA AGG AAG AAG GTT ACG CCA AAT GG
pNZ8048-*Δ2-19 cys-less aac2*	M114C	M114C rev	GAA ACC AAA ACA GGC CTT GAT CTT GTC CTT GAA GGC GAA ATT CAA AGC
pNZ8048-*Δ2-19 cys-less aac2*	E120C	E120C for	TCA AGA AGT GCG AAG GTT ACG CCA AAT GGT TTG CCG GTA ACT TGG C
pNZ8048-*Δ2-19 cys-less aac2*	E120C	E120C rev	GTA ACC TTC GCA CTT CTT GAA ACC AAA CAT GGC CTT GAT CTT GTC C

Plasmid	Mutation	Primer name	Primer sequence (5'-3')
pNZ8048-*Δ2-19 cys-less aac2*	A124C	A124C for	AAG GTT ACT GCA AAT GGT TTG CCG GTA ACT TGG CAT CTG GTG
pNZ8048-*Δ2-19 cys-less aac2*	A124C	A124C rev	AAA CCA TTT GCA GTA ACC TTC TTC CTT CTT GAA ACC AAA CAT GGC C
pNZ8048-*Δ2-19 cys-less aac2*	W126C	W126C for	ACG CCA AAT GTT TTG CCG GTA ACT TGG CAT CTG GTG
pNZ8048-*Δ2-19 cys-less aac2*	W126C	W126C rev	ACC GGC AAA ACA TTT GGC GTA ACC TTC TTC CTT CTT GAA AC
pNZ8048-*Δ2-19 cys-less aac2*	N130C	N130C for	TTG CCG GTT GTT TGG CAT CTG GTG GTG CTG CTG GTG CC
pNZ8048-*Δ2-19 cys-less aac2*	N130C	N130C rev	AGA TGC CAA ACA ACC GGC AAA CCA TTT GGC GTA ACC TTC TTC CTT C
pNZ8048-*Δ2-19 cys-less aac2*	G134C	G134C for	TGG CAT CTT GTG GTG CTG CTG GTG CCT TGT C
pNZ8048-*Δ2-19 cys-less aac2*	G134C	G134C rev	AGC AGC ACC ACA AGA TGC CAA GTT ACC GGC AAA C
pNZ8048-*Δ2-19 cys-less aac2*	A136C	A136C for	CTG GTG GTT GTG CTG GTG CCT TGT CAT TAC TAT TTG TTT ACT CTT TG
pNZ8048-*Δ2-19 cys-less aac2*	A136C	A136C rev	GGC ACC AGC ACA ACC ACC AGA TGC CAA GTT ACC G

Plasmid	Mutation	Primer name	Primer sequence (5'-3')
pNZ8048-*Δ2-19 cys-less aac2*	G138C	G138C for	GTG CTG CTT GTG CCT TGT CAT TAC TAT TTG TTT ACT CTT TGG ATT ATG
pNZ8048-*Δ2-19 cys-less aac2*	G138C	G138C rev	TGA CAA GGC ACA AGC AGC ACC ACC AGA TGC C
pNZ8048-*Δ2-19 cys-less aac2*	S147C	S147C for	TTG TTT ACT GTT TGG ATT ATG CAA GAA CTA GAT TGG CTG CTG ACT C
pNZ8048-*Δ2-19 cys-less aac2*	S147C	S147C rev	ATA ATC CAA ACA GTA AAC AAA TAG TAA TGA CAA GGC ACC AGC AGC AC
pNZ8048-*Δ2-19 cys-less aac2*	K179C	K179C for	GTC TAC AAG TGC ACC TTA AAA TCT GAT GGT GTT GCT GGT CTT TAC AGA G
pNZ8048-*Δ2-19 cys-less aac2*	K179C	K179C rev	GAT TTT AAG GTG CAC TTG TAG ACA TCG ATC AAA CCG TTG AAT TGA CGA GC
pNZ8048-*Δ2-19 cys-less aac2*	A187C	A187C for	ATG GTG TTT GTG GTC TTT ACA GAG GTT TCT TAC CTT CTG TCG TTG G
pNZ8048-*Δ2-19 cys-less aac2*	A187C	A187C rev	CTG TAA AGA CCA CAA ACA CCA TCA GAT TTT AAG GTC TTC TTG TAG ACA TC

Plasmid	Mutation	Primer name	Primer sequence (5'-3')
pNZ8048-*Δ2-19 cys-less aac2*	Y203C	Y203C for	TTG TTG TCT GTA GAG GTC TAT ACT TCG GTA TGT ACG ATT CTT TGA AGC
pNZ8048-*Δ2-19 cys-less aac2*	Y203C	Y203C rev	TAG ACC TCT ACA GAC AAC AAT ACC AAC GAC AGA AGG TAA GAA ACC TC
pNZ8048-*Δ2-19 cys-less aac2*	R204C	R204C for	TTG TCT ACT GTG GTC TAT ACT TCG GTA TGT ACG ATT CTT TGA AGC CTC
pNZ8048-*Δ2-19 cys-less aac2*	R204C	R204C rev	GTA TAG ACC ACA GTA GAC AAC AAT ACC AAC GAC AGA AGG TAA GAA ACC
pNZ8048-*Δ2-19 cys-less aac2*	Y207C	Y207C for	GAG GTC TAT GTT TCG GTA TGT ACG ATT CTT TGA AGC CTC TAT TGT TG
pNZ8048-*Δ2-19 cys-less aac2*	Y207C	Y207C rev	CAT ACC GAA ACA TAG ACC TCT GTA GAC AAC AAT ACC AAC GAC AGA AG
pNZ8048-*Δ2-19 cys-less aac2*	F208C	F208C for	GTC TAT ACT GTG GTA TGT ACG ATT CTT TGA AGC CTC TAT TGT TGA CTG
pNZ8048-*Δ2-19 cys-less aac2*	F208C	F208C rev	GTA CAT ACC ACA GTA TAG ACC TCT GTA GAC AAC AAT ACC AAC GAC AG

Plasmid	Mutation	Primer name	Primer sequence (5'-3')
pNZ8048-*Δ2-19 cys-less aac2*	Y211C	Y211C for	TCG GTA TGT GTG ATT CTT TGA AGC CTC TAT TGT TGA CTG GTT CTT TGG
pNZ8048-*Δ2-19 cys-less aac2*	Y211C	Y211C rev	CAA AGA ATC ACA CAT ACC GAA GTA TAG ACC TCT GTA GAC AAC AAT ACC
pNZ8048-*Δ2-19 cys-less aac2*	D212C	D212C for	GAG GTC TAT ACT TCG GTA TGT ACT GTT CTT TGA AGC CTC TAT TGT TGA
pNZ8048-*Δ2-19 cys-less aac2*	D212C	D212C rev	TCA ACA ATA GAG GCT TCA AAG AAC AGT ACA TAC CGA AGT ATA GAC CTC
pNZ8048-*Δ2-19 cys-less aac2*	K215C	K215C for	CGA TTC TTT GTG CCC TCT ATT GTT GAC TGG TTC TTT GGA AGG TTC ATT C
pNZ8048-*Δ2-19 cys-less aac2*	K215C	K215C rev	CAA CAA TAG AGG GCA CAA AGA ATC GTA CAT ACC GAA GTA TAG ACC TCT G
pNZ8048-*Δ2-19 cys-less aac2*	P216C	P216C for	CTT TGA AGT GTC TAT TGT TGA CTG GTT CTT TGG AAG GTT CAT TCT TGG
pNZ8048-*Δ2-19 cys-less aac2*	P216C	P216C rev	GTC AAC AAT AGA CAC TTC AAA GAA TCG TAC ATA CCG AAG TAT AGA CCT C
pNZ8048-*Δ2-19 cys-less aac2*	L217C	L217C for	TGA AGC CTT GCT TGT TGA CTG GTT CTT TGG AAG GTT CAT TCT TGG C
pNZ8048-*Δ2-19 cys-less aac2*	L217C	L217C rev	CAG TCA ACA AGC AAG GCT TCA AAG AAT CGT ACA TAC CGA AGT ATA GAC C

Plasmid	Mutation	Primer name	Primer sequence (5'-3')
pNZ8048-*Δ2-19 cys-less aac2*	S222C	S222C for	TGA CTG GTT GTT TGG AAG GTT CAT TCT TGG CTT CAT TCT TGT TG
pNZ8048-*Δ2-19 cys-less aac2*	S222C	S222C rev	ACC TTC CAA ACA ACC AGT CAA CAA TAG AGG CTT CAA AGA ATC G
pNZ8048-*Δ2-19 cys-less aac2*	E224C	E224C for	GTT CTT TGT GCG GTT CAT TCT TGG CTT CAT TCT TGT TGG GTT GGG TTG
pNZ8048-*Δ2-19 cys-less aac2*	E224C	E224C rev	CAA GAA TGA ACC GCA CAA AGA ACC AGT CAA CAA TAG AGG CTT CAA AGA ATC
pNZ8048-*Δ2-19 cys-less aac2*	S226C	S226C for	TGG AAG GTT GTT TCT TGG CTT CAT TCT TGT TGG GTT GGG TTG TTA C
pNZ8048-*Δ2-19 cys-less aac2*	S226C	S226C rev	AGC CAA GAA ACA ACC TTC CAA AGA ACC AGT CAA CAA TAG AGG CTT C
pNZ8048-*Δ2-19 cys-less aac2*	S230C	S230C for	TCT TGG CTT GTT TCT TGT TGG GTT GGG TTG TTA CTA CTG GTG C
pNZ8048-*Δ2-19 cys-less aac2*	S230C	S230C rev	CAA CAA GAA ACA AGC CAA GAA TGA ACC TTC CAA AGA ACC AGT CAA C
pNZ8048-*Δ2-19 cys-less aac2*	G234C	G234C for	TCT TGT TGT GTT GGG TTG TTA CTA CTG GTG CTT CTA CAG C
pNZ8048-*Δ2-19 cys-less aac2*	G234C	G234C rev	AAC AAC CCA ACA CAA CAA GAA TGA AGC CAA GAA TGA ACC TTC C

Plasmid	Mutation	Primer name	Primer sequence (5'-3')
pNZ8048-*Δ2-19 cys-less aac2*	T238C	T238C for	GGG TTG TTT GTA CTG GTG CTT CTA CAG CTT CTT ACC CAT TGG
pNZ8048-*Δ2-19 cys-less aac2*	T238C	T238C rev	AGC ACC AGT ACA AAC AAC CCA ACC CAA CAA GAA TGA AGC CAA G
pNZ8048-*Δ2-19 cys-less aac2*	T243C	T243C for	GTG CTT CTT GCG CTT CTT ACC CAT TGG ATA CCG TTA GAA GAA GAA TG
pNZ8048-*Δ2-19 cys-less aac2*	T243C	T243C rev	GTA AGA AGC GCA AGA AGC ACC AGT AGT AAC AAC CCA ACC CAA CAA G
pNZ8048-*Δ2-19 cys-less aac2*	R273C	R273C for	ACG CTT TGT GTA AGA TTG TTG CTG CTG AAG GTG TTG GTT CTC TAT TC
pNZ8048-*Δ2-19 cys-less aac2*	R273C	R273C rev	AAC AAT CTT ACA CAA AGC GTC AAA GGC ACC GTC GTA CTT AAC AGC
pNZ8048-*Δ2-19 cys-less aac2*	A278C	A278C for	TTG TTG CTT GTG AAG GTG TTG GTT CTC TAT TCA AGG GTG CTG G
pNZ8048-*Δ2-19 cys-less aac2*	A278C	A278C rev	AAC ACC TTC ACA AGC AAC AAT CTT CCT CAA AGC GTC AAA GGC AC
pNZ8048-*Δ2-19 cys-less aac2*	A297C	A297C for	GAG GTG TCT GTG GTG CTG GTG TTA TCT CAA TGT ACG ACC AAC TGC
pNZ8048-*Δ2-19 cys-less aac2*	A297C	A297C rev	ACC AGC ACC ACA GAC ACC TCT TAA GAT GTT AGC ACC AGC ACC C

Plasmid	Mutation	Primer name	Primer sequence (5'-3')
pNZ8048-*Δ2-19 cys-less aac2*	G298C	G298C for	GTG TCG CAT GTG CTG GTG TTA TCT CAA TGT ACG ACC
pNZ8048-*Δ2-19 cys-less aac2*	G298C	G298C rev	AAC ACC AGC ACA TGC GAC ACC TCT TAA GAT GTT AGC AC
pNZ8048-*Δ2-19 cys-less aac2*	A299C	A299C for	TCG CAG GTT GTG GTG TTA TCT CAA TGT ACG ACC AAC TGC AAA TG
pNZ8048-*Δ2-19 cys-less aac2*	A299C	A299C rev	GAT AAC ACC ACA ACC TGC GAC ACC TCT TAA GAT GTT AGC ACC
pNZ8048-*Δ2-19 cys-less aac2*	V301C	V301C for	GTG CTG GTT GTA TCT CAA TGT ACG ACC AAC TGC AAA TGA TCT TGT TTG
pNZ8048-*Δ2-19 cys-less aac2*	V301C	V301C rev	CAT TGA GAT ACA ACC AGC ACC TGC GAC ACC TCT TAA GAT GTT AG
pNZ8048-*Δ2-19 cys-less aac2*	I302C	I302C for	CTG GTG TTT GCT CAA TGT ACG ACC AAC TGC AAA TGA TCT TGT TTG G
pNZ8048-*Δ2-19 cys-less aac2*	I302C	I302C rev	GTA CAT TGA GCA AAC ACC AGC ACC TGC GAC ACC TCT TAA G
pNZ8048-*Δ2-19 cys-less aac2*	Y305C	Y305C for	TCT CAA TGT GCG ACC AAC TGC AAA TGA TCT TGT TTG GTA AGA AG
pNZ8048-*Δ2-19 cys-less aac2*	Y305C	Y305C rev	CAG TTG GTC GCA CAT TGA GAT AAC ACC AGC ACC TG

Plasmid	Mutation	Primer name	Primer sequence (5'-3')
pNZ8048-*Δ2-19 cys-less aac2*	D306C	D306C for	GGT GCT GGT GTT ATC TCA ATG TAC TGT CAA CTG CAA ATG TTG TTT GGT
pNZ8048-*Δ2-19 cys-less aac2*	D306C	D306C rev	ACC AAA CAA GAT CAT TTG CAG TTG ACA GTA CAT TGA GAT AAC ACC AGC ACC
pNZ8048-*Δ2-19 cys-less aac2*	Q309C	Q309C for	GTA CGA CCA ACT GTG CAT GAT CTT GTT TGG TAA GAA GTT CAA ATA AGC TAG AG
pNZ8048-*Δ2-19 cys-less aac2*	Q309C	Q309C rev	CAA GAT CAT GCA CAG TTG GTC GTA CAT TGA GAT AAC ACC AGC ACC TGC
pNZ8048-*Δ2-19 cys-less aac2*	I311C	I311C for	CTG CAA ATG TGC TTG TTT GGT AAG AAG TTC AAA TAA GCT AGA GAG CTC
pNZ8048-*Δ2-19 cys-less aac2*	I311C	I311C rev	ACC AAA CAA GCA CAT TTG CAG TTG GTC GTA CAT TGA GAT AAC ACC AG
pNZ8048-*Δ2-19 cys-less aac2*	G314C	G314C for	GAT CTT GTT TTG TAA GAA GTT CAA ATA AGC TAG AGA GCT CAA GCT TTC
pNZ8048-*Δ2-19 cys-less aac2*	G314C	G314C rev	GAA CTT CTT ACA AAA CAA GAT CAT TTG CAG TTG GTC GTA CAT TGA G

Appendix II

Transport and labelling statistics

A summary of the statistics for all of the single cysteine mutants of Aac2p expressed in whole cells of *L. lactis* discussed in Chapters 3, 4 and 5 is listed in Table A.3. These include statistics for transport assays, inhibition of transport and labelling studies.

To test whether the initial transport rate (nmol ADP min^{-1}) was significantly above background, the average of the initial transport rate of each single cysteine mutant was compared to the average of the initial transport rate of the empty vector construct. An unpaired, one-tailed Student's *t*-test assuming unequal variance was used ($P<0.05$). In addition, the average of the specific initial uptake rate (nmol ADP min^{-1} mg^{-1} Aac2p) for each single cysteine mutant was compared to G134C Aac2p, which had the lowest average specific initial uptake rate (data not shown). An unpaired, one-tailed Student's *t*-test assuming unequal variance was used ($P<0.05$). The results of the *t*-tests are in agreement.

To test whether the average inhibition of the specific initial uptake rate by CATR for each single cysteine mutant of Aac2p was not significantly different or greater than the average inhibition of the specific initial uptake rate by CATR for Δ2-19 cys-less Aac2p, an unpaired, two-tailed Student's *t*-test assuming unequal variance was used ($P<0.05$). The same test was used to compared BKA-inhibited single cysteine mutant Aac2p to BKA-inhibited Δ2-19 cys-less Aac2p.

To test whether eosin-5-maleimide labelling of single cysteines of Aac2p was significantly above background, the average fluorescence intensity of each single cysteine mutant of Aac2p in the presence of CATR or BKA was compared to the average fluorescence intensity of the empty vector construct in the presence of CATR or BKA, respectively. An unpaired, one-tailed Student's *t*-test assuming unequal variance was used ($P<0.05$).

To test whether eosin-5-maleimide labelling of individual single cysteines was significantly different in the presence of BKA or CATR, the average specific fluorescence intensity (mg^{-1} Aac2p) in the presence of BKA was compared to the average in the presence of CATR for individual single cysteine mutants of Aac2p. An unpaired, two-tailed Student's *t*-test assuming unequal variance was used ($P<0.05$).

Table A.3 Summary of the statistics for transport and labelling for single cysteine mutants of Aac2p. NT is an abbreviation for 'not transporting', NI for 'not inhibited' and NL for 'not labelled'.

Single cysteine mutant of Aac2p	Is the initial transport rate (nmol ADP min^{-1}) significantly higher than the background?	Is inhibition by CATR not significantly different or significantly higher than Δ2-19 cys-less Aac2p?	Is inhibition by BKA not significantly different or significantly higher than Δ2-19 cys-less Aac2p?	Is labelling in the presence of BKA significantly higher than the background?	Is labelling in the presence of CATR significantly higher than the background?	Is labelling significantly different in the presence of BKA and CATR?
N22C	yes	yes	yes	no	no	NL
D26C	yes	yes	yes	no	yes	yes
G30C	yes	yes	NI	NI	NI	NI
A34C	no	NT	NT	NT	NT	NT
L50C	yes	yes	yes	no	no	NL
T79C	yes	yes	yes	no	no	NL
T100C	yes	yes	yes	no	no	NL
Q101C	yes	yes	yes	no	no	NL
N104C	yes	yes	no	NI	NI	NI
F105C	yes	yes	yes	no	no	NL
K108C	yes	yes	yes	no	no	NL
D109C	yes	yes	yes	no	yes	yes
K112C	yes	yes	yes	no	yes	yes
A113C	yes	yes	yes	yes	yes	yes
M114C	yes	yes	yes	no	yes	yes
E120C	yes	yes	yes	yes	no	no
A124C	yes	yes	yes	no	yes	yes
W126C	yes	yes	yes	no	yes	yes
N130C	yes	yes	yes	yes	yes	yes
G134C	no	NT	NT	NT	NT	NT
A136C	yes	yes	yes	no	no	NL
G138C	no	NT	NT	NT	NT	NT
S147C	yes	yes	yes	no	no	NL
K179C	yes	yes	yes	no	no	NL
A187C	yes	yes	yes	no	no	NL
Y203C	yes	yes	no	NI	NI	NI
R204C	no	NT	NT	NT	NT	NT
Y207C	yes	yes	yes	no	no	NL
F208C	no	NT	NT	NT	NT	NT
Y211C	yes	yes	NI	NI	NI	NI
D212C	yes	yes	no	NI	NI	NI
K215C	yes	yes	yes	no	yes	yes
P216C	yes	yes	yes	yes	yes	no

Single cysteine mutant of Aac2p	Is the initial transport rate (nmol ADP min^{-1}) significantly higher than the background?	Is inhibition by CATR not significantly different or significantly higher than Δ2-19 cys-less Aac2p?	Is inhibition by BKA not significantly different or significantly higher than Δ2-19 cys-less Aac2p?	Is labelling in the presence of BKA significantly higher than the background?	Is labelling in the presence of CATR significantly higher than the background?	Is labelling significantly different in the presence of BKA and CATR?
L217C	yes	yes	yes	yes	yes	no
S222C	yes	yes	yes	yes	yes	no
E224C	yes	yes	yes	yes	yes	no
S226C	yes	yes	yes	no	no	NL
S230C	yes	yes	yes	no	yes	yes
G234C	no	NT	NT	NT	NT	NT
T238C	yes	yes	NI	NI	NI	NI
T243C	yes	yes	yes	no	no	NL
R273C	yes	yes	yes	no	no	NL
A278C	yes	yes	yes	no	no	NL
A297C	yes	yes	yes	no	no	NL
G298C	no	NT	NT	NT	NT	NT
A299C	no	NT	NT	NT	NT	NT
V301C	yes	yes	yes	no	no	NL
I302C	yes	yes	yes	yes	yes	yes
Y305C	yes	yes	NI	NI	NI	NI
D306C	yes	yes	yes	no	yes	yes
Q309C	yes	yes	yes	no	no	NL
I311C	yes	yes	yes	no	yes	no
G314C	yes	yes	yes	no	yes	no

Appendix III

Specific initial uptake rates of single cysteine mutants

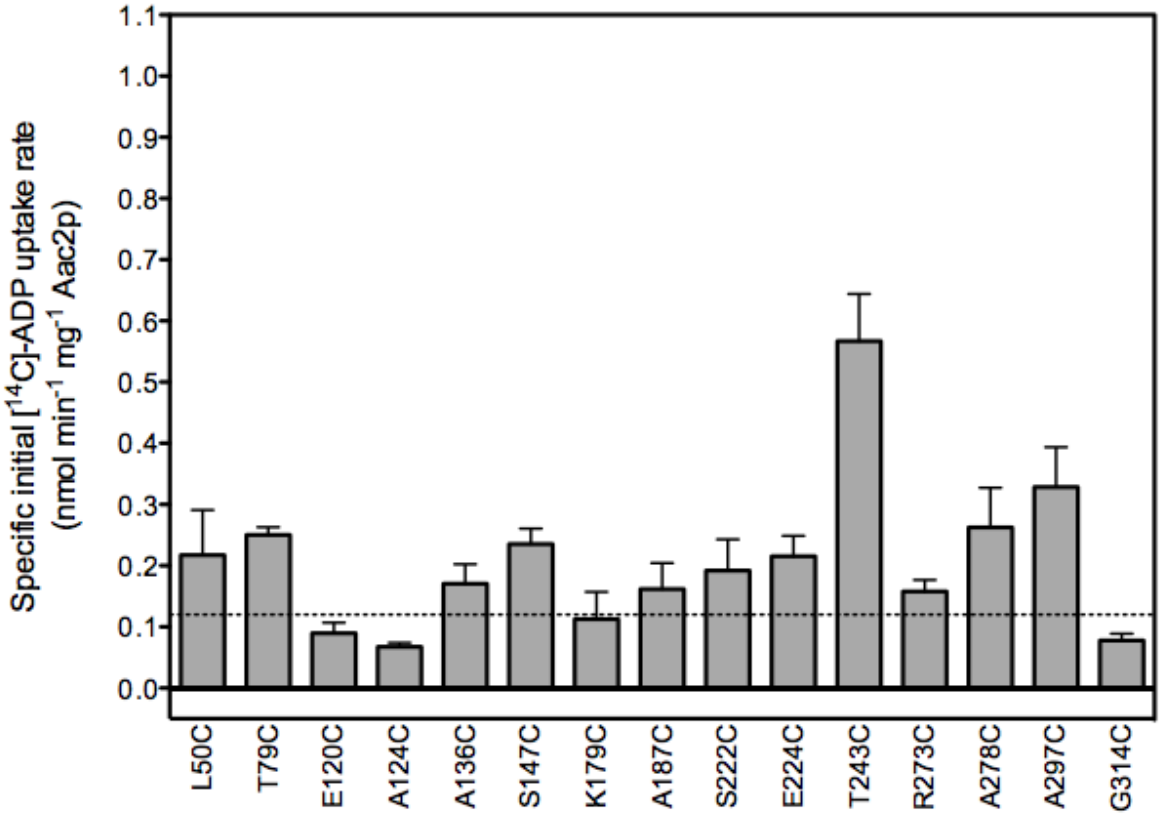

Figure A.1 Specific initial ADP uptake rates of Aac2p control mutants. See Figure 3.10 for legend details. See Table 4.1 for a list of individual mutations.

Appendix IV

Expression level of single cysteine mutants

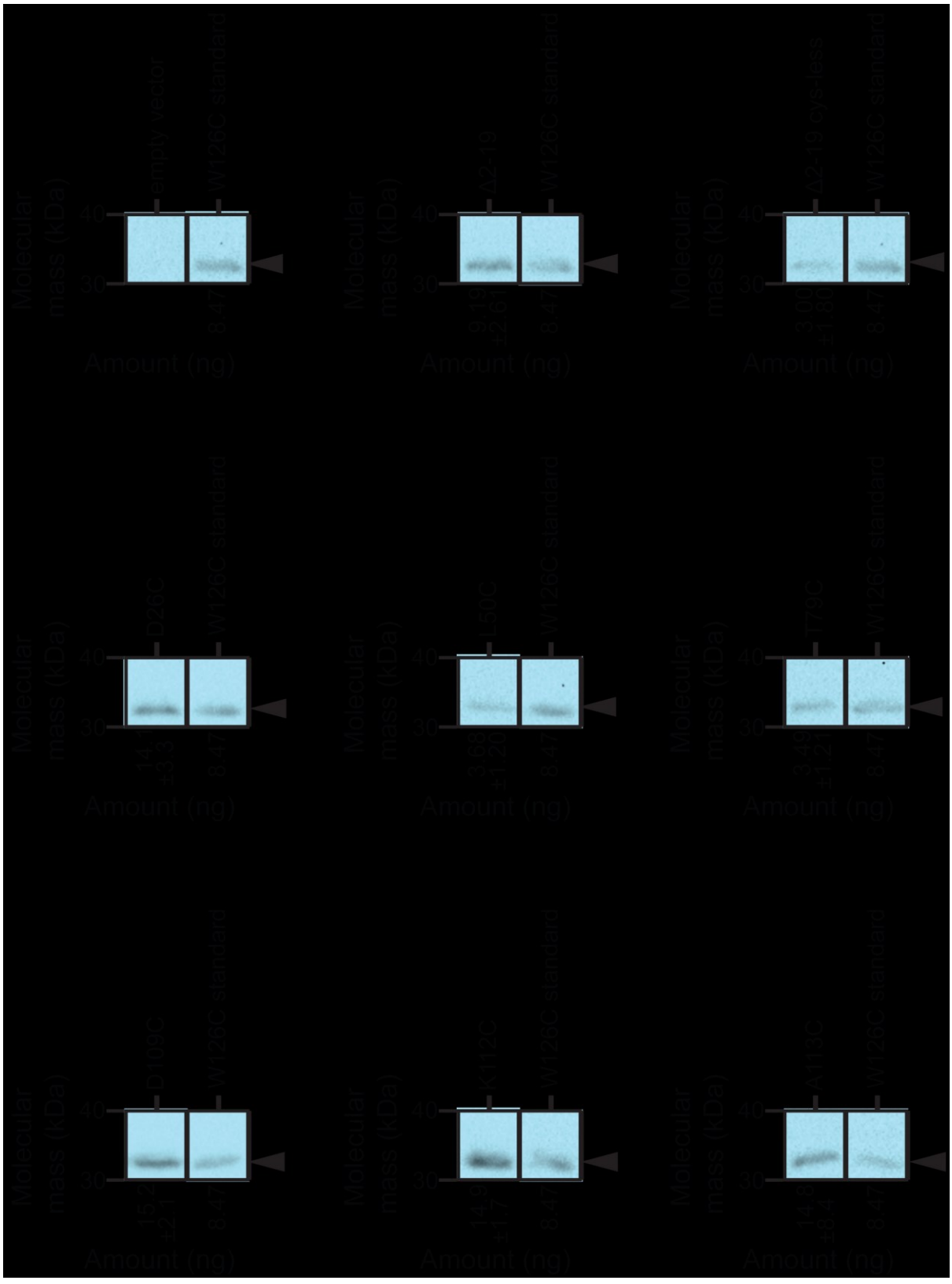

Figure A.2 Expression of bongkrekic acid or carboxy-atractyloside inhibited, eosin-5-maleimide labelled single cysteine mutants of Aac2p for orientation studies. For legend details, see the last page of the figure.

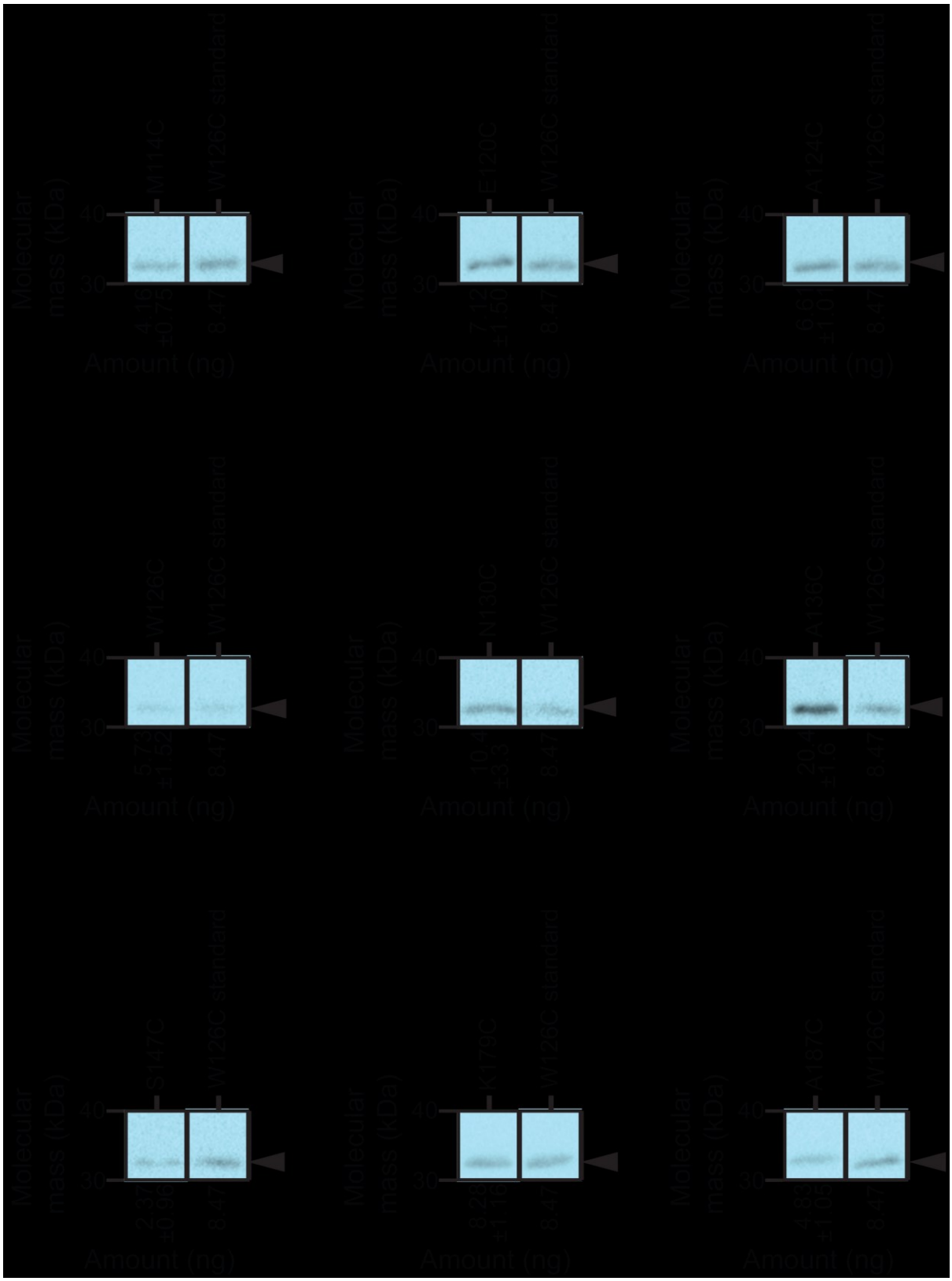

Figure A.2 continued Expression of bongkrekic acid or carboxy-atractyloside inhibited, eosin-5-maleimide labelled single cysteine mutants of Aac2p for orientation studies. For legend details, see the last page of the figure.

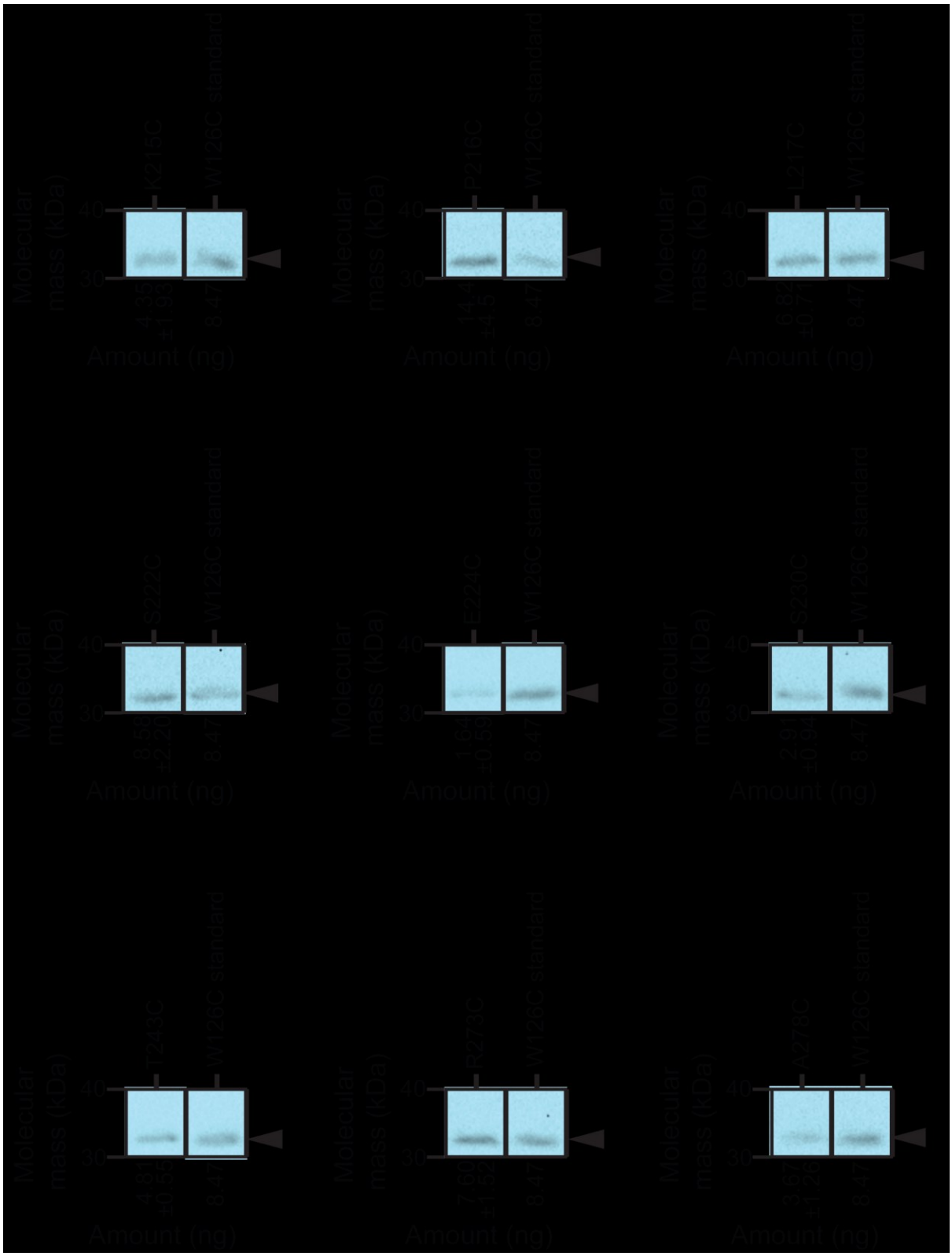

Figure A.2 continued Expression of bongkrekic acid or carboxy-atractyloside inhibited, eosin-5-maleimide labelled single cysteine mutants of Aac2p for orientation studies. For legend details, see the next page.

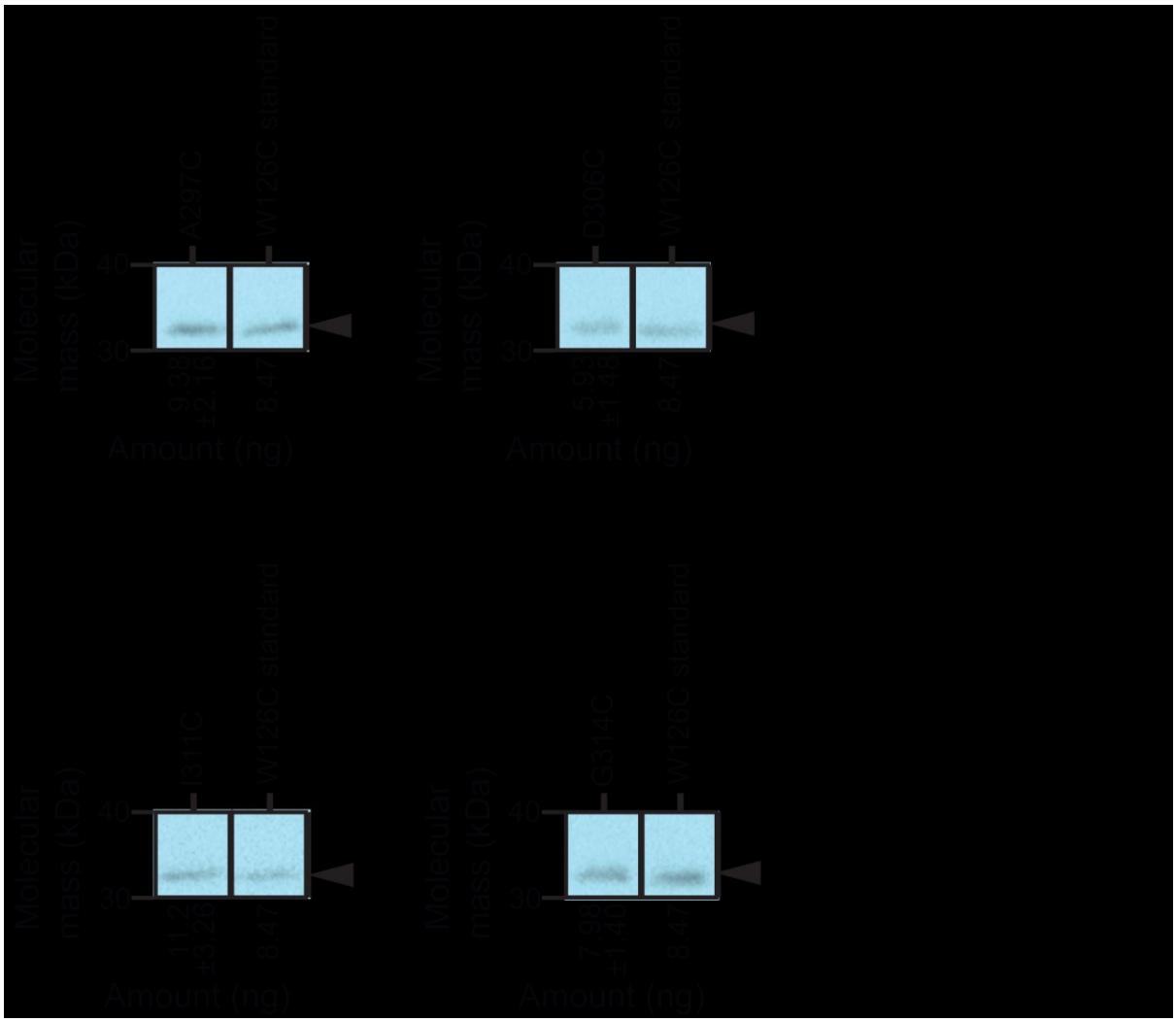

Figure A.2 continued Expression of bongkrekic acid or carboxy-atractyloside inhibited, eosin-5-maleimide labelled single cysteine mutants of Aac2p for orientation studies. Western blot analysis of single cysteine mutants constructed in Δ2-19 cys-less Aac2p and expressed in whole cells of *L. lactis*. 30 µg total cellular protein was loaded per lane. The antibody is directed against α-helix H5 of Aac2p. Imaged for 2-14 min using Chemi-doc XRS+, depending on the intensity of the W126C control. The bands for Aac2p are indicated by a solid black arrowhead. The total signals were quantified, with the empty vector background subtracted, using Image Lab (see Figure 4.6 and Table 4.2 for an example). Each single cysteine mutant is shown next to its corresponding W126C reference standard, for comparison. The data represent the average and the standard deviation (*n*=6) including both BKA- (*n*=3) and CATR-inhibited (*n*=3) samples.

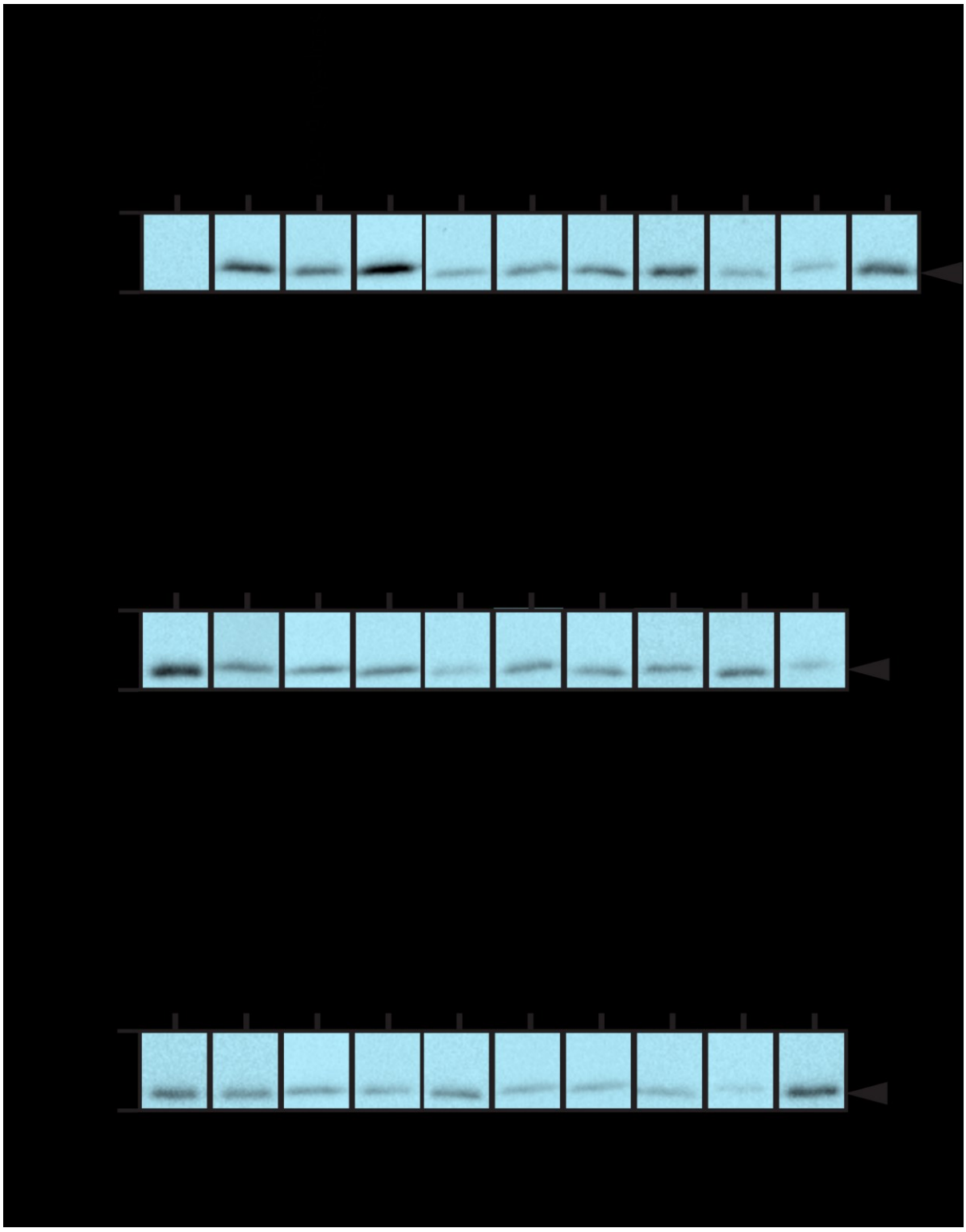

Figure A.3 Expression levels of single cysteine mutants of Aac2p that were used in transport assays for orientation studies. For details, see the legend of Figure 3.8.

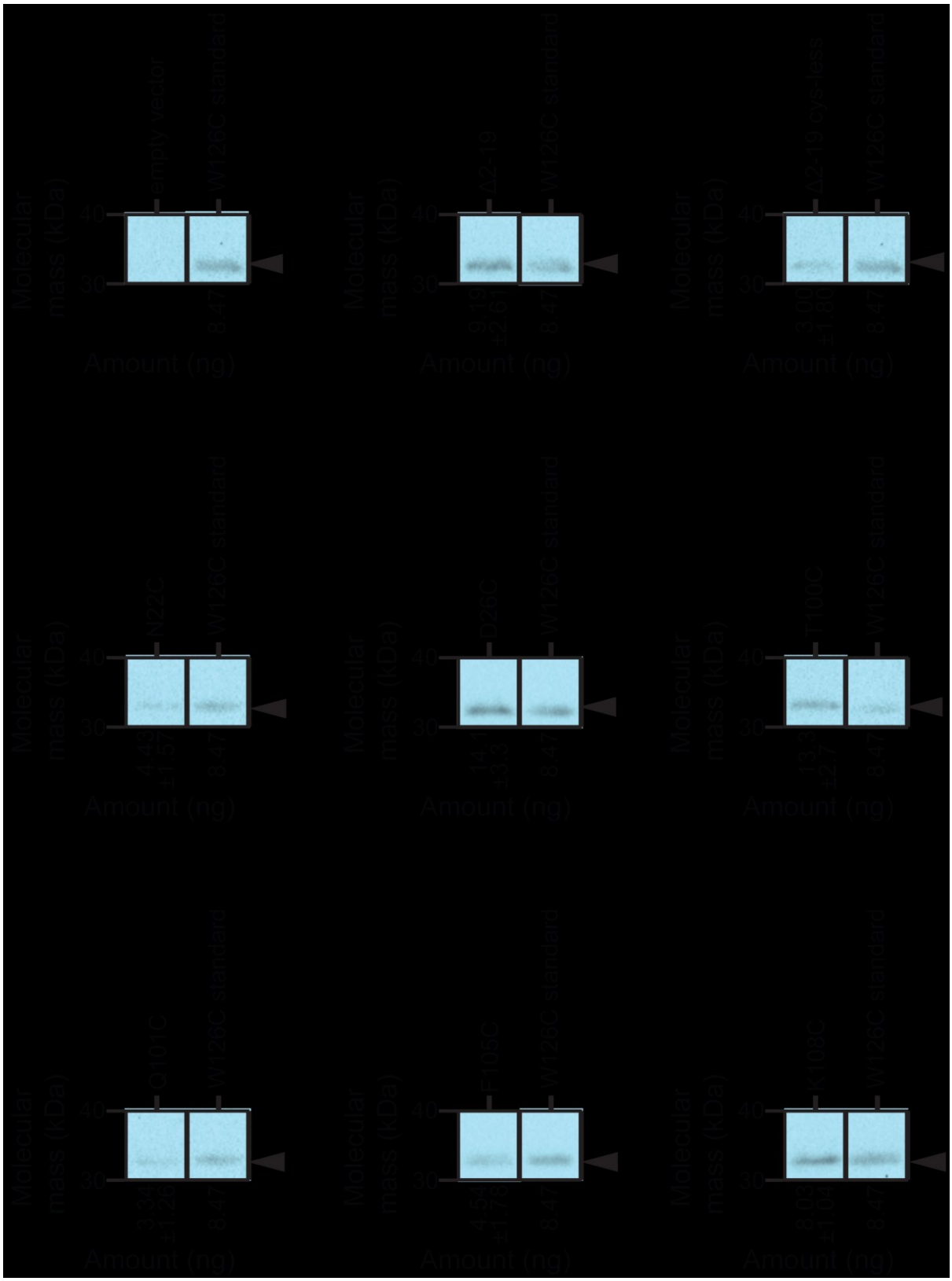

Figure A.4 Expression of bongkrekic acid or carboxy-atractyloside inhibited, eosin-5-maleimide labelled single cysteine mutants of Aac2p for labelling studies. For details, see legend of Figure A.2.

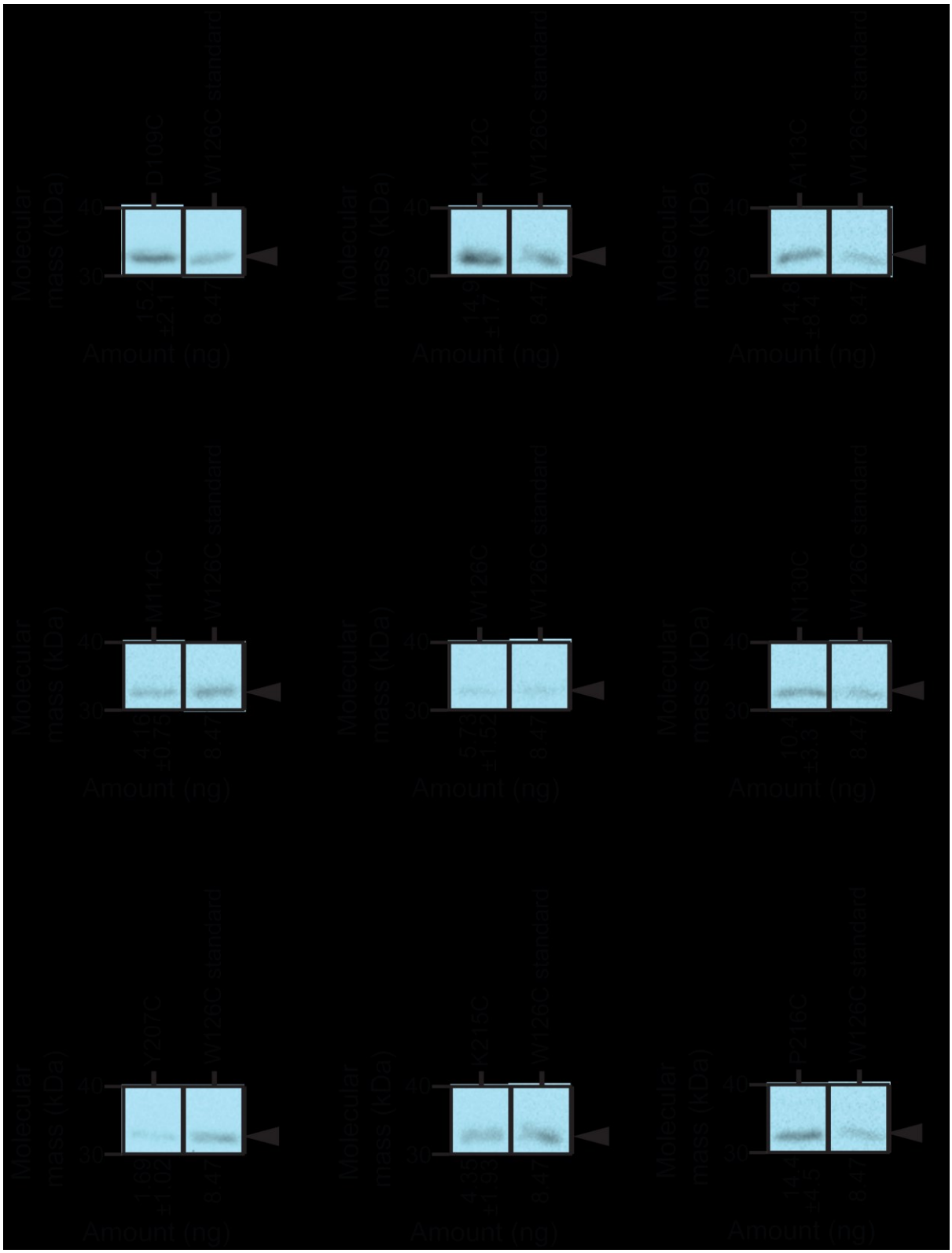

Figure A.4 continued Expression of bongkrekic acid or carboxy-atractyloside inhibited, eosin-5-maleimide labelled single cysteine mutants of Aac2p for labelling studies. For details, see legend of Figure A.2.

Figure A.4 continued Expression of bongkrekic acid or carboxy-atractyloside inhibited, eosin-5-maleimide labelled single cysteine mutants of Aac2p for labelling studies. For details, see legend of Figure A.2.

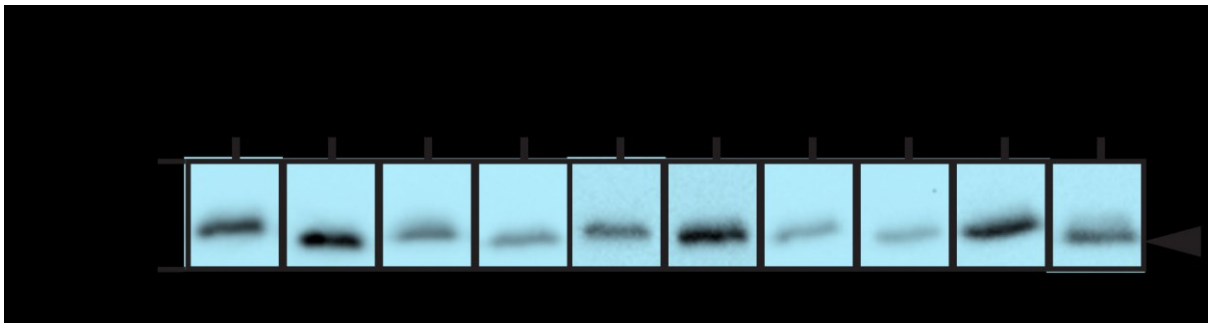

Figure A.5 Expression of single cysteine mutants of Aac2p for substrate studies. Western blot analysis of mutants of Aac2p that showed significant differences in labelling between the BKA- and CATR-inhibited states (Figure 5.5 and Section 5.4.2) in the absence or presence of 2.5 mM ADP. 30 µg total cellular protein was loaded per lane. The antibody is directed against α-helix H5 of Aac2p. ECL prime was substituted for standard ECL. Imaged for 30-180 s using Chemi-doc XRS+, depending on the intensity of the W126C control. The total signals were quantified, with the empty vector background subtracted, using Image Lab (see Figure 4.6 and Table 4.2 for an example). The bands for Aac2p are indicated by a solid black arrowhead. The data represent the average and the standard deviation (*n*=3).

Bibliography

Abrahams, J.P., Leslie, A.G., Lutter, R. & Walker, J.E. (1994) Structure at 2.8 Å resolution of F_1-ATPase from bovine heart mitochondria. *Nature*, 370 (6491), pp.621–628.

Aquila, H., Link, T.A. & Klingenberg, M. (1987) Solute carriers involved in energy transfer of mitochondria form a homologous protein family. *FEBS letters*, 212 (1), pp.1–9.

Aquila, H., Link, T.A. & Klingenberg, M. (1985) The uncoupling protein from brown fat mitochondria is related to the mitochondrial ADP/ATP carrier. Analysis of sequence homologies and of folding of the protein in the membrane. *The EMBO journal*, 4 (9), pp.2369–2376.

Aquila, H., Misra, D., Eulitz, M. & Klingenberg, M. (1982) Complete amino acid sequence of the ADP/ATP carrier from beef heart mitochondria. *Hoppe-Seyler's Zeitschrift für physiologische Chemie*, 363 (3), pp.345–349.

Axelrod, H.L., Feher, G., Allen, J.P., Chirino, A.J., Day, M.W., Hsu, B.T. & Rees, D.C. (1994) Crystallization and X-ray structure determination of cytochrome c2 from Rhodobacter sphaeroides in three crystal forms. *Acta crystallographica Section D, Biological crystallography*, 50 (Pt 4), pp.596–602.

Babot, M., Blancard, C., Pélosi, L., Lauquin, G.J.M. & Trézéguet, V. (2012) The transmembrane prolines of the mitochondrial ADP/ATP carrier are involved in nucleotide binding and transport and its biogenesis. *The Journal of biological chemistry*, 287 (13), pp.10368–10378.

Baker, L.A., Watt, I.N., Runswick, M.J., Walker, J.E. & Rubinstein, J.L. (2012) Arrangement of subunits in intact mammalian mitochondrial ATP synthase determined by cryo-EM. *Proceedings of the National Academy of Sciences of the United States of America*, 109 (29), pp.11675–11680.

Bamber, L., Harding, M., Butler, P.J.G. & Kunji, E.R.S. (2006) Yeast mitochondrial ADP/ATP carriers are monomeric in detergents. *Proceedings of the National Academy of Sciences of the United States of America*, 103 (44), pp.16224–16229.

Bamber, L., Harding, M., Monné, M., Slotboom, D.-J. & Kunji, E.R.S. (2007a) The yeast mitochondrial ADP/ATP carrier functions as a monomer in mitochondrial membranes. *Proceedings of the National Academy of Sciences of the United States of America*, 104 (26), pp.10830–10834.

Bamber, L., Slotboom, D.-J. & Kunji, E.R.S. (2007b) Yeast mitochondrial ADP/ATP carriers are monomeric in detergents as demonstrated by differential affinity purification. *Journal of molecular biology*, 371 (2), pp.388–395.

Berardi, M.J., Shih, W.M., Harrison, S.C. & Chou, J.J. (2011) Mitochondrial uncoupling protein 2 structure determined by NMR molecular fragment searching. *Nature*, 476 (7358), pp.109–113.

Berliner, L.J. (1983) The spin-label approach to labeling membrane protein sulfhydryl groups. *Annals of the New York Academy of Sciences*, 414, pp.153–161.

Birrell, J.A., King, M.S. & Hirst, J. (2011) A ternary mechanism for NADH oxidation by positively charged electron acceptors, catalyzed at the flavin site in respiratory complex I. *FEBS letters*, 585 (14), pp.2318–2322.

Bogner, W., Aquila, H. & Klingenberg, M. (1986) The transmembrane arrangement of the ADP/ATP carrier as elucidated by the lysine reagent pyridoxal 5-phosphate. *European journal of biochemistry / FEBS*, 161 (3), pp.611–620.

Brandolin, G., Doussiere, J., Gulik, A., Gulik-Krzywicki, T., Lauquin, G.J. & Vignais, P.V. (1980) Kinetic, binding and ultrastructural properties of the beef heart adenine nucleotide carrier protein after incorporation into phospholipid vesicles. *Biochimica et biophysica acta*, 592 (3), pp.592–614.

Brandolin, G., Boulay, F., Dalbon, P. & Vignais, P.V. (1989) Orientation of the N-terminal region of the membrane-bound ADP/ATP carrier protein explored by antipeptide antibodies and an arginine-specific endoprotease. Evidence that the accessibility of the N-terminal residues depends on the conformational state of the carrier. *Biochemistry*, 28 (3), pp.1093–1100.

Bricker, D.K., Taylor, E.B., Schell, J.C., Orsak, T., Boutron, A., Chen, Y.-C., Cox, J.E., Cardon, C.M., Van Vranken, J.G., Dephoure, N., Redin, C., Boudina, S., Gygi, S.P., Brivet, M., Thummel, C.S. & Rutter, J. (2012) A mitochondrial pyruvate carrier required for pyruvate uptake in yeast, Drosophila, and humans. *Science (New York, NY)*, 337 (6090), pp.96–100.

Brierley, G. & O'Brien, R.L. (1965) Compartmentation of heart mitochondria. II. Mitochondrial adenine nucleotides and the action of atractyloside. *The Journal of biological chemistry*, 240 (11), pp.4532–4539.

Briggs, C., Mincone, L. & Wohlrab, H. (1999) Replacements of basic and hydroxyl amino acids identify structurally and functionally sensitive regions of the mitochondrial phosphate transport protein. *Biochemistry*, 38 (16), pp.5096–5102.

Broustovetsky, N., Bamberg, E., Gropp, T. & Klingenberg, M. (1997) Biochemical and physical parameters of the electrical currents measured with the ADP/ATP carrier by photolysis of caged ADP and ATP. *Biochemistry*, 36 (45), pp.13865–13872.

Bruni, A. & Luciani, S. (1962) Effects of atractyloside and oligomycin on magnesium-stimulated adenosine triphosphatase and on adenosine triphosphate-induced contraction of swollen mitochondria. *Nature*, 196, pp.578–580.

Bruni, A., Luciani, S. & Contessa, A.R. (1964) Inhibition by atractyloside of the binding of adenine-nucleotides to rat-liver mitochondria. *Nature*, 201, pp.1219–1220.

Brustovetsky, N., Becker, A., Klingenberg, M. & Bamberg, E. (1996) Electrical currents associated with nucleotide transport by the reconstituted mitochondrial ADP/ATP carrier. *Proceedings of the National Academy of Sciences of the United States of America*, 93 (2), pp.664–668.

Buchanan, B.B., Eiermann, W., Riccio, P., Aquila, H. & Klingenberg, M. (1976) Antibody evidence for different conformational states of ADP, ATP translocator protein isolated from mitochondria. *Proceedings of the National Academy of Sciences of the United States of America*, 73 (7), pp.2280–2284.

Capobianco, L., Brandolin, G. & Palmieri, F. (1991) Transmembrane topography of the mitochondrial phosphate carrier explored by peptide-specific antibodies and enzymatic digestion. *Biochemistry*, 30 (20), pp.4963–4969.

Cappello, A.R., Curcio, R., Valeria Miniero, D., Stipani, I., Robinson, A.J., Kunji, E.R.S. & Palmieri, F. (2006) Functional and structural role of amino acid residues in the even-numbered transmembrane alpha-helices of the bovine mitochondrial oxoglutarate carrier. *Journal of molecular biology*, 363 (1), pp.51–62.

Cappello, A.R., Miniero, D.V., Curcio, R., Ludovico, A., Daddabbo, L., Stipani, I., Robinson, A.J., Kunji, E.R.S. & Palmieri, F. (2007) Functional and structural role of amino acid residues in the odd-numbered transmembrane alpha-helices of the bovine mitochondrial oxoglutarate carrier. *Journal of molecular biology*, 369 (2), pp.400–412.

Chan, S.H. & Barbour, R.L. (1983) Adenine nucleotide transport in hepatoma mitochondria. Characterization of factors influencing the kinetics of ADP and ATP uptake. *Biochimica et biophysica acta*, 723 (1), pp.104–113.

Chappell, J.B. (1968) Systems used for the transport of substrates into mitochondria. *British medical bulletin*, 24 (2), pp.150–157.

Chappell, J.B. & Crofts, A.R. (1965) The effect of atractylate and oligomycin on the behaviour of mitochondria towards adenine nucleotides. *The Biochemical journal*, 95, pp.707–716.

Chappell, J.B. & Greville, G.D. (1958) Dependence of mitochondrial swelling on oxidizable substrates. *Nature*, 182 (4638), pp.813–814.

Chen, L.L., Rosa, J.J., Turner, S. & Pepinsky, R.B. (1991) Production of multimeric forms of CD4 through a sugar-based cross-linking strategy. *The Journal of biological chemistry*, 266 (27), pp.18237–18243.

Cherry, R.J. & Nigg, E.A. (1981) Rotational diffusion of erythrocyte membrane proteins. *Progress in clinical and biological research*, 51, pp.59–77.

Clémençon, B., Rey, M., Trézéguet, V., Forest, E. & Pélosi, L. (2011) Yeast ADP/ATP carrier isoform 2: conformational dynamics and role of the RRRMMM signature sequence methionines. *The Journal of biological chemistry*, 286 (41), pp.36119–36131.

Colombini, M. (2012) VDAC structure, selectivity, and dynamics. *Biochimica et biophysica acta*, 1818 (6), pp.1457–1465.

Dautant, A., Velours, J. & Giraud, M.-F. (2010) Crystal structure of the Mg·ADP-inhibited state of the yeast F_1c_{10}-ATP synthase. *The Journal of biological chemistry*, 285 (38), pp.29502–29510.

David, C., Arnou, B., Sanchez, J.-F., Pélosi, L., Brandolin, G., Lauquin, G.J.M. & Trézéguet, V. (2008) Two residues of a conserved aromatic ladder of the mitochondrial ADP/ATP carrier are crucial to nucleotide transport. *Biochemistry*, 47 (50), pp.13223–13231.

de Ruyter, P.G., Kuipers, O.P. & de Vos, W.M. (1996) Controlled gene expression systems for *Lactococcus lactis* with the food-grade inducer nisin. *Applied and environmental microbiology*, 62 (10), pp.3662–3667.

Dehez, F., Pebay-Peyroula, E. & Chipot, C. (2008) Binding of ADP in the mitochondrial ADP/ATP carrier is driven by an electrostatic funnel. *Journal of the American Chemical Society*, 130 (38), pp.12725–12733.

Devaux, P.F., Bienvenüe, A., Lauquin, G., Brisson, A.D., Vignais, P.M. & Vignais, P.V. (1975) Interaction between spin-labeled acyl-coenzyme A and the mitochondrial adenosine diphosphate carrier. *Biochemistry*, 14 (6), pp.1272–1280.

Dickson, V.K., Silvester, J.A., Fearnley, I.M., Leslie, A.G.W. & Walker, J.E. (2006) On the structure of the stator of the mitochondrial ATP synthase. *The EMBO journal*, 25 (12), pp.2911–2918.

Dierks, T., Riemer, E. & Krämer, R. (1988) Reaction mechanism of the reconstituted aspartate/glutamate carrier from bovine heart mitochondria. *Biochimica et biophysica acta*, 943 (2), pp.231–244.

Dolce, V., Scarcia, P., Iacopetta, D. & Palmieri, F. (2005) A fourth ADP/ATP carrier isoform in man: identification, bacterial expression, functional characterization and tissue distribution. *FEBS letters*, 579 (3), pp.633–637.

Don, R.H., Cox, P.T., Wainwright, B.J., Baker, K. & Mattick, J.S. (1991) 'Touchdown' PCR to circumvent spurious priming during gene amplification. *Nucleic acids research*, 19 (14), p.4008.

Drees, M. & Beyer, K. (1988) Interaction of phospholipids with the detergent-solubilized ADP/ATP carrier protein as studied by spin-label electron spin resonance. *Biochemistry*, 27 (23), pp.8584–8591.

Drgon, T., Sabová, L., Gavurniková, G. & Kolarov, J. (1992) Yeast ADP/ATP carrier (AAC) proteins exhibit similar enzymatic properties but their deletion produces different phenotypes. *FEBS letters*, 304 (2-3), pp.277–280.

Duee, E.D. & Vignais, P.V. (1969) Kinetics and specificity of the adenine nucleotide translocation in rat liver mitochondria. *The Journal of biological chemistry*, 244 (14), pp.3920–3931.

Duyckaerts, C., Sluse-Goffart, C.M., Fux, J.P., Sluse, F.E. & Liebecq, C. (1980) Kinetic mechanism of the exchanges catalysed by the adenine-nucleotide carrier. *European journal of biochemistry / FEBS*, 106 (1), pp.1–6.

Efremov, R.G. & Sazanov, L.A. (2011) Structure of the membrane domain of respiratory complex I. *Nature*, 476 (7361), pp.414–420.

Efremov, R.G., Baradaran, R. & Sazanov, L.A. (2010) The architecture of respiratory complex I. *Nature*, 465 (7297), pp.441–445.

Erdelt, H., Weidemann, M.J., Buchholz, M. & Klingenberg, M. (1972) Some principle effects of bongkrekic acid on the binding of adenine nucleotides to mitochondrial membranes. *European journal of biochemistry / FEBS*, 30 (1), pp.107–122.

Facey, S.J. & Kuhn, A. (2004) Membrane integration of E. coli model membrane proteins. *Biochimica et biophysica acta*, 1694 (1-3), pp.55–66.

Ferreira, G.C., Pratt, R.D. & Pedersen, P.L. (1990) Mitochondrial proton/phosphate transporter. An antibody directed against the COOH terminus and proteolytic cleavage experiments provides new insights about its membrane topology. *The Journal of biological chemistry*, 265 (34), pp.21202–21206.

Fiermonte, G., De Leonardis, F., Todisco, S., Palmieri, L., Lasorsa, F.M. & Palmieri, F. (2004) Identification of the mitochondrial ATP-Mg/Pi transporter. Bacterial expression, reconstitution, functional characterization, and tissue distribution. *The Journal of biological chemistry*, 279 (29), pp.30722–30730.

Fiermonte, G., Paradies, E., Todisco, S., Marobbio, C.M.T. & Palmieri, F. (2009) A novel member of solute carrier family 25 (SLC25A42) is a transporter of coenzyme A and adenosine 3‘,5’-diphosphate in human mitochondria. *The Journal of biological chemistry*, 284 (27), pp.18152–18159.

Fiore, C., Trézéguet, V., Le Saux, A., Roux, P., Schwimmer, C., Dianoux, A.C., Noel, F., Lauquin, G.J., Brandolin, G. & Vignais, P.V. (1998) The mitochondrial ADP/ATP carrier: structural, physiological and pathological aspects. *Biochimie*, 80 (2), pp.137–150.

Fontanesi, F., Palmieri, L., Scarcia, P., Lodi, T., Donnini, C., Limongelli, A., Tiranti, V., Zeviani, M., Ferrero, I. & Viola, A.M. (2004) Mutations in AAC2, equivalent to human adPEO-associated ANT1 mutations, lead to defective oxidative phosphorylation in *Saccharomyces cerevisiae* and affect mitochondrial DNA stability. *Human molecular genetics*, 13 (9), pp.923–934.

Fonyó, A., Palmieri, F. & Quagliariello, E. (1976) Carrier-mediated transport of metabolites in mitochondria. *Horizons in biochemistry and biophysics*, 2, pp.60–105.

Frelet-Barrand, A., Boutigny, S., Moyet, L., Deniaud, A., Seigneurin-Berny, D., Salvi, D., Bernaudat, F., Richaud, P., Pebay-Peyroula, E., Joyard, J. & Rolland, N. (2010) *Lactococcus lactis*, an alternative system for functional expression of peripheral and intrinsic Arabidopsis membrane proteins. *PloS one*, 5 (1), p.e8746.

Frey, T.G. & Mannella, C.A. (2000) The internal structure of mitochondria. *Trends in biochemical sciences*, 25 (7), pp.319–324.

Gabbita, S.P., Subramaniam, R., Allouch, F., Carney, J.M. & Butterfield, D.A. (1998) Effects of mitochondrial respiratory stimulation on membrane lipids and proteins: an electron paramagnetic resonance investigation. *Biochimica et biophysica acta*, 1372 (2), pp.163–173.

Giangregorio, N., Tonazzi, A., Console, L., Indiveri, C. & Palmieri, F. (2010) Site-directed mutagenesis of charged amino acids of the human mitochondrial carnitine/acylcarnitine carrier: insight into the molecular mechanism of transport. *Biochimica et biophysica acta*, 1797 (6-7), pp.839–845.

Gordon, E., Horsefield, R., Swarts, H.G.P., de Pont, J.J.H.H.M., Neutze, R. & Snijder, A. (2008) Effective high-throughput overproduction of membrane proteins in *Escherichia coli*. *Protein expression and purification*, 62 (1), pp.1–8.

Gorin, G., Martic, P.A. & Doughty, G. (1966) Kinetics of the reaction of *N*-ethylmaleimide with cysteine and some congeners. *Archives of biochemistry and biophysics*, 115 (3), pp.593–597.

Griffiths, D.G., Partis, M.D., Sharp, R.N. & Beechey, R.B. (1981) *N*-polymethylenecarboxymaleimides -- a new class of probes for membrane sulphydryl groups. *FEBS letters*, 134 (2), pp.261–263.

Gropp, T., Brustovetsky, N., Klingenberg, M., Müller, V., Fendler, K. & Bamberg, E. (1999) Kinetics of electrogenic transport by the ADP/ATP carrier. *Biophysical journal*, 77 (2), pp.714–726.

Hackenbrock, C.R. (1966) Ultrastructural bases for metabolically linked mechanical activity in mitochondria. I. Reversible ultrastructural changes with change in metabolic steady state in isolated liver mitochondria. *The Journal of cell biology*, 30 (2), pp.269–297.

Hashimoto, M., Majima, E., Goto, S., Shinohara, Y. & Terada, H. (1999) Fluctuation of the first loop facing the matrix of the mitochondrial ADP/ATP carrier deduced from intermolecular cross-linking of Cys56 residues by bifunctional dimaleimides. *Biochemistry*, 38 (3), pp.1050–1056.

Hashimoto, M., Majima, E., Hatanaka, T., Shinohara, Y., Onishi, M., Goto, S. & Terada, H. (2000) Irreversible extrusion of the first loop facing the matrix of the bovine heart mitochondrial ADP/ATP carrier by labeling the Cys(56) residue with the SH-reagent methyl methanethiosulfonate. *Journal of biochemistry*, 127 (3), pp.443–449.

Hatanaka, T., Kihira, Y., Shinohara, Y., Majima, E. & Terada, H. (2001) Characterization of loops of the yeast mitochondrial ADP/ATP carrier facing the cytosol by site-directed mutagenesis. *Biochemical and biophysical research communications*, 286 (5), pp.936–942.

Heidkämper, D., Müller, V., Nelson, D.R. & Klingenberg, M. (1996) Probing the role of positive residues in the ADP/ATP carrier from yeast. The effect of six arginine mutations on transport and the four ATP versus ADP exchange modes. *Biochemistry*, 35 (50), pp.16144–16152.

Heijne, von, G. (1986) The distribution of positively charged residues in bacterial inner membrane proteins correlates with the trans-membrane topology. *The EMBO journal*, 5 (11), pp.3021–3027.

Heijne, von, G. (1989) Control of topology and mode of assembly of a polytopic membrane protein by positively charged residues. *Nature*, 341 (6241), pp.456–458.

Heijne, von, G. & Gavel, Y. (1988) Topogenic signals in integral membrane proteins. *European journal of biochemistry / FEBS*, 174 (4), pp.671–678.

Henderson, P.J. & Lardy, H.A. (1970) Bongkrekic acid. An inhibitor of the adenine nucleotide translocase of mitochondria. *The Journal of biological chemistry*, 245 (6), pp.1319–1326.

Henderson, P.J., Lardy, H.A. & Dorschner, E. (1970) Factors affecting the inhibition of adenine nucleotide translocase by bongkrekic acid. *Biochemistry*, 9 (17), pp.3453–3457.

Hermanson, G.T. (2008) *Bioconjugate Techniques, Second Edition*. 2nd ed. Academic Press.

Herzig, S., Raemy, E., Montessuit, S., Veuthey, J.-L., Zamboni, N., Westermann, B., Kunji, E.R.S. & Martinou, J.-C. (2012) Identification and functional expression of the mitochondrial pyruvate carrier. *Science (New York, NY)*, 337 (6090), pp.93–96.

Hirst, J., King, M.S. & Pryde, K.R. (2008) The production of reactive oxygen species by complex I. *Biochemical Society transactions*, 36 (Pt 5), pp.976–980.

Hornblow, H.M., Laverty, R., Logan, B.J. & Peake, B.M. (1985) The use of 2,2,6,6-tetramethyl-4-maleimido-piperidin-1-oxyl in electron paramagnetic resonance spin label studies of drug interactions with erythrocyte membranes. *Journal of pharmacological methods*, 14 (3), pp.229–241.

Horváth, L.I., Munding, A., Beyer, K., Klingenberg, M. & Marsh, D. (1989) Rotational diffusion of mitochondrial ADP/ATP carrier studied by saturation-transfer electron spin resonance. *Biochemistry*, 28 (1), pp.407–414.

Horváth, L.I., Drees, M., Beyer, K., Klingenberg, M. & Marsh, D. (1990) Lipid-protein interactions in ADP-ATP carrier/egg phosphatidylcholine recombinants studied by spin-label ESR spectroscopy. *Biochemistry*, 29 (47), pp.10664–10669.

Houstěk, J. & Pedersen, P.L. (1985) Adenine nucleotide and phosphate transport systems of mitochondria. Relative location of sulfhydryl groups based on the use of the novel fluorescent probe eosin-5-maleimide. *The Journal of biological chemistry*, 260 (10), pp.6288–6295.

Huang, L.-S., Shen, J.T., Wang, A.C. & Berry, E.A. (2006) Crystallographic studies of the binding of ligands to the dicarboxylate site of Complex II, and the identity of the ligand in the 'oxaloacetate-inhibited' state. *Biochimica et biophysica acta*, 1757 (9-10), pp.1073–1083.

Hubbell, W.L., Cafiso, D.S. & Altenbach, C. (2000) Identifying conformational changes with site-directed spin labeling. *Nature structural biology*, 7 (9), pp.735–739.

Hunte, C., Zickermann, V. & Brandt, U. (2010) Functional modules and structural basis of conformational coupling in mitochondrial complex I. *Science (New York, NY)*, 329 (5990), pp.448–451.

Indiveri, C., Dierks, T., Krämer, R. & Palmieri, F. (1991) Reaction mechanism of the reconstituted oxoglutarate carrier from bovine heart mitochondria. *European journal of biochemistry / FEBS*, 198 (2), pp.339–347.

Indiveri, C., Prezioso, G., Dierks, T., Krämer, R. & Palmieri, F. (1993) Kinetic characterization of the reconstituted dicarboxylate carrier from mitochondria: a four-binding-site sequential transport system. *Biochimica et biophysica acta*, 1143 (3), pp.310–318.

Indiveri, C., Tonazzi, A. & Palmieri, F. (1994) The reconstituted carnitine carrier from rat liver mitochondria: evidence for a transport mechanism different from that of the other mitochondrial translocators. *Biochimica et biophysica acta*, 1189 (1), pp.65–73.

Indiveri, C., Tonazzi, A., Stipani, I. & Palmieri, F. (1999) The purified and reconstituted ornithine/citrulline carrier from rat liver mitochondria catalyses a second transport mode: ornithine+/H+ exchange. *The Biochemical journal*, 341 (Pt 3), pp.705–711.

Indiveri, C., Tonazzi, A., Stipani, I. & Palmieri, F. (1997) The purified and reconstituted ornithine/citrulline carrier from rat liver mitochondria: electrical nature and coupling of the exchange reaction with H+ translocation. *The Biochemical journal*, 327 (Pt 2), pp.349–355.

Iwahashi, A., Ishii, A., Yamazaki, N., Hashimoto, M., Ohkura, K., Kataoka, M., Majima, E., Terada, H. & Shinohara, Y. (2008) Functionally important conserved length of C-terminal regions of yeast and bovine ADP/ATP carriers, identified by deletion mutants studies, and water accessibility of the amino acids at the C-terminal region of the yeast carrier. *Mitochondrion*, 8 (2), pp.196–204.

Iwahashi, A., Kihira, Y., Majima, E., Terada, H., Yamazaki, N., Kataoka, M. & Shinohara, Y. (2006) The structure of the second cytosolic loop of the yeast mitochondrial ADP/ATP carrier AAC2 is dependent on the conformational state. *Mitochondrion*, 6 (5), pp.245–251.

Iwata, S., Lee, J.W., Okada, K., Lee, J.K., Iwata, M., Rasmussen, B., Link, T.A., Ramaswamy, S. & Jap, B.K. (1998) Complete structure of the 11-subunit bovine mitochondrial cytochrome bc_1 complex. *Science (New York, NY)*, 281 (5373), pp.64–71.

Jardetzky, O. (1966) Simple allosteric model for membrane pumps. *Nature*, 211 (5052), pp.969–970.

Jezek, P. (1987) Sulfhydryl groups are involved in H+ translocation via the uncoupling protein of brown adipose tissue mitochondria. *FEBS letters*, 211 (1), pp.89–93.

Kadenbach, B., Schneyder, B., Mell, O., Stroh, S. & Reimann, A. (1991) Respiratory chain proteins. *Revue neurologique*, 147 (6-7), pp.436–442.

Kaplan, R.S., Mayor, J.A., Brauer, D., Kotaria, R., Walters, D.E. & Dean, A.M. (2000) The yeast mitochondrial citrate transport protein. Probing the secondary structure of transmembrane domain IV and identification of residues that likely comprise a portion of the citrate translocation pathway. *The Journal of biological chemistry*, 275 (16), pp.12009–12016.

Karrasch, S. & Walker, J.E. (1999) Novel features in the structure of bovine ATP synthase. *Journal of molecular biology*, 290 (2), pp.379–384.

Kemp, A., Out, T.A., Guiot, H.F. & Souverijn, J.H. (1970) The effect of adenine nucleotides and pH on the inhibition of oxidative phosphorylation by bongkrekic acid. *Biochimica et biophysica acta*, 223 (2), pp.460–462.

Kenyon, G.L. & Bruice, T.W. (1977) Novel sulfhydryl reagents. *Methods in enzymology*, 47, pp.407–430.

Kihira, Y., Iwahashi, A., Majima, E., Terada, H. & Shinohara, Y. (2004) Twisting of the second transmembrane alpha-helix of the mitochondrial ADP/ATP carrier during the transition between two carrier conformational states. *Biochemistry*, 43 (48), pp.15204–15209.

Kihira, Y., Majima, E., Shinohara, Y. & Terada, H. (2005) Cysteine labeling studies detect conformational changes in region 106-132 of the mitochondrial ADP/ATP carrier of *Saccharomyces cerevisiae*. *Biochemistry*, 44 (1), pp.184–192.

Kim, J.S. & Raines, R.T. (1995) Dibromobimane as a fluorescent crosslinking reagent. *Analytical biochemistry*, 225 (1), pp.174–176.

Klingenberg, M. (2005) Ligand-protein interaction in biomembrane carriers. The induced transition fit of transport catalysis. *Biochemistry*, 44 (24), pp.8563–8570.

Klingenberg, M. (1989) Molecular aspects of the adenine nucleotide carrier from mitochondria. *Archives of biochemistry and biophysics*, 270 (1), pp.1–14.

Klingenberg, M. (2008) The ADP and ATP transport in mitochondria and its carrier. *Biochimica et biophysica acta*, 1778 (10), pp.1978–2021.

Klingenberg, M., Appel, M., Babel, W. & Aquila, H. (1983) The binding of bongkrekate to mitochondria. *European journal of biochemistry / FEBS*, 131 (3), pp.647–654.

Klingenberg, M., Grebe, K. & Heldt, H.W. (1970) On the inhibition of the adenine nucleotide translocation by bongkrekic acid. *Biochemical and biophysical research communications*, 39 (3), pp.344–351.

Klug, C.S., Su, W. & Feix, J.B. (1997) Mapping of the residues involved in a proposed beta-strand located in the ferric enterobactin receptor FepA using site-directed spin-labeling. *Biochemistry*, 36 (42), pp.13027–13033.

Kolarov, J., Kolarova, N. & Nelson, N. (1990) A third ADP/ATP translocator gene in yeast. *The Journal of biological chemistry*, 265 (21), pp.12711–12716.

Kumar, S. & Nussinov, R. (2002) Close-range electrostatic interactions in proteins. *Chembiochem : a European journal of chemical biology*, 3 (7), pp.604–617.

Kunji, E.R.S. (2004) The role and structure of mitochondrial carriers. *FEBS letters*, 564 (3), pp.239–244.

Kunji, E.R.S. & Crichton, P.G. (2010) Mitochondrial carriers function as monomers. *Biochimica et biophysica acta*, 1797 (6-7), pp.817–831.

Kunji, E.R.S. & Harding, M. (2003) Projection structure of the atractyloside-inhibited mitochondrial ADP/ATP carrier of *Saccharomyces cerevisiae*. *The Journal of biological chemistry*, 278 (39), pp.36985–36988.

Kunji, E.R.S. & Robinson, A.J. (2010) Coupling of proton and substrate translocation in the transport cycle of mitochondrial carriers. *Current opinion in structural biology*, 20 (4), pp.440–447.

Kunji, E.R.S. & Robinson, A.J. (2006) The conserved substrate binding site of mitochondrial carriers. *Biochimica et biophysica acta*, 1757 (9-10), pp.1237–1248.

Kunji, E.R.S., Chan, K.W., Slotboom, D.-J., Floyd, S., O'Connor, R. & Monné, M. (2005) Eukaryotic membrane protein overproduction in *Lactococcus lactis*. *Current opinion in biotechnology*, 16 (5), pp.546–551.

Kunji, E.R.S., Harding, M., Butler, P.J.G. & Akamine, P. (2008) Determination of the molecular mass and dimensions of membrane proteins by size exclusion chromatography. *Methods (San Diego, Calif.)*, 46 (2), pp.62–72.

Kunji, E.R.S., Slotboom, D.-J. & Poolman, B. (2003) *Lactococcus lactis* as host for overproduction of functional membrane proteins. *Biochimica et biophysica acta*, 1610 (1), pp.97–108.

Lanzarotti, E., Biekofsky, R.R., Estrin, D.A., Marti, M.A. & Turjanski, A.G. (2011) Aromatic-aromatic interactions in proteins: beyond the dimer. *Journal of chemical information and modeling*, 51 (7), pp.1623–1633.

Larkin, M.A., Blackshields, G., Brown, N.P., Chenna, R., McGettigan, P.A., McWilliam, H., Valentin, F., Wallace, I.M., Wilm, A., Lopez, R., Thompson, J.D., Gibson, T.J. & Higgins, D.G. (2007) Clustal W and Clustal X version 2.0. *Bioinformatics (Oxford, England)*, 23 (21), pp.2947–2948.

Lauquin, G.J. & Vignais, P.V. (1976) Interaction of (3H) bongkrekic acid with the mitochondrial adenine nucleotide translocator. *Biochemistry*, 15 (11), pp.2316–2322.

Lawson, J.E. & Douglas, M.G. (1988) Separate genes encode functionally equivalent ADP/ATP carrier proteins in *Saccharomyces cerevisiae*. Isolation and analysis of AAC2. *The Journal of biological chemistry*, 263 (29), pp.14812–14818.

Lindhurst, M.J., Fiermonte, G., Song, S., Struys, E., De Leonardis, F., Schwartzberg, P.L., Chen, A., Castegna, A., Verhoeven, N., Mathews, C.K., Palmieri, F. & Biesecker, L.G. (2006) Knockout of Slc25a19 causes mitochondrial thiamine pyrophosphate depletion, embryonic lethality, CNS malformations, and anemia. *Proceedings of the National Academy of Sciences of the United States of America*, 103 (43), pp.15927–15932.

Liu, S., Kondo, N., Long, Y., Xiao, D., Iwamoto, A. & Matsuda, Z. (2010) Membrane topology analysis of HIV-1 envelope glycoprotein gp41. *Retrovirology*, 7, p.100.

Liu, Y., Engelman, D.M. & Gerstein, M. (2002) Genomic analysis of membrane protein families: abundance and conserved motifs. *Genome biology*, 3 (10), pp.1–12.

Loo, T.W. & Clarke, D.M. (2001) Determining the dimensions of the drug-binding domain of human P-glycoprotein using thiol cross-linking compounds as molecular rulers. *The Journal of biological chemistry*, 276 (40), pp.36877–36880.

Macara, I.G. & Cantley, L.C. (1981) Interactions between transport inhibitors at the anion binding sites of the band 3 dimer. *Biochemistry*, 20 (18), pp.5095–5105.

Macara, I.G., Kuo, S. & Cantley, L.C. (1983) Evidence that inhibitors of anion exchange induce a transmembrane conformational change in band 3. *The Journal of biological chemistry*, 258 (3), pp.1785–1792.

Majima, E., Ikawa, K., Takeda, M., Hashimoto, M., Shinohara, Y. & Terada, H. (1995) Translocation of loops regulates transport activity of mitochondrial ADP/ATP carrier deduced from formation of a specific intermolecular disulfide bridge catalyzed by copper-*o*-phenanthroline. *The Journal of biological chemistry*, 270 (49), pp.29548–29554.

Majima, E., Koike, H., Hong, Y.M., Shinohara, Y. & Terada, H. (1993) Characterization of cysteine residues of mitochondrial ADP/ATP carrier with the SH-reagents eosin 5-maleimide and *N*-ethylmaleimide. *The Journal of biological chemistry*, 268 (29), pp.22181–22187.

Majima, E., Shinohara, Y., Yamaguchi, N., Hong, Y.M. & Terada, H. (1994) Importance of loops of mitochondrial ADP/ATP carrier for its transport activity deduced from reactivities of its cysteine residues with the sulfhydryl reagent eosin-5-maleimide. *Biochemistry*, 33 (32), pp.9530–9536.

Majima, E., Takeda, M., Miki, S., Shinohara, Y. & Terada, H. (2002) Close location of the first loop to the third loop of the mitochondrial ADP/ATP carrier deduced from cross-linking catalyzed by copper-o-phenanthroline of the solubilized carrier with Triton X-100. *Journal of biochemistry*, 131 (3), pp.461–468.

Majima, E., Yamaguchi, N., Chuman, H., Shinohara, Y., Ishida, M., Goto, S. & Terada, H. (1998) Binding of the fluorescein derivative eosin Y to the mitochondrial ADP/ATP carrier: characterization of the adenine nucleotide binding site. *Biochemistry*, 37 (1), pp.424–432.

Mannella, C.A. (2000) Introduction: our changing views of mitochondria. *Journal of bioenergetics and biomembranes*, 32 (1), pp.1–4.

McBride, H.M., Neuspiel, M. & Wasiak, S. (2006) Mitochondria: more than just a powerhouse. *Current biology : CB*, 16 (14), pp.R551–60.

McDonald, T.P. & Henderson, P.J. (2001) Cysteine residues in the D-galactose-H+ symport protein of *Escherichia coli*: effects of mutagenesis on transport, reaction with *N*-ethylmaleimide and antibiotic binding. *The Biochemical journal*, 353 (Pt 3), pp.709–717.

McGivan, J.D. & Klingenberg, M. (1971) Correlation between H+ and anion movement in mitochondria and the key role of the phosphate carrier. *European journal of biochemistry / FEBS*, 20 (3), pp.392–399.

Miniero, D.V., Cappello, A.R., Curcio, R., Ludovico, A., Daddabbo, L., Stipani, I., Robinson, A.J., Kunji, E.R.S. & Palmieri, F. (2011) Functional and structural role of amino acid residues in the matrix alpha-helices, termini and cytosolic loops of the bovine mitochondrial oxoglutarate carrier. *Biochimica et biophysica acta*, 1807 (3), pp.302–310.

Miroux, B. & Walker, J.E. (1996) Over-production of proteins in *Escherichia coli*: mutant hosts that allow synthesis of some membrane proteins and globular proteins at high levels. *Journal of molecular biology*, 260 (3), pp.289–298.

Mitchell, P. (1961) Coupling of phosphorylation to electron and hydrogen transfer by a chemi-osmotic type of mechanism. *Nature*, 191, pp.144–148.

Mitchell, P. (1976) Possible molecular mechanisms of the protonmotive function of cytochrome systems. *Journal of theoretical biology*, 62 (2), pp.327–367.

Mitchell, P. (1979) Keilin's respiratory chain concept and its chemiosmotic consequences. *Science (New York, NY)*, 206 (4423), pp.1148–1159.

Mitra, K., Wunder, C., Roysam, B., Lin, G. & Lippincott-Schwartz, J. (2009) A hyperfused mitochondrial state achieved at G1-S regulates cyclin E buildup and entry into S phase. *Proceedings of the National Academy of Sciences of the United States of America*, 106 (29), pp.11960–11965.

Mollaaghababa, R., Steinhoff, H.J., Hubbell, W.L. & Khorana, H.G. (2000) Time-resolved site-directed spin-labeling studies of bacteriorhodopsin: loop-specific conformational changes in M. *Biochemistry*, 39 (5), pp.1120–1127.

Monné, M., Chan, K.W., Slotboom, D.-J. & Kunji, E.R.S. (2005) Functional expression of eukaryotic membrane proteins in *Lactococcus lactis*. *Protein science : a publication of the Protein Society*, 14 (12), pp.3048–3056.

Monné, M., Miniero, D.V., Daddabbo, L., Robinson, A.J., Kunji, E.R.S. & Palmieri, F. (2012) Substrate specificity of the two mitochondrial ornithine carriers can be swapped by single mutation in substrate binding site. *The Journal of biological chemistry*, 287 (11), pp.7925–7934.

Müller, M., Krebs, J.J., Cherry, R.J. & Kawato, S. (1984) Rotational diffusion of the ADP/ATP translocator in the inner membrane of mitochondria and in proteoliposomes. *The Journal of biological chemistry*, 259 (5), pp.3037–3043.

Müller, M., Krebs, J.J., Cherry, R.J. & Kawato, S. (1982) Selective labeling and rotational diffusion of the ADP/ATP translocator in the inner mitochondrial membrane. *The Journal of biological chemistry*, 257 (3), pp.1117–1120.

Müller, V., Basset, G., Nelson, D.R. & Klingenberg, M. (1996) Probing the role of positive residues in the ADP/ATP carrier from yeast. The effect of six arginine mutations of oxidative phosphorylation and AAC expression. *Biochemistry*, 35 (50), pp.16132–16143.

Müller, V., Heidkämper, D., Nelson, D.R. & Klingenberg, M. (1997) Mutagenesis of some positive and negative residues occurring in repeat triad residues in the ADP/ATP carrier from yeast. *Biochemistry*, 36 (50), pp.16008–16018.

Munding, A., Beyer, K. & Klingenberg, M. (1983) Binding of spin-labeled carboxyatractylate to mitochondrial adenosine 5‘-diphosphate/adenosine 5’-triphosphate carrier as studied by electron spin resonance. *Biochemistry*, 22 (8), pp.1941–1947.

Munding, A., Drees, M., Beyer, K. & Klingenberg, M. (1987) Probing of sulfhydryl groups in the adenosine 5‘-diphosphate/adenosine 5’-triphosphate carrier by maleimide spin-labels. *Biochemistry*, 26 (26), pp.8637–8644.

Narendra, D.P., Jin, S.M., Tanaka, A., Suen, D.-F., Gautier, C.A., Shen, J., Cookson, M.R. & Youle, R.J. (2010) PINK1 is selectively stabilized on impaired mitochondria to activate Parkin. *PLoS biology*, 8 (1), p.e1000298.

Nelson, D.R. (1996) The yeast ADP/ATP carrier. Mutagenesis and second-site revertants. *Biochimica et biophysica acta*, 1275 (1-2), pp.133–137.

Nelson, D.R. & Douglas, M.G. (1993) Function-based mapping of the yeast mitochondrial ADP/ATP translocator by selection for second site revertants. *Journal of molecular biology*, 230 (4), pp.1171–1182.

Nelson, D.R., Felix, C.M. & Swanson, J.M. (1998) Highly conserved charge-pair networks in the mitochondrial carrier family. *Journal of molecular biology*, 277 (2), pp.285–308.

Neuhaus, H.E. & Wagner, R. (2000) Solute pores, ion channels, and metabolite transporters in the outer and inner envelope membranes of higher plant plastids. *Biochimica et biophysica acta*, 1465 (1-2), pp.307–323.

Nicholls, D.G. & Ferguson, S.J. (2002) *Bioenergetics 3*. Academic Press.

Okamoto, K. & Shaw, J.M. (2005) Mitochondrial morphology and dynamics in yeast and multicellular eukaryotes. *Annual review of genetics*, 39, pp.503–536.

Palade, G.E. (1953) An electron microscope study of the mitochondrial structure. *The journal of histochemistry and cytochemistry : official journal of the Histochemistry Society*, 1 (4), pp.188–211.

Palade, G.E. (1952) The fine structure of mitochondria. *The Anatomical record*, 114 (3), pp.427–451.

Palmer, C.S., Osellame, L.D., Stojanovski, D. & Ryan, M.T. (2011) The regulation of mitochondrial morphology: intricate mechanisms and dynamic machinery. *Cellular signalling*, 23 (10), pp.1534–1545.

Palmieri, F. (2008) Diseases caused by defects of mitochondrial carriers: a review. *Biochimica et biophysica acta*, 1777 (7-8), pp.564–578.

Palmieri, F. (2004) The mitochondrial transporter family (SLC25): physiological and pathological implications. *Pflügers Archiv : European journal of physiology*, 447 (5), pp.689–709.

Palmieri, F. & Pierri, C.L. (2010) Structure and function of mitochondrial carriers - role of the transmembrane helix P and G residues in the gating and transport mechanism. *FEBS letters*, 584 (9), pp.1931–1939.

Palmieri, F., Bisaccia, F., Capobianco, L., Dolce, V., Fiermonte, G., Iacobazzi, V. & Zara, V. (1993a) Transmembrane topology, genes, and biogenesis of the mitochondrial phosphate and oxoglutarate carriers. *Journal of bioenergetics and biomembranes*, 25 (5), pp.493–501.

Palmieri, F., Indiveri, C., Bisaccia, F. & Krämer, R. (1993b) Functional properties of purified and reconstituted mitochondrial metabolite carriers. *Journal of bioenergetics and biomembranes*, 25 (5), pp.525–535.

Palmieri, L., Alberio, S., Pisano, I., Lodi, T., Meznaric-Petrusa, M., Zidar, J., Santoro, A., Scarcia, P., Fontanesi, F., Lamantea, E., Ferrero, I. & Zeviani, M. (2005) Complete loss-of-function of the heart/muscle-specific adenine nucleotide translocator is associated with mitochondrial myopathy and cardiomyopathy. *Human molecular genetics*, 14 (20), pp.3079–3088.

Palmieri, L., Rottensteiner, H., Girzalsky, W., Scarcia, P., Palmieri, F. & Erdmann, R. (2001) Identification and functional reconstitution of the yeast peroxisomal adenine nucleotide transporter. *The EMBO journal*, 20 (18), pp.5049–5059.

Pebay-Peyroula, E., Dahout-Gonzalez, C., Kahn, R., Trézéguet, V., Lauquin, G.J.M. & Brandolin, G. (2003) Structure of mitochondrial ADP/ATP carrier in complex with carboxyatractyloside. *Nature*, 426 (6962), pp.39–44.

Perkins, G., Renken, C., Martone, M.E., Young, S.J., Ellisman, M. & Frey, T. (1997) Electron tomography of neuronal mitochondria: three-dimensional structure and organization of cristae and membrane contacts. *Journal of structural biology*, 119 (3), pp.260–272.

Perkins, G.A. & Frey, T.G. (2000) Recent structural insight into mitochondria gained by microscopy. *Micron*, 31 (1), pp.97–111.

Pershad, H.R., Hirst, J., Cochran, B., Ackrell, B.A. & Armstrong, F.A. (1999) Voltammetric studies of bidirectional catalytic electron transport in Escherichia coli succinate dehydrogenase: comparison with the enzyme from beef heart mitochondria. *Biochimica et biophysica acta*, 1412 (3), pp.262–272.

Pfaff, E. & Klingenberg, M. (1968) Adenine nucleotide translocation of mitochondria. 1. Specificity and control. *European journal of biochemistry / FEBS*, 6 (1), pp.66–79.

Pfaff, E., Klingenberg, M. & Heldt, H.W. (1965) Unspecific permeation and specific exchange of adenine nucleotides in liver mitochondria. *Biochimica et biophysica acta*, 104 (1), pp.312–315.

Phelps, A., Briggs, C., Mincone, L. & Wohlrab, H. (1996) Mitochondrial phosphate transport protein. replacements of glutamic, aspartic, and histidine residues affect transport and protein conformation and point to a coupled proton transport path. *Biochemistry*, 35 (33), pp.10757–10762.

Plessis, du, D.J.F., Berrelkamp, G., Nouwen, N. & Driessen, A.J.M. (2009) The lateral gate of SecYEG opens during protein translocation. *The Journal of biological chemistry*, 284 (23), pp.15805–15814.

Plessis, du, D.J.F., Nouwen, N. & Driessen, A.J.M. (2011) The Sec translocase. *Biochimica et biophysica acta*, 1808 (3), pp.851–865.

Poelarends, G.J. & Konings, W.N. (2002) The transmembrane domains of the ABC multidrug transporter LmrA form a cytoplasmic exposed, aqueous chamber within the membrane. *The Journal of biological chemistry*, 277 (45), pp.42891–42898.

Pozueta-Romero, J., Frehner, M., Viale, A.M. & Akazawa, T. (1991) Direct transport of ADPglucose by an adenylate translocator is linked to starch biosynthesis in amyloplasts. *Proceedings of the National Academy of Sciences of the United States of America*, 88 (13), pp.5769–5773.

Pressman, B.C. (1958) Intramitochondrial nucleotides. I. Some factors affecting net interconversions of adenine nucleotides. *The Journal of biological chemistry*, 232 (2), pp.967–978.

Prisner, T., Rohrer, M. & MacMillan, F. (2001) Pulsed EPR spectroscopy: biological applications. *Annual review of physical chemistry*, 52, pp.279–313.

Ravaud, S., Bidon-Chanal, A., Blesneac, I., Machillot, P., Juillan-Binard, C., Dehez, F., Chipot, C. & Pebay-Peyroula, E. (2012) Impaired Transport of Nucleotides in a Mitochondrial Carrier Explains Severe Human Genetic Diseases. *ACS chemical biology*.

Rees, D.M., Leslie, A.G.W. & Walker, J.E. (2009) The structure of the membrane extrinsic region of bovine ATP synthase. *Proceedings of the National Academy of Sciences of the United States of America*, 106 (51), pp.21597–21601.

Reginsson, G.W. & Schiemann, O. (2011) Pulsed electron-electron double resonance: beyond nanometre distance measurements on biomacromolecules. *The Biochemical journal*, 434 (3), pp.353–363.

Rey, M., Man, P., Clémençon, B., Trézéguet, V., Brandolin, G., Forest, E. & Pélosi, L. (2010) Conformational dynamics of the bovine mitochondrial ADP/ATP carrier isoform 1 revealed by hydrogen/deuterium exchange coupled to mass spectrometry. *The Journal of biological chemistry*, 285 (45), pp.34981–34990.

Riccio, P., Aquila, H. & Klingenberg, M. (1975a) Purification of the carboxy-atractylate binding protein from mitochondria. *FEBS letters*, 56 (1), pp.133–138.

Riccio, P., Aquila, H. & Klingenberg, M. (1975b) Solubilization of the carboxy-atractylate binding protein from mitochondria. *FEBS letters*, 56 (1), pp.192–132.

Robinson, A.J. & Kunji, E.R.S. (2006) Mitochondrial carriers in the cytoplasmic state have a common substrate binding site. *Proceedings of the National Academy of Sciences of the United States of America*, 103 (8), pp.2617–2622.

Robinson, A.J., Overy, C. & Kunji, E.R.S. (2008) The mechanism of transport by mitochondrial carriers based on analysis of symmetry. *Proceedings of the National Academy of Sciences of the United States of America*, 105 (46), pp.17766–17771.

Rorbach, J. & Minczuk, M. (2012) The post-transcriptional life of mammalian mitochondrial RNA. *The Biochemical journal*, 444 (3), pp.357–373.

Rubinstein, J.L., Walker, J.E. & Henderson, R. (2003) Structure of the mitochondrial ATP synthase by electron cryomicroscopy. *The EMBO journal*, 22 (23), pp.6182–6192.

Runswick, M.J., Powell, S.J., Nyren, P. & Walker, J.E. (1987) Sequence of the bovine mitochondrial phosphate carrier protein: structural relationship to ADP/ATP translocase and the brown fat mitochondria uncoupling protein. *The EMBO journal*, 6 (5), pp.1367–1373.

Runswick, M.J., Walker, J.E., Bisaccia, F., Iacobazzi, V. & Palmieri, F. (1990) Sequence of the bovine 2-oxoglutarate/malate carrier protein: structural relationship to other mitochondrial transport proteins. *Biochemistry*, 29 (50), pp.11033–11040.

Saraste, M. & Walker, J.E. (1982) Internal sequence repeats and the path of polypeptide in mitochondrial ADP/ATP translocase. *FEBS letters*, 144 (2), pp.250–254.

Sazanov, L.A. & Hinchliffe, P. (2006) Structure of the hydrophilic domain of respiratory complex I from Thermus thermophilus. *Science (New York, NY)*, 311 (5766), pp.1430–1436.

Scherer, B. & Klingenberg, M. (1974) Demonstration of the relationship between the adenine nucleotide carrier and the structural changes of mitochondria as induced by adenosine 5'-diphosphate. *Biochemistry*, 13 (1), pp.161–170.

Schneider, D. & Engelman, D.M. (2004) Motifs of two small residues can assist but are not sufficient to mediate transmembrane helix interactions. *Journal of molecular biology*, 343 (4), pp.799–804.

Schopfer, L.M. & Salhany, J.M. (1998) Spectroscopic and kinetic characterization of eosin-5-maleimide. *Analytical biochemistry*, 257 (2), pp.139–148.

Scouten, W.H., Visser, A.J., Grande, H.J., De Kok, A., De Graaf-Hess, A.C. & Veeger, C. (1980) Fluorescence polarization and energy-transfer studies on the pyruvate dehydrogenase complex of Escherichia coli. *European journal of biochemistry / FEBS*, 112 (1), pp.9–16.

Sherratt, H.S. (1991) Mitochondria: structure and function. *Revue neurologique*, 147 (6-7), pp.417–430.

Shvetsov, A., Stamm, J.D., Phillips, M., Warshaviak, D., Altenbach, C., Rubenstein, P.A., Hideg, K., Hubbell, W.L. & Reisler, E. (2006) Conformational dynamics of loop 262-274 in G- and F-actin. *Biochemistry*, 45 (20), pp.6541–6549.

Skou, J.C. & Esmann, M. (1980) Effects of ATP and protons on the Na : K selectivity of the (Na+ + K+)-ATPase studied by ligand effects on intrinsic and extrinsic fluorescence. *Biochimica et biophysica acta*, 601 (2), pp.386–402.

Slater, E.C. (1953) Mechanism of phosphorylation in the respiratory chain. *Nature*, 172 (4387), pp.975–978.

Sluse, F.E., Evens, A., Dierks, T., Duyckaerts, C., Sluse-Goffart, C.M. & Krämer, R. (1991) Kinetic study of the aspartate/glutamate carrier in intact rat heart mitochondria and comparison with a reconstituted system. *Biochimica et biophysica acta*, 1058 (3), pp.329–338.

Smyth, D.G., Blumenfeld, O.O. & Konigsberg, W. (1964) Reactions of *N*-ethylmaleimide with peptides and amino acids. *The Biochemical journal*, 91 (3), pp.589–595.

Stappen, R. & Krämer, R. (1994) Kinetic mechanism of phosphate/phosphate and phosphate/OH- antiports catalyzed by reconstituted phosphate carrier from beef heart mitochondria. *The Journal of biological chemistry*, 269 (15), pp.11240–11246.

Stipani, V., Cappello, A.R., Daddabbo, L., Natuzzi, D., Miniero, D.V., Stipani, I. & Palmieri, F. (2001) The mitochondrial oxoglutarate carrier: cysteine-scanning mutagenesis of transmembrane domain IV and sensitivity of Cys mutants to sulfhydryl reagents. *Biochemistry*, 40 (51), pp.15805–15810.

Stock, D., Gibbons, C., Arechaga, I., Leslie, A.G. & Walker, J.E. (2000) The rotary mechanism of ATP synthase. *Current opinion in structural biology*, 10 (6), pp.672–679.

Stock, D., Leslie, A.G. & Walker, J.E. (1999) Molecular architecture of the rotary motor in ATP synthase. *Science (New York, NY)*, 286 (5445), pp.1700–1705.

Sun, F., Huo, X., Zhai, Y., Wang, A., Xu, J., Su, D., Bartlam, M. & Rao, Z. (2005) Crystal structure of mitochondrial respiratory membrane protein complex II. *Cell*, 121 (7), pp.1043–1057.

Symersky, J., Pagadala, V., Osowski, D., Krah, A., Meier, T., Faraldo-Gómez, J.D. & Mueller, D.M. (2012) Structure of the c(10) ring of the yeast mitochondrial ATP synthase in the open conformation. *Nature structural & molecular biology*, 19 (5), pp.485–91– S1.

Terada, H. & Majima, E. (1997) Important role of loops in the transport activity of the mitochondrial ADP/ATP carrier. *Progress in Colloid & Polymer Science*. K. Kawasaki, B. Lindman, & H. Okabayashi eds. Darmstadt, Steinkopff, pp.193-198.

Thompson, J.D., Higgins, D.G. & Gibson, T.J. (1994) CLUSTAL W: improving the sensitivity of progressive multiple sequence alignment through sequence weighting, position-specific gap penalties and weight matrix choice. *Nucleic acids research*, 22 (22), pp.4673–4680.

Tonazzi, A., Console, L., Giangregorio, N., Indiveri, C. & Palmieri, F. (2012) Identification by site-directed mutagenesis of a hydrophobic binding site of the mitochondrial carnitine/acylcarnitine carrier involved in the interaction with acyl groups. *Biochimica et biophysica acta*, 1817 (5), pp.697–704.

Tsaousis, A.D., Kunji, E.R.S., Goldberg, A.V., Lucocq, J.M., Hirt, R.P. & Embley, T.M. (2008) A novel route for ATP acquisition by the remnant mitochondria of *Encephalitozoon cuniculi. Nature*, 453 (7194), pp.553–556.

Tsukihara, T., Aoyama, H., Yamashita, E., Tomizaki, T., Yamaguchi, H., Shinzawa-Itoh, K., Nakashima, R., Yaono, R. & Yoshikawa, S. (1996) The whole structure of the 13-subunit oxidized cytochrome c oxidase at 2.8 Å. *Science (New York, NY)*, 272 (5265), pp.1136–1144.

van der Giezen, M., Slotboom, D.-J., Horner, D.S., Dyal, P.L., Harding, M., Xue, G.-P., Embley, T.M. & Kunji, E.R.S. (2002) Conserved properties of hydrogenosomal and mitochondrial ADP/ATP carriers: a common origin for both organelles. *The EMBO journal*, 21 (4), pp.572–579.

Vignais, P.V., Vignais, P.M. & Defaye, G. (1973) Adenosine diphosphate translocation in mitochondria. Nature of the receptor site for carboxyatractyloside (gummiferin). *Biochemistry*, 12 (8), pp.1508–1519.

Vignais, P.V., Vignais, P.M. & Defaye, G. (1971) Gummiferin, an inhibitor of the adenine-nucleotide translocation. Study of its binding properties to mitochondria. *FEBS letters*, 17 (2), pp.281–288.

Vignais, P.V., Vignais, P.M. & Stanislas, E. (1962) Action of potassium atractylate on oxidative phosphorylation in mitochondria and in submitochondrial particles. *Biochimica et biophysica acta*, 60, pp.284–300.

Walker, J.E. & Runswick, M.J. (1993) The mitochondrial transport protein superfamily. *Journal of bioenergetics and biomembranes*, 25 (5), pp.435–446.

Wang, Y. & Tajkhorshid, E. (2008) Electrostatic funneling of substrate in mitochondrial inner membrane carriers. *Proceedings of the National Academy of Sciences of the United States of America*, 105 (28), pp.9598–9603.

Watmough, N.J. & Frerman, F.E. (2010) The electron transfer flavoprotein: ubiquinone oxidoreductases. *Biochimica et biophysica acta*, 1797 (12), pp.1910–1916.

Watt, I.N., Montgomery, M.G., Runswick, M.J., Leslie, A.G.W. & Walker, J.E. (2010) Bioenergetic cost of making an adenosine triphosphate molecule in animal mitochondria. *Proceedings of the National Academy of Sciences of the United States of America*, 107 (39), pp.16823–16827.

Weidemann, M.J., Erdelt, H. & Klingenberg, M. (1970) Effect of bongkrekic acid on the adenine nucleotide carrier in mitochondria: tightening of adenine nucleotide binding and differentiation between inner and outer sites. *Biochemical and biophysical research communications*, 39 (3), pp.363–370.

Weil, J.A., Bolton, J.R. & Wertz, J.E. (1994) *Electron Paramagnetic Resonance: Elementary Theory and Practical Applications*. 1st ed. Wiley-Interscience.

Whitehurst, C.B., Soderblom, E.J., West, M.L., Hernandez, R., Goshe, M.B. & Brown, D.T. (2007) Location and role of free cysteinyl residues in the Sindbis virus E1 and E2 glycoproteins. *Journal of virology*, 81 (12), pp.6231–6240.

Wikström, M. (1984) Two protons are pumped from the mitochondrial matrix per electron transferred between NADH and ubiquinone. *FEBS letters*, 169 (2), pp.300–304.

Wilson, K. & Walker, J. (2010) *Principles and Techniques of Biochemistry and Molecular Biology*. Cambridge Univ Pr.

Wohlrab, H., Annese, V. & Haefele, A. (2002) Single replacement constructs of all hydroxyl, basic, and acidic amino acids identify new function and structure-sensitive regions of the mitochondrial phosphate transport protein. *Biochemistry*, 41 (9), pp.3254–3261.

Xu, Y., Kakhniashvili, D.A., Gremse, D.A., Wood, D.O., Mayor, J.A., Walters, D.E. & Kaplan, R.S. (2000) The yeast mitochondrial citrate transport protein. Probing the roles of cysteines, Arg(181), and Arg(189) in transporter function. *The Journal of biological chemistry*, 275 (10), pp.7117–7124.

Yankovskaya, V., Horsefield, R., Törnroth, S., Luna-Chavez, C., Miyoshi, H., Léger, C., Byrne, B., Cecchini, G. & Iwata, S. (2003) Architecture of succinate dehydrogenase and reactive oxygen species generation. *Science (New York, NY)*, 299 (5607), pp.700–704.

Yoshikawa, S., Shinzawa-Itoh, K., Nakashima, R., Yaono, R., Yamashita, E., Inoue, N., Yao, M., Fei, M.J., Libeu, C.P., Mizushima, T., Yamaguchi, H., Tomizaki, T. & Tsukihara, T. (1998) Redox-coupled crystal structural changes in bovine heart cytochrome c oxidase. *Science (New York, NY)*, 280 (5370), pp.1723–1729.

Youle, R.J. & Narendra, D.P. (2011) Mechanisms of mitophagy. *Nature reviews Molecular cell biology*, 12 (1), pp.9–14.

Zara, V. & Palmieri, F. (1988) Inhibition and labelling of the mitochondrial 2-oxoglutarate carrier by eosin-5-maleimide. *FEBS letters*, 236 (2), pp.493–496.

Zhang, J., Frerman, F.E. & Kim, J.-J.P. (2006) Structure of electron transfer flavoprotein-ubiquinone oxidoreductase and electron transfer to the mitochondrial ubiquinone pool. *Proceedings of the National Academy of Sciences of the United States of America*, 103 (44), pp.16212–16217.

Zu, Y., Shannon, R.J. & Hirst, J. (2003) Reversible, electrochemical interconversion of NADH and NAD+ by the catalytic (Ilambda) subcomplex of mitochondrial NADH:ubiquinone oxidoreductase (complex I). *Journal of the American Chemical Society*, 125 (20), pp.6020–6021.